Université Mohammed V
Faculté des Sciences
Rabat

ULPGC
GRUPO FEAM

UNIVERSIDAD DE LAS PALMAS
DE GRAN CANARIA

PROGRAMA DE DOCTORADO EN INGENIERÍAS, QUÍMICA, MECÁNICA Y DE FABRICACIÓN

CENTRE: EAU, RESSOURCES NATURELLES, ENVIRONNEMENT ET DÉVELOPPEMENT DURABLE (CERN2D)

DOCTORAL THESIS

DEGRADATION AND ELIMINATION OF SOME POLLUTANTS, PESTICIDES, DYES FROM WATER PHOTOCATALYTICALLY

Wiâm EL-ALAMI

Las Palmas de Gran Canaria — **Spain**

Rabat — **Morocco**

09-06-2018

PROGRAMA DE DOCTORADO EN INGENIERÍAS, QUÍMICA, MECÁNICA Y DE FABRICACIÓN

CENTRE: EAU, RESSOURCES NATURELLES, ENVIRONNEMENT ET DÉVELOPPEMENT DURABLE (CERN2D)

DOCTORAL THESIS

DEGRADATION AND ELIMINATION OF SOME POLLUTANTS, PESTICIDES, DYES FROM WATER PHOTOCATALYTICALLY

Wiâm EL-ALAMI

Président :

EL HAJJAJI SOUAD: PES, Université Mohammed 5, Rabat, Maroc.

Examinateurs :

JOSÉ MIGUEL DOÑA RODRÍGUEZ: PES, Université Las Palmas de Gran Canaria, Espagne.

OSCAR GONZÁLEZ DÍAZ: PES, Université Las Palmas de Gran Canaria, Espagne.

CHIBAN MOHAMED: PH, Université Ibn Zohr, Agadir, Maroc.

ELHOURCH ABDERRAHIM: PES, Université Mohammed 5, Rabat, Maroc.

EL AZZOUZI MOHAMED: PES, Université Mohammed 5, Rabat, Maroc.

Las Palmas de Gran Canaria **Rabat**
Spain **Morocco**

09-06-2018

Dedication

In memory of my grandparents,

Who would be very happy to learn that their little girl was able to realize her dream.

May God give you a paradise of your choice.

To my parents,

To my close friends, who have engraved in my heart tenderness, love and gentleness.

All the words of the world cannot express the immense love which I bear to you, nor the deep gratitude which I testify to you for all the efforts and the sacrifices which you have never ceased to consent for my education and my well-being. It is through your support, your encouragement and your prayers that I was able to realize myself and be what I am. I would always be grateful to you.

May God bless you and gives you health, happiness and long life.

My love for you is so strong and eternal.

To my brother and my little sister,

Your lights are warming my oceans of dreams, evaporating the obstacles of my fears.

I love you so much my dears

DEDICATION

To those who have not abandoned their academic career and are doing their best to work on their thesis.

To all my family and friends,

I wish them much success and happiness

To all who helped me,

To all who love me,

I dedicate this thesis.

Wiâm

Acknowledgment

Praise to God alone, after all I implore Almighty to have granted me patience, health and serenity in my life, without God I would not have arrived at this day and at this level.

I would like to express the deepest appreciation to the people who helped me during the study period both in Spanish University of Las Palmas de Gran Canaria and Moroccan University Mohammed V of Rabat.

I would like to acknowledge:

My supervisor in Spain and co-supervisor in Morocco, Dr. Prof. José Miguel DOÑA RODRÍGUEZ of university Las Palmas de Gran Canaria, for providing me with the opportunity to work in CIDIA laboratory. His support and guidance were of great help to me. I also acknowledge him for his patience, availability, advice and encouragement. Please find in this work the expression of my sincere gratitude and my great respect.

My supervisor in Morocco, Dr. Prof. EL AZZOUZI Mohammed of university Mohammed V of Rabat, for welcoming me into Spectroscopy, Molecular Modeling, Materials, Nanomaterials, Water and Environment Laboratory (S2MN2E). Water, Natural resources, Environment and Sustainable Development Center. I also acknowledge him for his availability, his help, his encouragement and his confidence that he always gave me. That he finds in this thesis the expression of my respectful gratitude.

Dr. Prof. Javier ARAÑA for his passion and his help for research and scientific papers.

ACKOWLEDGMENT

Dr. Prof Óscar GONZÁLEZ DÍAZ for his encouragement and contributions in this work by transferring his knowledge into the analytical techniques used in this work.

Members of jury Prof. EL HAJJAJI Souad, Prof. Óscar GONZÁLEZ DÍAZ, Prof. ELHOURCH Abderrahim and Prof. CHIBAN Mohamed, I express my sincere thanks for the honor you give me in agreeing to judge this thesis.

I thank all my colleagues at S2MN2E moroccan laboratory as well as my colleagues at CIDIA spanish laboratory.

I would like to deeply thank Mr. Prof. Lferd Mohamed, former director of the Center for Doctoral Studies at the university Mohammed V Rabat, for his invaluable help despite his many concerns and responsibilities.

I would like also to acknowledge:

My dear parents,

It is with my parents that I found the necessary energy, my permanent support since all these years of studies, they are my inexhaustible source of love and tenderness. I wish them a long life with a very good health.

My brother Simohammed and my sister Chaymae,

With all the love that I bear to them, in testimony of the affection that I have always reserved to them, that they find through this thesis the expression of my deep love.

INDEX

INDEX

INDEX

Resumen

El principio de la fotocatálisis consiste en iluminar un semiconductor con una fuente de luz ultravioleta. Esta configuración conduce a una reacción fisicoquímica que destruye a la inmensa mayoría de los contaminantes no biodegradables que están presentes en el agua transformándolos en CO_2 y H_2O. La fotocatálisis puede inducir numerosos tipos de reacciones: oxidaciones parciales o totales, deshidrogenaciones, transferencia de hidrógeno, intercambios isotópicos, depósitos de metales en fase acuosa o gaseosa, etc. La fotocatálisis puede producirse en fase acuosa, gaseosa o una fase líquida puramente orgánica. Como toda reacción de catálisis heterogénea, las reacciones fotocatalíticas pueden ser descompuestas en cinco etapas. La primera etapa es la transferencia de moléculas de la fase líquida (o gaseosa) a la superficie del catalizador semiconductor, a través de la capa límite. La segunda es la adsorción de superficie del catalizador semiconductor. La tercera es la reacción de las moléculas adsorbidas. La cuarta es la desorción de los productos de reacción. Y la quinta etapa es la transferencia de los productos de la capa límite a la solución.

En general, una reacción fotocatalítica puede ser descrita como una reacción de óxido-reducción catalizada por un material semiconductor excitado, sobre el cual, los reactivos se encuentran adsorbidos. La reacción fotocatalítica es iniciada por la absorción de fotones, por el material semiconductor. Es la única diferencia con un procedimiento heterogéneo convencional de catálisis térmica.

La absorción de un fotón de energía superior a la anchura de la banda deenergías prohibidas (band gap), que separa la banda de valencia de la banda de conducción del material, induce la promoción de un electrón de valencia a la banda de conducción y la formación de un hueco positivo en la banda de valencia. La formación de los pares electrón / hueco (e^-/h^+) en el semiconductor es el principio básico de su actividad fotocatalítica.

Los pares electrón / hueco pueden iniciar reacciones de oxido-reducción que conducen a la formación de especies radicalarias altamente reactivos, OH• entre otros, capaces

de oxidar los contaminantes presentes en la superficie del catalizador. Sin embargo, debido a su reactividad muy fuerte, la corta vida útil de los OH• induce a la mayoría de autores a pensar que las oxidaciones por la acción de OH• se producen en la superficie del semiconductor.

Los mecanismos de eliminación de los contaminantes son pues múltiples, como la oxidación directa a través de los huecos, la reducción por los e^- libres de la banda de conducción, o la oxidación por las especies radicalarias formadas en la superficie del catalizador por los mecanismos que se ilustran en la figura 1.

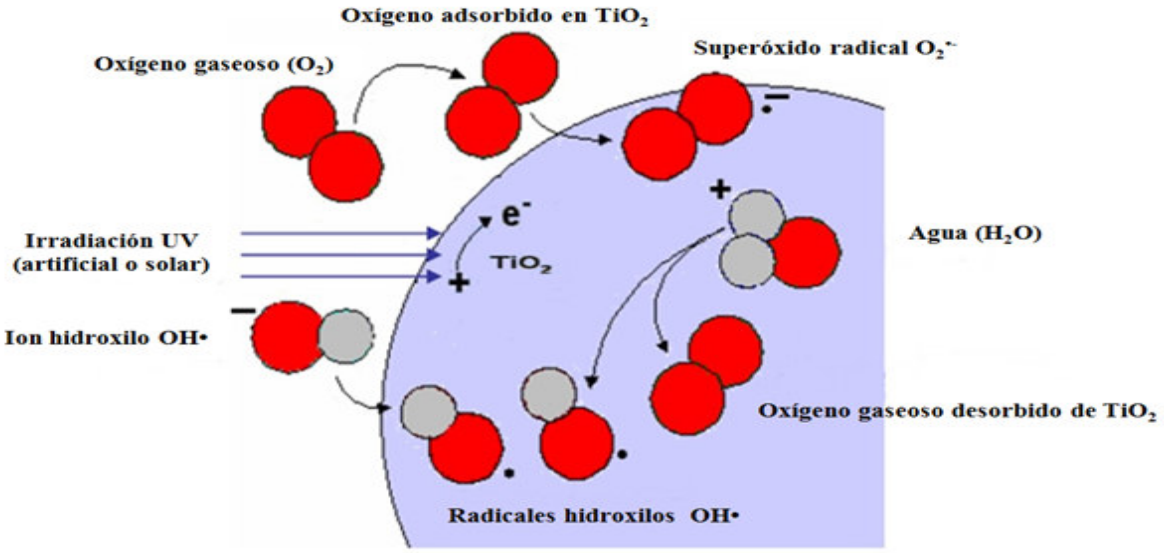

Figura 1: formación de radicales hidroxilos y superóxido a partir de agua, de oxígeno disuelto y de iones hidróxido

Sabemos que la fotocatálisis encuentra su aplicación en diferentes campos, entre los que se encuentra la detoxificación de agua.

Las moléculas que se adsorben en la superficie del TiO_2 pueden ser unos contaminantes orgánicos o inorgánicos, pero también moléculas de agua, iones hidroxilos oxígeno disuelto por ejemplo.

Los compuestos orgánicos, incluido los fenoles, están entre los contaminantes más comunes en los efluentes que provienen de industrias del plástico, del papel, del petróleo, de las resinas y las tinturas [1, 2, 3]. Los fenoles están considerados como

compuestos tóxicos perjudiciales para la salud humana, la vida acuática y las plantas [4]. La ingestión de los fenoles en concentración entre 10 y 240 $mg.l^{-1}$ durante períodos largos, provoca irritación de la boca, trastornos de la visión y diarrea [5]. Los compuestos y derivados fenólicos están considerados como contaminantes prioritarios por la agencia americana de protección medioambiental [6, 7]. La concentración máxima admisible de fenol en el agua potable es 1 $\mu g \cdot l^{-1}$ (Organización Mundial de la Salud) [8], por ello se necesita el desarrollo del procedimiento de tratamiento eficaces para eliminarlos de las aguas residuales [9, 10].

En esta tesis se estudia la fotocatálisis heterogénea como tratamiento para la destoxificación de aguas. Se han sintetizado y modificado diferentes catalizadores para este fin. La síntesis hidrotermal parece ser una alternativa prometedora, permitiendo producir materiales eficientes y baratos. Un método utilizado ha sido la síntesis sol-gel. Esta técnica permite la síntesis de una gran variedad de óxidos semiconductores con diferentes estructuras.

Varios semiconductores (TiO_2, ZnO, ZrO_2, ...) pueden desempeñar el papel de fotocatalizadores, pero el TiO_2 ha sido el más estudiado debido a su elevada reactividad, su toxicidad reducida, su estabilidad química, su bajo coste, su capacidad de descomponer los contaminantes orgánicos e incluso su capacidad para provocar una mineralización completa de ciertos compuestos orgánicos. Además, puede ser dopado para mejorar sus propiedades. Los diferentes semiconductores estudiados en esta tesis han sido también modificados con el fin de mejorar su actividad y se ha estudiado y comparado las mejoras producidas. En esta tesis se pretende evaluar la factibilidad de la utilización de los productos a base de TiO_2 y otros óxidos semiconductores para reducir la contaminación del agua mediante fotocatálisis.

Résumé

Le principe de la photocatalyse consiste à éclairer un semi-conducteur avec une source de lumière ultraviolette. Cette configuration conduit à une réaction physico-chimique qui détruit la plupart des polluants non biodégradables présents dans l'eau en les transformant en CO_2 et H_2O. La photocatalyse peut induire de nombreux types de réactions: oxydations partielles ou totales, déshydrogénations, transfert d'hydrogène, échanges isotopiques, dépôts métalliques en phase aqueuse ou gazeuse, etc. La photocatalyse peut se produire en phase aqueuse, gazeuse ou dans une phase liquide purement organique. Comme toute réaction de catalyse hétérogène, les réactions photocatalytiques peuvent être décomposées en cinq étapes. La première étape est le transfert des molécules de la phase liquide (ou gazeuse) à la surface du catalyseur semi-conducteur, à travers la couche limite. La seconde est l'adsorption de surface du catalyseur semi-conducteur. La troisième est la réaction des molécules adsorbées. La quatrième est la désorption des produits de réaction. Et la cinquième étape est le transfert des produits de la couche limite à la solution.

En général, une réaction photocatalytique peut être décrite comme une réaction d'oxydo-réduction catalysée par un matériau semi-conducteur excité, sur lequel, les réactifs sont adsorbés. La réaction photocatalytique est initiée par l'absorption de photons, par le matériau semi-conducteur. C'est la seule différence avec un procédé hétérogène classique de catalyse thermique.

L'absorption d'un photon d'énergie supérieure à la largeur de la bande d'énergie interdite (band gap), qui sépare la bande de valence de la bande de conduction du matériau, induit la promotion d'un électron de valence dans la bande de conduction et formation d'un trou positif dans la bande de valence. La formation des paires électron/trou (e^-/h^+) dans le semi-conducteur est le principe de base de son activité photocatalytique.

Les paires électron/trou peuvent initier des réactions d'oxydo-réduction conduisant à la formation d'espèces radicalaires hautement réactives, OH• entre autres, capables

d'oxyder les contaminants présents à la surface du catalyseur. Cependant, en raison de sa très forte réactivité, la courte durée de vie des OH• incite la plupart des auteurs à penser que des oxydations par l'action de OH• se produisent à la surface du semi-conducteur.

Les mécanismes d'élimination des contaminants sont donc multiples, tels que l'oxydation directe à travers les trous, la réduction par les e^- libre de la bande de conduction, ou l'oxydation par les espèces radicalaires formées à la surface du catalyseur par les mécanismes qui sont illustrés dans la figure 1.

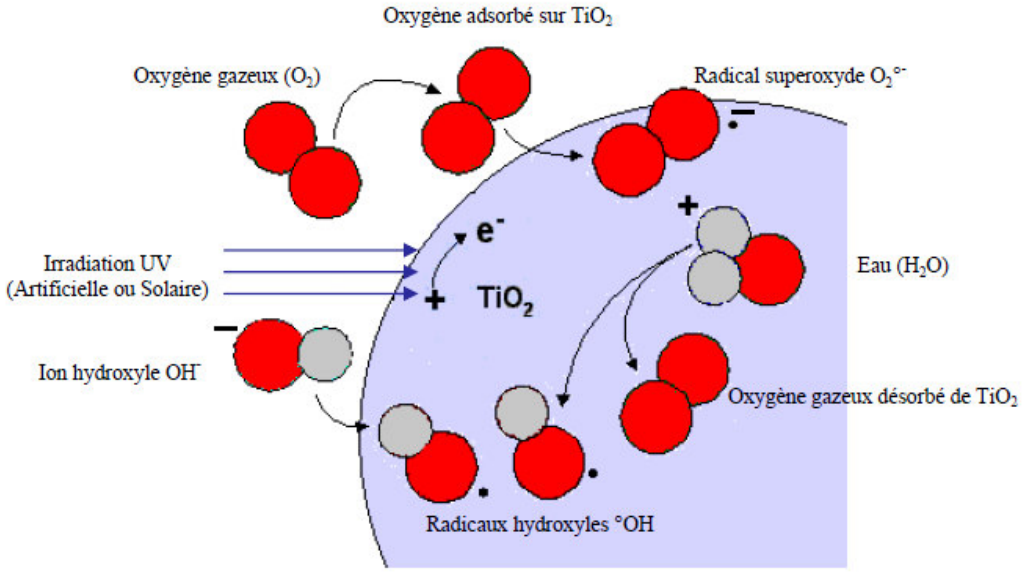

Figure 1: formation des radicaux hydroxyles et de superoxyde à partir d'eau, d'oxygène dissous et d'ions hydroxyde

On connait bien que la photocatalyse trouve son application dans différents domaines dont la désintoxication de l'eau.

Les molécules qui s'adsorbent à la surface de TiO_2 peuvent être des polluants organiques ou inorganiques, mais aussi des molécules d'eau, des ions hydroxyles ou de l'oxygène dissous par exemple.

Les composés organiques, y compris les phénols, sont parmi les polluants les plus courants dans les effluents provenant des industries des plastiques, du papier, du

pétrole, des résines et des colorants [1, 2, 3]. Les phénols sont considérés comme des composés toxiques nocifs pour la santé humaine, la vie aquatique et les plantes [4]. L'ingestion des phénols à une concentration comprise entre 10 et 240 $mg \cdot L^{-1}$ pendant de longues périodes provoque une irritation de la bouche, des troubles de la vision et de la diarrhée [5]. Les composés et les dérivés phénoliques sont considérés comme des polluants prioritaires par l'agence américaine de protection de l'environnement [6, 7]. La concentration maximale admissible de phénol dans l'eau potable est de 1 $\mu g \cdot L^{-1}$ (Organisation mondiale de la santé) [8], par conséquent, le développement des procédés de traitement efficaces est nécessaire pour les éliminer des eaux usées [9, 10].

Dans cette thèse, la photocatalyse hétérogène est étudiée en tant que traitement pour la désintoxication de l'eau. Pour ceci différents catalyseurs ont été synthétisés et modifiés. Une méthode nommée la synthèse sol-gel a été utilisée. Cette technique permet la synthèse d'une grande variété d'oxydes semi-conducteurs avec des structures différentes.

Plusieurs semi-conducteurs (TiO_2, ZnO, ZrO_2, ...) peuvent jouer le rôle de photocatalyseurs, mais le TiO_2 a été le plus étudié en raison de sa réactivité élevée, de sa toxicité réduite, de sa stabilité chimique, de son faible coût et de sa capacité à décomposer contaminants organiques et même sa capacité à achever une minéralisation complète de certains composés organiques. De plus, il peut être dopé pour améliorer ses propriétés. Les différents semiconducteurs étudiés dans cette thèse ont également été modifiés afin d'améliorer leur activité, et les améliorations produites ont été étudiées et comparées. Cette thèse vise à évaluer la faisabilité de l'utilisation des produits à base de TiO_2 et d'autres oxydes semi-conducteurs pour réduire la contamination de l'eau par photocatalyse.

General introduction

The principle of photocatalysis consists in illuminating a semiconductor with an ultraviolet light source. This configuration leads to a physico-chemical reaction which destroys most of the non-biodegradable pollutants present in water by converting them into CO_2 and H_2O. Photocatalysis can induce many types of reactions: partial or total oxidations, dehydrogenations, hydrogen transfer, isotopic exchanges, metal deposition In aqueous or gaseous phase. The photocatalysis can take place in an aqueous, gaseous or pure organic liquid phase. As any heterogeneous catalysis reaction, photocatalytic reactions can be decomposed into five steps. The first step is the transfer of molecules from the liquid (or gaseous) phase to the surface through the boundary layer. The second is surface adsorption of TiO_2. The third is the reaction of the adsorbed molecule. The fourth is the desorption of the Reaction Products. And the fifth step is the transfer of products from the boundary layer to the solution.

In general, a photocatalytic reaction can be described as an oxidation-reduction reaction catalyzed by an excited semiconductor material, which on it's the surface the reagents are adsorbed. The photocatalytic reaction is initiated by the absorption of photons by the semiconductor material. This is the only difference with a conventional heterogeneous catalysis process activated by thermal elevation.

The absorption of a photon of energy greater than the width of the band gap separating the valence band from the conduction band of the material induces the promotion of a valence electron to the conduction band and the formation of a positive hole on the valence band. The formation of electron/hole pairs (e^-/h^+) on the surface of the semiconductor is at the origin of its photocatalytic activity.

Electron-hole pairs can initiate oxidation-reduction reactions leading to the formation of highly reactive OH• radical species, among others capable of oxidizing the pollutants present on the surface of the catalyst. However, due to their very high reactivity, the short lifetime of OH• induces the majority of authors to think that these OH• oxidations take place on the surface of the semiconductor.

The mechanisms for eliminating pollutants are therefore multiple, as direct oxidation through holes, reduction by e^- frequencies of the conduction band, or oxidation by the radical species formed on the surface of the catalyst by the mechanisms illustrated in figure 1.

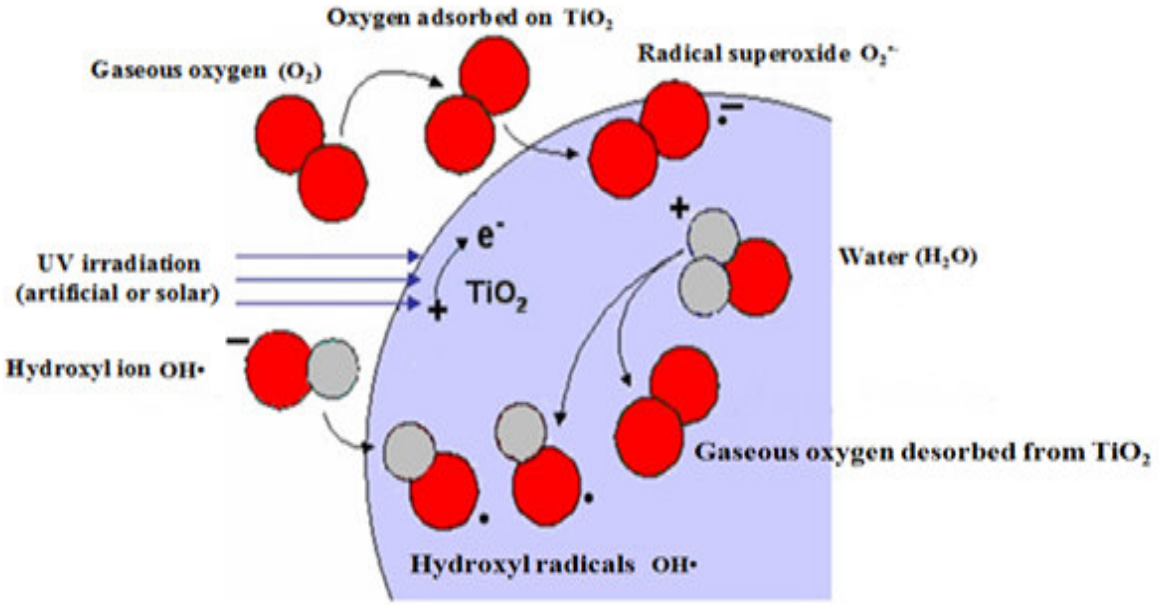

Figure 1: Formation of hydroxyl and superoxide radicals from water, dissolved oxygen and hydroxide ions

As known, the photocatalysis finds its application in different fields in particular the detoxification of water.

The molecules which adsorb on the surface of TiO_2 can be organic or inorganic pollutants, but also water molecules, hydroxyl ions, or dissolved oxygen, for example.

Organic compounds, including phenols, are among the most common pollutants in effluents from the plastics, paper, petroleum, resins and dyes industries [1, 2, 3]. Phenols are considered toxic compounds that are harmful to human health, aquatic life and plants [4]. Ingestion of phenols at concentration between 10 and 240 $mg \cdot L^{-1}$ for long periods causes irritation of the mouth, blurred vision and diarrhea [5]. Phenolic compounds and derivatives are considered as priority pollutants by the environmental protection american agency [6, 7]. The maximum allowable concentration of phenol in

drinking water is 1 $\mu g \cdot L^{-1}$ (World Health Organization) [8], therefore the development of effective treatment processes is necessary to remove them from wastewater [9, 10].

In this thesis, heterogeneous photocatalysis is studied as a treatment for the detoxification of water. For this, different catalysts have been synthesized and modified. A method named sol-gel have been used. This technique allows the synthesis of a wide variety of semiconductor oxides under different structures.

Several semiconductors (TiO_2, ZnO, ZrO_2,...) can act as photocatalysts but TiO_2 has been the most studied one due to its high reactivity, reduced toxicity, chemical stability, lower costs, and its ability to break down organic pollutants and even achieve complete mineralization. And since among their main characteristics is the ability to be doped to improve their properties, then we will dope all the semiconductors that we will use, and study the improvement occurred by comparing them. This thesis aimed at evaluating the feasibility of using TiO_2 based products, and different other products, to alleviate the water pollution by photocatalysis.

References:

[1] Charge Transfer Processes at Semiconductor-Electrolyte Interfaces in Connection With Problems of Catalysis. H. Gerischer. Surface Science. 18 (1969) 97.

[2] Destruction of Water Contaminants. D.F. Ollis, E. Pelizzetti and N. Serpone. Environ. Sci. Technol. 25(9) (1991) 1523.

[3] Heterogeneous Photocatalysis: fundamentals and applications to the renoval of various types of aquous pollutants. J.M Herrmann. Catalysis Today. 53 (1999) 115.

[4] Homogeneous and Heterogeneous Photocatalysis. E Pelizzetti. La Chimica e L'Industria. 68(10) (1986) 51.

[5] Photochemical Inactivation of Organic Pollutants from Water. A. Archer and S. Saltzman, pp. 302-319 in: Ecological studies, Vol. 73 "Toxic Organic Chemicals in Porous Media". Springer-Verlag Berlin Heidelberg, 1989.

[6] Photoelectrochemistry and Heterogeneous Photocatalysis at Semiconductors. A.J. Bard. Journal of Photochemistry, 10 (1979) 59.

[7] Putting Photocatalysis to Work. E. Borgarello, N. Serpone, M. Barbeni, C. Minero, E. Pelizzetti and E. Pramauro. La Chimica e L'Industria. 68(10) (1986) 53.

[8] Solar Assisted Photocatalysis for Water Purification: Issues, Data, Questions. D.F. Ollis, pp. 593-622 in: “Photochemical Conversion and Storage of Energy”. Ed. E Pelizzetti and M. Schiavello. Kluwer Academic Publishers. The Netherlands, 1991.

[9] Araña, J., Doña-Rodríguez, J.M., Portillo-Carrizo, D., Fernández-Rodríguez, C., Pérez-Peña, J., González Díaz, O., Navío, J.A., Macías, M. Photocatalytic degradation of phenolic compounds with new TiO2 catalysts. (2010) Applied Catalysis B: Environmental, 100 (1-2), pp. 346-354.

[10] Colón, G., Hidalgo, M.C., Navío, J.A., Pulido Melián, E., González Díaz, O., Doña Rodríguez, J.M. Highly photoactive ZnO by amine capping-assisted hydrothermal treatment. (2008) Applied Catalysis B: Environmental, 83 (1-2), pp. 30-38.

CHAPTER I

STATE OF THE ART

State of the art

1. Advanced Oxidation Processes (AOP)

1.1 Generality

Advanced Oxidation Processes are defined as very interesting alternatives for the degradation of non-biodegradable organic pollutants which cannot be eliminated by biological treatment. These AOP involve the formation of OH· hydroxyl radicals in sufficient quantity and at room temperature to oxidize organic pollutants [1, 2, 3]. This hydroxyl radical can be produced by photochemical and non-photochemical processes:

- **Non-photochemical processes :**
  - aElectrochemical
  - Electro-Fenton
  - Fenton (Fe^{2+}/H_2O_2)
  - Peroxonation (O_3/H_2O_2)
  - Sonolysis
  - Radiolysis

- **Photochemical processes :**
  - Photolysis of water (UV /H_2O)
  - Photolysis of hydrogen peroxide (UV/H_2O_2)
  - Photolysis of ozone (UV / O_3)
  - UV/H_2O_2/O_3
  - Heterogeneous photocatalysis
  - Photo-Fenton (Fe^{2+}/ H_2O_2/ UV)

The AOP are complementary to the conventional processes of flocculation, precipitation, adsorption on activated carbon, etc. They are very effective for the degradation of recalcitrant organic pollutants. However, in the case of high concentrations of total organic carbon or in the case of waste waters with a chemical oxygen demand greater than 5 g/l (COD>5 g/l) (Figure I.1) [4], it becomes inadequate

to use AOP, so in the case where the COD is very high, the chosen methods will be incineration or wet air oxidation.

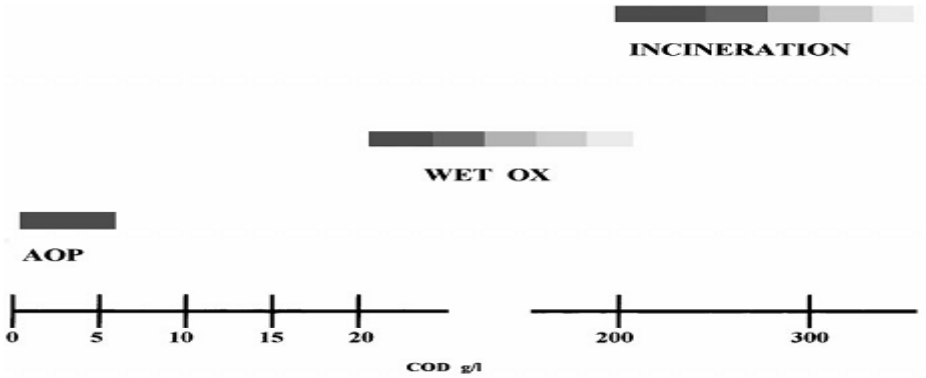

Figure I.1: Techniques for wastewater treatment according to the COD content [4]

The AOP have several advantages:

- Transformation of refractory pollutants to biodegradable products easy to process by inexpensive biological treatment methods.
- Complete mineralization of the majority of pollutants to CO_2 and H_2O.
- Minimum energy consumption compared to other methods such as incineration.
- Reduction of the use of disinfectants and oxidants such as chlorine whose residues can have adverse/harmful effects on health.

1.2 Description and characteristics of the hydroxyl radical OH·

The hydroxyl radical (**OH·**) is a molecule composed of an oxygen and a hydrogen atom having an unpaired electron (single electron) on its external orbital. In contrary to ions, the hydroxyl radicals are produced from an homolytic rupture of a covalent bond, that means that the two electrons involved in this bond are also divided, one electron for each bound atom [5]. This characteristic gives it a strongly polar character and, consequently, high reactivity [4] for several organic compounds (aromatic and aliphatic), inorganic compounds and bacteria. It has one of the strongest oxidizing power, after Fluorine, with an oxidation potential of 2.80V compared to the normal

hydrogen electrode [Table I.1]. The OH· radical is characterized by a half-life of the order of 10^{-9} sec [6] and an electrophilic character. This is why compounds with donor groups react more rapidly with OH· radical leading mainly to the formation of hydroxylated compounds. It is by far one of the most powerful oxidants that can be used in water treatment.

Species	Oxidation potential (V)
Fluorine	**3.03**
Hydroxyl radical	**2.80**
Atomic oxygen	**2.42**
Ozone	**2.07**
Hydrogen peroxide	**1.78**
Perhydroxyl radical	**1.70**
Permanganate	**1.68**
Hypobromous acid	**1.59**
Chloride dioxide	**1.57**
Hypochlorous acid	**1.49**
Hypoiodous acid	**1.45**
Chlorine	**1.36**
Bromine	**1.09**
Iodine	**0.54**

TableI.1: Oxidation potentials of some oxidants [7]

The hydroxyl radical OH· can react with organic molecules in three different ways [Eq. I.1-I.3] [7].

- Hydrogen abstraction: $OH^{\bullet} + RH \rightarrow R^{\bullet} + H_2O$ **(I.1)**
- Electron addition: $OH^{\bullet} + R \rightarrow ROH^{\bullet}$ **(I.2)**
- Electron transfer: $OH^{\bullet} + RX \rightarrow OH^{-} + RX^{\bullet+}$ **(I.3)**

Radical-radical recombination must also be also taken into account.

$$2\ OH\bullet \rightarrow H_2O_2$$

Some ions present in the water to be treated are known as OH· scavengers because of the speed with which they react. They could limit the action of the hydroxyl radicals. Among the OH· scavengers we find carbonates and bicarbonates which form the carbonate radical anion ($CO_3^{\cdot -}$) less reactive than OH· [8].

1.3 Advanced non-photochemical oxidation processes

1.3.1. Electrochemical processes / Electro-Fenton

This technique is based on the generation of hydroxyl radicals by applying oscillations of low electrical current intensities (<10 amperes) to a solution containing hydrogen peroxide [9].

Several factors can affect the reaction rate, the temperature, the current, the configuration of the electrodes and their composition. This process has certain disadvantages such as its high cost compared to other processes, the need to have a conductive effluent, and therefore the addition of a salt in the case low conductive effluents.

The hydroxyl radicals can be generated in solution to be treated by direct or indirect electrochemical reactions [10]. Anodic direct oxidation allows the complete oxidation of a large number of organic molecules contained in wastewater. By-products resulting from anodic oxidation are carbonic acid, water, ammonia and other products. In many cases, the anodic oxidation of organic or inorganic pollutants leads to the formation of simpler, non-toxic or less toxic and biodegradable compounds [11, 12]. For example, at the anode, phenols are oxidized to maleic acid, cyanides to cyanates, sulphides to sulphates, and so on [11, 12]. It is important to emphasize that these electrodes allow to oxidize compounds chemically non-oxidizable or hardly oxidizable [13].

On the other hand, indirect oxidation (electro-Fenton process) uses the Fenton reaction to produce these radicals [Eq. I.4-I.6][14].

$$\mathbf{O_2 + 2H^+ + 2e^- \leftrightarrow H_2O_2} \qquad \textbf{(I.4)}$$

$$\mathbf{H_2O_2 + Fe^{2+} \rightarrow Fe^{3+} + OH^- + OH^{\cdot}} \qquad \textbf{(I.5)}$$

$$Fe^{3+} + e^{-} \leftrightarrow Fe^{2+} \quad \text{(I.6)}$$

In summary, electrochemical treatments constitute interesting methods for water treatment and effluents aimed, firstly, at reducing the quantity of reagents (decrease in the volume of generated sludge) and, on the other hand, to reduce the volume of equipment (decreased retention time in the reactor). Several physical and chemical processes can simultaneously intervene during the electrolytic treatment of an effluent (anodic oxidation, cathodic reduction, adsorption, flotation, etc.), which, in most cases, contribute to a better treatment efficiency compared to conventional chemical or biological techniques commonly used.

1.3.2 Fenton reaction (H_2O_2/Fe^{2+})

The Fenton process, known since the end of the 19th century [15], was discovered for the first time by H.J.H. Fenton in 1894 [16] when he noticed that it is possible to activate H_2O_2 with a ferrous salt and then to oxidize tartaric acid. It was only later, in 1934, that Haber and Weiss [17] hypothesized that the oxidizing agent in the Fenton reaction was the hydroxyl radical generated by the catalytic decomposition of H_2O_2 into acidic medium. The oxidation reaction proceeds as described below. In a first step, hydroxyl radicals are produced by reaction between H_2O_2 and Fe^{2+} ions (equation I.7). Hydrogen peroxide (H_2O_2) can react with ferric ions Fe^{3+} or HO• radicals (equation I.7 and I.9) formed, leading to the production of hydroperoxyl radicals (HOO•) having an oxidizing potential lower than that of hydroxyl radicals [18,19].

$$Fe^{2+} + H_2O_2 \rightarrow Fe^{3+} + OH^{-} + OH^{\cdot} \quad \text{(I.7)}$$

$$Fe^{3+} + H_2O_2 \rightarrow Fe^{2+} + H^{+} + HO_2^{\cdot} \quad \text{(I.8)}$$

$$OH^{\cdot} + H_2O_2 \rightarrow H_2O + HO_2^{\cdot} \quad \text{(I.9)}$$

The radicals OH• and HO_2• can oxidize the organic substrate RH to an alkyl radical by abstraction of a proton [20,21,22] :

$$RH + OH^{\cdot} \rightarrow R^{\bullet} + H_2O \quad \text{(I.10)}$$

$$RH + HO_2^{\cdot} \rightarrow R^{\bullet} + H_2O_2 \quad \textbf{(I.11)}$$

The hydroperoxyl radical leads, by various reactions, to the formation of molecular oxygen [23]:

$$HO_2^{\cdot} + H_2O_2 \rightarrow H_2O + OH^{\cdot} + O_2 \quad \textbf{(I.12)}$$

$$HO_2^{\cdot} + Fe^{3+} \rightarrow Fe^{2+} + H^{+} + O_2 \quad \textbf{(I.13)}$$

In general, the Fenton reaction requires a low pH [24] and improves with temperature increase. A pH <3 is important to keep the ferric ion (Fe^{3+}) in solution. For a 3< pH<5, Fe^{3+} will be in colloidal form in the solution. For a pH above 5 (pH>5), Fe^{3+} precipitates as $Fe(OH)_3$ and will decompose H_2O_2 into oxygen. This reaction has an observable effect at temperatures between 5°C and 20°C and when the temperature rises above 40°C the accelerated decomposition of H_2O_2 into oxygen and water decreases the efficiency of the use of H_2O_2.

1.3.3 Peroxonation H_2O_2/O_3

The principle of the peroxonation process is based on the coupling between ozone and hydrogen peroxide to produce free radicals. This combined system is more efficient than ozonation alone. In this process, hydroxyl radicals, the main oxidants of peroxonation, are formed by reaction between ozone and hydrogen peroxide (Eq. I.14) [25]. Although this method is more efficient than ozonation, it is affected by many parameters such as temperature, pH, reactions consuming the hydroxyl radicals, the type of pollutant, as well as the low solubility of O_3 [26].

$$O_3 + H_2O_2 \rightarrow OH^{\cdot} + HOO^{\cdot} + O_2 \quad \textbf{(I.14)}$$

On the other hand, ozonation and peroxonation have the advantage over processes with UV irradiation that they can operate in water with high turbidity because the system does not depend on the transmittance of the radiation through the effluent [27].

1.3.4 Sonolysis

Sonolysis is a technique using ultrasound to degrade pollutants in aqueous medium.

Ultrasounds are increasingly used in industrial settings to accelerate or activate a reaction mechanism. The interest of ultrasound resides in their non-polluting appearance and their ease of automation. In an aqueous medium, ultrasound can act according to two modes of action, either by chemical action (indirect), or by a physical action (direct). The indirect action, usually obtained at high frequency, leads to the generation of free radicals (OH·, HO_2· and O·) induced by homolytic rupture of the molecule of water or oxygen. [28]. The direct action induced by ultrasound is also interesting for the treatment of industrial effluents. Indeed, ultrasound generates cavitation bubbles. Inside these bubbles the extreme conditions of temperature and pressure lead to the dissociation of water and the production of OH·, HOO· radicals, etc. Also, the ultrasound can have biocide effect induced by these phenomena of cavitation which break the bacterial cells [29].

$$\mathbf{H_2O + ultrasound \rightarrow OH^{\cdot} + H^{\cdot}} \qquad \textbf{(I.15)}$$ [30]

1.3.5 Radiolysis

The radiolysis of water is a phenomenon that was observed at the beginning of the 20th century by Giesel, Ramsey and Soddy and which has been widely studied by many researchers [31]. As the radiolysis phenomenon is observed for the first time in 1903 by F.Giesel [32] by irradiating pure water with the β radiation of natural radio-elements. Radiolysis comprises different steps and several chemical species are produced during each step. A first attempt to understand the radiolysis of pure water goes back to 1914 [33], when Debierne made the hypothesis of the dissociation of water under the influence of radiation into H atoms and OH· radicals.

After the passage of the electron in water, the radiolysis process can be divided into three successive phases according to the following scheme [34] (figure I.2) **:**

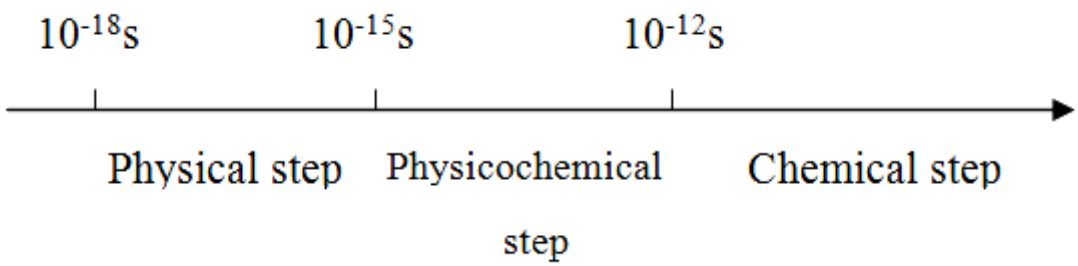

Figure I.2 : Descriptive diagram of the stages of radiolysis of water [34]

a - Physical step : the physical step starts just after **the collision** between the electron and the target molecule. The duration of this step extends from 10^{-18} to 10^{-15}s after the collision. It actually concerns the transfer of energy from the electron/ionizing radiation to the water molecules.

b- Physicochemical step: Species previously formed during the physical stage are unstable and react with each other and with surrounding water molecules. This step concerns the products of the physical step, H_2O^+, the electron e^- and the excited water molecules noted as H_2O^*. This step takes place between 10^{-15} and 10^{-12}s [35] after the incident electron.

c- Chemical step: The species from the previous steps are located in clusters (short trajectories or drops) independent from each other. The concentration of these species is therefore not homogeneous throughout the solution. Thus, some reactions occur within clusters according to the radiolytic species present. Then, with the spread of these species in the rest of the solution, the clusters overlap and reactions between species from different clusters are possible. The chemical step can be divided into 2 sub-steps: the step of heterogeneous chemistry, when the clusters are independent and the homogeneous chemistry step when the radiolytic species concentrations can be considered homogeneous over the entire solution.

1.4 Advanced photochemical oxidation processes

Advanced photochemical oxidation processes allow the production of hydroxyl radicals by direct photolysis of water (H_2O), or of an additive (H_2O_2, O_3) or by the excitation of a semiconductor. The most used methods for generating the hydroxyl radical by advanced photochemical oxidation processes are as follows:

1.4.1 Photolysis of water (UV/H_2O)

This advanced oxidation process is based on an irradiation at λ <190 nm, which causes the breakdown of bonds and the degradation of organic matter in the condensed and gaseous phases. Due to the absorption of air, it is necessary to evacuate the devices working at these low wavelengths, which are generally called Vacuum Ultraviolet (VUV). This process produces also a breakdown of the water molecule producing hydroxyl radicals and hydrogen atoms which can give place to other radicals.

$$H_2O + h\upsilon \rightarrow OH^{\cdot} + H^{\cdot} \qquad \textbf{(I.16)}$$

The high concentration of radicals in the solution leads to high rates of degradation.

However, it is impossible to commercially think on this technique only with the energy of the sun, so an additional source of energy is needed, which increases the cost of installation.

1.4.2 Photolysis of hydrogen peroxide (UV/H_2O_2)

Photolysis of hydrogen peroxide, at wavelengths between 200 et 300 nm, causes a break in the O — O bond of the H_2O_2 molecule forming two hydroxyl radicals [Eq.(I.17)] which also participate, by secondary reactions, in the decomposition of hydrogen peroxide [8] according to the equations [Eq. (I.18)-(I.23)].

$$H_2O_2 + h\upsilon \rightarrow 2OH^{\cdot} \qquad \textbf{Initiation} \qquad \textbf{(I.17)}$$

$$HO_2^{\cdot} + H_2O_2 \rightarrow H_2O + HO_2^{\cdot} \qquad \textbf{Spread} \qquad \textbf{(I.18)}$$

$$HO_2^{\cdot} + H_2O_2 \rightarrow OH^{\cdot} + H_2O + O_2 \qquad \textbf{(I.19)}$$

$$OH^{\cdot} + HO_2^{-} \rightarrow HO_2^{\cdot} + OH^{-} \qquad \textbf{(I.20)}$$

$$2\,HO_2^{\cdot} \rightarrow H_2O_2 + O_2 \qquad \textbf{Termination} \qquad \textbf{(I.21)}$$

$$OH^{\cdot} + HO_2^{\cdot} \rightarrow H_2O + O_2 \qquad \textbf{(I.22)}$$

$$2OH^{\cdot} \rightarrow H_2O_2 \qquad \textbf{(I.23)}$$

The speed of production of free radicals depends on several factors [36] as pH, the characteristics of UV lamps (emission spectrum, energy), and the characteristics of the medium (turbidity). Thus, turbid waters containing organic compounds can absorb UV radiation, hence the need to increase the UV dose. The reaction is faster in a basic medium. For pH less than 10, speeds are low.

This process is often used for the decontamination of underground water and for the removal of pollutants such as trichlorethylene (TCE), tetrachlorethylene, and benzene [37] and also to remove phosphoric esters from drinking water [23].

1.4.3 Photolysis of ozone (UV/O_3) :

Ozone in aqueous solution absorbs UV radiations with a maximum adsorption at 253.7nm [38]**.** This reaction leads to the production of free radicals [Eq.(I.24) - (I.28)] which are very reactive, oxidative and effective species in removing organic pollutants and bacteria.

$$O_3 + H_2O + h\upsilon \rightarrow 2OH^{\cdot} + O_2 \qquad \textbf{Initiation} \qquad \textbf{(I.24)}$$

$$O_3 + OH^{\cdot} \rightarrow HO_2^{\cdot} + O_2 \qquad \textbf{Spread} \qquad \textbf{(I.25)}$$

$$O_3 + HO_2^{\cdot} \rightarrow OH^{\cdot} + 2\,O_2 \qquad \textbf{(I.26)}$$

$$OH^{\cdot} + HO_2^{\cdot} \rightarrow H_2O + O_2 \qquad \textbf{Termination} \qquad \textbf{(I.27)}$$

$$OH^{\cdot} + OH^{\cdot} \rightarrow H_2O_2 \qquad \textbf{(I.28)}$$

The process UV/O_3 is more effective than UV/H_2O_2 for the generation of hydroxyl radicals for equal concentrations of oxidants and using low pressure UV lamps. This coupling (UV/O_3) has been studied for the treatment of effluents containing various types of organic pollutants such as pesticides [39], herbicides [40] and dyes[41].

1.4.4 Process $UV/H_2O_2/O_3$

The addition of H_2O_2 to the process UV/O_3 accelerates the decomposition of ozone resulting in an increase of the concentration of hydroxyl radicals. This process $UV/H_2O_2/O_3$ allows a considerable reduction of carbon and rapid mineralization for

pollutants. This is the most efficient process for highly polluted effluents. This process is the combination of the two systems UV/H_2O_2 and UV/O_3. The global equation of this process UV/H_2O_2/O_3 is [Eq. (I.29)] :

$$2O_3 + H_2O_2 + h\upsilon \rightarrow 2OH^{\cdot} + 3O_2 \qquad \textbf{(I.29)}$$

The degradation of salicylic acid by different processes has been studied by Mandavgane et al. [42]: photoperoxone (UV/H_2O_2/O_3), photofenton (UV/Fe^{2+}/H_2O_2) photoperoxydation (UV/H_2O_2) and photolysis (UV). They found that using the process UV/H_2O_2/O_3 the degradation is faster.

1.4.5 Photo-Fenton process (UV/Fe^{2+}/H_2O_2)

The photo-Fenton process relies on the Fenton reaction between H_2O_2 (oxidizing agent) and Fe^{2+} (catalyst) (Eq. 45) coupled with irradiation UV/visible to increase the rate of free radicals production by stimulating the reduction of Fe^{3+} to Fe^{2+} for the treatment of wastewater. The radiation UV/ visible increases considerably the speed of the formation of the radicals HO• by coupling the Fenton reaction (Eq. I.30) with ferric iron reduction (Eq. I.31) and photolysis of hydrogen peroxide (Eq. I.32), but its contribution to the photo-Fenton method is negligible because H_2O_2 absorbs little of these radiations.

$$H_2O_2 + Fe^{2+} + H^+ \rightarrow Fe^{3+} + H_2O + OH^{\cdot} \qquad \textbf{(I.30)}$$

$$Fe^{3+} + H_2O + h\upsilon \rightarrow Fe^{2+} + OH^{\cdot} + H^+ \qquad \textbf{(I.31)}$$

$$H_2O_2 + h\upsilon \rightarrow 2OH^{\cdot} \qquad \textbf{(I.32)}$$

The effectiveness of photo-Fenton treatment depends mainly on Fe^{3+} and H_2O_2 ion concentrations and obviously the light intensity. The higher the concentration of Fe^{2+} and/or H_2O_2, the higher the amount of HO· produced [43].

In fact, the reaction limiting step during the catalytic action of iron in the Fenton process (without irradiation) is the reduction of Fe^{3+}. Thus, the irradiation allows the regeneration of ferrous ions (Fe^{2+}) by photoreduction of ferric ions (Fe^{3+}) without consuming hydrogen peroxide, while forming an additional hydroxyl radical [44].

The researchers studied the photo-Fenton process in the atmosphere to clarify the natural mechanisms of the production of hydroxyl radical HO· [45]. This photo-fenton process occurs naturally in the atmosphere. Indeed, water droplets contain hydrogen peroxide and iron ions which are a source of HO· radicals, especially under solar irradiation by photo-Fenton reaction. The major disadvantage of the photo-Fenton process is the need to work at low pH values. An optimal value was frequently found at pH 2.8 [46, 47]. In fact, at this pH the precipitation has not yet taken place and the dominant species of iron in solution is $[Fe(OH)]^{2+}$. Beyond the pH values between 3.0 and 5.0, iron (Fe^{2+} and Fe^{3+}) is susceptible to precipitate and form iron hydroxides, inducing to a low catalytic activity.

1.5 Photocatalysis: definition, areas of application and advantages:

Photocatalysis is a natural phenomenon in which a substance, the photocatalyst, initiates a chemical reaction due to the action of light, without degrading itself.

Its principle is simple: it lies in the decomposition and degradation of the material under the action of light rays mainly ultraviolet. Oxidation and reduction reactions can occur between photoexcited species and absorbed chemical substances.

Photocatalysis is particularly noteworthy in the depollution of our environment. The pollutants are destroyed when in contact with a catalyst, usually titanium dioxide TiO_2, activated by the ultraviolet rays of the sun or artificial lighting. Titanium dioxide is an inert compound used as a pigment in paints and cosmetics. It remains the raw material chosen by most manufacturers. Titanium dioxide, an inert compound used as a pigment in paints and cosmetics, remains the raw material chosen by most of industrialists. It participates in the oxidation-reduction reaction but it's not consumed. As long as it is in contact with light and pollutants, this raw material remains stable and effective. The titanium dioxide particles therefore act for a very long time. The surface of the catalyst must be the largest possible to promote the absorption of photons. The speed, at which the reactions take place, therefore depends on the intensity of the light, the amount of titanium dioxide used, the contact surface, the contact time between the TiO_2 and the polluting molecules present.

The photoactivity of titanium dioxide was described for the first time in 1921 by Carl

Renz [48] where he discussed the change of color of irradiated TiO_2 by natural light in the presence of organic compounds. A few years later, in 1929,Keidel [49] observed the decomposition of certain additives in paints in the presence of illuminated TiO_2. The oxidation of CO on irradiated ZnO was studied for the first time by Doerffler and Hauffe in 1964 [50].

Photocatalysis has several applications in the field of the environment: water treatment and air purification, such as the elimination of odors [51, 52-57], the removal of atmospheric nitrogen oxides (NO_x) that cause acid rain [58, 59], application in self-cleaning coatings of surfaces (glass, metals, concretes, cements, etc.) [60-63]. Photocatalysis is also used for the production of hydrogen [64], the synthesis of organic compounds [65] and cancer treatment [66-69].

Photocatalysis has several advantages which we quote:

- ✓ Nontoxic used catalyst, active in different physical forms, cheap
- ✓ It works at ambient temperature and pressure
- ✓ It is effective for low concentrations of pollutants
- ✓ Total mineralization is possible : formation of H_2O and CO_2 and other species
- ✓ It requires only low energy consumption.

1.6 Heterogeneous photocatalysis

1.6.1 Introduction

Heterogeneous photocatalysis is a catalytic process based on the excitation of a semiconductor by light radiation leading to the acceleration of photoreactions involving reactions between the electron/hole pairs and the organic products and/or water molecules adsorbed on the surface of a semiconductor.

The process of heterogeneous photocatalysis can be divided into 5 independent steps like any heterogeneous catalysis process [70]:

1 - Transfer of the reagent (s) from the fluid phase to the catalyst surface

2 - Adsorption of at least one reagent

3 - Reactions in adsorbed phase

4.- Desorption of intermediate and / or final products

5 - Transfer of these products from the surface region into the fluid phase.

1.6.2 Principle :

The principle of heterogeneous photocatalysis is based on the excitation of a semiconductor (usually titanium dioxide) by a radiation of energy higher than or equal to the semiconductor bandgap (3.2 eV for the TiO_2 in anatase form). So, photons having wavelengths λ <388 nm (E> 3.2 eV), excite electrons from the valence band (VB) to the conduction band (CB) thereby creating electron-hole pairs (e^--h^+) [71]:

$$\mathbf{TiO_2 + h\upsilon \rightarrow TiO_2\,(e_{BC}^- + h_{BV}^+)} \qquad \textbf{(I.33)}$$

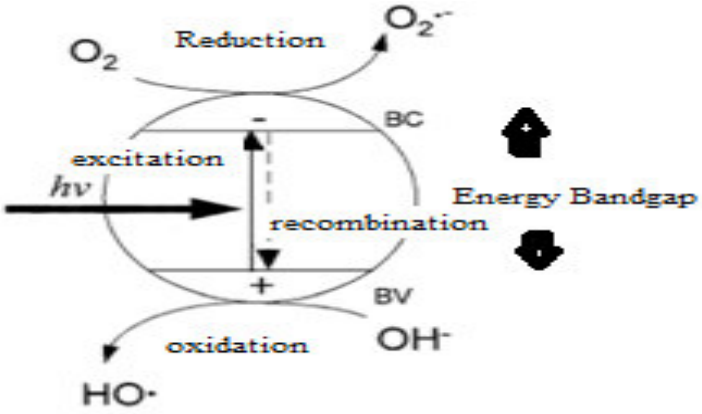

Figure I.3: Representation of the heterogeneous photocatalysis process in a TiO_2 particle

When a semiconductor (SC) absorbs photons of energy greater than the value of its bandgap (hυ>Eg), an electron is promoted from the valence band to the conduction band, creating an oxidative site (hole h^+) and a reductive site (electron e^-) [Eq. I.34].

$$\mathbf{SC + h\upsilon \rightarrow h^+ + e^-} \qquad \textbf{(I.34)}$$

The holes h^+ react with the donors of electrons such as H_2O, the anions OH^- and the organic products R adsorbed on the surface of the semiconductor forming OH• or

organic radicals [Eq. I.35-37].

$$H_2O_{ads} + h^+ \rightarrow H^+ + OH_{ads}^{\cdot} \quad \textbf{(I.35)}$$

$$OH_{ads}^{-} + h^+ \rightarrow OH_{ads}^{\cdot} \quad \textbf{(I.36)}$$

$$R_{ads} + h^+ \rightarrow R_{ads}^{\bullet +} \quad \textbf{(I.37)}$$

Electrons react with electron acceptors such as O_2 to form superoxide radicals $O_2^{\bullet}$- and thereafter H_2O_2 [Eq. I.38-40].

$$O_2 + e^- \rightarrow O_2^{\bullet -} \quad \textbf{(I.38)}$$

$$O_2^{\bullet -} + e^- + 2H^+ \rightarrow H_2O_2 \quad \textbf{(I.39)}$$

$$O_2^{\bullet -} + 2H^+ \rightarrow HOO^{\bullet} \quad \textbf{(I.40)}$$

1.6.3. The photocatalyst TiO_2 :

Titanium dioxide exists under eight crystalline forms: rutile [72], anatase [73,74], brookite [75], TiO_2(B) [76,77], hollandite (TiO_2(H)) [78], ramsdellite (TiO_2(R)) [79], and the phases of high pressure: columbite (type α-PbO_2 or TiO_2-II) [80,81], and baddeleyite (ZrO_2 type or TiO_2-III). Three of these crystalline forms adopt a stable structure: anatase (quadratic), rutile (quadratic) and brookite (orthorhombic). Two of these forms have demonstrated photocatalytic activity, anatase and rutile.

In both crystal structures (rutile and anatase), the titanium atoms are surrounded by six oxygen atoms and each oxygen atom is surrounded by three titanium atoms. In the case of rutile, Ti^{4+} cations occupy the vertices and the center of the parallelepiped with a square base. Each cation is then surrounded by 6 anions O^{2-}. Anatase is a tetrahedral structure elongated with irregular oxygen octahedra [Figure I.4].

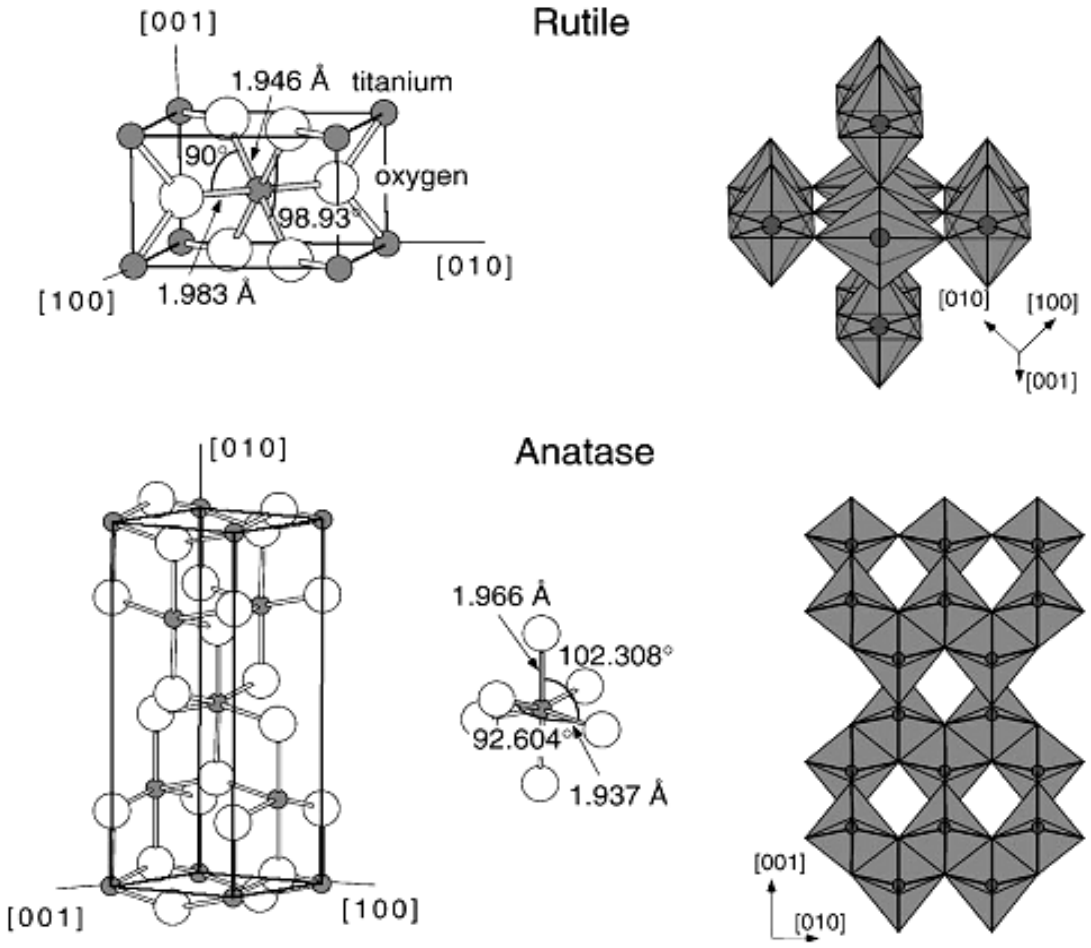

Figure I.4: Structure of anatase and rutile TiO_2 [82]

The anatase has a band gap energy Eg of 3.2 eV corresponding to an activation by photons of wavelength lower than 388 nm. The rutile Eg is 3.0 eV corresponding to an activation by photons having a wavelength less than 414 nm [83]. The anatase has been shown to be the most active form of TiO_2 [84].

The photocatalytic degradation of organic molecules can take place according to two different mechanisms:

(i) Direct reaction of the adsorbed molecule with the e-/h+ pair by a redox reaction (eg. photosensitization).

(ii) Reaction of the molecule with a radical or a reactive oxygenated species (ROS) formed during the reaction of water and oxygen adsorbed with the e^-/h^+ pair.

1.6.4 The photocatalyst ZrO_2

Zirconium oxide, called zirconia (ZrO_2), is a ceramic material that exists mainly under three stable crystalline structures at different temperatures.

Phase	Temperature range	Density (g/cm3)
Monoclinic	T < 1205 °C	5.56
Tetragonal	1075 °C< T < 2377 °C	6.1
Cubic	T > 2377 °C	5.83

Table I-2: Data on the 3 stable phases of zirconia (ZrO_2).

The cubic phase of ZrO_2 crystallizes in a face-centered cubic lattice of CaF_2 type with each Zr^{4+} cation in coordination and the oxygen ions arranged in two equal tetrahedrons. The tetragonal phase of ZrO_2 is a cubic centered face structure, derived from the cubic structure of fluorite by the movement of the oxygen anions following one of the cubic axes. The monoclinic ZrO_2 structure can be described as a distortion of the CaF_2 cubic structure.

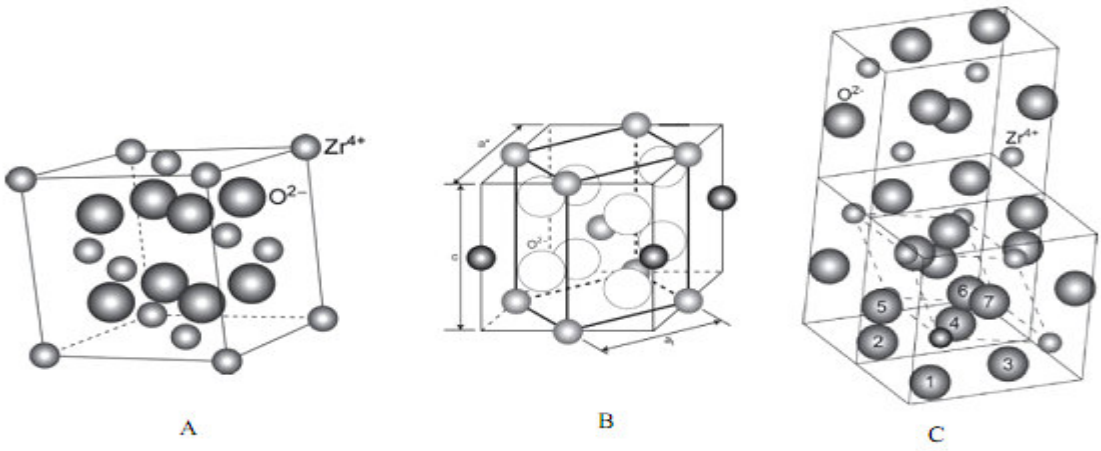

Figure I-5: ZrO_2 mesh structures(A : cubic, B : tetragonal, C : monoclinic).

The fields of application of zirconia (ZrO_2) are very diverse, since zirconia (ZrO_2) is of great interest in the aeronautical, nuclear and also in the field of microelectronics. The zirconia (ZrO_2) powder serves for example as catalyst or catalyst support. Zirconia

(ZrO_2) is also used as an element in fuel cells [85] or as a thermal barrier for high temperature materials [86].

Zirconia (ZrO_2) has a large band gap (Eg> 5 eV) [87-89]. Monoclinic zirconia (ZrO_2), at low pressures, has an n-type character, whereas at higher pressures it has a p-type character.

The determination of the mechanical properties of tetragonal and pure cubic zirconia (ZrO_2) is extremely difficult because of the very high temperatures for such measurements. Therefore, only monoclinic zirconia (ZrO_2) has been completely studied in its pure form. The Young's module of zirconia (ZrO_2) monoclinic structure is around 150 - 200 GPa [90,91], while that of tetragonal zirconia (ZrO_2) is higher, 220 GPa (undoped, nanocrystalline) [90]. The Young's module of cubic zirconia (ZrO_2) is between 171 and 288 GPa [91]. The hardness of zirconia (ZrO_2) is about 9.2 GPa for monoclinic samples with density > 98% [92].

1.6.5 The photocatalyst ZnO

Zinc oxide is a chemical compound of formula ZnO. It is in the solid state in the form of an odorless powder of off-white to light yellow color. As an oxide, it has certain advantages such as being neither combustible nor explosive in case of fire, or to be relatively inert to the human organism. It is insoluble in water but soluble in acids, bases, and alcohols. Its melting temperature is 2248K, its density is 5675 kg.m-3, his enthalpy of formation is 6,5.105 J.mol-1 and its module of shear is equal to 44 GPa.

1.6.5.1. Structural properties

Zinc oxide, known as zincite in the natural state, is a II-VI semiconductor. Its structure can be:

- Würtzite (hexagonal). This structure is the most stable thermodynamically at room temperature.
- Blende (cubic)
- Rocksalt (NaCl structure). This structure is obtained when a hydrostatic

pressure between 10 to 15 GPa is applied to the Würtzite structure.

Figure I.6 shows the three crystallographic phases of ZnO.

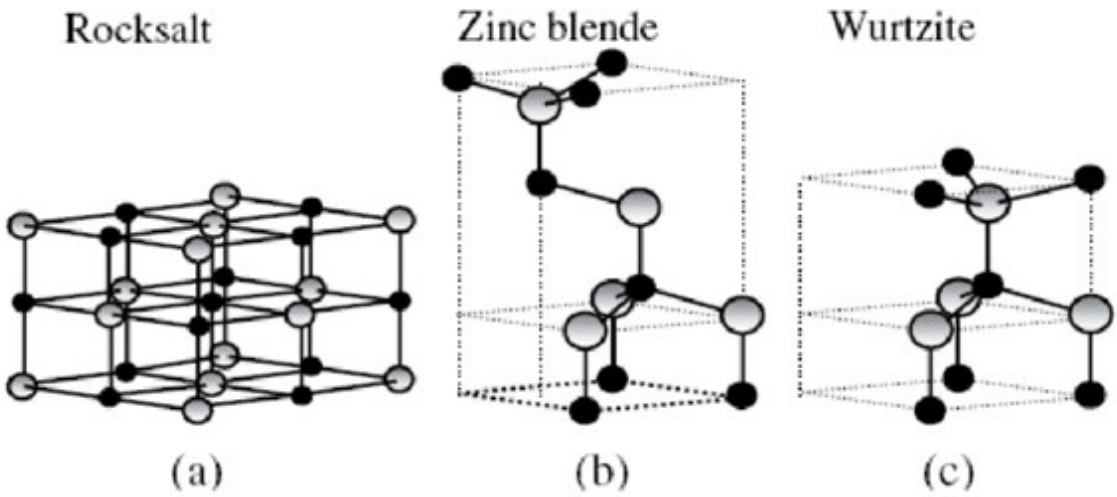

Figure I.6 : Representation of ZnO structures: (a) cubic rocksalt, (b) cubic zinc blende and (c) hexagonal würzite [93].

This specificity is linked to the mixed nature of the bonds within the crystal. In fact, the difference in electronegativity between the oxygen and zinc atoms is close to 1.79, placing the ZnO on the border between covalent polar semiconductor and ionic semiconductor. Nevertheless, the würtzite form is widely favored under normal conditions of temperature and pressure, and the blende phases of zinc and rocksalt have until now been able to be synthesized only under very specific experimental conditions [94].

Most ZnO crystals crystallize in the würtzite structure. This structure consists of an interpenetration of separated hexagonal meshes along the C axis by the *u* coordinate (translation coefficient) defined by: $u = 1/4 + c^2/3a^2$.

Each zinc atom is surrounded by four oxygen atoms and vice versa, giving a 4:4 coordinate. Figure I.7 shows the distribution of the atoms Zn and O to form the Würtzite crystallographic structure of ZnO:

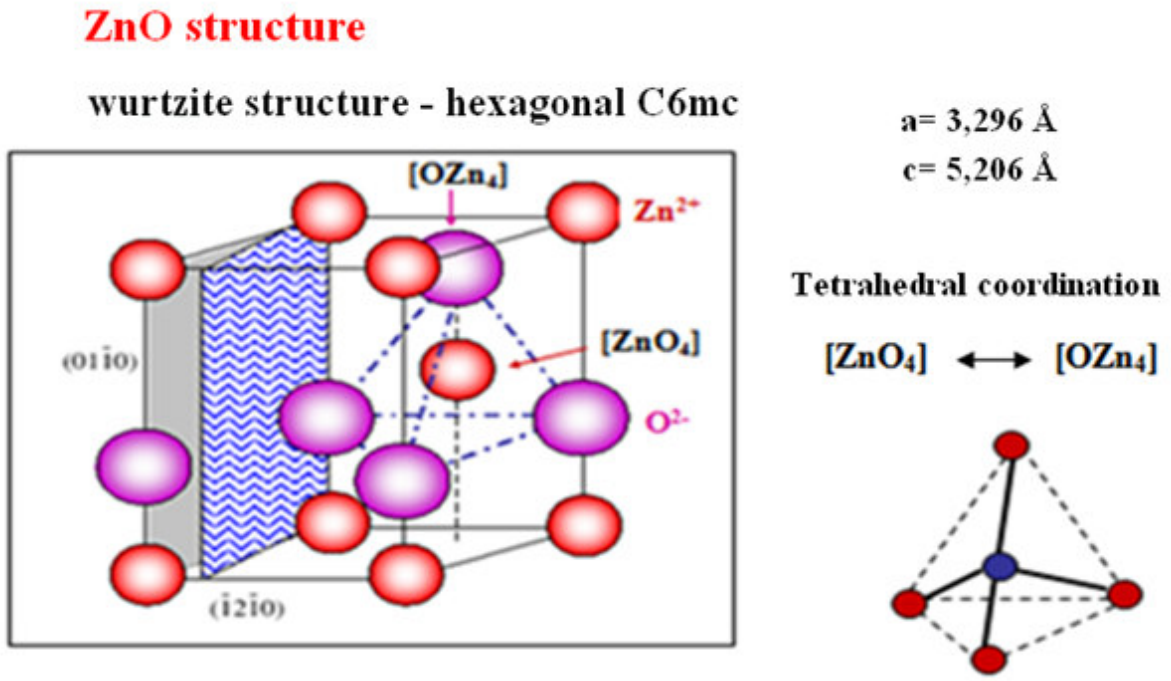

Figure I.7 : Crystal structure of ZnO (Würtzite) [95].

1.6.5.2. The characteristics of ZnO

Zinc oxide (ZnO) found in nature, Zincite, usually crystallizes in the hexagonal phase (würtzite). However it can be synthesized in the cubic phase (blende) when it is deposited on some substrates of cubic symmetry. The application of a high hydrostatic pressure to the ZnO of würtzite structure, transforms it into phase rocksalt which is metastable [96].

From the point of view of applications, ZnO is particularly interesting because it is transparent to visible light. The combination of its optical and magnetic properties of the transition metals used as doping elements, gives it magneto-optical properties.

1.6.5.3. Electrical properties of ZnO:

Zinc oxide is a semiconductor with a large direct bandgap equal to 3.4 eV at room temperature [97,98]. ZnO has a natural electrical conductivity of type n which is due to the presence of zinc atoms in interstitial position [99] and the oxygen vacancies in the ZnO matrix. The energy value of the bandgap can be modified by doping zinc oxide [100, 101].

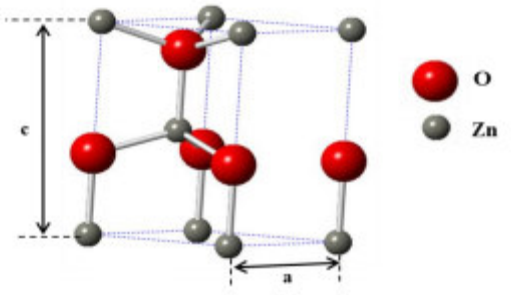

Figure I.8: Elementary mesh of the structure

1.6.5.4. Optical properties and luminescence

Zinc oxide has a high absorption of ultraviolet radiation. Under the action of photons whose energy E is higher than 3.4 eV, zinc oxide emits photons. This phenomenon corresponds to luminescence. In function of conditions of elaboration and ulterior treatments of the solid, different photoluminescence bands are observed. They go from the near UV (λ =350 nm), to visible (green color emission close to λ =550 nm).

1.6.5.5. Catalytic properties of ZnO

Zinc oxide also has catalytic properties, especially for oxidation and dehydrogenation reactions. For example, can be mentioned the oxidation of oxygen to ozone, the oxidation of ammonia to nitrate, the synthesis of hydrogen peroxide [102] and also the oxidation of phenols [103]. These catalytic properties depend essentially on the degree of perfection of its crystal lattice, which acts on its surface energy, and on semiconductor doping [104].

1.6.5.6. ZnO application in photocatalysis

The effect of a light radiation of energy higher than that of the width of the bandgap of the zinc oxide, causes the ejection of an electron from the valence band (VB) towards the conduction band (CB). It is generally accepted that the free electron is captured by oxygen, which leads to the formation of superoxide ions then, after protonation and dismutation, to hydrogen peroxide [105]. The positive hole created by the ejection of an electron can react with water, producing hydroxyl radicals. These radicals react with most aromatic compounds adsorbed on the surface of the solid [107-110].

Reaction mechanism of photocatalysis in the presence of ZnO in aqueous suspension

$$ZnO + h\upsilon \rightarrow e^- + h^+ \quad \textbf{(I.41)}$$

$$H_2O + h^+ \rightarrow OH^\bullet + H^+ \quad \textbf{(I.42)}$$

$$O_2 + e^- \rightarrow O_2^{\bullet -} \quad \textbf{(I.43)}$$

$$O_2^{\bullet -} + H^+ \rightarrow HO_2^\bullet \quad \textbf{(I.44)}$$

$$HO_2^\bullet + O_2^{\bullet -} \rightarrow HO_2^- + O_2 \quad \textbf{(I.45)}$$

$$HO_2^- + H^+ \leftrightarrow H_2O_2 \quad \textbf{(I.46)}$$

$$H_2O_2 + e^- \rightarrow + OH^\cdot + OH^- \quad \textbf{(I.47)}$$

$$H_2O_2 + O_2^{\bullet -} \rightarrow OH^\cdot + OH^- + O_2 \quad \textbf{(I.48)}$$

The creation of an electron-hole pair is at the origin of the photocatalytic activity of the semiconductor. If the photo-created charges recombine rapidly, the catalytic activity decreases. Indirect photo transformation often involves hydroxyl radicals, which are able to oxidize most organic compounds.

1.6.6 The photocatalyst WO_3

There are several crystallographic structures of tungsten oxide (WO_3) which derive by distortions of the cubic structure of rhenium oxide ReO_3. Each of these structures is described as a three-dimensional lattice (figure I.9) of WO_6 octahedron (figure I.10)connected by the vertices sharing their apical oxygen O_1 and their plane oxygen O_2, each tungsten having six neighboring oxygen.

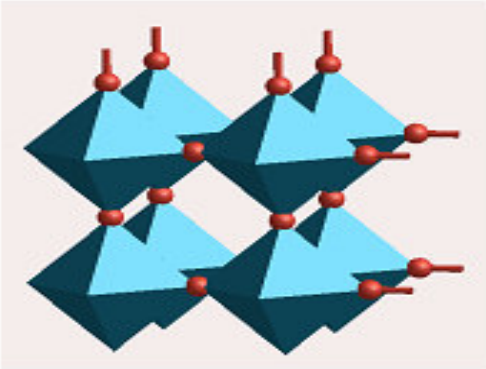

Figure I.9: Representation of a three-dimensional lattice WO_3

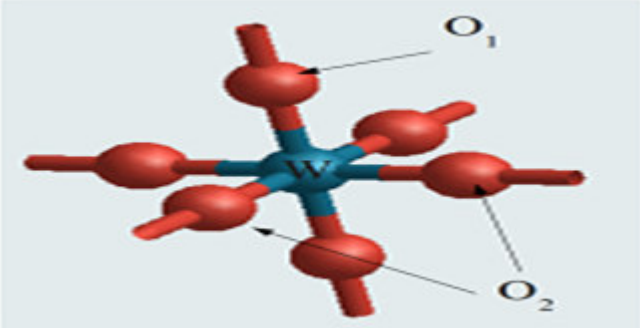

Figure I.10 : Regular octahedron WO_6: tungsten is in blue; the oxygens are in red (we note O_1 the apical oxygen and O_2 the plane oxygen)

According to the arrangement of octahedron, we obtain the phases presented in Table I.3: they are stable in well-defined temperature range.

Phase	Symmetry	Temperature range	Reference
h -WO_3	Hexagonal	Metastable	[111,112]
α - WO_3	Tetragonal	≥ 720 °C	[113]
β - WO_3	Orthorhombic	de 320 °C à 720 °C	[113]
γ - WO_3	Monoclinic	de 17 °C à 320 °C	[114]
δ - WO_3	Triclinic	de 40 °C à 17 °C	[114]
ε - WO_3	Monoclinic	≤ 40 °C	[114]

Table I.3: The different phases of WO_3 and their temperature stability range

Commercial tungsten trioxide, with a monoclinic structure, is stable in a temperature range of 17 ºC to 320 ºC. This structure is close to the cubic structure WO_3: we are talking about the pseudo cubic approximation. The hexagonal structure WO_3 is metastable: A particular synthesis is necessary to obtain it. This structure is still poorly known. Several models have been proposed in the literature without distortions [111] or with distortions [112] of octahedrons.

1.7 Factors influencing heterogeneous photocatalysis

The main factors influencing heterogeneous photocatalysis are :

- The pH
- The temperature
- The catalyst concentration
- The initial pollutant concentration
- The catalyst crystalline structure
- Surface area and particle size
- The luminous flux
- The wavelength

1.7.1 pH influence

The surface of the catalyst can be charged positively, negatively or neutrally depending on the pH of the solution. Indeed, the pH for which the surface charge of a catalyst is zero, is called Point of zero charge (pH_{PZC}) or isoelectric point (IEP). It is about 6.5 for the TiO_2 P25 which is the most used TiO_2 in experimental photocatalysis. Below and above this pH, the surface of the oxide is charged. In an aqueous medium and at acidic pH, the surface of TiO_2 is positively charged ($TiOH^{2+}$) which promotes the adsorption of the anions by electrostatic attraction. While in basic medium, the surface is negatively charged (TiO^-) and attracts the cations.

$pH < 6,5$ $\quad TiOH^{2+} \rightarrow TiOH + H^+$ $\quad$ (I.49) $\quad pK\ TiOH^{2+} = 2,4$ [115]

$pH > 6,5$ $\quad TiOH \rightarrow TiO^- + H^+$ $\quad$ (I.50) $\quad pKTiOH = 8$ [115]

The influence of pH on the size of TiO_2 particles in aqueous suspension is shown in Figure I.11.

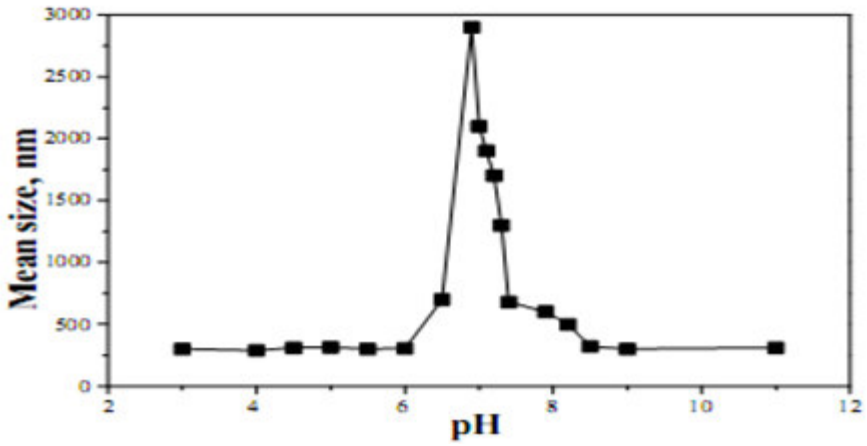

Figure I.11: Mean particle size of TiO_2 (P25) suspended in water versus pH. [TiO_2]=0.2g/L [116]

When the pH approaches pH_{PZC} (6.5), the surface charge of the oxide disappears. There is therefore much less electrostatic interaction between particles, which promotes the phenomenon of aggregation and formation of TiO_2 clusters [117].

1.7.2 Influence of temperature

The photocatalytic system doesn't need the input of heat, because it is a photonic activated process. The majority of the photo-reactions aren't sensitive to small temperature variations. The decrease in temperature favors adsorption which is a spontaneously exothermic phenomenon. On the contrary, when the temperature rises above 80°, the exothermic adsorption of the pollutants is disadvantaged.

1.7.3 Influence of catalyst concentration

In a photo reactor, the initial reaction rate is directly proportional to the mass of catalyst. This indicates that the catalytic system is really heterogeneous. However, above a certain limit of value of the mass, the reaction rate become independent of the mass of the catalyst. At high catalyst concentration, there will be an increase in opacity, which masks a part of the photosensitive surface; the light hardly reaches the reactor core, and therefore this affects the photocatalytic yield of the reaction.

1.7.4 Influence of the concentration of the pollutant

For a low pollutant concentration, the expression of the photo-mineralization rate of organic pollutants follows the Langmuir-Hinshelwood (L-H) law [118].

Four cases are possible:

- The reaction takes place between two adsorbed substances: the radical and the pollutant;

- The reaction occurs between a radical in solution and the adsorbed pollutant;

- The reaction occurs between a radical of the surface and the pollutant in solution;

- The reaction occurs between the two species in solution.

In all cases, the expression of the equation is similar to the L-H model. For kinetic studies only, it is not possible to determine if the process occurs on the surface of the catalyst or in solution. Although the L-H isotherm was quickly used in modeling, it is generally accepted that the rate constant and its order are « apparent ». They are used to describe the rate of degradation, and can be used to optimize a reactor, but they have no physical mean, and can't be used to identify surface reactions [119**].**

1.7.5 Influence of the crystalline structure

The photocatalytic yield of the catalyst TiO_2 varies considerably depending on its crystalline structure: anatase, rutile, and brookite. The brookite is not stable enough to be used in photocatalysis. The crystalline structure of rutile is denser, its bandgap is 3.0 eV, while that of anatase is 3.2 eV. The absorbed photons therefore have a wavelength of less than 414 nm for rutile and 388 nm for anatase.

Studies comparing the photocatalytic activity of anatase and rutile has shown that the recombination rate of e-/h+ pairs is higher for rutile than for anatase [120] which limits the formation of radicals and then slows down the degradation of pollutants.

Anatase is considered the most photoactive form, while rutile is considered to have low photocatalytic activity. However, a mixture of anatase (80%) and rutile (20%) which is known under the name of P25, gives a greater photoactivity than each form used alone [100]. The combination between these two crystalline forms is suggested to

decrease the recombination of photogenerated pairs and thus allow a better activity than the anatase used alone [121].

1.7.6 Influence of specific surface area and particle size

The decrease in particle size, which is inversely proportional to its specific surface and which has a paramount importance in the photocatalytic yield, is suggested increase the probability of recombination of e^-/h^+ pairs [122].

1.7.7 Influence of luminous flux

The interest for solar technologies allowing the depollution has steadily increased [123]. The use of a solar system for the treatment of water is very advantageous because the order of the rate of degradation is little influenced by the light intensity. Several authors [70, 124] have shown that photocatalytic degradation is proportional to light flux, which confirms the photo-induced character of the activation of the catalytic process. Some experiments have shown that above a certain photonic flux, the influence of the intensity on the reaction rate decreases from order 1 to order 0.5 [125, 126]. For an n-type semiconductor, such as titanium dioxide [127], photo induced holes are less numerous than electrons: $[h^+] << [e^-]$. Holes are therefore limiting active species.

Currently, this phenomenon appears more frequently in work with a supported catalyst, and/or when the stirring is weak, which implies a smaller surface in contact with the solution. The intensity at which the change of order occurs is different according to the experimental conditions of the system [128].

Indeed, for a luminous flux lower than $20 mW \cdot cm^{-2}$, the reaction rate is proportional to the luminous flux (I) (order 1) ($r = k I$), then varies according to 0.5 ($r = k I^{0.5}$), indicating that a high value of luminous flux produces an increase in the recombination rate of electron-hole pairs. At high intensities, the reaction rate does not depend on the light intensity ($r = k I^{0.0}$) [Figure I.12].

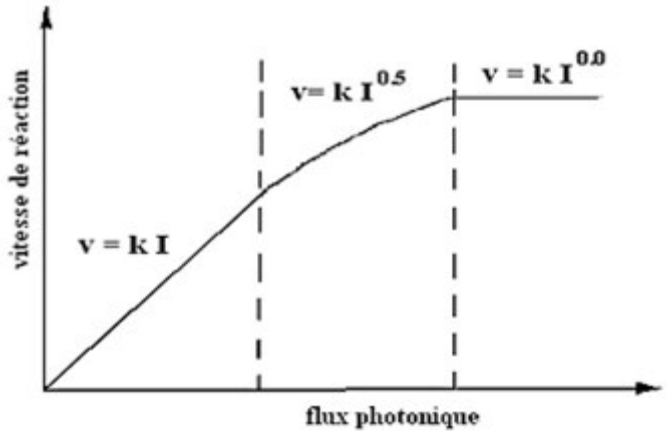

Figure I.12: Influence of the photon flux on the kinetics of photocatalytic degradation [70]

1.7.8 Influence of the wavelength

The variation of the reaction rate in terms of the wavelength follows the absorption spectrum of the catalyst, with a threshold corresponding to its bandgap energy. TiO2, having a band energy of 3.2 eV, absorbs in the near UV (λ <388 nm). It is therefore possible to use sunlight as a source of energy for the degradation of organic pollutants, but this leads to low energy efficiency since only 5% of the solar spectrum is used [129]. In addition, it must be verified that the reagents do not absorb at this wavelength in order to preserve the exclusive photoactivation of the catalyst for a true heterogeneous catalytic regime [130].

2. Pesticides

2.1 definition

Various anthropogenic activities generate wastewater, which contains both organic and inorganic pollutants. Some of the common pollutants are pesticides, dyes, solvents, etc. Pesticides and herbicides are important classes of aquatic pollutants. These pollutants are usually toxic and have harmful effects on human and animal life if they are present above a certain concentration.

A pesticide is a chemical compound allowing to repel or destroy organisms considered harmful or parasitic. Pesticides make it possible to increase the yield of agricultural production, by regulating the growth of plants, reducing the loss of fruit because of their fall or by safeguarding their quality during storage or transportation [131]. But it

is essential to treat water for the removal of pollutants before it is recycled. There has been growing interest in developing effective methods of degradation of these pesticides, which include precipitation and photocatalytic degradation.

Some of these processes have such limitations as more time and high handling costs. Thus, there is an urgent need for a fast, easy to use and low cost process. Overall, photocatalytic oxidation is one of the most appropriate technologies for the removal of organic compounds [132, 133]. Photocatalytic oxidation processes have been used successfully for the elimination-degradation of pesticides from water.

2.2 Pesticide history

The 19th century knew the development of mineral chemistry by discovering several types of inorganic pesticides based on copper salt. In the fifties, insecticides such as dichlorodiphenyldichloroethane (DDD) and dichlorodiphenyltrichloroethane (DDT) were used in large quantities in preventive medicine (to destroy the mosquito responsible for malaria) and in agriculture (elimination of the Colorado beetle). These compounds are today prohibited because of their low biodegradability and bioaccumulation in the food chain. During the 20th century, the use of pesticides was very frequent, therefore a success in terms of yield and production is well noticed, hence their indispensability in most activities. Indeed, the desire to increase yields in agriculture has led to the use of more and more chemicals. Pesticide treatments appear at the end of the 20th century because of their negative impact on the environment. Currently, reducing the use of pesticides is becoming a major concern [134].

2.3 Classification of Pesticides

Pesticides are classified into several categories at the level of their use:

- Fungicides: intended to treat fungal diseases of plants, but also bacterial and viral diseases.
- Insecticides: intended for the fight against insects, they intervene by killing them or preventing their reproduction.
- Herbicides: intended to control certain plants competing with cultivated plants.

Pesticides are usually classified according to target they target (Table below):

Types of pesticides	Targets
Herbicides	to fight against "weeds"
Fungicides	to destroy fungi
Insecticides	to kill insects
Corvicides	against birds
Rodenticides	to fight against rodents
Molluscicides	against slugs
Nematicides	against nematodes (small worms)

Table I.4: Classification of pesticides according to their target.

2.4. Persistent organic pollutants (POPs)

The increasing use of pesticides has generated in recent years questions about the risks to human health. In fact, these persistent organic pollutants (POPs) or pesticides are often transformed into many metabolites that persist for years in the environment. The danger

major of these persistent products or their metabolites is their capacity to enter in the food chain. Because of their toxicity and low degradation capacity, pesticides can accumulate in the food chain and / or the environment, it is known as bioaccumulation that puts life of living organism in danger [135,136].

This type of organic pollutants is very dangerous, which requires studying them and knowing their becoming in the environment.

2.5 Fate of Persistent Organic Pollutants in the Environment:

Several scientific works have confirmed the presence of organic pollutants in the environment [137-139], especially in the aquatic environment. As soon as they arrive on the ground (Figure .1), organic pollutants begin to distribute themselves. Indeed, the manifestation of the pollutant nature of the organic compound is closely linked to their fate in the soil. This is done in different ways.

The three main routes are:

2.5.1. Degradation

The degradation of a pesticide occurs when the pesticide is broken down into small molecules and eventually in carbon dioxide and water, through photochemical, chemical and biological reactions [140, 141]. Indeed, when a pesticide is degraded, it generates several stable by-products called metabolites, each of those has its own chemical properties, sometimes more toxic than the starting material.

2.5.2. Adsorption by plants

Soil particles can play a very important role in immobilizing pesticides through adsorption.

Also, plants incorporate these pesticides and weaken their availability, and therefore stop their migration into the environment. Adsorption refers to the attachment of the pesticide by soil particles.

The adsorption rate is a function of several parameters, namely: the characteristics of the soil and the nature of the pesticide. The adsorption of a given pesticide by the soil, depends on the pH [142], which subsequently determines the chemical structure of the pesticide in the environment.

2.5.3. Drainage in deepth or on the soil surface

The displacement of the pesticides is done either by the transfer which is provoked mainly by the rain (runoff, seepage and transfer to groundwater and streams), or by the volatilization being carried away by the wind drift. Indeed, droplets smaller than 100µm in size may be transported over very long distances. They end up by being deposited by dry route or by leaching of the atmosphere by the rains. The availability and transfer of pesticides to groundwater (Figure I.13) [143] constitute serious and redoubtable problems.

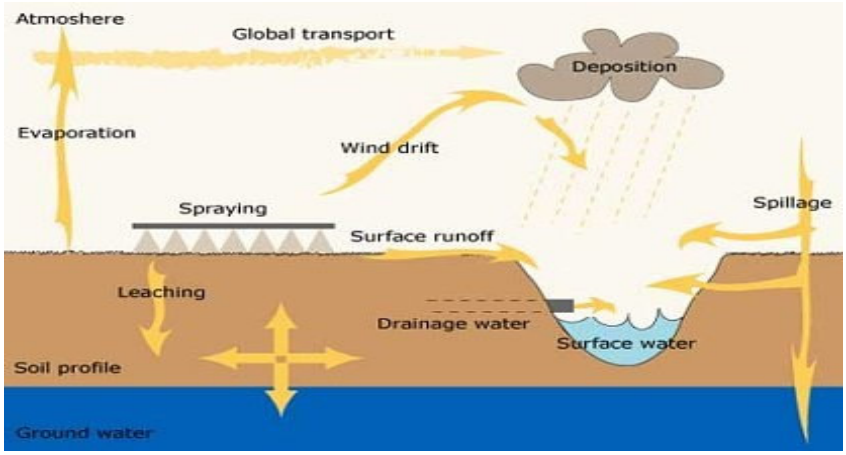

Figure I.13 : Process showing the fate of pesticides in the environment [144]

2.6. Toxicity of pesticides:

The use of pesticides has certainly led to agronomic progress, but it also represents a growing danger to the health of populations and the effects on ecosystems are difficult to evaluate and prevent. Although knowledge of short-term effects (acute toxicity) is increasing, long-term risks (chronic toxicity) remain difficult to assess.

2.6.1. Acute toxicity:

Acute toxicity is the ability of a substance to cause the harmful effects that develop rapidly after absorption, that is to say, in the short term.

2.6.2. Chronic toxicity:

Chronic toxicity is the ability of a substance to cause adverse health effects, it is a long-term manifestation. This toxicity has an impact on humans and the environment [145-147], in particular by carcinogenic, immunosuppressive, mutagenic, neurotoxic and teratogenic effects [148].

2.7. Treatment methods:

From the above, pesticides are a potential threat for water resources. Thus, this pollution primarily affects surface water where we observe contamination on all rivers. In order to protect the aquatic environment, the treatment of urban, industrial and agricultural wastewater is essential. The treatment can be achieved using different processes that are currently well controlled and applied on a large scale including physicochemical treatments, biological treatments and advanced oxidation processes

already described before.

3. Dyes:

3.1. Generality on dyes:

The use of dyes in human life dates back to ancient times. Primitive people used the paintings for body decorations. At that time, the dyestuffs used were of natural origin extracted either from plants like indigo or from animals like carmine that is extracted from cochineal. The use of these natural dyes lasted until the first half of the 19th century. Afterwards, they were gradually replaced by synthetic dyes. Today, dyes are a basic material in many industries such as textiles, leather, paper, plastics, pharmaceuticals, cosmetics, etc.

The release of dyes into the environment is a huge problem. The presence of these types of contaminants in the water is very visible and undesirable even at the trace state. Many studies have shown that the exhibition to the dyes begets negative effects on human health and the environment.

3.2. Synthetic dyes:

3.2.1. Definition:

A dye is a product that can provide color to a substance in a sustainable way. It is characterized by an assemblage of chromophore, autochromes and conjugated aromatic structures. These groups have the property of transforming white light in the visible spectrum (from 380 to 750 nm) into colored light. Chromophores are groups of atoms that contain at least one double bond and form with the rest of the molecule a conjugated sequence. These groups are responsible of the coloring of the molecule. The table (I.5) gives a list of the main chromophore groups classified by increasing intensity. Autochromes are groups of ionizable atoms able to change the adsorption frequency of a chromophore. They allow the fixation of dyes on the substance.

Chromophoric groups	Auochrome groups Electron donor groups
Azo (-N=N-) Nitro (-N=O) Carbonyl (>C=O) Vinyl (-C=CH_2) ou methine (>C=) Nitro (-NO_2) Thiocarbonyl (>C=S)	Amino (-NH_2) Methylamino (-$NHCH_3$) Dimethylamino (-$N(CH_3)_2$) Hydroxyl (-OH) Alkoxy (-OR)

Table I.5: The main chromophore groups classified by increasing intensity

3.2.2 Types of dyes:

The presence of these dyes in industrial effluents has a dangerous impact on the environment and on human health because they are stable and resistant to biodegradation.

- Azoic dyes: are characterized by the presence within the molecule of an azo group (-N = N-) connecting two benzene rings. This type of dye is widely used in the textile industry due to its resistive property to light, to acids, to bases and to oxygen [149].
- Triphenylmethane dye: it is a derivative of methane. It is composed of three phenyl rings linked to a central carbon. This hydrocarbon constitutes a basic structure in many dyes.
- Indigo Dye: This compound is considered one of the oldest known dyes with purple, which is a derivative dibromo-6,6-indigo. They are characterized by remarkable resistance to washing treatments.
- Xanthene dyes: are tricyclic organic compounds. They consist of a cycle of pyran framed by two cycles of benzene. The dyes of this family are characterized by intense fluorescence. They are used as food, cosmetic and textile dyes [150].
- Anthraquinone dyes: are derivatives of anthracene. They exist naturally in

certain plants (buckthorn, senna, aloe, rhubarb). The basic molecule of this group of dyes is anthraquinone which present the chromophore carbonyl group (> C═O) on a quinone nucleus. These products are used to coloring polyester fibers, cellulose acetate and triacetate.

- Phthalocyanines: This type of dyes is characterized by a complex structure having a central metal atom. They are mainly used in the manufacture of inks.
- Nitro and nitrosated dyes: They have a simple structure characterized by the presence of a nitro group (-NO_2) in the ortho position of an electro-donor. These nitro compounds are the basis of dispersed anionic dyes, or pigments in shades limited to yellow and brown. These dyes are less common and have a low industrial interest.

3.3. Toxicity of dyes:

The spill of effluents loaded with dyes into aquatic environments is a huge problem. Indeed, these compounds are known by their toxicity, linked mainly to their complex structures and their important molecular weights, that allow them to resist biodegradation, in addition to their accumulation.

3.4. The dye removal processes:

The intense and irrational use of dyes and the enormous risk to the quality of the environment and to human health, have been behind a number of projects aimed at eliminating these pollutants. Biological, physical and chemical processes have been developed to eradicate these dyes from aquatic environments, including heterogeneous photocatalysis using TiO_2/UV.

References:

[1] Glaze, William H., Joon-Wun Kang, and Douglas H. Chapin. "The chemistry of water treatment processes involving ozone, hydrogen peroxide and ultraviolet radiation." (1987): 335-352.

[2] La Porta, R., Lopez-de-Silanes, F., Shleifer, A., & Vishny, R. (2000). Investor protection and corporate governance. Journal of financial economics, 58(1), 3-27.

[3] Oppenländer, Thomas. Photochemical purification of water and air: advanced oxidation processes (AOPs)-principles, reaction mechanisms, reactor concepts. John Wiley & Sons, 2003.

[4] R.Andreozzi, V. Caprio, A. Insola, R. Marotta, Advanced oxidation processes (AOP) for water purification and recovery, Catalysis today 53 (1999) 51-59.

[5] Millet, M. "L'oxygène et les radicaux libres. I." Bios 23.1-2 (1992): 67-70.

[6] C.Pulgarin, N. Adler, P. Peringer, C. Comninellis, Electrochemical detoxification of a 1,4-benzoquinone solution in wastewater treatment, Water Research 28 (1994) 887-893.

[7] O.Legrini, E. Oliveros, A.M. Braun, Photochemical processes for water treatment, Chemical Reviews 93 (1993) 671-698.

[8] G.V. Buxton, C.L. Greenstock, W.P. Helman, A.B. Ross, Critical review of rate constant for reactions of hydrated electrons, hydrogen atoms and hydroxyl radicals (OH•/O-•) in aqueous solution, Journal of Physical Chemistry 17 (1988) 513-759.

[9] R.J.Scrudato , J.R. Chiarenzelli Electrochemical Preoxidation of PCBs and VOCs in Suspended Site Water and Sedmints, Presented at the pacific Basin Conference in Hazardous Waste, Kuala Lumpar (1996).

[10] Rajeshwar, Krishnan, and Jorge G. Ibanez. Environmental electrochemistry: Fundamentals and applications in pollution sensors and abatement. Academic press, 1997.

[11] Comninellis, Christos. "Electrochemical treatment of waste water containing phenol." Institution of Chemical Engineers Symposium Series. Vol. 127. No. GGEC-CHAPTER-1992-004. 1992.

[12] Poon, Calvin PC. "Electroflotation for groundwater decontamination." Journal of hazardous materials 55.1-3 (1997): 159-170.

[13] Kiwi, J., C. Pulgarin, and P. Peringer. "Effect of Fenton and photo-Fenton reactions on the degradation and biodegradability of 2 and 4-nitrophenols in water treatment." Applied Catalysis B: Environmental 3.4 (1994): 335-350.

[14] M.A. Oturan, J.J. Aaron, N. Oturan, J. Pinson, Degradation of chlorophenoxyacid herbicides in aqueous media, using a novel electrochemical method, Pesticide Science 55 (1999) 558-562.

[15] H.J.H. Fenton, Oxidation of Tartaric Acid in the Presence of Iron, J. Chem. Soc. Trans, 65 (1894) 899-910.

[16] H.J.H. Fenton, Oxidation of tartaric acid in the presence of iron, Journal of the Chemical Society 65 (1894) 899-910.

[17] F. Haber, J. Weiss, The catalytic decomposition of hydrogen peroxide by iron salt, Proceedings of the Royal Society A: Mathematical 147 (1934) 332-351.

[18] C. Walling, Fenton's Reagent Revisited, Acc. Chem. Res, 8 (1975) 125-131.

[19] J.J.Pignatello, Dark and Photoassisted Fe3+ Catalyzed Degradation of Chlorophenoxy Herbicides by Hydrogen Peroxide, Environ. Sci. Technol, 26 (1992) 944-951.

[20] C. Walling, Fenton's Reagent Revisited, Acc. Chem. Res, 8 (1975) 125-131.

[21] F.J. Rivas, S.T. Kolaczkowski, F.J. Beltrán, D.B. McLurgh, Development of a Model for the Wet Air Oxidation of Phenol Based on a Free Radical Mechanism, Chem. Eng. Sci, 53 (1998) 2575-2586.

[22] A.Sadana, J.R. Katzer, Involvement of Free Radicals in the Aqueous-Phase Catalytic Oxidation of Phenol Over Copper Oxide, J. Catal., 35 (1974) 140-152.

[23] A.Machairas, The UV/H2O2 advanced oxidation process in UV disinfection units : removal of selected phosphate esters by hydroxyl radical, Thesis, Massachusetts Institute of Technology. Dept. of Civil and Environmental Engineering (2004).

[24] Y.S. Jung, W.T. Lim, P. Joo-Yang, K. Young-Hun, Effect of pH on Fenton and Fenton-like oxidation, Environmental technology 30 (2009) 183-190.

[25] J.Staehelin, J. Hoigné, Decomposition of ozone in water: rate of initiation by hydroxide ion and hydrogen peroxide, Environmental Science & Technology 16 (1982) 676-680.

[26] R. Hernandez, M. Zappi, J. Colucci, R. Jones, Comparing the performance of various advanced oxidation processes for treatment of acetone contaminated water Journal of Hazardous Materials 92 (2002) 33-50.

[27] Kremer, M. L., and Gabriel Stein. "The catalytic decomposition of hydrogen peroxide by ferric perchlorate." Transactions of the Faraday Society 55 (1959): 959-973.

[28] Lorimer, John P., and Timothy J. Mason. "Sonochemistry. Part 1—the physical aspects." Chemical Society Reviews 16 (1987): 239-274.

[29] Hua, Inez, and Michael R. Hoffmann. "Optimization of ultrasonic irradiation as an advanced oxidation technology." Environmental Science & Technology 31.8 (1997): 2237-2243.

[30] A. Henglein, Sonochemistry-historical developments and modern aspects, Ultrasonics 25 (1987) 6-16.

[31] Ferradini, Christiane, and Jean-Paul Jay-Gerin. "La radiolyse de l'eau et des solutions aqueuses: historique et actualité." Canadian journal of chemistry 77.9 (1999): 1542-1575.

[32] Giesel, Fritz. "Ueber den Emanationskörper aus Pechblende und über Radium." European Journal of Inorganic Chemistry 36.1 (1903): 342-347.

[33] C. Ferradini, J.P. Jay-Gerin, La radiolyse de l'eau et des solutions aqueuses: historique et actualité, Canadian journal of chemistry 77 (1999) 1542-1575.

[34] Y. Tabata, Y. Ito et S. Tagawa : Handbook of Radiation Chemistry. CRC Press, Boca Raton, 1991.

[35] D. Swiatla-Wojcik, G.V. Buxton, Modeling of radiation spur processes in water at temperatures up to 300 degree, The Journal of Physical Chemistry 99 (1995) 11464-11471.

[36] CRISSOT, François. Oxydation catalytique de composés organiques en milieu aqueux par le peroxyde d'hydrogène en phase hétérogène. 1996. Thèse de doctorat. Poitiers.

[37] M. Doré, Chimie des oxydants et traitement des eaux, Tec. Doc. Lavoisier (Éditeur), Paris, France, (1989) 505.

[38] Van Craeynest, K., and H. Van Langenhove. "and RM Stuetz." Advanced oxidation processes for water and wastewater treatment (2004): 275.

[39] J. De Laat, M. Doré, H. Suty, Oxydation de S-triazines par les procédés d'oxydation radicalaire. Sous-produits de réaction et constantes cinétiques de réaction, Journal of Water Science 8 (1995) 23-42.

[40] F.J. Benitez, J. BeltrÃ¡n-Heredia, T. Gonzalez, Degradation By Ozone and UV Radiation of the Herbicide Cyanazine, Ozone: Science & Engineering 16 (1994) 213-234.

[41] H.Y. Shu, M.C. Chang, Decolorization effects of six azo dyes by O3, UV/O3 and UV/H2O2 processes, Dyes and Pigments 65 (2005) 25-31.

[42] S.A. Mandavgane, M.K.N. Yenkie, Dgradation of salicylic acid by UV, UV/ H2O2, UV/O3, photo-Fenton processes, RASlYAN Journal of Chemistry 4 (2011) 640-647.

[43] Kim, Jaheon, et al. "New cucurbituril homologues: syntheses, isolation, characterization, and X-ray crystal structures of cucurbit [n] uril (n= 5, 7, and 8)." Journal of the American Chemical Society 122.3 (2000): 540-541.

[44] F. Zaviska, P. Drogui, G. Mercier, J.-F. Blais, Procédés d'oxydation avancée dans le traitement des eaux et des effluents industriels :Application à la dégradation des polluants réfractaires, Revue des sciences de l'eau. 22 (2009) 535-564.

[45] B. Faust, J. Hoigné, Photolysis of hydroxy-complexes as sources of OH• radicals in clouds, fog and rain. , Atmospheric Environment 24A (1990) 79-89.

[46] J.J. Pignatello, Dark and photoassisted iron(3+)-catalyzed degradation of chlorophenoxy herbicides by hydrogen peroxide, Environmental Science & Technology 26 (1992) 944-951.

[47] A. Safarzadeh-Amiri , J.R. Bolton , S.R. Cater The use of iron in Advanced Oxidation Processes, J. Adv. Oxid. Techn 1 (1996) 18-26.

[48] C. Renz, Lichtreaktionen der Oxyde des Titans, Cers und der Erdsäuren., Helvetica Chimica Acta 4 (1921) 961-968.

[49] E. Keidel, Die Beeinflussung der Lichtechtheit von Teerfarblacken durch Titanweiss [Influence of titanium white on the fastness to light of coal-tar days], Farben-Zeitung 34 (1929) 1242-1243.

[50] W. Doerffler, K. Hauffe, Heterogeneous photocatalysis I. The influence of oxidizing and reducing gases on the electrical conductivity of dark and illuminated zinc oxide surfaces, Journal of Catalysis 3 (1964) 156-170.

[51] C. Guillard, T.H. Bui, C. Felix, V. Moules, B. Lina, P. Lejeune, Microbiological disinfection of water and air by photocatalysis, Comptes Rendus Chimie 11 (2008) 107-113.

[52] P. Yaron, Application of TiO2 photocatalysis for air treatment: Patents' overview, Applied Catalysis B: Environmental 99 (2010) 448-460.

[53] P. Pichat, J. Disdier, C. Hoang-Van, D. Mas, G. Goutailler, C. Gaysse, Purification/deodorization of indoor air and gaseous effluents by TiO2 photocatalysis, Catalysis today 63 (2000) 363-369.

[54] D.F. Ollis, Photocatalytic purification and remediation of contaminated air and water, Comptes Rendus de l'Académie des Sciences - Series IIC - Chemistry 3 (2000) 405-411.

[55] O. d'Hennezel, D.F. Ollis, Trichloroethylene-Promoted Photocatalytic Oxidation of Air Contaminants, Journal of Catalysis 167 (1997) 118-126.

[56] M.L. Sauer, M.A. Hale, D.F. Ollis, Heterogenous photocatalytic oxidation of dilute toluene-chlorocarbon mixtures in air, Journal of Photochemistry and photobiology A: Chemistry 88 (1995) 169-178.

[57] J. Peral, D.F. Ollis, Heterogeneous photocatalytic oxidation of gas-phase organics for air purification: Acetone, 1-butanol, butyraldehyde, formaldehyde, and m-xylene oxidation, Journal of Catalysis 136 (1992) 554-565.

[58] T. Ibusuki, K. Takeuchi, Removal of low concentration nitrogen oxides through photoassisted heterogeneous catalysis, Journal of Molecular Catalysis 88 (1994) 93-102.

[59] N. Negishi, K. Takeuchi, T. Ibusuki, Surface structure of the TiO2 thin film photocatalyst, Journal of Materials Science 33 (1998) 5789-5794.

[60] T. Yuranova, R. Mosteo, J. Bandara, D. Laub, J. Kiwi, Self-cleaning cotton textiles surfaces modified by photoactive SiO2/TiO2 coating, Journal of Molecular Catalysis A: Chemical 244 (2006) 160-167.

[61] S.S. Madaeni, N. Ghaemi, Characterization of self-cleaning RO membranes coated with TiO2 particles under UV irradiation, Journal of Membrane Science 303 (2007) 221-233.

[62] X. Ding, S. Zhou, L. Wu, G. Gu, J. Yang, Formation of supra-amphiphilic self-cleaning surface through sun-illumination of titania-based nanocomposite coatings, Surface and Coatings Technology 205 (2010) 2554-2561.

[63] Rathouský, J., Kalousek, V., Kolář, M., Jirkovský, J., & Barták, P. (2011). A study into the self-cleaning surface properties—the photocatalytic decomposition of oleic acid. Catalysis today, 161(1), 202-208.

[64] Kudo, Akihiko. "Photocatalysis and solar hydrogen production." Pure and Applied Chemistry 79.11 (2007): 1917-1927.

[65] J.S. Hubbard, J.P. Hardy, G.E. Voecks, E.E. Golub, Photocatalytic synthesis of organic compounds from CO and water: Involvement of surfaces in the formation and stabilization of products, Journal of Molecular Evolution 2 (1973) 149-166.

[66] A. Fujishima, J. Ohtsuki, T. Yamashita, S. Hayakawa, Behavior of tumor cells on photoexcited semiconductor surface, Photomed. Photobiol. 8 (1986) 45-46. .

[67] H. Sakai, R. Baba, K. Hashimoto, Y. Kubota, A. Fujishima, Selective killing of a single cancerous T24 cell with TiO2 semiconducting microelectrode under irradiation, Chem. Lett. (1995) 185-186.

[68] R. Cai, K. Hashimoto, Y. Kubota, A. Fujishima, Increment of photocatalytic killing of cancer cells using TiO2 with the aid of superoxide dismutase, Chem. Lett (1992) 427-430.

[69] D.M. Blake, P.C. Maness, Z. Huang, E.J. Wolfrum, J. Huang, W.A. Jacoby, Application of the Photocatalytic Chemistry of Titanium Dioxide to Disinfection and the Killing of Cancer Cells, Separation & Purification Reviews 28 (1999) 1-50.

[70] J.M. Herrmann, Heterogeneous photocatalysis: fundamentals and applications to the removal of various types of aqueous pollutants, Catalysis today 53 (1999) 115-129.

[71] Fujishima, Akira, Kazuhito Hashimoto, and Toshiya Watanabe. "TiO2 photocatalysis." Fundamentals and Applications, BKC Inc., Tokyo (1999): 66.

[72] Swope, R. Jeffrey, Joseph R. Smyth, and Allen C. Larson. "H in rutile-type compounds: I. Single-crystal neutron and X-ray diffraction study of H in rutile." American Mineralogist 80.5-6 (1995): 448-453.

[73] Weirich, Th E., et al. "Rietveld analysis of electron powder diffraction data from nanocrystalline anatase, TiO 2." Ultramicroscopy 81.3 (2000): 263-270.

[74] JCPDS ref. 21-1272; Nat. Bur. Stand. (US) Monogr. 25 (1969).

[75] Meagher, E. P., and George A. Lager. "Polyhedral thermal expansion in the TiO2 polymorphs; refinement of the crystal structures of rutile and brookite at high temperature." The Canadian Mineralogist 17.1 (1979): 77-85.

[76] Marchand, René, Luc Brohan, and Michel Tournoux. "TiO2 (B) a new form of titanium dioxide and the potassium octatitanate K2Ti8O17." Materials Research Bulletin 15.8 (1980): 1129-1133.

[77] Feist, Thomas P., and Peter K. Davies. "The soft chemical synthesis of TiO2 (B) from layered titanates." Journal of solid state chemistry 101.2 (1992): 275-295.

[78] Latroche, M., Brohan, L., Marchand, R., & Tournoux, M. (1989). New hollandite oxides: TiO2 (H) and K0. 06TiO2. Journal of Solid State Chemistry, 81(1), 78-82.

[79] Akimoto, J., Gotoh, Y., Oosawa, Y., Nonose, N., Kumagai, T., Aoki, K., & Takei, H. (1994). Topotactic oxidation of ramsdellite-type Li 0.5 TiO 2, a new polymorph of titanium dioxide: TiO 2 (R). Journal of Solid State Chemistry, 113(1), 27-36.

[80] N.A.Bendeliani; Geochem. Int. 3 (1966) 387.

[81] Simons, P. Y., and F. Dachille. "The structure of TiO2II, a high-pressure phase of TiO2." Acta Crystallographica 23.2 (1967): 334-336.

[82] Diebold, Ulrike. "The surface science of titanium dioxide." Surface science reports 48.5 (2003): 53-229.

[83] le Roux, Herman, and Leslie Glasser. "Transferable potentials for the Ti–O system." Journal of Materials Chemistry 7.5 (1997): 843-851.

[84] A. Sclafani, J.M. Herrmann, Comparison of the Photoelectronic and Photocatalytic Activities of Various Anatase and Rutile Forms of Titania in Pure Liquid Organic Phases and in Aqueous Solutions, The Journal of Physical Chemistry 100 (1996) 13655-13661.

[85] Gorte, Raymond J., and John M. Vohs. "Novel SOFC anodes for the direct electrochemical oxidation of hydrocarbons." Journal of catalysis 216.1 (2003): 477-486.

[86] Chen, Zhe. Relation microstructure et propriété mécanique des films de ZrO2 obtenus par MOCVD. Diss. Paris 11, 2011.

[87] C.Zhao, G.Roebben, H.Bender, T.Young, S.Haukka, M.Houssa, M.Naili, S.De Gendt, M.Heyns, O.Van Der Biest, Microelectronics Reliability. 41 (2001) 995.

[88] T.Ngai, W.J.Qi, R.Sharma, J.Fretwell, X.Chen, JC.Lee, S.Banerjee, Appl. Phys. Lett. 76 (2000) 502.

[89] M.Morita, H.Fukumoto, T.Imura, Y.Osaka, M.Ichihara, J. Appl. Phys. 58 (1985) 2407 12,13,14.

[90] Bernard, Olivier, et al. "Synthesis, structure, microstructure and mechanical characteristics of MOCVD deposited zirconia films." Applied Surface Science 253.10 (2007): 4626-4640.

[91] Shackelford, James F., and Robert H. Doremus. "Ceramic and glass materials." Structure, properties and processing. Springer (2008).

[92] Bravo-Leon, Alfonso, et al. "Fracture toughness of nanocrystalline tetragonal zirconia with low yttria content." Acta Materialia 50.18 (2002): 4555-4562.

[93] PATRA, Saroj Kumar. A novel chemical approach to fabricate ZnO Nanostructure. 2008. Thèse de doctorat. PhD thesis, Indian Institute of Technology Kharagpur.

[94] U. Özgür, Y. I. Alivov, C. Liu, A. Teke, M. A. Reshchikov, S. Doğan, V. Avrutin, S.-J. Cho, and H. Morkoç, "A comprehensive review of ZnO materials and devices," Journal of Applied Physics, vol. 98, p. 041301, Aug. 2005.

[95] WANG, Zhong Lin. ZnO nanowire and nanobelt platform for nanotechnology. Materials Science and Engineering: R: Reports, 2009, vol. 64, no 3-4, p. 33-71.

[96] B. Amrani, I. Chiboub , S. Hiadsi , T. Benmessabih , N. Hamdadou, "Structural and electronic properties of ZnO under high pressures", Solid State Communications 137 (2006) 395–399.

[97] J. Joussot-Dubien, NouveauTraité de ChimieMinérale, vol. V, Masson & Cie. Paris(1962).

[98] Z. Y. Xiao, Y. C. Liu, D. X. Zhao, J. Y. Zhang, Y. M. Lu, D. Z. Shen, X. W. Fan, J. Luminescence, 34 (2007) 122.

[99] S. J. Chen, Y. C. Liu, H. Jiang, Y. M. Lu, J. Y. Zhang, D. Z. Shen, X. W. Fan, J. Crystal Growth, 285 (2005) 24.

[100] G. C. Bond, Heterogeneous catalysis, Principale and Applications",second edition (Oxford) (1987).

[101] Davidson, J. Michael, Catriona H. Lawrie, and Khalid Sohail. "Kinetics of the absorption of hydrogen sulfide by high purity and doped high surface area zinc oxide." Industrial & Engineering Chemistry Research 34.9 (1995): 2981-2989.

[102] Berger, H., H. Tang, and F. Lévy. "Growth and Raman spectroscopic characterization of TiO2 anatase single crystals." Journal of crystal growth 130.1-2 (1993): 108-112.

[103] Castaneda, L., Alonso, J. C., Ortiz, A., Andrade, E., Saniger, J. M., & Banuelos, J. G. (2003). Spray pyrolysis deposition and characterization of titanium oxide thin films.Materials Chemistry and Physics, 77(3), 938-944.

[104] Fujishima, Akira, and Kenichi Honda. "Electrochemical photolysis of water at a semiconductor electrode." nature 238.5358 (1972): 37-38.

[105] Sehili, Tahar, Gisèle Bonhomme, and Jacques Lemaire. "Transformation des composes aromatiques chlores photocatalysee par de l'oxyde de zinc I-Comportement du chloro-3 phenol." Chemosphere 17.11 (1988): 2207-2218.

[106] Fujihira, Masamichi, Yoshiharu Satoh, and Tetsuo Osa. "Heterogeneous photocatalytic reactions on semiconductor materials. III. Effect of pH and Cu2+ ions on the photo-Fenton type reaction." Bulletin of the Chemical Society of Japan 55.3 (1982): 666-671.

[107] W. Klopffer, G. Kaufmann, R. Frank, Z. Naturforsch, Teil A, Nature, 40 (1985) 686.

[108] G. V. Buxton, C. L. Greenstock, W. P. Helman, A. B. Ross, J. Phys. Chem. Ref. Data, 17 (1988) 513.

[109] Cunningham, Joseph, and Somkiat Srijaranai. "Sensitized photo-oxidations of dissolved alcohols in homogenous and heterogeneous systems Part 2. TiO2-sensitized photodehydrogenations of benzyl alcohol." Journal of Photochemistry and Photobiology A: Chemistry 58.3 (1991): 361-371.

[110] Sclafani, A., L. Palmisano, and M. Schiavello. "Influence of the preparation methods of titanium dioxide on the photocatalytic degradation of phenol in aqueous dispersion." Journal of physical chemistry 94.2 (1990): 829-832.

[111] B. Gerand, G. Nowogrocki, J. Guenot, and M. Figlarz. Structural study of a new hexagonal form of tungsten trioxide. Journal of Solid State Chemistry, 29 :429-434, 1979.

[112] J. Oi, A. Kishimoto, T. Kudo, and M. Hiratani. Hexagonal tungsten trioxide obtained from peroxo-polytungstate and reversible lithium electro-intercalation into its framework. Journal of Solid State Chemistry, 96 :13-19, 1992.

[113] Salje, Ekhard. "The orthorhombic phase of WO3." Acta Crystallographica Section B: Structural Crystallography and Crystal Chemistry 33.2 (1977): 574-577.

[114] Woodward, P. M., A. W. Sleight, and T. Vogt. "Structure refinement of triclinic tungsten trioxide." Journal of Physics and Chemistry of Solids 56.10 (1995): 1305-1315.

[115] Kormann C., Bahnemann D., Hoffmann M. R., Photolysis of chloroform and other organic molecules in aqueous TiO2 suspensions, Environmental Science Technology, 25 (1991) 494-500.

[116] Malato, S., et al. "Photocatalytic treatment of water-soluble pesticides by photo-Fenton and TiO 2 using solar energy." Catalysis Today 76.2 (2002): 209-220.

[117] Xi W., Geissen S. U., Separation of TiO2 from photocatalytically treated water by crossflow microfiltration, Water Research, 35(5) (2001) 1256-1262.

[118] Cunningham J., Al-sayyed G., Sedlak P., Caffrey J., Aerobic and anaerobic TiO2- photocatalysed purifications of waters contaning organic pollutants, Catalysis Today, 53 (1999) 145-158.

[119] Cunningham J., Al-sayyed G., Sedlak P., Caffrey J., Aerobic and anaerobic TiO2- photocatalysed purifications of waters contaning organic pollutants, Catalysis Today, 53 (1999) 145-158.

[120] K.M. Schindler, M. Kunst, Charge-carrier dynamics in titania powders, The Journal of Physical Chemistry 94 (1990) 8222-8226 Schindler, Karl Michael, and Marinus Kunst. "Charge-carrier dynamics in titania powders." Journal of Physical Chemistry 94.21 (1990): 8222-8226.

[121] T.E. Agustina, H.M. Ang, V.K. Vareek, A review of synergistic effect of photocatalysis and ozonation on wastewater treatment, Journal of Photochemistry and Photobiology C: Photochemistry Reviews 6 (2005) 264-273.

[122] G. Rothenberger, J. Moser, M. Graetzel, N. Serpone, D.K. Sharma, Charge carrier trapping and recombination dynamics in small semiconductor particles, Journal of the American Chemical Society 107 (1985) 8054-8059.

[123] Beydoun D., Amal R., Low G., McEVOY S., Role of nanoparticles in photocatalysis, Journal of Nanoparticle Rsearch, 1, (1999) 439-458.

[124] D.F. Ollis, E. Pelizzetti, N. Serpone, Photocatalyzed destruction of water contaminants, Environmental Science & Technology 25 (1991) 1522-1529.

[125] Ollis D. F., Solar-assisted photocatalysis for water purification : issues, data, questions, Photochemical Conversion and Storage of Solar Energy, Kluwer Academic Publishers, (1991) 593-622.

[126] Blazkova A., Csolleova I., Brezova V., Effect of light sources on the phenol degradation using Pt/TiO2 photocatalysts immobilized on glass fibres, Journal of Photochemistry and Photobiology A: Chemistry, 113 (1998) 251-256.

[127] Bard, Allen J., Larry R. Faulkner, and Jean Louis Brisset. Electrochimie: principes, méthodes et applications. Masson, 1983.

[128] Blazkova A., Csolleova I., Brezova V., Effect of light sources on the phenol degradation using Pt/TiO2 photocatalysts immobilized on glass fibres, Journal of Photochemistry and Photobiology A: Chemistry, 113 (1998) 251-256.

[129] Lhomme, 2006.

[130] Herrmann, Jean-Marie. "Heterogeneous photocatalysis: fundamentals and applications to the removal of various types of aqueous pollutants." Catalysis today 53.1 (1999): 115-129.

[131] P. Cherin, E. Voronska, N. Fraoucene, et C. de Jaeger, « Toxicité aiguë des pesticides chez l'homme », Médecine Longévité, vol. 4, no 2, p. 68□74, juin 2012.

[132] M. Kerzhentsev, C. Guillard, J. M. Herrmann, P. Pichat, Photocatalytic pollutant removal in water at room temperature : Case study of the total degradation of the insecticide fenitrothion (phosphorothioic acid O,O-dimethyl-O-(3-methyl-4-nitro-phenyl) ester), Catal. Today 27 (1996) 215-220.

[133] R. Doong, W. Chang, Photoassisted titanium dioxide mediated degradation of organophosphorus pesticides by hydrogen peroxide, J. Photochem. Photobiol., 107A, (1997) 239 -244.

[134] J.P. Butault, N. Delame, F. Jacquet, et G. Zardet, « L'utilisation des pesticides en France : état des lieux et perspectives de réduction », Socio-Économiques NESE, no 35, p. 7□26, 2011.

[135] A. Lazartigues, M. Thomas, D. Banas, J. Brun-Bellut, C. Cren-Olivé, et C. Feidt, « Accumulation and half-lives of 13 pesticides in muscle tissue of freshwater fishes through food exposure », Chemosphere, vol. 91, no 4, p. 530□535, avr. 2013.

[136] T. Wang, Y. Wang, C. Liao, Y. Cai, et G. Jiang, « Perspectives on the Inclusion of Perfluorooctane Sulfonate into the Stockholm Convention on Persistent Organic Pollutants1 », Environ. Sci. Technol., vol. 43, no 14, p. 5171□5175, juill. 2009.

[137] Gunningham, Neil, and Darren Sinclair. "Policy instrument choice and diffuse source pollution." Journal of Environmental Law 17.1 (2005): 51-81.

[138] D. W. Kolpin, J. E. Barbash, et R. J. Gilliom, « Occurrence of pesticides in shallow groundwater of the United States: Initial results from the National Water-Quality Assessment program », Environ. Sci. Technol., vol. 32, no 5, p. 558□566, 1998.

[139] G. Moussavi, H. Hosseini, et A. Alahabadi, « The investigation of diazinon pesticide removal from contaminated water by adsorption onto NH4Cl-induced activated carbon », Chem. Eng. J., vol. 214, p. 172□179, janv. 2013.

[140] S. Ahmed, M. G. Rasul, R. Brown, et M. A. Hashib, « Influence of parameters on the heterogeneous photocatalytic degradation of pesticides and phenolic contaminants in wastewater: A short review », J. Environ. Manage., vol. 92, no 3, p. 311□330, mars 2011.

[141] W. Mulbry et P. C. Kearney, « Degradation of pesticides by micro-organisms and the potential for genetic manipulation », Crop Prot., vol. 10, no 5, p. 334□346, oct. 1991.

[142] D. Gondar, R. López, J. Antelo, S. Fiol, et F. Arce, « Effect of organic matter and pH on the adsorption of metalaxyl and penconazole by soils », J. Hazard. Mater., vol. 260, p. 627□633, sept. 2013.

[143] M. Schiavon, C. Perrin-Ganier, et J. Portal, « La pollution de l'eau par les produits phytosanitaires : état et origine », Agronomie, vol. 15, no 3□4, p. 157□170, 1995.

[144] Picture made by: Mikaela Gonczi, Centre for Chemical Pesticides (CKB), SLU, Sweden.

[145] T. Colborn, F. S. vom Saal, et A. M. Soto, « Developmental effects of endocrine-disrupting chemicals in wildlife and humans. », Environ. Health Perspect., vol. 101, no 5, p. 378-384, oct. 1993.

[146] A. M. Soto, K. L. Chung, et C. Sonnenschein, « The pesticides endosulfan, toxaphene, and dieldrin have estrogenic effects on human estrogen-sensitive cells. », Environ. Health Perspect., vol. 102, no 4, p. 380-383, avr. 1994.

[147] Viel, J. F., Challier, B., Pitard, A., & Pobel, D. (1998). Brain cancer mortality among French farmers: the vineyard pesticide hypothesis. Archives of Environmental Health: An International Journal, 53(1), 65-70.

[148] van der Werf, Hayo MG. "Assessing the impact of pesticides on the environment." Agriculture, Ecosystems & Environment 60.2-3 (1996): 81-96.

[149] Shu, Hung-Yee, and Ming-Chin Chang. "Decolorization effects of six azo dyes by O 3, UV/O 3 and UV/H2O2 processes." Dyes and Pigments 65.1 (2005): 25-31.

[150] Nestmann ER, Douglas GR, Matula TI, Grant CE, Kowbel DJ: Mutagenic activity of rhodamine dyes and their impurities as detected by mutation induction in salmonella and DNA damage in chinese hamster ovary cells. Cancer research 1979;39:4412-4417.

CHAPTER II

PHOTOCATALYTIC TECHNOLOGY

Photocatalytic technology

1. Photocatalytic technology

1.1Introduction :

Under light irradiation conditions, hydrogen was produced from the decomposition of water on a TiO_2 electrode [1], which caused a scientific boom. So the research on water has attracted the attention of several authors, who have reported their fascinating results.

When a semiconductor is irradiated with light, the absorption of a photon with sufficient energy causes the separation of charges due to the promotion of an electron (e^-) in the conduction band (CB) and the formation of a hole (h^+) in the valence band (VB). The photogenerated electrons and holes are not immediately recombined and can migrate to the semiconductor surface and transferred to the solution or gaseous phase, thereby oxidizing or reducing the adsorbed substances.

Then, the photocatalytic process can be summarized in the following reaction:

$$(Ox_1)_{ads} + (Red_2)_{ads} \longrightarrow Red_1 + Ox_2$$

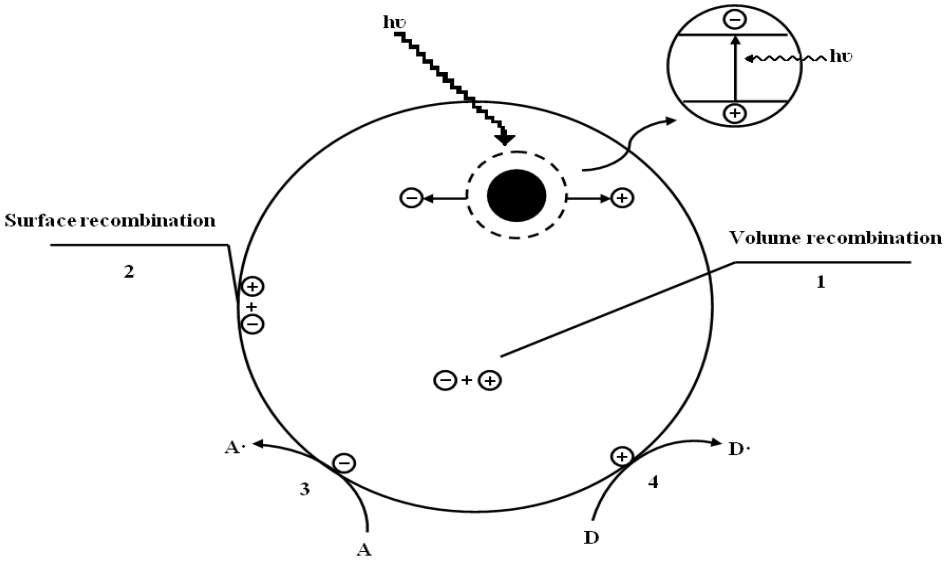

Figure II.1: Photocatalytic reaction process of semiconductors

Figure II.1 shows the response of a semiconductor after absorbing photons of energy equal to or greater than its bandgap.

The process of reducing and oxidizing substances on the semiconductive surface, causes the photocatalytic reaction that is performed. These are steps 3 and 4 respectively. Steps 1 and 2 are the recombination process, which is inefficient for the photocatalytic reaction. Therefore, in order to prevent electrons from recombining at the surface and in the volume of the semiconductor particles (steps 1 and 2), the reactive species must be pre-adsorbed on the semiconductor. Titanium dioxide TiO_2, which is the main semiconductor used in this work, is n-type with a wide bandgap Eg=3.2eV. When irradiated with photons of energy higher than the bandgap width ($\lambda \leq 387.5nm$) [2], the electrons from the valence band (e^-) are excited to cross the bandgap and enter into the conduction band, while leaving a hole charged positively (h^+) at the valence band. The electrons of the conduction band and the holes of valence band can be recombined inside or on the surface of TiO_2, in a very short time, to release energy in the form of heat or light. Photogenerated electron-hole pairs can migrate under the action of an electric field or by diffusion, and react with adsorbed species on the surface of the catalyst producing oxidoreduction reactions (redox), such as the decomposition of water into hydrogen and oxygen or the degradation of organic matter.

However, the photocatalytic decomposition of water into hydrogen and oxygen must fill certain conditions. Figure II.2 shows the conduction and valence band energy positions required to produce the water decomposition compared with the positions of these bands for some semiconductor materials.

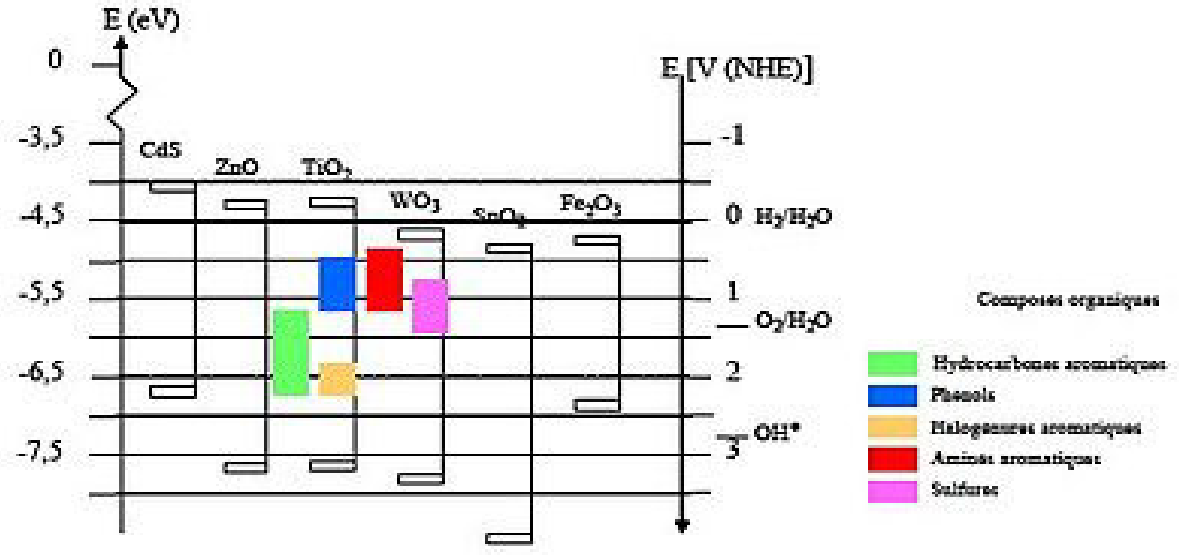

Figure II.2: Relationship between the band structure of various semiconductor compounds and the potential for decomposition of water into H_2 and O_2 [3, 4]

Therefore, it is necessary that the energy of the band gap (Eg) of the photocatalyst fill in the electrochemical requirements.

More specifically, the electrochemical potential of the valence band should be slightly larger than that of the O_2/H_2O electrode and the position of the conduction band should be slightly lower than that of the H_2 / H_2O electrode to produce hydrogen and oxygen.

So that it is necessary to have a specific position of the semiconductor bands energy and a certain redox potential of the adsorbate in order that a semiconductor would be able to be used as photocatalyst [5]. The lower energy level of the conduction band corresponds to the potential of the reduction of photogenerated electrons. The higher energy level of the valence band defines the oxidation capacity of the photo-holes.

From a thermodynamic point of view, an adsorbed species can be photocatalytically reduced by the electrons of the conduction band if it has a redox potential more positive than the potential level of the conduction band and can be oxidized by holes in the valence band if it has a potential more negative than the potential level of the valence band.

The necessary lifetime of the pair e^-/h^+ is assumed to spread on the surface of the catalyst and initiate the redox reaction. This is because the semiconductors, dissimilar to metals, don't have a continuity of band states to allow recombination of the photogenerated pair electron-hole.

Among the different semiconductors that exists in nature, TiO_2 has been the most successful for its application in these processes. This semiconductor exhibits photo-induced processes due to the characteristics of its "bandgap". Thus, when photons having an energy higher than that of the "bandgap" come into contact with the TiO_2, they can be absorbed by activating it [6].

As described in the previous chapter, among the polymorphic structures of TiO_2 that exists in nature, those having photocatalytic activity are the anatase and rutile phases. Differences in the crystal lattice of these two TiO_2 phases produce different electron band densities and structures, giving rise to different bandwidths (3.20eV for anatase and 3.02eV for rutile). In this way, the absorption threshold of the anatase and rutile TiO_2 phases, for well-crystallized samples, corresponds to 384 and 410 nm respectively [7, 8].

Taking into account the electrochemical potential of the holes and electrons in TiO_2 it can be used for the photocatalytic production of hydrogen [9].

Khan et al [10] have proposed the conditions for the photocatalytic decomposition of water to produce hydrogen:

1- High stability, to avoid photo-corrosion;

2- Cheap;

3- Can fill-in the thermodynamic requirements for water decomposition;

4- Can absorb sunlight.

Pure TiO_2 fill-in the first three requirements, but cannot absorb visible light. Many researchers have modified the TiO_2 so that it can absorb visible light [11].

The photocatalytic reaction of organics in wastewater under the action of a photocatalyst is the result of the reaction of pollutants with highly active groups such as OH· and O_2·$^-$ which have an extremely strong oxidizing capacity.

OH·, O_2·$^-$, and other ROS groups are produced after the n-type nanoscale semiconductor (TiO_2), absorbs light of no less than the energy of the width of its band gap. This species are generated by h^+ and e^- after the reaction with adsorbed of H_2O and O_2 on the TiO_2 surface. These species can degrade organic matter. Competing with the production of ROS, electrons and holes can be recombined at the same time. The whole process is as follows [12, 13]:

$$\mathbf{TiO_2 + h\upsilon \rightarrow e^- + h^+} \quad \textbf{(II.1)}$$

$$\mathbf{h^+ + H_2O \rightarrow H^+ + OH^{\cdot}} \quad \textbf{(II.2)}$$

$$\mathbf{e^- + O_2 \rightarrow O_2^{\cdot -} \rightarrow^{H+} \rightarrow HO_2^{\cdot}} \quad \textbf{(II.3)}$$

$$\mathbf{2\,HO_2^{\cdot} \rightarrow O_2 + H_2O_2} \quad \textbf{(II.4)}$$

$$\mathbf{H_2O_2 + O_2^{\cdot -} \rightarrow OH^{\cdot} + OH^- + O_2} \quad \textbf{(II.5)}$$

$$\mathbf{e^- + h^+ \rightarrow h\upsilon \quad or \quad heat} \quad \textbf{(II.6)}$$

Regarding oxidation of organic matter, the effect of nano-TiO_2 on organic polluting molecules is as follows:

1- The organic molecules in the liquid phase diffuses on the surface of the titanium dioxide.

2- Organic molecules are adsorbed on the surface of titanium dioxide or concentrated near the catalyst surface.

3- The hydroxyl radicals and the photo-generated holes react with organic substances, on the surface of the titanium dioxide or in the near liquid phase.

4- If the degradation of the titanium dioxide take place on the surface, the product of the resulting small molecules are desorbed.

In short, the organic pollutant molecules are first adsorbed on the surface of the nano-TiO_2 particles where can be directly suffer redox reactions or react with ROS. The organic pollutants are then oxidized into small molecules and even mineralized into CO_2 and salt ions.

As a new technology for pollution control, heterogeneous photocatalysis with semiconductor has recently made great progress. There have been numerous reports on the photocatalytic removal of various important organic compounds such as dyes, pesticides, herbicides, oils, hydrocarbons and polycyclic aromatic hydrocarbons, halogenated aromatic compounds, phenols, cyanides.

The research on organic compounds has shown that photocatalytic technology can effectively decolorize, degrade, detoxify and mineralize them into small inorganic molecules, to eliminate or reduce the impact of pollutants on the environment.

1.2 Applications to the purification of the environment:

Compared to the photocatalytic oxidation treatment method of the traditional treatment methods have lower efficiency in certain conditions. In particular, this methods cannot effectively remove low concentrations of no-biodegradable organic pollutants in water.

Therefore, this economical and effective way is preferred to remove organic pollutants in low concentration. The heterogeneous photocatalytic reaction involving TiO_2 is carried out at the liquid-solid or gas-solid interface. The photocatalytic reaction in the liquid phase is suitable for dye wastewater, pesticide wastewater, surfactants, chlorinated wastewater, Freon and oily wastewater.

Compared to the photocatalytic degradation of organic matter in the liquid phase, the photocatalytic reaction in gas phase has many advantages:

- Can be developed at room temperature and at atmospheric pressure. With oxygen in the atmosphere as an oxidizing agent the removal efficiency is high.
- The reaction is not affected by the solvent's molecules.
- The air absorption of ultraviolet light is smaller than the water one. A low energy light source can be used.

- The oxidation of volatile organic compounds is complete, and the reaction rate is fast.
- The molecular diffusion rate is high and facilitates mass transfer and chain reaction.

1.3 Wastewater treatment:

At the current level of production, it is unavoidable to reduce domestic wastewater and wastewater of industrial production. The uninterrupted spill of industrial wastewater and domestic wastewater is one of the main and major causes of environmental pollution. According to the source, the organic pollutants contained in wastewater can be divided into: organic wastewater of pesticide, organic wastewater of petroleum, organic wastewater of dye, tannery wastewater, surfactant wastewater, wastewater of textile factory.

Depending on the molecular structure of the pollutants in the wastewater, they can be divided into: cyanide, aliphatic hydrocarbons, chlorinated hydrocarbons, aldehydes, ketones, anthraquinones, compounds containing triazine group, compounds of β-naphthol structure, aniline containing a structure with double bond nitrogen-nitrogen. Wastewater contains harmful substances, causing physical and chemical changes in natural water, in way that the quality of the water deteriorates. Water pollution not only affects the aquatic ecosystem and impedes industrial and agricultural production but also endangers, directly or indirectly, the health of the human beings. Governments have invested a lot of workforce and resources for the research about industrial wastewater treatment.

To ensure that the water is not contaminated, it is necessary to treat this pollutants before to be released into water. The quality requirements are not the same because industrial wastewater and domestic wastewater differ in the quality and quantity of water, and also because of the different factories producing raw materials. So it's required to use different production processes. The choice of wastewater treatment methods should be based on the quality of water and the amount of wastewater to adopt different methods of treatment. At the same time, it must be taken into account

the effect of treatment methods, operating costs, wastewater post treatment processes required by sludge and sediment treatment, problems of secondary pollution and recycling, etc.

In short, wastewater treatment consists of separating the pollutants present in the wastewater, or breaking them down transforming them into harmless substances.

In order to fill in the increasing standards of wastewater discharge, traditional methods (such as biological methods, adsorption methods, etc.) continue to be improved. Also new methods (photocatalysis, photoelectrocatalysis, ultrasonic method, etc.) continue to emerge to be adapted to different sources (such as printing, dyeing, papermaking, pharmaceuticals, fine chemicals, pesticides , electrolysis of wastewater, etc.).

Photocatalytic oxidation is a technology for water pollution treatment, developed at the beginning of 1970s.

The use of photocatalytic oxidation for organic wastewater treatment has the following advantages:

- A variety of organic compounds can be completely degraded to CO_2 and water,
- No necessity of additional electron's acceptors (such as hydrogen peroxide),
- Suitable photocatalysts are cheap, nontoxic, stable and can be reused,
- Solar energy can be used as a light source to activate the catalyst.

The photocatalytic degradation is critically dependent on the photocatalyst, such as crystalline structure, lattice defects, crystalline surface, catalyst particle size, which have an impact on photocatalytic activity. The nano-anatase TiO_2 crystal has a high photocatalytic oxidation capacity. Until now, more than 100 species have been studied in detail [14] most of which are a substances of very high concern to the environment. Like harmful gases, pesticides, dyes, surfactants, odorous substances, etc.
Since photocatalytic oxidation is very promising as a water treatment technology, there is a lot of research work to be done in basic research such as:

- Improve the knowledge of photocatalytic mechanism at the solid-liquid interface,
- Structure of the energy levels at the semiconductor/liquid interface and influence of the density of surface electronic states,
- Mechanism of metal or metallic oxide loading,
- Reduction of the recombination of photogenerated carriers,
- Reactivity of organic material related to its molecular structure.

In the field of applied research, just like general catalytic studies, the core/heart of photocatalytic research is to find excellent photocatalyst performance. Therefore, the screening and the preparation of an efficient photocatalyst is the main issue of the photocatalytic research.

2. Water pollution:

2.1 Introduction:

The pollution refers to all wastes of chemical, biological or physical nature that are **potentially** toxics and that humans release into the ecosystem. It also means substances that can be very dangerous to the organisms and have a disruptive influence on the **natural functioning of ecosystems**. In other words, the pollution is an unfavorable modification that disturbs the environment with the possibility of affecting humans directly or indirectly through biological or agricultural water resources. It can also affect or alter the physical environment and recreational opportunities in nature [15].

2.2 The different types of water pollution:

Our water resources are affected by various types of pollution: water pollution damages seriously the ecological environment and affects the survival of humans. To achieve the sustainable development of human society, we must first resolve the problem of water pollution of which there are two types: one is natural pollution, the other is pollution due to humans. This last pollution is the main one. Water pollution

can be divided into different categories: chemical pollution, physical pollution and biological pollution, according to the different types of pollutants.

2.2.1 Chemical pollution:

Chemical pollutants can be inorganic pollutants, organic toxic pollutants, aerobic pollutants, plant nutrients, petroleum substances, etc. This type of pollution is classified into two categories:

- Non-biodegradable pollution: Among the non-biodegradable pollutants are the mineral substances and some organic compounds such as aromatic compounds.
- Biodegradable pollution: Biodegradable compounds consist of organic compounds containing nitrogen and phosphoric.

In general, the chemical pollution is divided into:

- **Chemical pollution of mineral origin:**

Mineral substances can be classified in :

- Essential elements : N, P, Na...
- Desirable elements : Fe, Mn, Zn, Cu...
- Toxic elements : Pb, Se, Hg, As, Cr, Sn, Cd...

- **Chemical pollution of organic origin:**

This type of pollution is an **important** part of water pollution. Among the chemical pollutants of organic origin:

- Phenols.
- Pesticides.
- Detergents.
- Hydrocarbons.
- Organic materials (proteins, lipids….).

2.2.2 Biological / bacteriological pollution :

Biological pollution mainly refers to diseases caused by pathogens present in water (diseases through water transmission), among these diseases can be mentioned:

- Typhoid.
- Salmonellose.
- Cholera.

2.2.3 Physical pollution :

Physical pollution can be divided into thermal pollution and radioactive pollution. An example of the first one is the industrial water cooling of some technologies which increases the temperature to 300ºC or more. Regarding radioactive pollution, it comes from the use of radioactive substances and is especially worrying when it is due to products with very long lifetime, such as plutonium [16].

3. Air pollution :

Air pollution is the possibility of inciting harmful effects on health and the environment by the presence of gases and particles (pollutants) in the atmosphere. [17].

3.1 Sources of air pollution:

Air pollution can be either from natural sources (such as volcanic eruption, forest fires, and bush fires), or from sources related to human activity (anthropogenic sources) [18].

3.1.1 Natural Sources:

Because it discards large clouds of sulfur dioxide, the volcanic eruption is considered the largest natural polluter. It also produces nitrogen oxides due to the heat that get away, and mineral dust.

Pollens are also considered as pollutants, because they annoy a lot of people who are allergic to it [19].

3.1.2 Anthropogenic sources:

Air pollution is often attached to human activities. It's considered the direct result of industrial progress, usually with a continuous emission and sometimes with unsuspecting emission of pollutants associated with combustion processes (energy produced by combustion, traffic /motor vehicles, industrial installations, heating...).

Generally, all activities that use fossil fuels (coal, petroleum,…) emit pollutants to the atmosphere, such as nitrogen oxides, carbon oxides, sulfur dioxide, dusts, but also other compounds such as benzene.

It must be realized and known that any energy production using these fossil fuels has an impact on pollution. For years, studies have shown a relationship between the degradation of human health and the environment, and have shown the presence of these pollutants in the atmosphere [20, 21, 22, 23].

- **Transports:**

Whatever the mean of transport, air, sea or vehicle, it contributes to emissions of air pollutants. Among the Pollutants emitted by this sector, can be quoted: carbon monoxide (CO), particles in exhaust gases, nitrogen oxides (NO_x), etc.

- **Domestic activities:**

When we cook, or when we use household products, paints, etc, we all emit atmospheric pollutants such as volatile organic compounds.

- **Incineration of household garbage:**

The combustion of garbage either in a dedicated installation or by an individual, it generates pollution emissions, such as: hydrochloric acid (HCl), metals, dioxins.

- **Electricity production :**

Most of the atmospheric emissions are at the origin of the industrial sector. It is where the electricity is produced that pollutants are emitted but not at the place of

consumption. In this sector there is emission of pollutants like: materials, dusts, sulfur dioxide (SO_2), volatile organic compounds (VOC).

- **Individual and / or collective air-conditioning :**

The air-conditioning generates emissions because of its high electricity consumption. The pollutants generally emitted by this sector are: fine particles, carbon monoxide (CO), sulfur dioxide (SO_2), nitrogen oxides.

- **Agriculture :**

The use of phytosanitary products or spreading (ammonia emission) in this sector, as well as the use of machines give this sector the responsibility of contributing to air pollution. Examples of agricultural emitted pollutants are: ammonia (NH_3), dusts.

3.2 The air pollutants :

Pollutants can be classified as primary or secondary.

3.2.1 Primary pollutants :

Primary pollutants can be defined as pollutants that come directly from one of the identified pollutant sources:

- **Carbon monoxide (CO):** It comes from combustion processes (coals, fuels...) and it presents in the exhaust gases of cars.
- **Sulfur Dioxide (SO_2):** This gas can be produced by various industrial processes such as petroleum refineries and metallurgical industries [18], it's also naturally produced by volcanoes.
- **Nitrogen oxides (NO_x):** These oxides include nitrogen monoxide (NO) and nitrogen dioxide (NO_2). These are gases that result from the nitrogen oxidation in the air by oxygen at high temperature. This phenomenon usually occurs during combustion processes, particularly in internal combustion engines and thermal power stations [17].

- **Volatile Organic Compounds (VOCs):** The emission of VOCs into atmosphere comes from various anthropogenic sources, such as the evaporation of refined products, incomplete combustion in engines, paints, the use of solvents in industry...
- **Particulate Matter (PM):**These particles can come from anthropogenic sources (fossils combustion, industrial emissions), or from natural sources (volcanic eruptions, forest fires, pollen).

3.2.2 Secondary pollutants :

Secondary pollutants can be defined as pollutants not directly emitted by the identified sources. But, they are formed in the atmosphere following reactions that involve compounds emitted by primary sources. Their presence in the atmosphere is difficult to regulate because their existence doesn't come directly from anthropogenic activities [24].

- **Tropospheric Ozone :**It is formed in the lower atmosphere, but once formed, it reacts very quickly, with the NO whose input in the atmosphere is constant. The ozone will therefore be partly consumed and generally present in small quantities.
- **Secondary VOCs :** Also called peroxy acetyl nitrates (PAN).

4. Photocatalytic degradation of organic pollutants:

In the 21st century, social, energetic and environmental problems have been the focus of global concern for reducing pollution, protecting the ecological equilibrium and solving the environmental problems. At the moment, water as the most precious resource of humanity, has attracted more and more attentions. The development of a simple and very effective way to control water pollution is an urgent problem for human society. Although there are many ways, the technology of photocatalytic organic pollutants treatment has become the subject of research because of its advantages: inexpensive, economical in energy, nontoxic and effective.

In our daily life, there are also many volatile organic compounds (VOCs) released to the environment, they not only have caused serious damage to the environment but also threatened human health and even human lives. For example, various petrochemicals products present in decorations, daily necessities, especial coatings and other commonly used construction materials such as paints. These compounds provoke a severe environmental pollution.

5. Chosen pollutant; phenol: molecule model

5.1 Introduction:

Phenol is found in wastewater from different factories, such as: textiles, pesticides, paints, petroleum refinery, coal processing, pharmaceutical, tannery, and other industries. It is a very common pollutant in many industrial effluents.

The family of aromatic organic compounds includes phenol as one of its first constituents [24]. Although it has an alcohol function, phenol has unique properties and is not classified as an alcohol. Its structure is that of a hydroxyl group -OH bonded to a carbon atom of the benzene cycle. It is also known as: phenic acid, carbolic acid and hydroxybenzene [25]. It is present in many plants and has a simple molecular structure (figure II.3).

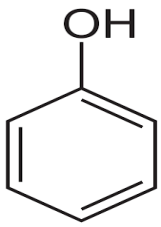

Figure II.3: Structure of the phenol molecule

5.2 Properties of phenol:

Pure phenol, C_6H_5OH, is a colorless solid, crystallized at room temperature. It is hygroscopic and has a pungent and sweetish smell [26]. In contact with the air or under the influence of humidity, the phenol oxidizes slightly to give traces of Quinone. It takes a pink color, then red. Its solubility in water is limited: 80 $g \cdot L^{-1}$ at 25 °C. It is

very soluble in many organic solvents such as acetone, ethanol, diethyl ether. It is easily soluble in ether [27].

Some of its physicochemical properties are mentioned in the following table:

Brute formula	C_6H_6O
Molar masse ($g \cdot mol^{-1}$)	94,11
T_{Fusion}(°C)	43
$T_{Boiling}$(°C)	182
Solubility in water ($g \cdot L^{-1}$)	80
Density ($g \cdot cm^{-3}$)	1,073
pK_a	9,95

Table II.1 : Physicochemical properties of phenol.

5.3 Methods of phenol synthesis:

Although phenol is present in the environment and can be extracted from tars or waste water, it is mostly produced synthetically. Industrially phenol is produced by several methods. An older method consisted on the alkaline fusion of a sulfonic acid salt [28]. This reaction requires the use of highly concentrated sodium hydroxide and a high temperature; that's why it's little used. The other method is a catalytic chlorination of benzene followed by basic hydrolysis of the obtained chlorobenzene [29].A method called DOW consists of oxidation of toluene and the formation of benzoic oxide, then oxidative decarboxylation to obtain phenol [30]. However, the main method of producing phenol was developed by Hock and Lang in 1944 [31] and it has been in use since the 1950s [32], it produces about 95% of phenol in the world [33]. This method has three phases [34]:

- Phase of benzene alkylation with propene to form the isopropylbenzene (cumene):

- Phase consisting in oxidizing cumene or isopropylbenzene by oxygen in the air at a temperature between 90 and 130°C, under a pressure of 5 to 10 bars, in liquid phase and at a pH about 9,5. It gives cumylhydroperoxide:

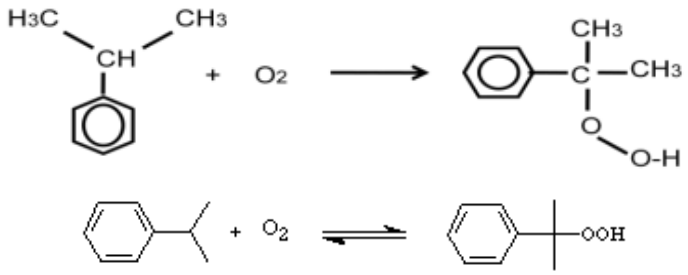

- Phase of the split of cumylhydroperoxide into phenol and acetone, in acidic medium at low temperature:

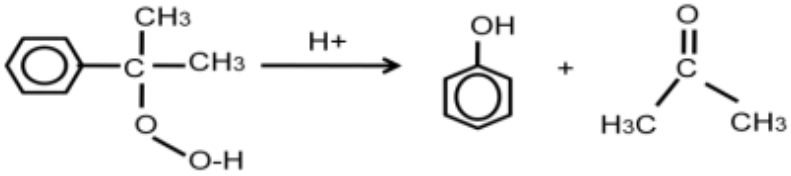

5.4 The different uses of phenol:

Phenol is used to produce the Bisphenol A, the polyphenylene oxide, the phenolic resins (composite materials), the fiber intermediates (caprolactam, cyclohexanol and cyclohexanone). It's also the basis of the production of a large number of products such as: alkylphenols, diphenols, chlorophenols such as pentachlorophenol used in the treatment of wood, nitrophenols, aminophenols such as intermediate paraminophenol in the pharmaceutical industry [35] as well as aniline [36, 24].

The use of phenol is carried out in very varied fields, such as the manufacture of chemicals, drugs, coke, rubber, fertilizers, dyes, perfumes, disinfectants, bactericides, fungicides and oil refining [35, 26, 25]. However, bisphenol A is used in the production of polycarbonates, epoxy resins, polysulfonates and caprolactam to produce nylon 6 [35, 37].Phenol can also be found in some consumer products [38, 26].

5.5 Main sources of phenol exposure:

5.5.1 Natural sources:

The phenol in the natural state can be usually found in wood and pine needles, in the urine of herbivores and in tar of coal [39].

There are also other natural factors responsible for the natural presence of phenol in the environment. Among them, the decomposition of various organic wastes, and human and animal metabolism [38, 37] can be mentioned. The natural concentrations can increase by forest fires [26, 37].

5.5.2 Anthropogenic sources:

Phenol is manufactured as an intermediate of the preparation of other chemicals and can be released as a by-product or contaminant [26].

Exhausts of thermal engines [34, 40] and photochemical degradation of benzene [37, 41] also emit phenol into the atmosphere. It's the same for coking and carbonization factories of wood and tobacco combustion at low temperature [34, 38, 39].

5.6 Behavior in the environment:

Phenol is a pollutant that can be detected throughout the environment and at different concentrations.

5.6.1 In waters :

Phenol has been detected in superficial water, groundwater [42, 43], drinking water, rainwater, urban runoff water and industrial effluents. Phenol is heavier than water and therefore it tends to settle and dissolve slowly to form toxic solutions [39]. Phenol is completely miscible with water at a temperature above 68,4ºC [44].

5.6.2 In the grounds:

Phenol is rapidly adsorbed / desorbed, oxidized but generally biodegraded or drained in water and / or volatilized in air [39]. That is why there is only few data of phenol in the ground.

5.6.3 In the air:

Phenol vapors are heavier than air and form an explosive mixtures. Phenol is oxidized in air, and this oxidation process is accelerated by light or by catalytic effect impurities [26]. A part is leached by rain [41].

5.6.4 In sediments:

Considering its physicochemical properties, there is little chance that phenol accumulate in sediments [34]. There isn't enough data showing the presence of phenol in sediments.

5.7 Toxicity :

Phenolic compounds are amply used, in industrial and daily life and have been proven to be a common pollutant of the water bodies. Owing to its carcinogenic character and its stability, the phenol has been classified as a toxic pollutant for microorganisms, animals, plants and humans at different concentrations [45].

5.7.1 In humans :

Phenol is rapidly absorbed by all routes of exposure: the lungs, the liver and the gastrointestinal mucosa are the main phenol metabolism sites [34].

The low volatility of phenol limits the inhalation risk of important large concentrations. However, phenol vapors are very unpleasant for the upper airways and could cause severe lesions of respiratory mucosa.

Locally, phenol produces a corrosive action on the tissues, it is a severe irritant for skin and eyes. Inhalation gives respiratory irritation signs with cough and dyspnea [25]. Prolonged exposure causes paralysis of the central nervous system as well as renal and pulmonary damage. This paralysis can lead to death. The poisoning is

accompanied by symptoms such as: headache, dizziness, buzzing, gastric and intestinal disorders, poisoning, collapse, irregular breathing, respiratory failure, unconsciousness, cardiac troubles, and sometimes convulsions [39]. The ingestion of 1g of phenol is deadly for humans [38, 39, 46]. The International Agency for Cancer Research and the EPA (United States of Environmental Protection Agency) have classified phenol as non-carcinogenic to humans [24, 38].

5.7.2 In animals and plants:

Following oral and dermal exposures at doses of acute phenol toxicity, many effects were observed in laboratory animals. These effects include necrosis of skin or of throat mucous membranes, neuromuscular convulsions, trembling, and histopathological effects on the kidney, liver, spleen and thymus. There are also hematological effects, suppression of the immune reaction [26] and effects on nervous system [25].

Phenol is toxic to aquatic organisms and these may be endangered in superficial or marine waters contaminated with phenol. Phenol concentrations above 50 ppb are toxic for some aquatic life [47].

The phenol is disruptive and inhibitor of the growth for plants [48].

5.8 Phenols and health:

Because of their toxicities, proven even at low concentrations, phenols are considered as pollutants to be treated first. Because of this toxicity, various phenols have been classified as priority pollutants by the EPA [38, 48]. Likewise the European Union has limited the maximum permissible concentration for drinking water to 0.5 $\mu g \cdot L^{-1}$ (0.5 ppb) [38, 39, 48, 49]. The EPA has established a water purification standard of less than 1 ppb of phenol in superficial water, while the phenol limits for wastewater emissions are 0.5 $mg \cdot L^{-1}$ [38].

References:

[1] Fujishima A, Honda K. Electrochemical Photolysis of Water at a Semiconductor Electrode [J]. Nature, 1972, 238: 37-38.

[2] D.H. Quiñones Murillo, Eliminacíon de contaminantes emergentes del agua mediante ozonation solar fotocatalítica, 2014.

[3] SERPONE, Nick et PELIZZETTI, Ezio. Photocatalysis: fundamentals and applications. Wiley-Interscience, 1989.

[4] GRÄTZEL, Michael. Photoelectrochemical cells. nature, 2001, vol. 414, no 6861, p. 338.

[5] RAJESHWAR, K. Photoelectrochemistry and the environment. Journal of Applied Electrochemistry, 1995, vol. 25, no 12, p. 1067-1082.

[6] www.cnrs.fr/cw/dossiers/dosnano/glossaire/mot/bandesPlus.htm

[7] A. Fujishima, K. Hashimoto, T. Watanabe TiO2 photocatalysis. Fundaments and applications, 1st ed. Tokyo: BKC; 1999.

[8] MARDARE, Diana, TASCA, M., DELIBAS, M., et al.On the structural properties and optical transmittance of TiO2 of sputtered thin films. Applied Surface Science, 2000, vol. 156, no 1-4, p. 200-206.

[9] PUGA, Alberto V. Photocatalytic production of hydrogen from biomass-derived feedstocks. Coordination Chemistry Reviews, 2016, vol. 315, p. 1-66.

[10] KHAN, Shahed UM, AL-SHAHRY, Mofareh, et INGLER, William B. Efficient photochemical water splitting by a chemically modified n-TiO2. science, 2002, vol. 297, no 5590, p. 2243-2245.

[11] http://openyoureyes.over-blog.ch/-dioxyde-de-titane-une-bombe-%C3%A0-retardement.

[12] FUJISHIMA, Akira, RAO, Tata N., et TRYK, Donald A. Titanium dioxide photocatalysis. Journal of photochemistry and photobiology C: Photochemistry reviews, 2000, vol. 1, no 1, p. 1-21.

[13] C. ZINSOU, cours de métabolisme :Energétiques des réactions biochimiques.

[14] HOFFMANN, Michael R., MARTIN, Scot T., CHOI, Wonyong, et al. Environmental applications of semiconductor photocatalysis. Chemical reviews, 1995, vol. 95, no 1, p. 69-96.

[15] CARTIER, Clément, BESNER, Marie-Claude, BARBEAU, Benoit, et al. Evaluating aerobic endospores as indicators of intrusion in distribution systems. Le traitement des eaux :Rymonddesjardins, ingénieur : professeur à l'écolepolytechnique de Montréal. American Water Works Association. Journal, 2009, vol. 101, no 7, p. 46.

[16] CHOCAT, Bernard, BERTRAND-KRAJEWSKI, Jean-Luc, et BARRAUD, Sylvie. Eaux pluviales urbaines et rejetsurbains par temps de pluie. 2007.

[17] MILER, S. Exposition prolongée à la pollution de l'air et incidence des évènementscardiovasculaires chez la femme. revue Environnement. Risques et santé, 2007, vol. 6, no 04, p. 2.

[18] MAYER, T., PTACEK, C., et ZANINI, L. Sediments as a source of nutrients to hypereutrophic marshes of Point Pelee, Ontario, Canada. Water Research, 1999, vol. 33, no 6, p. 1460-1470.

[19] http://www.futura-sciences.com/sciences/actualites/recherche-lien-pollution-urbaine-augmentation-allergies-5471/

[20] MONK, Lorna S., FAGERSTEDT, Kurt V., et CRAWFORD, Robert MM. Oxygen toxicity and superoxide dismutase as an antioxidant in physiological stress. PhysiologiaPlantarum, 1989, vol. 76, no 3, p. 456-459.

[21] BREMNER, S. Anderson, ANDERSON, H. R., ATKINSON, R. W., et al. Short-term associations between outdoor air pollution and mortality in London 1992-4. Occupational and environmental medicine, 1999, vol. 56, no 4, p. 237-244.

[22] CENKO, S. Bradley, FOX, Derek B., PENPRASE, Brian E., et al. GRB 070125: the first long-duration gamma-ray burst in a halo environment. The Astrophysical Journal, 2008, vol. 677, no 1, p. 441.

[23] www.fnors.org - Septembre 2008.

[24] HORCH, R., SPILKER, G., et STARK, G. B. Phenol burns and intoxications. Burns, 1994, vol. 20, no 1, p. 45-50.

[25] A. Baulig, A. Pichard, Seuils de Toxicitéaigue :Phénol, Rapport d'étude N°06DR058, 2008. DES SUBSTANCES CHIMIQUES, Expertise Toxicologique. Seuils de Toxicitéaiguë-Phénol, 2008.

[26] W. Bruce, M.E. Meek, R. Newhook, Environnement et Santé Canada, Liste des substances d'intérêt prioritaire, Rapport d'évaluation pour le phénol, N°Cat En40-215/45F, ISBN 0-662-84220-0, 2000.

[27] www.inrs.fr - 2008.

[28] SIROIS, J. et RICHARDS, J. S. Transcriptional regulation of the rat prostaglandin endoperoxide synthase 2 gene in granulosa cells. Evidence for the role of a cis-acting C/EBP beta promoter element. Journal of Biological Chemistry, 1993, vol. 268, no 29, p. 21931-21938.

[29] ACID-BINDING, Single-stranded Nucleic. Bibliography of the current world literature. Proc Natl Acad Sci USA, 1994, vol. 91, p. 7202-7206.

[30] EHTASH, Moamer. Purification des eaux polluées par du phénol dans un pertracteur à disques tournants. 2011. Thèse de doctorat. Rouen, INSA.

[31] Perrin and Scharff, 1993

[32] KUJAWSKI, Wojciech, WARSZAWSKI, Andrzej, RATAJCZAK, Włodzimierz, et al. Removal of phenol from wastewater by different separation techniques. Desalination, 2004, vol. 163, no 1-3, p. 287-296.

[33] FISK, P. R., GIRLING, A. E., et WILDEY, R. J. Prioritisation of flame retardants for environmental risk assessment. Wallingford, UK : Environment Agency. Phenol, Ullmann, Band 18, p. 177-190, 1972

[34] A. Pichard, Fiche de données toxicologiques et environnementales des substances chimiques, Phénol, INERIS, INERIS-DRC-01-25590-01DR021, N°2-1, 2005.

[35] A. Chemikaliengesetz, Risk Assessment, Phénol, CAS-N°108-95-2, EINECS-N°203-632-7, Dortmund, Allemagne, 2002.

[36] S. Imamura, Y. Tonomura, M. Terada et T. Kitao, Oxidation of Oxygen Containing Organic Compounds in Water, MizuShoriGigutsu, 20 (1979) 317-321.

[37] SHEETS, FACT. BREAST CANCER & THE ENVIRONMENT RESEARCH CENTERS. 2007.

[38] G. Busc, S. Berardinelli, C. Resini, L. Arrighi, Technologies for the Removal of Phenol From Fluid Streams: A Short Review of Recent Developments. J. Hazard. Mater, 160 (2008) 265-288.

[39] C. Horn, K. Roy, P. Frank,T. Just, Shock-tube Study on the High-temperature Pyrolysis of Phenol, Proc. Combust. Inst, 27 (1998) 321-328.

[40] S.K. Nadavala, K. Swayampakula, V.M. Boddu, K. Abburi, Biosorption of Phenol and o-cholorophenol from Aqueous Solutions on to Chitosan-calcium Alginate Blended Beads, J. Hazard. Mater, 162 (2009) 482-489.

[41] Health and Safety Guide No. 88: Phenol, IPCS-INCHEM, ISBN 92-4-151088-9, ISSN 0259-7268, World Health Organization, Genève, Suisse, 1994.

[42] Toxicological Profile for Phenol, Agency for Toxic Substances and Disease Registry, Atlanta, Géorgie. -SWAN, Shanna H. Environmental phthalate exposure in relation to reproductive outcomes and other health endpoints in humans. Environmental research, 2008, vol. 108, no 2, p. 177-184.

[43] GIANFREDA, L., SANNINO, F., RAO, M. A., et al. Oxidative transformation of phenols in aqueous mixtures. Water research, 2003, vol. 37, no 13, p. 3205-3215.

[44] SØRENSEN, Jens M., MAGNUSSEN, Thomas, RASMUSSEN, Peter, et al. Liquid-liquid equilibrium data: Their retrieval, correlation and prediction Part I: Retrieval. Fluid Phase Equilibria, 1979, vol. 2, no 4, p. 297-309.

[45] K. Yamada, Y. Akiba, K. Shibuya, A. Kashiwada, K. Matsuda, M. Hirata, Water Purification through Bioconversion of Phenol Compounds by Tyrosinase and Chemical Adsorption by Chitosan Beads, Biotechnol. Prog, 21 (2005) 823-829.

[46] NUHOGLU, Alper et YALCIN, Beste. Modelling of phenol removal in a batch reactor. Process Biochemistry, 2005, vol. 40, no 3-4, p. 1233-1239.

[47] SEETHARAM, Gayathri B. et SAVILLE, Bradley A. Degradation of phenol using tyrosinase immobilized on siliceous supports. Water Research, 2003, vol. 37, no 2, p. 436-440.

[48] NAMANE, Abdelkader. Adsorption-biodégradation du phénol par PseudomonasAeruginosaimmobilisé sur du charbonactif en grains. 2006. Thèse de doctorat. Ecolenationalesupérieurepolytechnique.

[49] BRUN, Alexandre. La gestion de l'eau. Gestion de l'eau, 2012, p. 63. [Les normes européennes, Centre d'information sur l'eau CIEAU (www.cieau.com), France, 2005].

CHAPTER III

Materials and methods

Materials and methods

1. The main used photocatalysts:

Along this work, ZnO, ZrO_2, WO_3 and two types of titanium dioxide, commercial and synthesized, were mainly used.

1.1 The commercial photocatalysts:

The commercial photocatalysts we have worked with are:

- Merck ZnO
- Chemco ZrO_2
- Evonik Aeroxide TiO_2-P25
- Evonik Aeroxide TiO_2-P90
- Millenium TiO_2-PC100
- Sigma Aldrich TiO_2
- Kemira650TiO_2

1.2 The lab-made photocatalysts:

1.2.1 Synthesis of ZnO

A mass of zinc acetate dihydrate ($Zn(CH_3COO)_2$,$2H_2O$) was dissolved in 100ml of distilled water. To this mixture was added, dropwise 20 ml of one molar solution of NaOH. The mixture obtained is heated with constant stirring at 60°C for 1 hour - the final pH of the mixture was 5,58- and then filtered under vacuum. The obtained solid is washed several times with distilled water and then dried overnight in an oven at 100°C [1].

The reaction mechanism for ZnO formation from zinc acetate is as :

$$\mathbf{Zn(CH_3COO)_{2(aq)} + 2NaOH \rightarrow Zn(OH)_{2(s)} + 2CH_3COONa + H_2O} \qquad \textbf{(III.1)}$$

$$\mathbf{Zn(OH)_{2(S)} + 2H_2O \rightarrow Zn(OH_4)^{2-} + 2H^+} \qquad \textbf{(III.2)}$$

$$Zn(OH_4)^{2-} \rightarrow ZnO + H_2O + 2OH^- \quad \text{(III.3)}$$

1.2.2 Synthesis of WO_3

Tungsten oxide is synthesized by the hydrothermal synthesis method. The method used is based on that proposed by Jinmin Wang et al. but with some modifications [2]. In this method, sodium tungstate (Na_2WO_4, $2H_2O$) is used as a precursor. 3.30 g of the tungstate salt and 1.16g NaCl are solubilized in 75ml of an aqueous solution of distilled water. The pH is adjusted to 3 with 3M HCl and the mixture is poured into a 100 ml steel autoclave.

The autoclave is placed in an oven at 180°C for 24 hours. The whitish solid is filtered under vacuum using a 0.45µm millipore filter membrane. The solid is washed with water. The dried solid is recovered and calcined in air at 500 °C for 3 hours.

1.2.3 Synthesis of TiO_2 nanoparticles :

Several laboratory processes have been developed. Among these methods, the sol-gel process [3, 4] which consists in synthesizing an amorphous inorganic solid by a simple chemical reaction and at a relatively low temperature (20-150 °C) is one of the most used.

Degussa P25 titanium dioxide is the photocatalyst used as a reference in photocatalysis studies, since it is found in the majority of cases as the most effective titanium dioxide. TiO_2 P25 is derived from the oxidation of $TiCl_4$ titanium chloride in a flame reactor and used as a white powder.

In this thesis, TiO_2 was then prepared from titanium trichloride ($TiCl_3$). This way, the synthesized TiO_2 is expected to be similar to Degussa P25.

The synthesis method is:

9.65 ml of titanium trichloride are placed in 500.78 ml of distilled water. A 1 $mol \cdot L^{-1}$ NaOH solution is added little by little. The obtained solution is heated under continuous stirring for 24 hours and then centrifuged. The separated solid is then

rinsed once with a hydrochloric acid solution and several times with distilled water. Finally, it is dried overnight in an oven at 120 °C.

The following diagram summarizes the different steps of the preparation of TiO_2 :

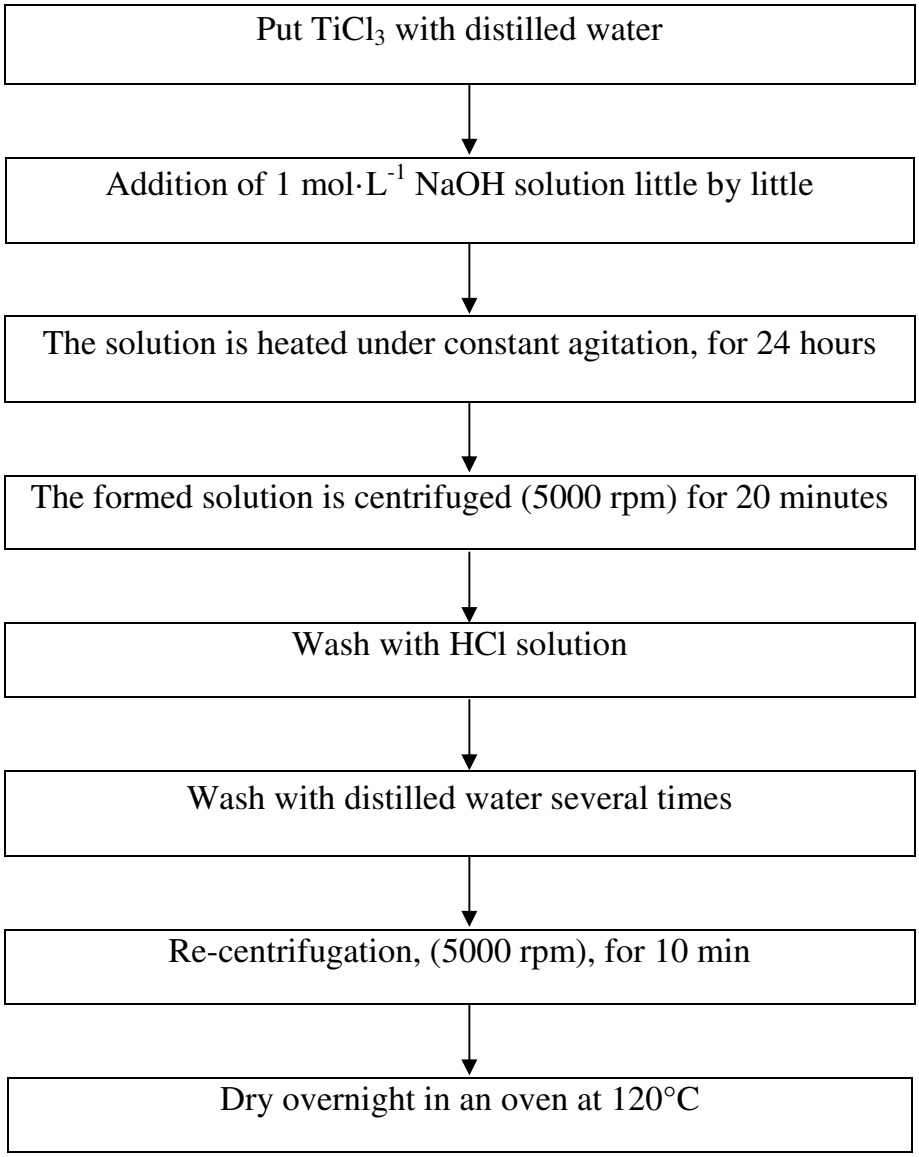

Figure III.1 : Diagram of the different steps of synthesis of titanium dioxide

The reaction mechanism for forming titanium dioxide from titanium trichloride is:

$$\mathbf{Ti(Cl)_3 + 3NaOH \rightarrow Ti(OH)_3 + 2NaCl} \qquad \textbf{(III.4)}$$

$$\mathbf{Ti(OH)_3 \rightarrow TiO_2 + H_2O + \frac{1}{2}H_2} \qquad \textbf{(III.5)}$$

1.3 Doping:

1.3.1 Doping of semiconductors :

Any disturbance of the crystalline structure such as defects or chemical impurities will make the forbidden gap "accessible", by creating some localized states. This property is commonly used to control the semiconductor materials properties by implanting them with well-chosen atoms called dopants [5].

Doping causes the appearance of new acceptor and donor electrons levels in the band structure of doped material. These levels are localized in the gap between the conduction band and the valence band.

The effect caused by a dopant depends on the number of valence electrons of the doping atom compared to the atom it replaces. P doping is produced by atoms with less valence electrons that the substituted one (Figure III.2: a), while n doping is produced by dopant atoms with excess of valence electrons compared to the substituted atom [6] (Figure III.2: b) [7].

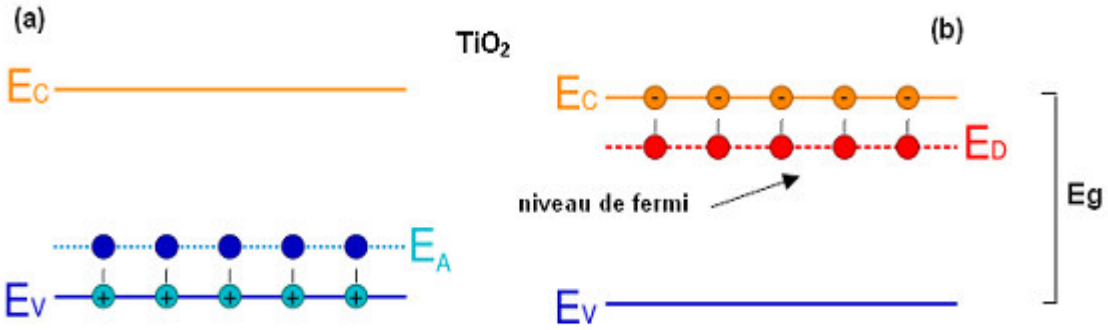

Figure III.2: (a) Semiconductor of type (P);
(b) Semiconductor of type (N) [7]

1.3.2 Anionic doping of TiO_2 (the important catalyst in this thesis):

In the early 1990s, Sato et al. reported the first study on TiO_2 anionic doping. They used nitrogen as a doping element [8,9]. Asahi et al. published in 2001 [10] a work reporting the photocatalytic activity of nitrogen-doped TiO_2 in the visible range. This study was developed to produce TiO_2 active in the visible range.

For the production of the doped and active TiO_2photocatalyst under visible radiation, the basic conditions have been defined by Asahi and his collaborators [10]:

* The minimum of the conduction band (BC) and the energetic state of the doped TiO_2 should be greater than or equal to the redox potential of water H_2/H_2O, to guarantee the necessary photo-reduction for photocatalysis.

* The energy state formed by the dopant in the forbidden band must overlap/interact sufficiently with the energy band of TiO_2. So that it can transfer the photoexcited charge carriers to the reactive sites on the TiO_2 surface.

* The dopant must create an energy level in the band gap of TiO_2, which will absorb visible light.

Calculations made by the method of density of states (DOS) by Asahi et al. [10] on the doping of anatase TiO_2 with different non-metallic anions (C, N, F, P, and S), lead to the fact that ***nitrogen and fluorine are the most effective dopants*** among the studied elements.

1.3.3 Anionic fluoride doping:

In order to prepare a fluorinated photocatalyst (F-MO_x) we start with the preparation of a 2M solution of sodium fluoride (NaF) (pH 6.5). Then the desired MO_x is added to that solution in a concentration of $40g \cdot L^{-1}$. The solution is stirred continuously for 30 min. Then filtered with Whatman TM 1005-125 (grade 5, diameter: 12.5cm, pore size: 2.5µm) and washed with 1 liter of ultra-pure water Milli-Q until neutral pH. The filtrate is a little turbid (the non-desorption of fluoride and sodium was observed). The catalyst was subsequently dried at 100 °C for 12 hours. After that the white powder is grinded in a mortar and stored for being used. It should be noted that different filters were tested with different pore diameters and that important photocatalytic performances were only obtained with the Whatman TM mentioned (fig.III.3).

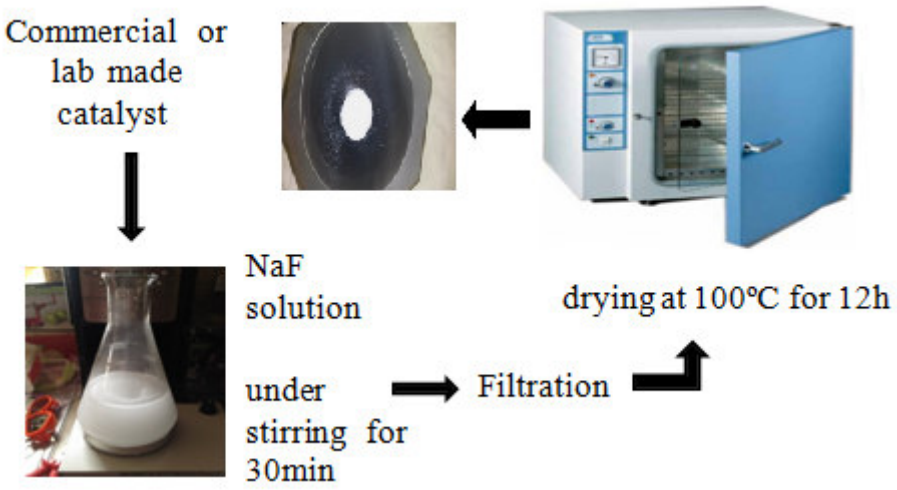

Figure III.3 : The experimental process of doping the catalysts by fluorine (F-MO_x)

1.4 Reaction Protocol:

1.4.1 In liquid phase:

The photocatalytic degradation studies in liquid phase were done in a 250 ml cylindrical Pyrex glass reactor by filling it with 200ml of pollutant solution and 200mg of MO_x or F-MO_x. Afterwards, the pH of the solution is adjusted with diluted H_2SO_4 or NaOH.

This suspension is maintained in darkness with aeration at a constant flux and under magnetic stirring at 750 rpm for 10 min in order to guarantee the adsorption equilibrium of the pollutant on the photocatalyst.

After the 10 minutes of adsorption, the concentration of the pollutant is determined as the initial concentration (C_o) and the UV lamp, located at a distance of 15 cm from the reactor, is activated. The UV lamp is a 60W Philips Solarium HB175 (equipped with 4 fluorescent tubes, 15 W Philips CLEO) with emission spectrum between 300 and 400nm (λ_{max} = 365 nm, irradiance: 9 mW·cm^{-2}).

The samples are extracted and filtered using a syringe equipped with filters Millex HA MF Millipore with a pore diameter of 0.45µm, in order to withdraw the photocatalyst and therefore make it possible to analyze the samples.

The sampling interval is determined by the initial concentration of the pollutant and the kinetics of photodegradation. At each predetermined time interval, 15ml of the solution was extracted as a sample at that time, and so on for 90-120 minutes. The concentration of pollutant was determined either by high performance liquid chromatography (HPLC) or by ionic chromatography (IC). The mineralization of the pollutant was determined by TOC analyzer (fig III.4).

Figure III.4 : Liquid phase study using the fluorescent lamp Philips HB175.

1.4.2 In gas phase:

The photocatalytic degradation studies in gas phase were done in a 250ml cylindrical Pyrex glass vessel with a stopper connected to a pump that injects air and produces bubbles at the bottom of the solution placed within. This vessel is connected to a glass tube filled with the catalyst and **under darkness**. The gas mixture from the vessel passes through this reactor. All the process is studied at room temperature under a fume hood.

Two different solutions were used as gas mixture precursor, ethanol or ammonium.

In the case of ethanol 100ml of a 2:1 ethanol/water solution bubbled at a constant air flow of 60 $cm^3 \cdot min^{-1}$ was used. The gas stream was injected into a tube (150mm, 4mm) containing 20mg of the commercial catalyst or 0.1g of the synthesized one, in darkness. After that, the gas stream is injected into a second reactor containing water. The reaction takes 90min.

In the case of ammonia we used the same device except that the solution is a concentrated ammonia in the first reactor and the second reactor contains a 1:1 sulfuric acid (H_2SO_4)/water solution. The reaction also takes 90 min.

In both cases, after the reaction time (adsorption time), the catalyst is carefully removed from the glass tube and placed in the middle of two CaF_2 windows to be analyzed by FTIR.

After the first FTIR spectrum, the two windows containing our catalyst are exposed to UV illumination produced by the fluorescent lamp (as mentioned above). This process is repeated at different sampling times followed by a FTIR spectrum recording. The Brönsted and Lewis acid centers in the various used photocatalysts were determined using the ammonia adsorption FTIR spectra.

2. Reagents :

2.1 Aqueous phase studies:

In aqueous phase degradation studies:

- Phenol C_6H_5OH ≥99 % Sigma-Aldrich,
- Formic acid 99% Panreac,
- Aniline ($C_6H_5NH_2$) Sigma-Aldrich,
- Muconic acid (Trans,Trans-Muconic acid) 98% Aldrich,
- Oxalic acid (99% Sigma-Aldrich),
- Sodium hydroxide (≥97% Sigma-Aldrich) and chlorhydric acid (37% Merck) were used to adjust the pH of the samples.

2.2 In gas phase :

- Ethanol (≥ 99,5 % Panreac)
- Ammonium (25-27 % Panreac)
- Sulfuric acid (H2SO4) (≥ 99% Panreac),

- NO_x (Copper + Pan REAC nitric acid HNO_3)

3. Physicochemical characterization of catalysts:

The catalysts were characterized by different physicochemical techniques.

3.1 Transmission Electron Microscopy (TEM) :

A transmission electron microscope uses an electron beam instead of light, exploiting the duality wave-particle of electrons. It is made up of source of electrons, electromagnetic lenses and electron detector. A very thin sample is placed on the path of electrons. An electron beam is produced, accelerated, and then concentrated on the sample through the lenses. The beam crosses through the sample which modifies it, according to its shape and nature and prints its image to the beam. The beam is then enlarged by other lenses and then detected by fluorescence.

A transmission electron microscope (TEM) allows the image of thin samples to be enlarged to atomic resolutions.

Electron microscopy is one of the first characterizations made on samples. Unlike optical microscopy, electron microscopy uses electrons instead of photons to obtain images with magnifications up to 10^5 times. The contrasts in the electron microscopy images are obtained due to the effective sections specific to each atom. If the images are obtained from the electrons that cross the nanoparticles, the technique will be called Transmission Electron Microscopy (TEM).

Information such as morphology, size distribution, and chemical contrast in nanoparticles can be deducted from electron microscopy images. In our case, we use TEM to check the general morphology of samples and make size distribution measurements.

3.2 Scanning Electron Microscopy coupled to EDAX (MET/EDS, EDX or EDAX):

Electron microscope consists of a source of electrons, electromagnetic lenses and an electron detector. It uses an electron beam instead of light, exploiting electrons duality

wave-particle. This beam is produced, accelerated, then concentrated on the sample due to the lenses. The sample then emits secondary electrons which are detected later. The number of electrons detected depends on the variation of sample surface. By scanning the beam and detecting the variation in scattered electrons number, the surface topography can be reconstructed. The electron beam can also ionize atoms to emit X-rays. The energy of these rays depends on the elemental composition of the sample. By scanning the beam again and detecting the emitted X-rays energy, the chemical nature of the compound and its spatial variations can be deduced. Other types of interactions between the beam and the surface also allow different complementary analyzes. The scanning electron microscopy (SEM) thus provides an enlarged surface image of thick samples and also allows to analyze their composition.

After that a primary electron beam interacts with the atoms of the material to be analyzed, X photons are created (de-excitation phenomenon). These photons are collected by a specific detector coupled to SEM to complete the imaging by elemental chemical analysis of surface (denoted EDS, EDX or EDAX).

The samples were prepared under pellets shape using a Specac Eurolabo pelletizer, and analyzed by a scanning electron microscope (FEI Quanta 200) equipped with an EDAX probe (Quantax 70, Bruker) for surface microanalysis. Three image amplifications were carried out for all analysis (300, 3,000 and 30,000) with 5 sampling points in each increase and an exposure time of 300 seconds (fig.III.5).

Figure III.5 :EDAX probe (Quantax70,Bruker)

3.3 X-Ray Diffraction (XRD) :

X-rays have a wavelength of the order of thousandths of a micron, which corresponds exactly to the distances that will be studied in the material.

The X-ray observation of the material is a way to obtain information, at the Angstrom scale, on its internal structure and its organization degree. When order is important the material is said crystalline, its observation by X-ray diffraction is then possible. The internal organization of the material determines further the physical properties of the materials. The determination of the crystalline material structure is based on the analysis of the diffraction figures, which are obtained during the illumination of a material sample by a monochromatic X-ray beam. This measurement is performed by a diffractometer. X-rays invisible to eyes are visualized using a detector to control the irradiation zone. The Bragg law allows to decrypt the diffraction figures; it links the diffracted beam angle to the distances separating the atomic planes in a crystal lattice.

$$2d_{hkl}\sin\theta = n\lambda \qquad \textbf{(III.6)}$$

where d_{hkl} is the interplanar distance between the family plans (hkl),

θ :the diffraction angle,

n :the reflection index,

λ :the X-rays wavelength.

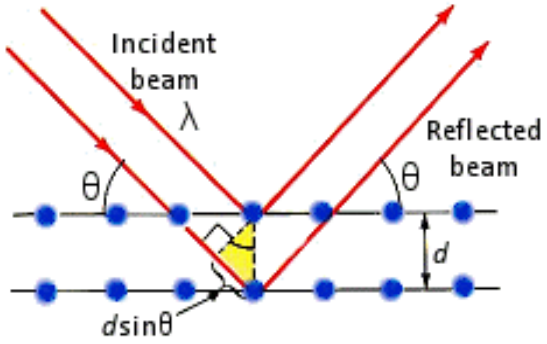

Figure III.6 :X-ray diffraction diagram. θ is the Bragg angle

So depending on the geometry of the crystallographic system and the atoms that compose it, crystalline phases will present diffractograms with diffraction angles and specific intensities to each crystalline phase. These diffractograms are listed in databases such as the International Center for Diffraction Data (ICDD), the American Minerologist Crystal Structure Database (AMCSD) or the Crystal Open Database (COD). It's possible to attribute crystalline phases of a diffractogram by comparing it to the databases references. Given the assigned crystalline phases, it's possible to calculate their lattice parameters from the diffraction angles and the lattice geometry.

For example, for a cubic system, where a=b=c and α=β=γ=90°, the interplanar distance d_{hkl} is related to the lattice parameters by the equation:

$$\boldsymbol{d_{hkl} = \frac{a}{\sqrt{h^2+k^2+l^2}}} \qquad \textbf{(III.7)}$$

The diffractograms of the samples were recorded with a copper anode, $K_{\alpha 1}$=0.15406 nm, at 1.6 kW (40 kV, 40 mA) (figure III.7)**.** The XRD thus allows to identify the main crystalline phases of our material and to estimate the crystallites size (fig III.7).

Figure III.7 : Diffractometer XRD Bruker D8 Advance

3.4 Specific BET surface:

The specific surface expressed in $m^2 \cdot g$ refers to the actual area of an object as opposed to its apparent surface. The measurement consists of determining the nitrogen molecules amount that can be adsorbed at 77 K, its liquefaction temperature, in a monolayer on the material surface. It reminds us that adsorption is the creation of bond between the adsorbed molecule and the surface. This is a weak Van der Waals bond. Knowing the area occupied by a nitrogen molecule allows them to calculate the total surface of the sample analyzed. In fact, nitrogen doesn't adsorb in a single layer on the material surface but in several layers whose number depends on the nitrogen partial pressure above the material.

To describe this phenomenon, Brunauer, Emmet and Teller proposed a model called BET. This model allows to determine the number of nitrogen moles in the first layer, and that's from the recording of adsorbed nitrogen amount depending on its partial pressure.

The device includes:

* A V_c volume measuring cell containing the sample,

* A liquid nitrogen Dewar allowing the sample temperature to reach 77K,

* A ball (flask) with calibrated volume noted V_b,

* A tube set of V_t volume,

* Valves to put in communication the different parts of the assembly,

* A pumping group to evacuate the device,

* A pressure gauge,

* Finally, two cylinders containing nitrogen and helium.

Initially the flask is filled with a nitrogen pressure and the rest of the device is under vacuum. By progressive opening of the valve v_1, the tubes set are filled with a nitrogen pressure P_1.Knowing tubes volume and temperature, the perfect gas law allows us to

calculate the number of moles N_1 in tubes volume. By opening the valve, the gas filled the entire volume, tube + cell, and a new pressure P_2 is reached. The perfect gas law allows to determine the number of moles N_2 of nitrogen, in the gas phase. The difference between $N_1$and N_2 corresponds to the adsorbed nitrogen under equilibrium pressure P_2 ($N_1 - N_2 = N_{ads}$).To make this calculation, it is necessary to know V_t tubing volume and V_c cell volume, for this, the same process is done with helium which doesn't adsorb at 77K.The conservation of the moles number allows to deduce the volumes V_c and V_t.

A micromeritic model analyzer 2010 instrument was used for the determination of BET surface (Brunauer-Emmett-Teller). Behold figure III.8.

Figure III.8 : BET Micromeritics 2010 insctrument

The samples are degassed at 160°C for 1h30min under vacuum, to evacuate the most volatile compounds, and then weighed accurately.

3.5 Diffuse reflectance spectroscopy (DRS, UV-Visible):

DRS (Diffuse Reflectance Spectroscopy) is one of the most important techniques to obtain information about the electronic structure of components of heterogeneous system. Reflectance corresponds to the photons quantity diffusely reflected on the surface of a solid after absorbing incident photons. Reflectance of the samples in the UV-VIS range was measured in percentage, using a UV-visible spectrophotometer

(Varian Cary 5, UV-Vis). DRS was also used to deduce the width of the material band gap (E_g).

To determine the absorption wavelengths of different samples, the Kubelka-Munk method [11] based on the absorption spectrum was used. (fig III.9).

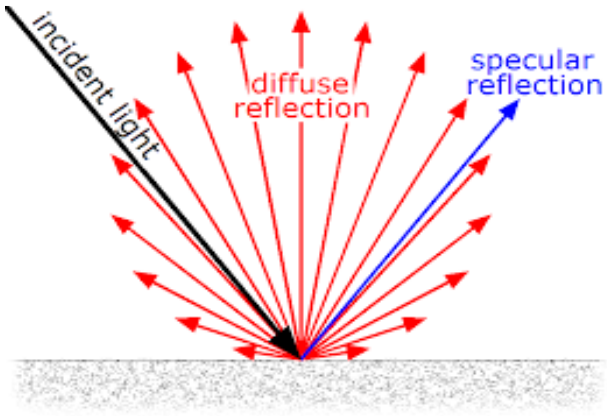

Figure III.9 : Diffuse Reflectance Spectroscopy

The values of the reflectance R can be related to the solid absorption coefficient by the Kubelka-Munk method by the expression :

$$\alpha = \frac{(1-R)^2}{2R} \qquad \textbf{(III.8)}$$

For a semiconductor with an indirect gap such as TiO_2 (the main catalyst in this work), the E_g energy value can be obtained from Tauc's equation:

$$\alpha h\upsilon = B(h\upsilon - E_g)^2 \qquad \textbf{(III.9)}$$

Where:

h :Planck's constant,

ν :Photon frequency,

B :Constant.

The curve $(\alpha h\upsilon)^{1/2}$ in terms of hυ has a point of inflection. The intersection between the tangent passing through this point and the x-axis corresponds exactly to E_g value.

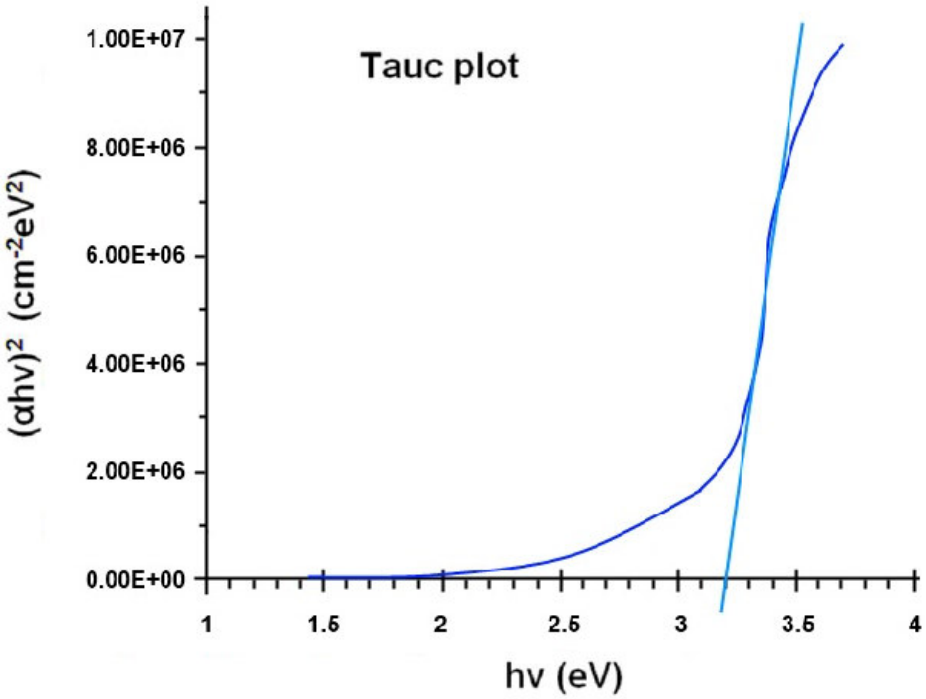

Figure III.10 :Example of indirect gap

The DRS $(\alpha h\upsilon)^{1/2}$= f (hυ) spectrum were recorded on a Varian Cary 5 spectrometer equipped with an integrating sphere using polytetrafluoroethylene (PTFE) as reference.

3.6 Fourier Transform InfraRed spectroscopy (FTIR) :

To obtain an infrared spectrum, electromagnetic radiation is focused on the sample. This radiation is between visible and microwave ranges. Therefore, the IR wavelength is greater than the visible one, which corresponds to lower energy. The incident intensity is called I_0 and the outgoing intensity **I** is measured. And a graph representing absorbance vs. wavelength is obtained. The device used is called a Fourier transform spectrophotometer.

Transmittance evaluates the ratio of the outgoing intensity **I** to the incoming intensity I (I_0):

$$\mathbf{T = \frac{I}{I_0}} \qquad \textbf{(III.10)}$$

If T = 100%, it means that all of the radiation has passed through the window and that the chemical species has not absorbed the electromagnetic radiation.

If T < 100%, only part of the incident radiation has passed indicating that the chemical species of the sample have absorbed part of this radiation.

Then, the transmittance (%) is plotted against the wavenumber (from right to left), which is related to wavelength by the following relation:

$$\bar{\nu}\,(\mathbf{cm^{-1}}) = \frac{\mathbf{1}}{\boldsymbol{\lambda}\,(\mathbf{cm})} \qquad \textbf{(III.11)}$$

For the study of spectrums concerning the different molecules to be analyzed the wavenumber range will be from 500 cm^{-1} to 4000 cm^{-1} which corresponds to the average infrared.

To understand an infrared spectrum, we must first consider molecules as a set of masses (atoms of different masses) connected by variable stiffness springs (bonds). It means that each bond corresponds to a more or less tense /stretched spring and that each atom represents a more or less heavy mass.

The energy of infrared electromagnetic vibrations will be converted into vibration energy. Indeed, each molecule bond will oscillate more and more strongly and enter into resonance for a frequency that will be proper to it. So each bond vibrates at a precise frequency. Elongation vibrations correspond to distance variation between two atoms along the bond axis. There are two types of molecular vibration for this type of vibrations, asymmetrical elongation and symmetrical elongation. But also there are angular deformations which correspond to angle variation separating two successive bonds, as for example:

* The rocking/sway between the two bonds,

* Or the shear,

* Or simply the rotation between the two successive bonds,

* Or finally the twist.

Each of these vibrations will result in the infrared spectrum by different absorption bands. Infrared spectroscopy is therefore widely used to determine the functional groups of a molecule.

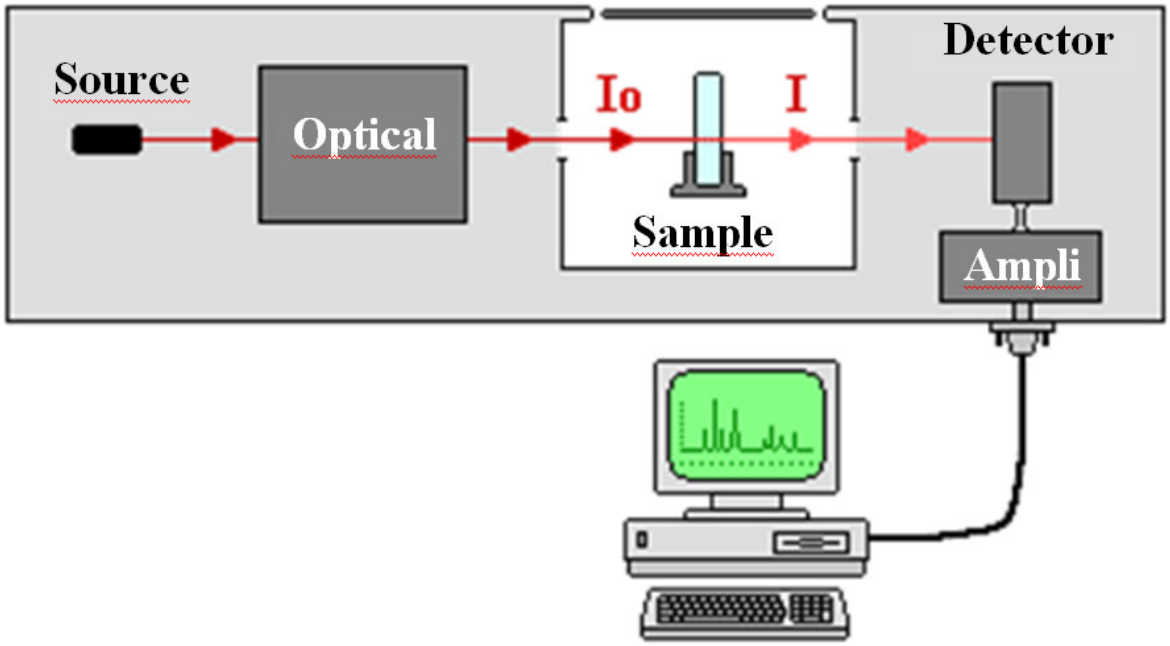

Figure III.11 :Operatingprinciple of FTIR

The powders of the samples were analyzed by a Fourier transform infrared spectrometer (Thermo-Scientific-Nicolet iS10) having a custom-madecell equipped with CaF_2 windows performing 32 scans with a spectral resolution of 4 cm^{-1} where the band range varied from 500 to 4000 cm^{-1}.

Figure III.12 : Fourier transform infrared spectrometer model Thermo-Scientific-NicoletiS10

4. Analytical techniques :

4.1 Analysis of Total Organic Carbon concentration:

The TOC value completely determines the biochemically difficult and non biodegradable compounds that are important for the assessment of water pollution. In order to determine the total carbon content, the organic molecules must be converted into a molecular form that can be quantitatively measured. This molecular form is carbon dioxide (CO_2). So this analysis aims to oxidize organic carbon, transform it into carbon dioxide, and then measure it. The conversion requires the use of chemical agents (such as persulfates), exposition to ionizing radiation (e.g. ultraviolet light)or combustion (T=680°C in the presence of a platinum catalyst), and pure oxygen to convert organic carbon to inorganic carbon (CO_2).

During this work, the TOC contents were measured using a TOC-meter model TOC-L CSH / CSN Shimatdzu (Figure III.13).

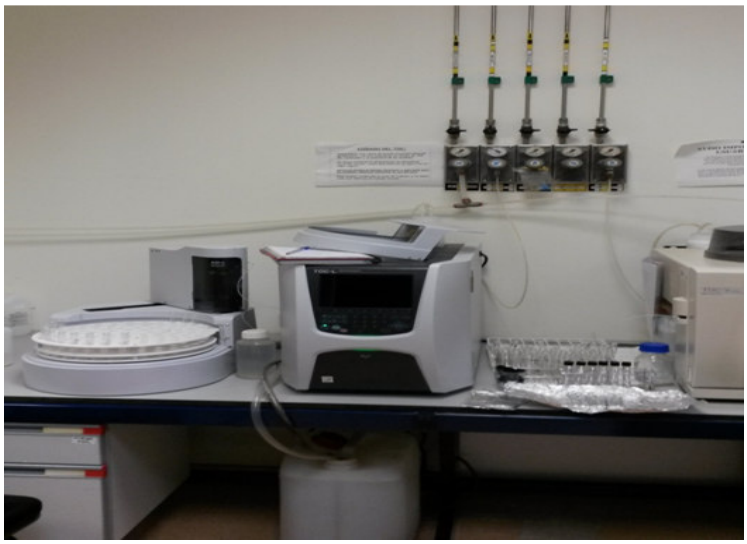

Figure III.13 : Experimental apparatus for the Total Organic Carbon measurement

Catalytic combustion at 680°C allows the complete combustion of the sample by heating at high temperature in an environment rich of oxygen. This is facilitated by using a catalyst made of platinum supported on alumina beads. The oxidation through combustion does not require any pretreatment or post-treatment using oxidizing agents which greatly simplifies the system. The resulting carbon dioxide is detected by a Non Dispersive Infra Red sensor NDIR.

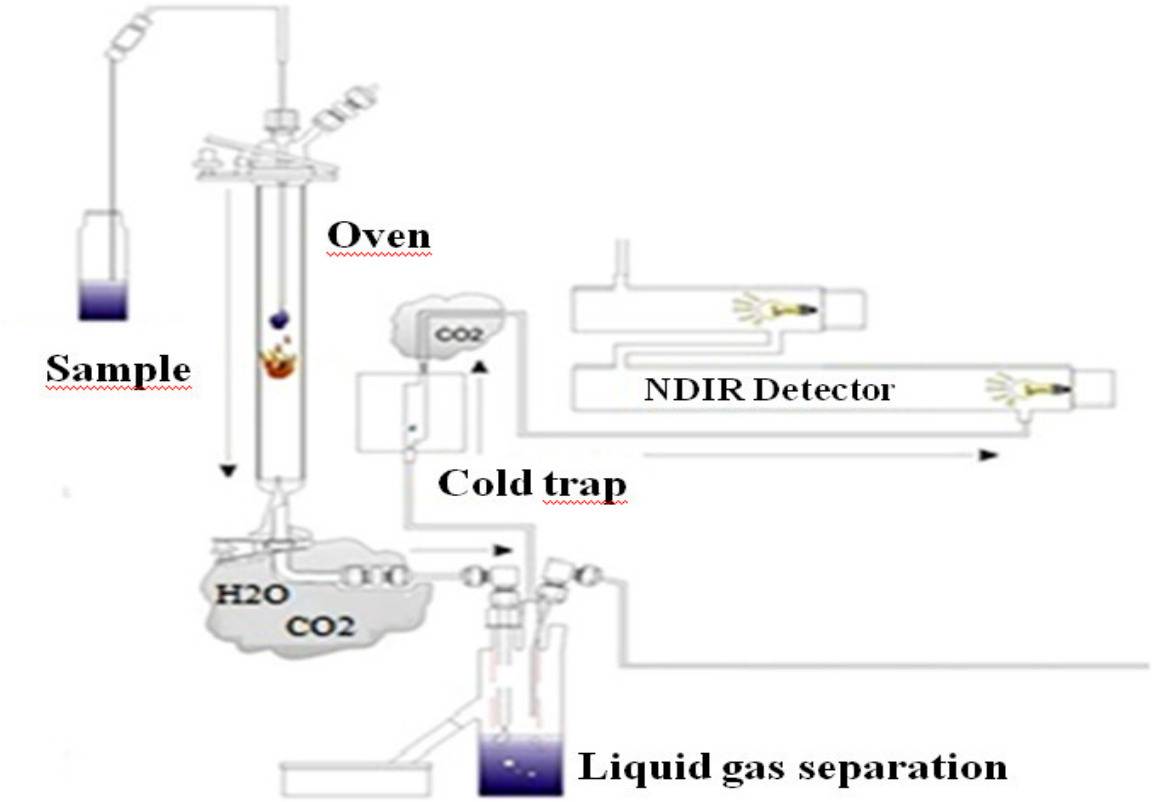

Figure III.14 :TOC-meter operating principle.

Knowing that total carbon (TC) is the sum of total organic carbon (TOC) and total inorganic carbon (TIC), TOC is calculated by the following formula:

$$TOC = TC - TIC \qquad \text{(III.12)}$$

For the total inorganic carbon (TIC) determination, the device only considers the bicarbonates (HCO_3^-) and carbonates ($CO_3^{=}$). This TIC is determined by acidifying the sample with H_3PO_4. Then the CO_2 being purged / removed from the sample by air bubbling corresponds to the TIC.

A calibration curve is carried out with organic carbon solutions (potassium phthalate) and inorganic carbon solutions (carbon and sodium bicarbonate). The calibration values (TC and TIC) are checked every working day.

4.2 High Performance Liquid Chromatography (HPLC) analysis:

High performance liquid chromatography HPLC is a technique that separates compounds from a mixture, based on the use of two phases, mobile phase and stationary phase. The liquid mobile phase displaces the sample, and the stationary phase is located inside the column. Substances to be separated (solutes) are dissolved in a solvent. This mixture is introduced into the liquid mobile phase (eluent). Chromatographic conditions used correspond to the reverse phase chromatography, according to the polarity of the stationary and mobile phases, and the isocratic mode was used in connection with the composition of the mobile phase. Mobile phase composition was kept constant. No gradient was applied.

Depending on the nature of the molecules, they will interact more or less with the stationary phase contained within a chromatographic column. And, depending on the strength of the interaction, it will take a longer or shorter time to leave the column pushed by the elution forces of the mobile phase that flows constantly through the system. These time distribution is collected in a chromatogram that contains a set of peaks were registered by proper detector. Whenever a peak is recorded on the chromatogram, it is obtained the retention time of a given molecule included in the mixture which is injected.

The mobile phase is driven by a pump under high pressure, runs through the chromatographic system. The mixture to be analyzed is injected then transported through this system. And the compounds to be separated are selectively distributed between the mobile phase and the stationary phase according to their molecular weight, size or charge. With the aid of a proper detector at the column outlet, the different solutes are characterized by peaks each one with a specific retention time. The set of recorded peaks is called chromatogram.

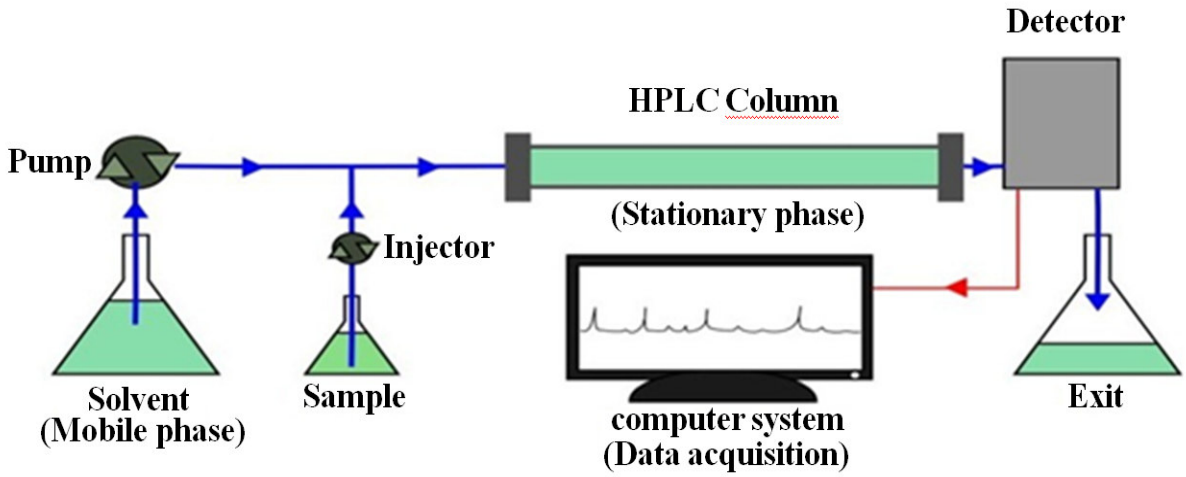

Figure III.15: HPLC operating principle.

Two experimental set ups were used in this study.

The first one, an Agilent ProStar, is used to identify phenol and its reaction intermediates. This device is equipped with:

- A UV/Vis detector with 8 diode.
- Wavelength was fixed at 270 nm.
- A Supelco Discovery C18 column (250mm in length, inner diameter of 4.6mm, 5 µm particles size).

Figure III.16: The first HPLC device

The analysis conditions are grouped in the following table :

Product	Phenol
Mobile Phase	30% Acetonitrile (ACN) + 70% Water
Quantity injected	10 µL
Flow	1 mL·min^{-1}
Wavelength	270 nm
Column	SupelcoDiscoveryC18 (4.6 x 250mm)
Temperature	Room temperature

Tableau III.1: Chromatographic conditions for HPLC analysis.

The second equipment, a Varian instrument (detector and pump) with a Pro-Star 410 automatic sampler, was used for the identification of oxalic acid and formic acid, equipped with:

- A spectrophotometric detector of photodiodes in the ultraviolet visible range (UV-Vis with a diode-array).
- A ternary and isocratic pump alternatively were used. The first one was a Varian model 9010 and second one ProStar 220. Both were used in Isocratic mode.
- A Supelco Discovery C18 column (250 x 4.6mm, 5µm particles size).
- Oven for the column, model Methaterm (temperature was fixed at 25ºC).

Figure III.17: The second HPLC device

The analysis conditions are grouped in the following table:

Product	Acids
Mobile Phase	Aqueous solution phosphoric acid 0.1% $_{wt}$
Quantity injected	20 µL
Flow	1 mL·min^{-1}
Wave length	210nm
Column	Supelcogel C-610H (300 x 7.8mm)

Tableau III.2: Chromatographic conditions for HPLC analysis

4.3 Ion chromatography (IC) analysis:

This technique is used to separate and identify ions in solution and to measure its concentration. In this thesis a DIONEX ion chromatograph LC25, with an AS40 autosampler was used. The device is equipped with:

- ED50 Electrochemical detector,
- LC25 chromatography Oven,

- IonPac AS11-HC columnfor anions(250x4mm), with an AG11-HC (4x 50mm) precolumn, Dionex AERS 500 4mm suppressor with an applied current of 90mA. Mobile phase was (NaOH 60mM 50%$_{vol}$: 50%$_{vol}$ water) to a flow of 1.5ml·min^{-1},
- IonPac CS11-HC columnfor cations (250 x 4 mm), with a CG12A (4 x 50mm) precolumn, Dionex CERS 500 4mm suppressor with an applied current of 59mA. Mobile phase (Aqueous 20mM methane sulfonic acid) to a flow of 1.5ml·min^{-1}, (this column did not use in this Thesis).
- GP50 gradient pump.

Figure III.18: Ion chromatography equipment

The analysis conditions are grouped in the following table:

Product	Formic acid
Mobile Phase	NaOH 60mM 50%$_{vol}$: 50%$_{vol}$ water
Quantity injected	25 µL
Flow	1.5 mL·min^{-1}
Column	IonPac AS11-HC (4x250mm)
Temperature	30ºC

Table III.3: Conditions of ion chromatograph analysis

4.4 Toxicity analysis by *Vibrio Fischeri* bacteria luminescence tests:

The bacterium ***Vibrio fischeri*** is a marine microorganism that naturally emits light. The bioluminescence phenomenon in this bacterium is related to the energy cycle of the cell. A bioluminescence inhibition can therefore be interpreted as a disturbance of the bacterium energetic metabolism.

The objective of this study is the use of *Vibrio fischeri* emitting light to detect water samples and chemicalstoxicity. The intensity of the bioluminiscence depends on the toxicity to *Vibrio fischeri* of the compounds present in the medium.

The samples are incubated at a temperature of 15°C in contact with *Vibrio Fischeri* bacteria (NRRL B-11177) for 30min. The intensity of luminescence after incubation is measured by the Microtox apparatus, and compared to the luminescence intensity of pure bacteria. The method is fast and practically sensitive to the presence of phenol. The sample is considered toxic if the inhibition percentage is greater than 10% according to the standard ISO 11348-2: 2007.

The device used to measure the bioluminescence emitted by the bacteria was a luminometer OPTOCOMP I - MGM Instrument equipped with a photon counter. The luminometer was programated and calibrated to present results in inhibition percentage.

Figure III.19: Toxicity apparatus

5. Analytical techniques for gas phase studies:

All the experiments done in gas phase were carried out in the system mentioned in Figure (III.20) under fume hood.

This system consists of a pump with an air flow of 60 $mL \cdot min^{-1}$ connected to reactor filled by a solution containing ethanol:water $(2:1)_{vol}$. The resulting air, which contains ethanol-water vapors was introduced into cylindrical glass reactor (20cm long * 4mm inner diameter) containing the catalyst. We covered this cylindrical reactor to make darkness inside. Masses introduced of our studied catalyst were different, 0.02g if it's commercial and 0.1g if it's lab-made one. The system consists also of a second reactor connected to the cylindrical reactor and filled by water. The experiment lasts 60 min.

The same system is used for the ammonium gas analysis, but with filling the first reactor by ammonium (25%) and the second reactor by a solution containing H_2SO_4:H_2O $(1:1)_{vol}$. Catalysts were treated with gas generated by bubbling air through the ammonium at room temperature for 90 min and then placed in the cell for FTIR analysis.

Blank experiments of photolytic evolution of were carried out in the absence of catalyst and under the same experimental conditions, reactants remained unaltered throughout the assay.

Figure III.20: Experimental setup of gas phase studies

References:

[1] LEE, Jim, EASTEAL, A. J., PAL, U., et al. Evolution of ZnO nanostructures in sol–gel synthesis. Current Applied Physics, 2009, vol. 9, no 4, p. 792-796.

[2] Wang, J., Khoo, E., Lee, P. S., & Ma, J. (2009). Controlled synthesis of WO3 nanorods and their electrochromic properties in H2SO4 electrolyte. The Journal of Physical Chemistry C, 113(22), 9655-9658.

[3] BRINKER, C. Jeffrey et SCHERER, George W. Sol-gel science: the physics and chemistry of sol-gel processing. Academic press, 2013.

[4] DING, Xing-Zhao, QI, Zhen-Zhong, et HE, Yi-Zhen. Effect of hydrolysis water on the preparation of nano-crystalline titania powders via a sol-gel process. Journal of Materials Science Letters, 1995, vol. 14, no 1, p. 21-22.

[5] Materiaux, Guillaume Speurt, Juin2010.

[6] Course "Les semi-conducteurs".

[7] BASE, DEVELOPPEMENT D.'UN REACTEUR A. Anne DANION. 2004. Thèse de doctorat. ECOLE CENTRALE DE LYON.

[8] T. Morikawa R. Asahi, T. Ohwaki, K. Aoki, Y. Taga. Band-Gap Narrowing of Titanium Dioxide by Nitrogen Doping. Jpn. J. Appl. Phys. 2001, 40, 561-563.

[9] S. Sato. Photocatalytic activity of NOx-doped TiO2 in the visible light region. Chemical Physics Letters. 1986, 123, 126-128.

[10] R. Asahi, T. Morikawa, T. Ohwaki, K. Aoki, Y. Taga. Visible-Light Photocatalysis in Nitrogen-Doped Titanium Oxides. Science. 2001, 293, 269-271.

[11] K. Macounova. J. Urban, H. Krysova, J. Jirkovsky, J. Ludvik. Photodegradation of Metamitron (4-Amino-6-Phenyl-3-Methyl-1, 2, 4-Triazin- 5(4H)-One) on TiO2. J. Photochem. Photobiol. A: Chem. 2001, 140, 93-98.

CHAPTER IV

SCREENING OF BARE AND MODIFIED ZnO, ZrO_2, WO_3 AND TiO_2(CL) PHOTOCATALYSTS FOR PHOTOCATALYTIC DEGRADATION OF PHENOL

Screening of bare and modified ZnO, ZrO_2, WO_3 and TiO_2(Cl) photocatalysts for photocatalytic degradation of phenol

1- Introduction

The aim of this part of work is to study the degradation of phenol in liquid phase, using different catalysts including ZrO_2, ZnO, WO_3 and TiO_2, to select the best material to be studied in this thesis. A study is also undertaken of the effect of the fluorination of these materials on degradation. These studies were carried out as explained before in the part of reaction protocols (chapter 3).

2- Experimental procedure

2.1 – Photocatalysts

This experiments were carried out using 4 types of photocatalysts :

- Commercial ZnO
- Synthesized ZnO
- Synthesized WO_3
- Commercial ZrO_2
- Synthesized TiO_2

2.2 – Pollutants:

In this aqueous phase degradation studies, the organic pollutant used as test target is phenol (C_6H_5OH) because it is a vastly studied molecule in this field and our results can be compared with those obtained by many researchers as reference.

2.3 - Liquid phase studies :

This photocatalytic degradation studies were developed in a cylindrical Pyrex glass reactor by filling it with 200ml of pollutant and $1g \cdot L^{-1}$ of photocatalyst.

The experiments were carried out following exactly the procedure described in the paragraph: Degradation Protocol- In liquid phase from chapter 3.

2.4 – Characterization :

The efficiency of the different catalysts for photocatalytic purposes was studied by High Performance Liquid Chromatography (HPLC) and Total Organic Carbon (TOC). The image of the surface of the products obtained were analyzed by Scanning Electron Microscopy (SEM). BET surface area measurements were carried out.

3- Results and discussion:

Merck ZnO (ZnO,com) and Chemco ZrO_2 (ZrO_2) are the commercial catalysts studied. ZnO (ZnO,syn), WO_3 (WO_3,syn) and TiO_2 (TiO_2(Cl)) were synthesized for this study.

3.1- BET area and SEM analyses:

The following table shows the surface area and particle size of non-fluorinated studied catalysts:

Catalyst	surface area ($m^2 \cdot g^{-1}$)	Diameter (nm)
ZrO_2	15.10	70-90
ZnO,com	12.09	30
ZnO,syn	9.67	40
WO_3,syn	14.31	40-50
TiO_2(Cl)	47.18	3 - 6

Table IV.1 - Characteristics of the non-fluorinated studied catalysts

The sequence of surface area, is:

$$\mathbf{TiO_2(Cl) > ZrO_2 > WO_3, syn > ZnO, com > ZnO, syn}$$

The sequence of particle size, is:

$$\mathbf{ZrO_2 > WO_3, syn > ZnO, syn > ZnO, com > TiO_2(Cl)}$$

Figures (IV-1)-(IV-5) shows the SEM micrographs of the different photocatalysts mentioned above. The SEM images show the differences in particle sizes of these materials.

The ZnO,syn and WO_3,syn have more or less similar particle sizes on the order of 40nm. The ZrO_2 and WO_3,syn have more or less similar surface areas, having values of 15.10 $m^2 \cdot g^{-1}$ and 14.31 $m^2 \cdot g^{-1}$ respectively. And they have a more irregular particle distribution with larger and smaller particles than the other catalysts, between 70-90nm and 40-50nm respectively.

It can also be seen that the TiO_2(Cl) have the largest surface area and the smallest particle size.

Different studies have shown a strong relation between particle size and photoactivity. In fact, it has been indicated that the size of the particles can influence on the absorption efficiency and photocatalytic activity [1,2,3].

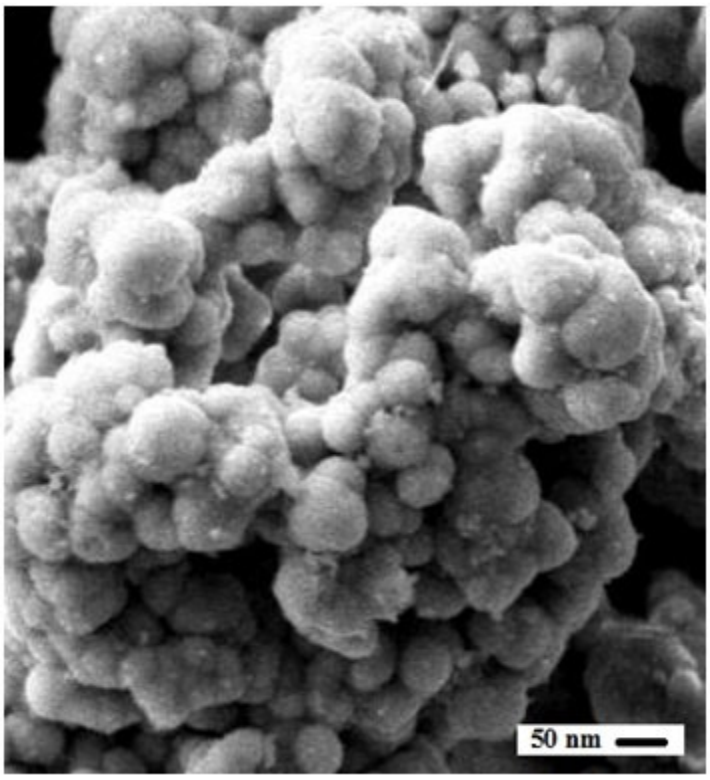

Figure IV-1: SEM image of ZrO_2

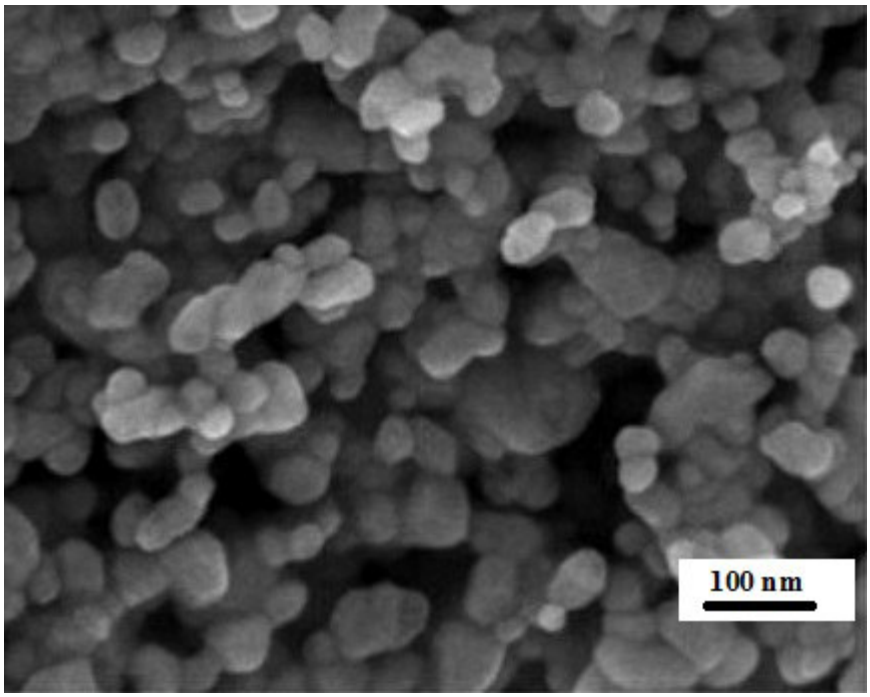

Figure IV-2: SEM image of commercial ZnO

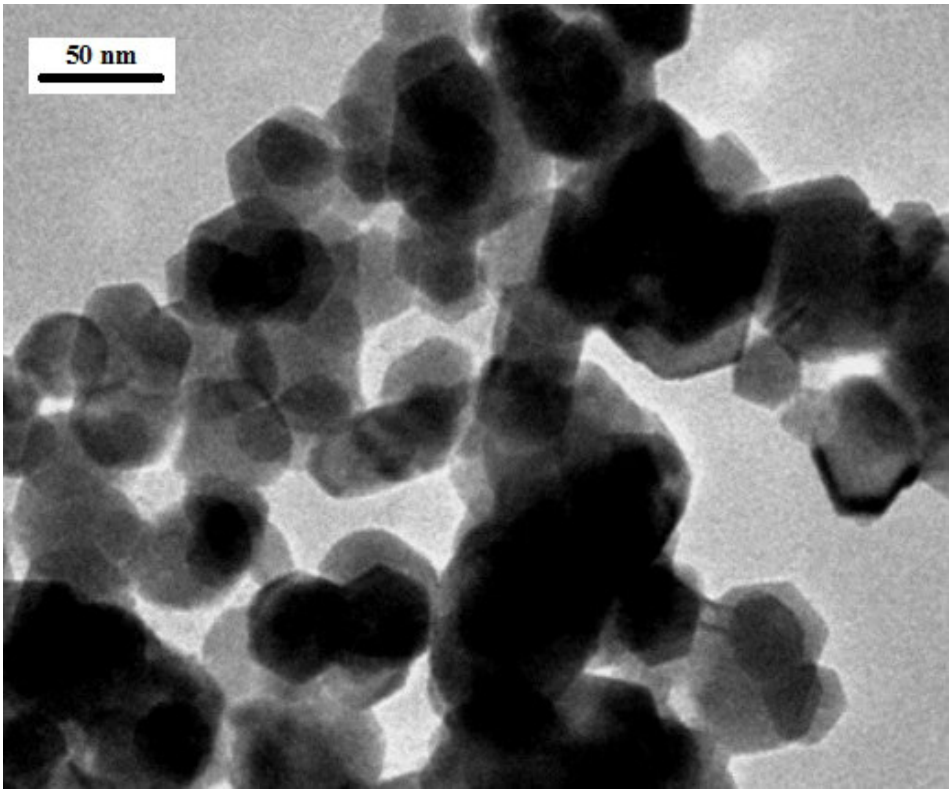

Figure IV-3: SEM image of synthesized ZnO

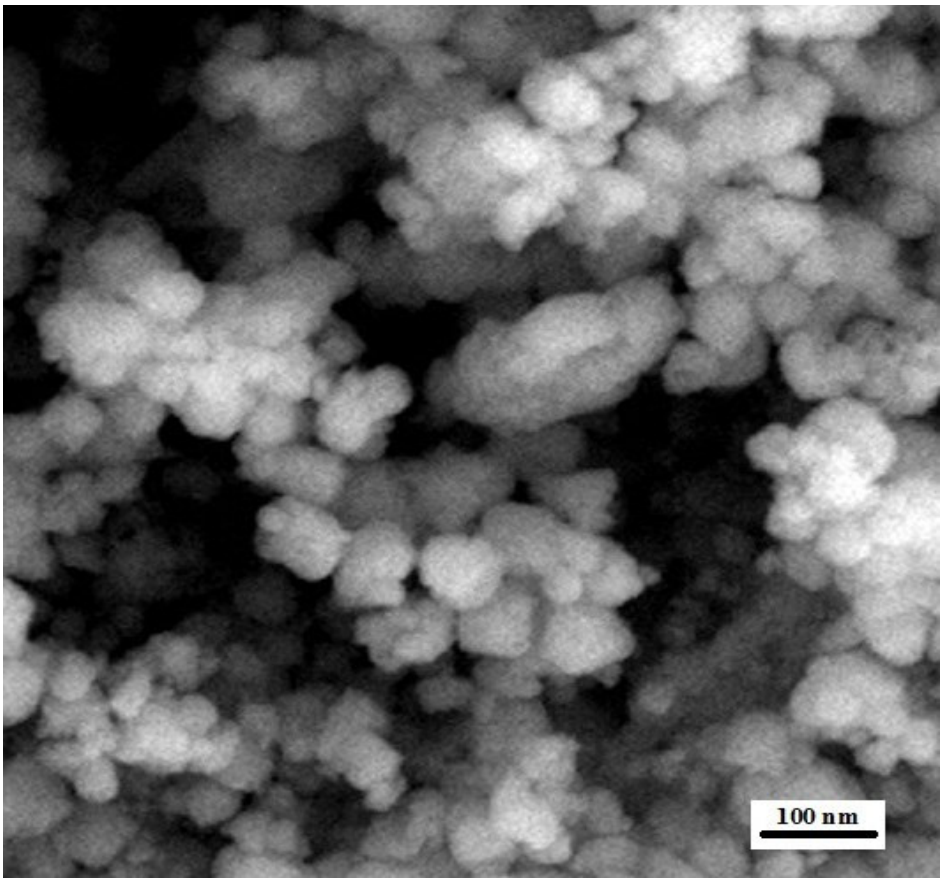

Figure IV-4: SEM image of synthesized WO_3

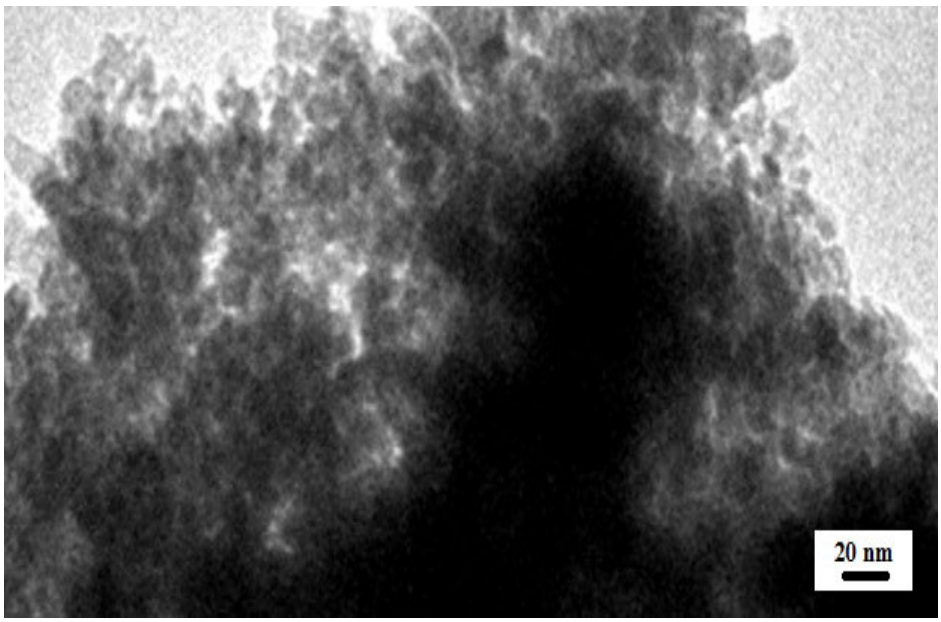

Figure IV-5: SEM image of synthesized TiO_2(Cl)

3.2- Degradation of phenol:

Degradation studies of phenol in aqueous phase were developed at pH= 5 with all catalysts, including those fluorinated ones.

3.2.1- Non-fluorinated catalysts:

The sequence of rate constants, is:

$$\mathbf{TiO_2(Cl) > ZnO, syn = ZnO, com > WO_3, syn = ZrO_2}$$

The sequence of initial degradation rate, is:

$$\mathbf{TiO_2(Cl) > ZnO, syn \geq ZnO, com > WO_3, syn \geq ZrO_2}$$

The results obtained for the different rate constants and the initial degradation rate of the various studied photocatalysts show a clear relation if ignoring the TiO_2(Cl) in the sequences. Inverse correlation between the rate constants and the diameter of the particles and an inverse correlation between the initial degradation rate and the surface area have been observed. This phenomenon was already concluded by Thiele and Ernest in their study using mathematical treatment [4] and by Anju et al. [5].

Catalysts	$C_{0\ (mg\cdot L^{-1})}$	k (min^{-1})	R^2	$(-)r_{0\ (mg\cdot L^{-1}\cdot min^{-1})}$
ZrO_2	48,197	0,001	0,876	0,048
ZnO,com	48,534	0,004	0,977	0,194
ZnO,syn	49,015	0,004	0,999	0,196
WO_3,syn	48,924	0,001	0,975	0,049
TiO_2(Cl)	46,205	0,010	0,980	0,462

Table IV.2 – Kinetic results of phenol degradation using non-fluorinated photocatalysts

The photocatalysts which show the highest degradation rate constant after TiO_2(Cl) are synthesized and commercial ZnO and they showed similar rate constants. However,

the commercial ZrO_2 and synthesized WO_3 rate constants are similar and lower than the previous ones while they have the highest particle sizes. So, it should be noted that there is a clear relationship between the diameter of the particles and the degradation rate as mentioned above.

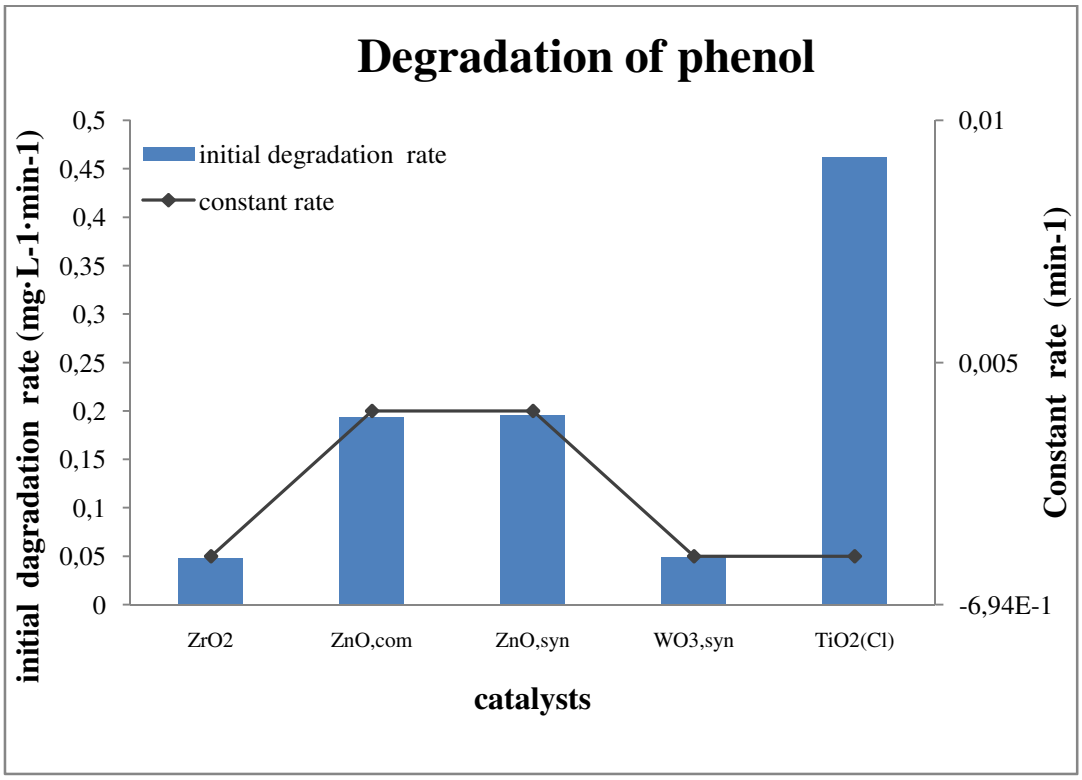

Figure IV.6 – Degradation of phenol

The percentages of mineralization of catalysts compiled in the following table. The percentage of mineralization using TiO_2(Cl) catalysts reached a maximum of 83,72%.

Catalysts	Mineralization
ZrO_2	4,43%
ZnO,com	19,81%
ZnO,syn	17,12%
WO_3,syn	4,56%
TiO_2(Cl)	83,72%

Table IV.3 - Percentages of mineralization of phenol

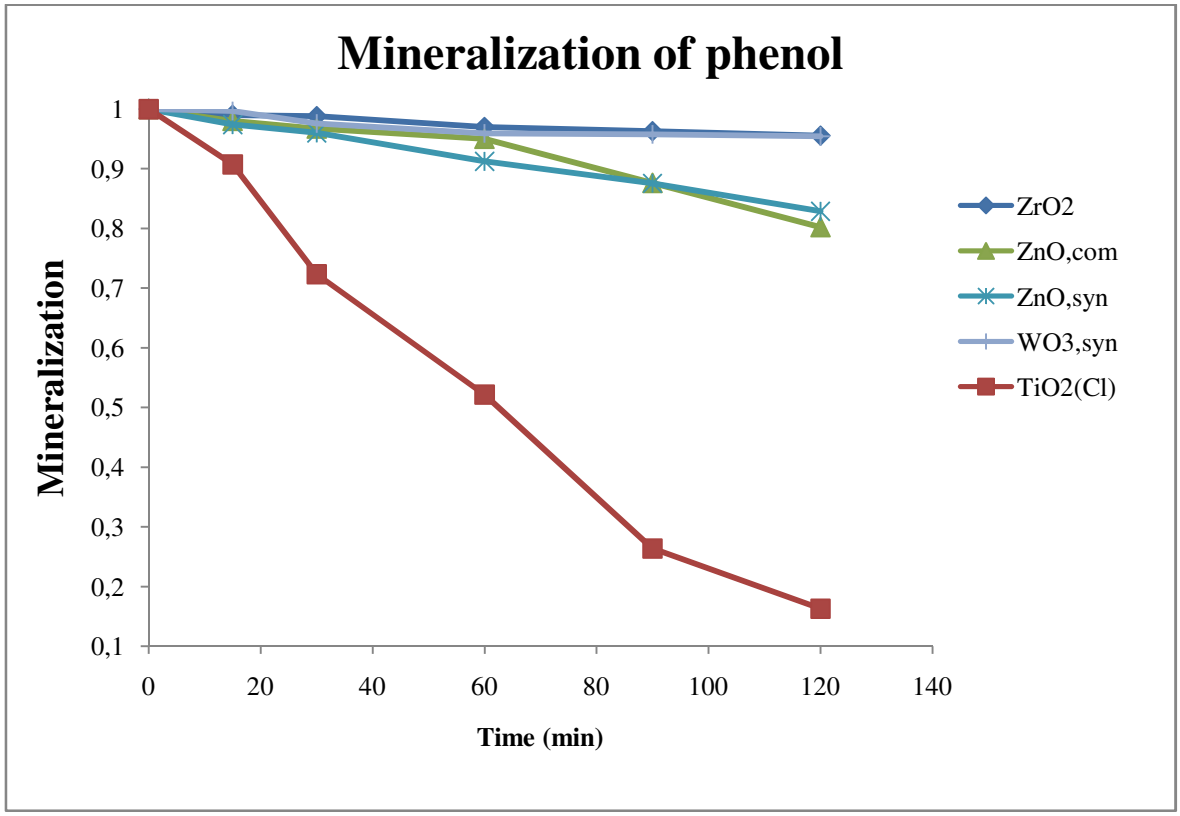

Figure IV.7 - Mineralization of phenol

The phenol mineralization sequence is:

$$\mathbf{TiO_2(Cl) > ZnO(com) \geq ZnO(syn) > WO_3 \geq ZrO_2}$$

Based on TOC analysis data when using commercial ZnO, the phenol mineralization with this catalysts under UV is divided into two stages: a slow decrease of TOC concentration and a second step which becomes faster after 60 minutes of illumination. Moreover, based on TOC analysis data of TiO_2(Cl), the phenol mineralization with this catalysts under UV is divided into two stages also: a fast and strong decrease of TOC concentration and a second step which becomes slower after 20 minutes of illumination. The opposite behavior has been observed in a study done before, where they showed two different stages also but inverse than our results, a slow first stage and a second faster one [6,7,8,9].

The following figures show the concentration profile of the intermediates of phenol degradation observed with ZrO_2, ZnO,com, ZnO,syn, WO_3,syn and TiO_2(Cl) catalysts (Figures IV.8-IV.12) .

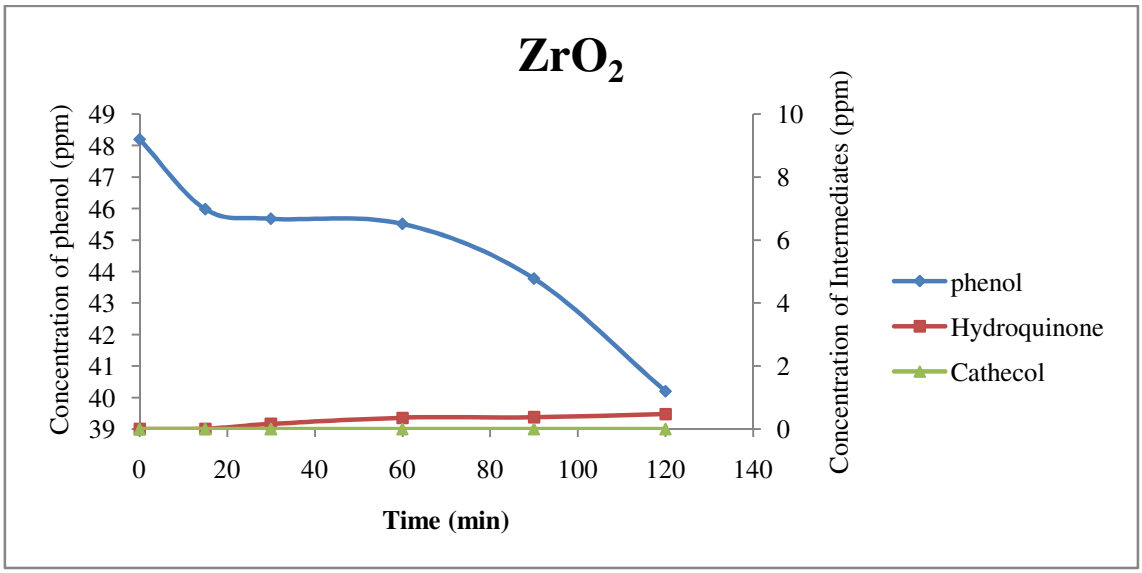

Figure IV.8- Concentration profile for phenol degradation and its degradation intermediates, catechol and hydroquinone with ZrO_2

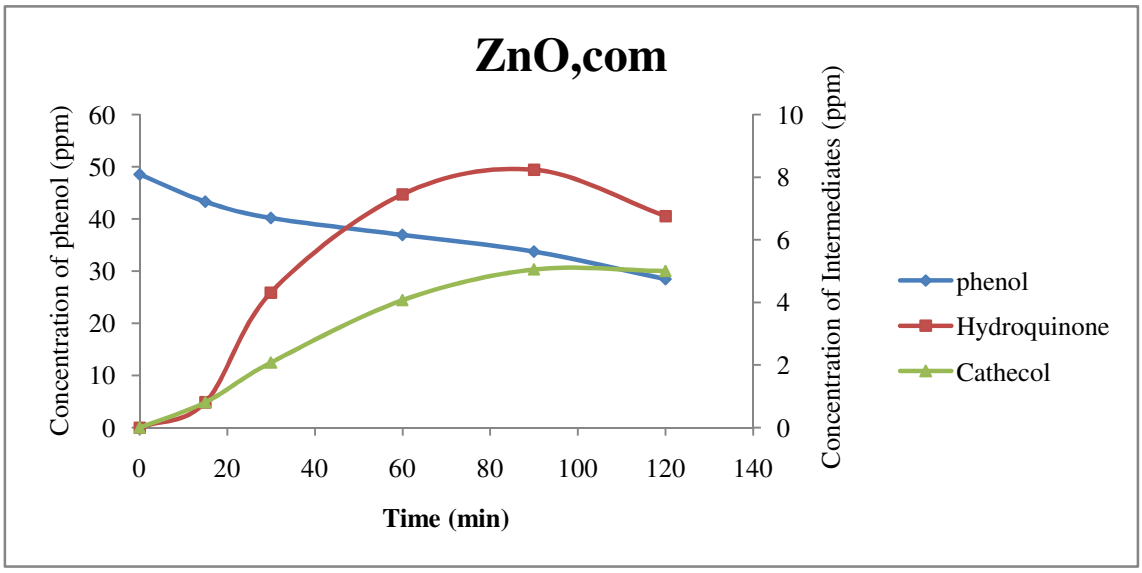

Figure IV.9- Concentration profile for phenol degradation and its degradation intermediates, catechol and hydroquinone with ZnO,com

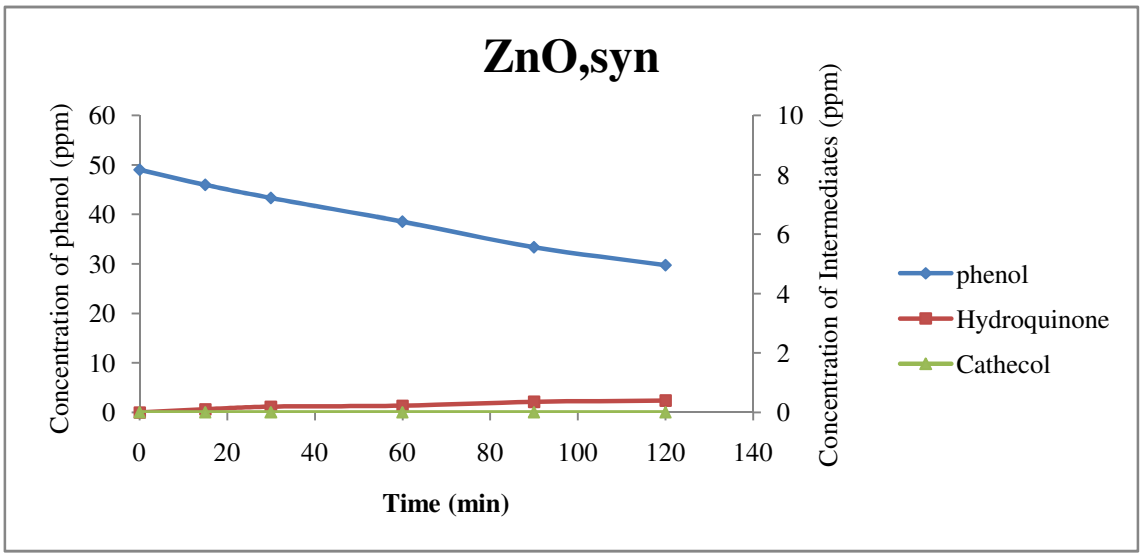

Figure IV.10- Concentration profile for phenol degradation and its degradation intermediates, catechol and hydroquinone with ZnO,syn

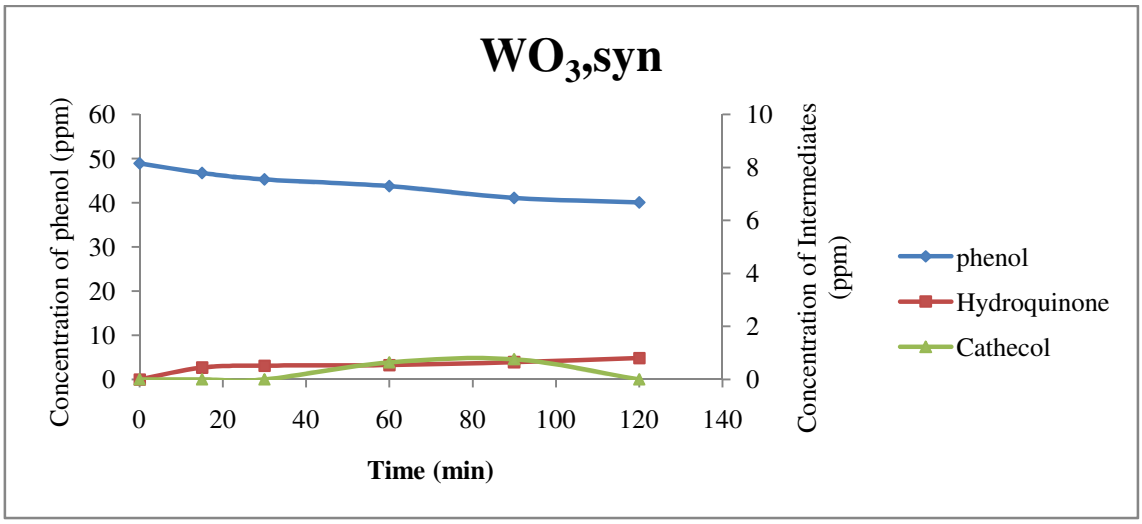

Figure IV.11- concentration profile for phenol degradation and its degradation intermediates, catechol and hydroquinone with WO_3,syn

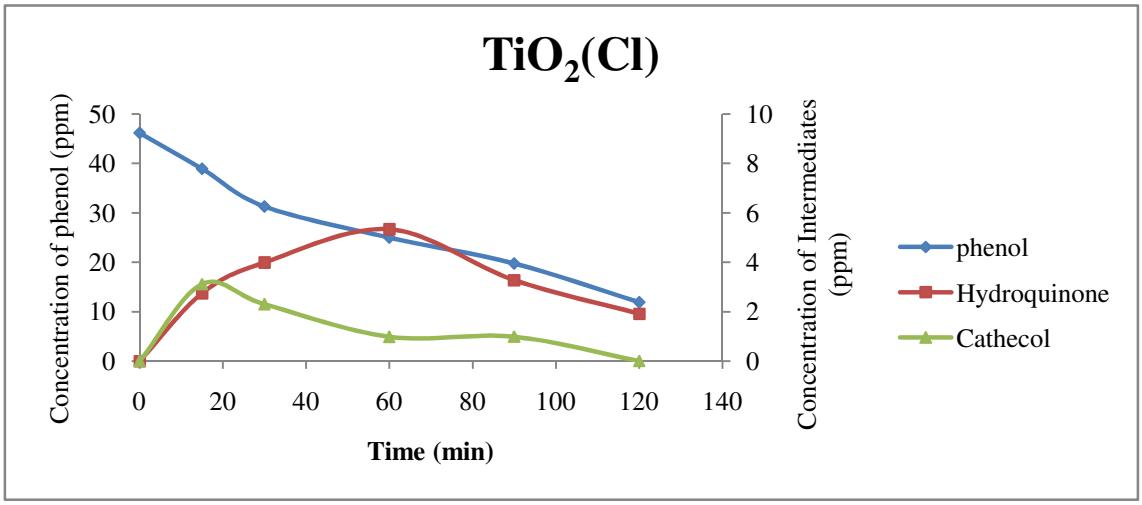

Figure IV.12- concentration profile for phenol degradation and its degradation intermediates, catechol and hydroquinone with TiO_2(Cl)

Catechol and hydroquinone are intermediate products of the phenol photocatalytic degradation reaction, and we can see that they don't appear when using ZrO_2, synthesized ZnO and WO_3.

By analyzing the evolution of phenol degradation intermediates for the commercial ZnO and TiO_2(Cl) photocatalysts, it is observed that as the phenol degrades, catechol and hydroquinone appear up to a maximum value from which they degrade completely in the case of TiO_2(Cl). However, the maximum intermediates concentrations are not the same for that two catalysts. We can see that the maximum formation of hydroquinone for both commercial ZnO and TiO_2(Cl) is reached at 60 min of phenol degradation.

3.2.2- Fluorinated catalysts:

In order to prepare a fluorinated photocatalyst (F-MO_x) we follow exactly the protocol explained before in the part of Anionic fluoride doping - chapter 3.

The results obtained for the different rate constants and the degradation rate of the fluorinated studied photocatalysts are shown in the following table:

Catalysts	$C_{0\ (mg\cdot L^{-1})}$	k (min^{-1})	R^2	$(-)r_{0\ (mg\cdot L^{-1}\cdot min^{-1})}$
$FZrO_2$	48,792	0,002	0,958	0,097
FZnO,com	47,453	0,035	0957	1,661
FZnO,syn	47,456	0,004	0,992	0,190
FWO3,syn	47,955	0,001	0,900	0,048
FTiO2(Cl)	47,837	0,013	0,969	0,621

Table IV.4 – The kinetic results of phenol degradation using fluorinated photocatalysts

The sequence of rate constants, is:

$$\mathbf{FZnO, com > FTiO_2(Cl) > FZnO, syn > FZrO_2 > FWO_3, syn}$$

The sequence of initial degradation rate, is:

$$\mathbf{FZnO, com > FTiO_2(Cl) > FZnO, syn > FZrO_2 > FWO_3, syn}$$

Comparing to both sequences of non-fluorinated photocatalysts, and ignoring the position of TiO_2(Cl), both of fluorinated and non-fluorinated photocatalysts show the same order in the sequence. The fluorinated commercial and synthesized ZnO show the highest initial degradation rate and rate constant. As well as fluorinated TiO_2(Cl).

On the contrary, the fluorinated commercial ZrO_2 and fluorinated synthesized WO_3 show the lowest rate constants and initial degradation rate.

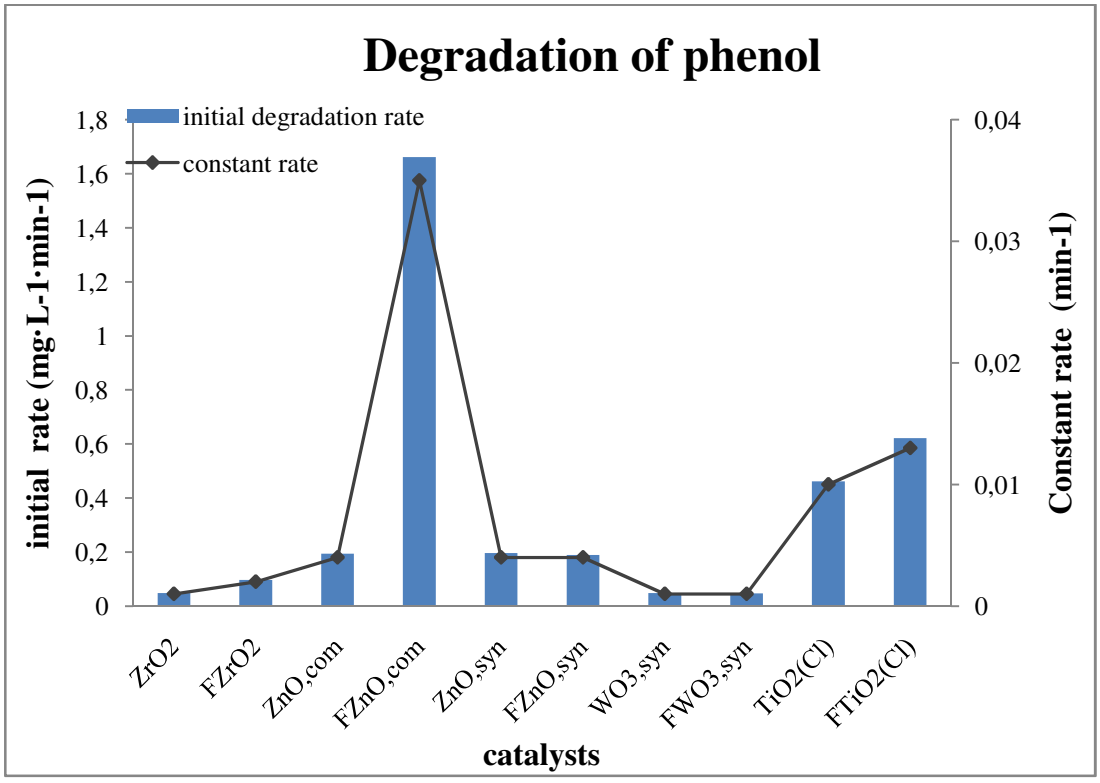

Figure IV.13 – Degradation of phenol using all studied photocatalysts

The percentages of mineralization of catalysts are presented in the following table. The percentage of mineralization using $FTiO_2$(Cl) catalysts reached a maximum of 88,29% and 85,83% for FZnO,com.

Catalysts	Mineralization
$FZrO_2$	9,23%
FZnO,com	85,83%
FZnO,syn	44,90%
FWO_3,syn	7,46%
$FTiO_2$(Cl)	88,29%

Table IV.5 - Percentages of mineralization of phenol with fluorinated photocatalysts

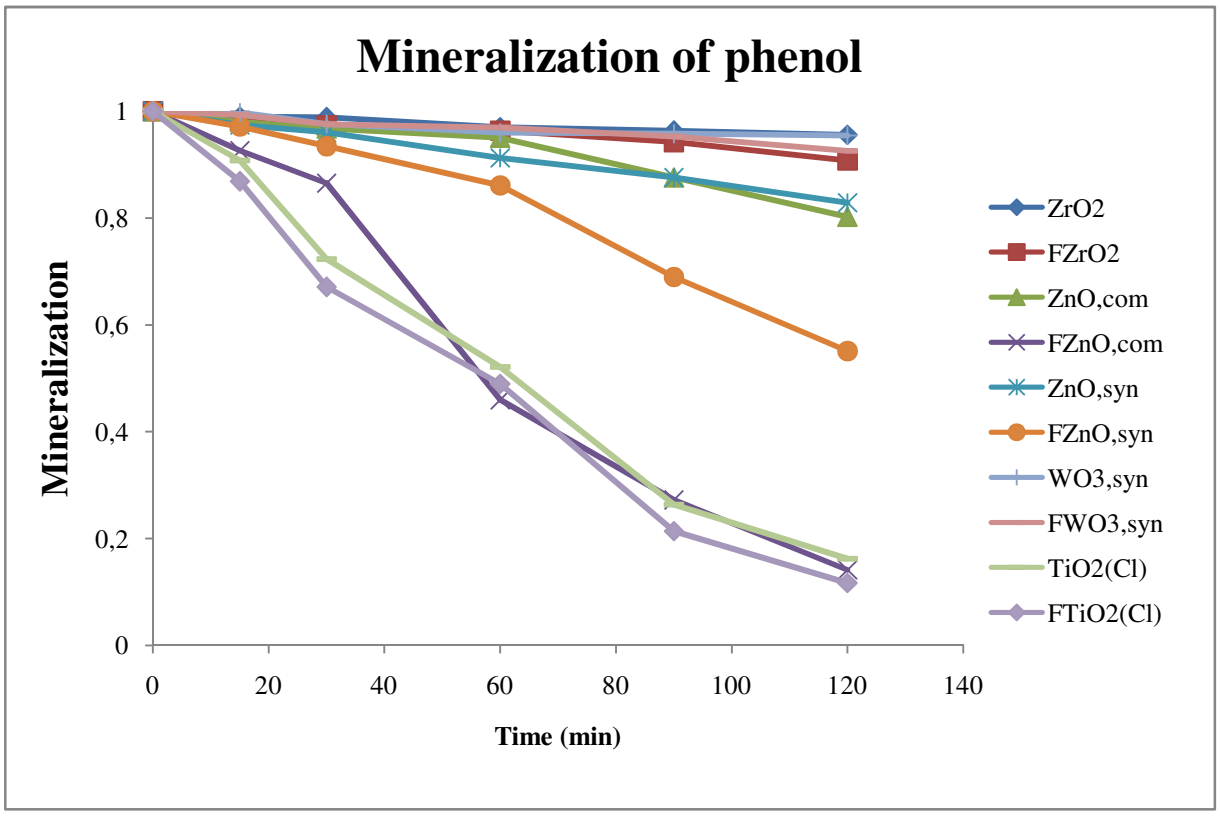

Figure IV.14 - Mineralization of phenol of all studied photocatalysts

The phenol mineralization sequence is as well as the one done for non-fluorinated photocatalysts:

$$\mathbf{FTiO_2(Cl) > FZnO(com) > FZnO(syn) > FZrO_2 \geq FWO_3, syn}$$

Based on TOC analysis data when using fluorinated synthesized ZnO, the phenol mineralization with this catalysts under UV is divided into two stages: a slow decrease of TOC concentration and a second step which becomes faster after 60 minutes of illumination**.** Concerning fluorinated commercial ZnO, the phenol mineralization with this catalysts under UV is divided into three stages: a slow decrease of TOC concentration, a second step which becomes faster after 30 minutes of illumination, and a third step which becomes more faster after 60 minutes of illumination.

Also based on TOC analysis data of $FTiO_2$(Cl), the phenol mineralization with this catalysts under UV is divided into three stages also: a fast and strong decrease of TOC

concentration, a second step which becomes less fast after 30 minutes of illumination, and a third step which becomes slower after 60 minutes of illumination.

The following figures show the intermediates of phenol observed with $FZrO_2$, FZnO,com, FZnO,syn, FWO_3,syn and $FTiO_2$(Cl) catalysts (Figures IV.15-IV.19).

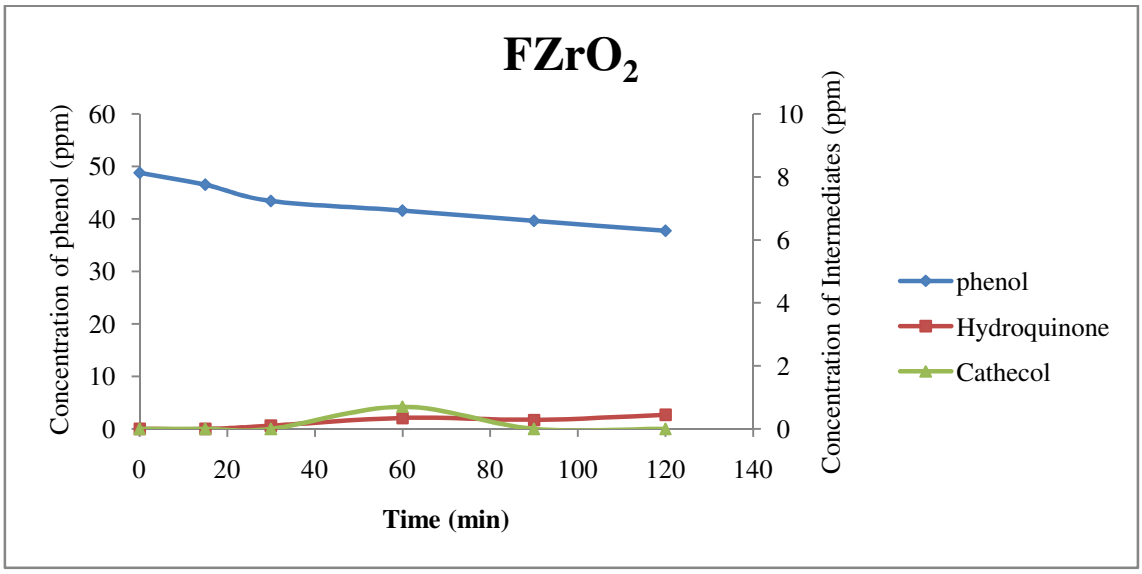

Figure IV.15- Concentration profile for phenol degradation and its degradation intermediates, catechol and hydroquinone with $FZrO_2$

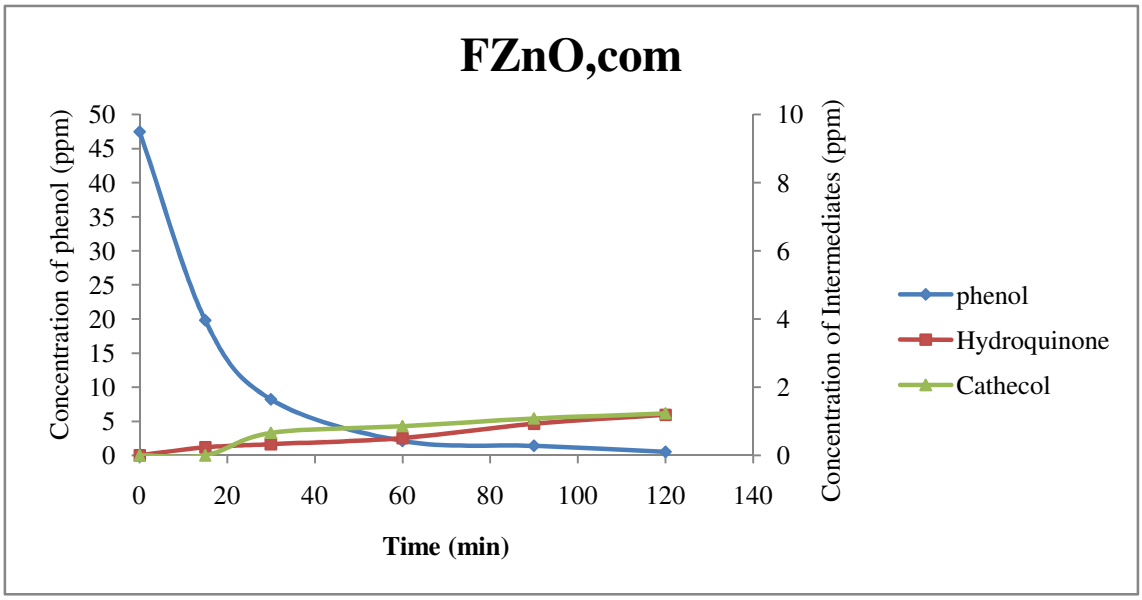

Figure IV.16- Concentration profile for phenol degradation and its degradation intermediates, catechol and hydroquinone with FZnO,com

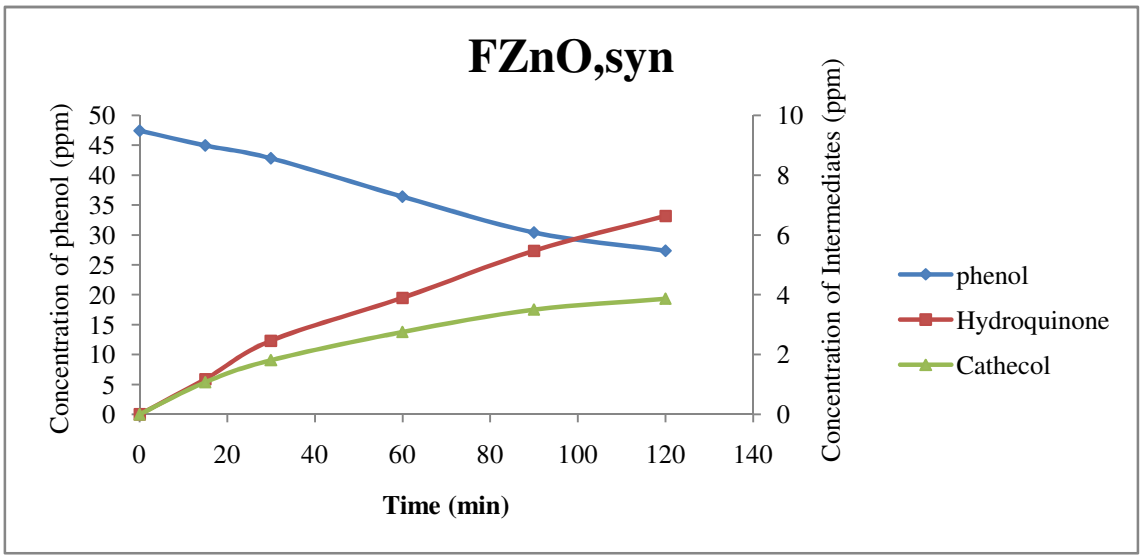

Figure IV.17- Concentration profile for phenol degradation and its degradation intermediates, catechol and hydroquinone with FZnO,syn

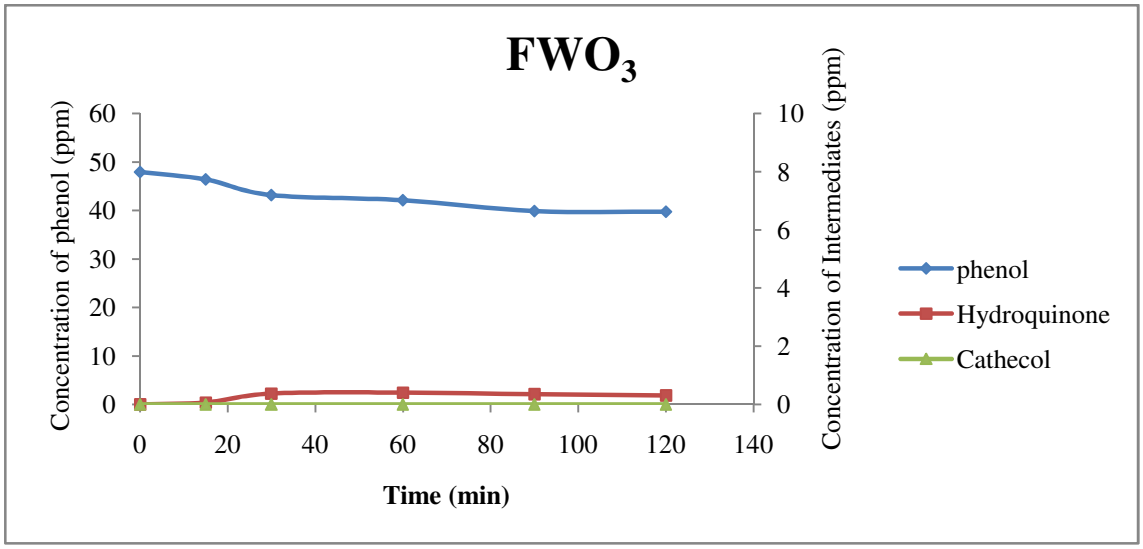

Figure IV.18- concentration profile for phenol degradation and its degradation intermediates, catechol and hydroquinone with FWO_3,syn

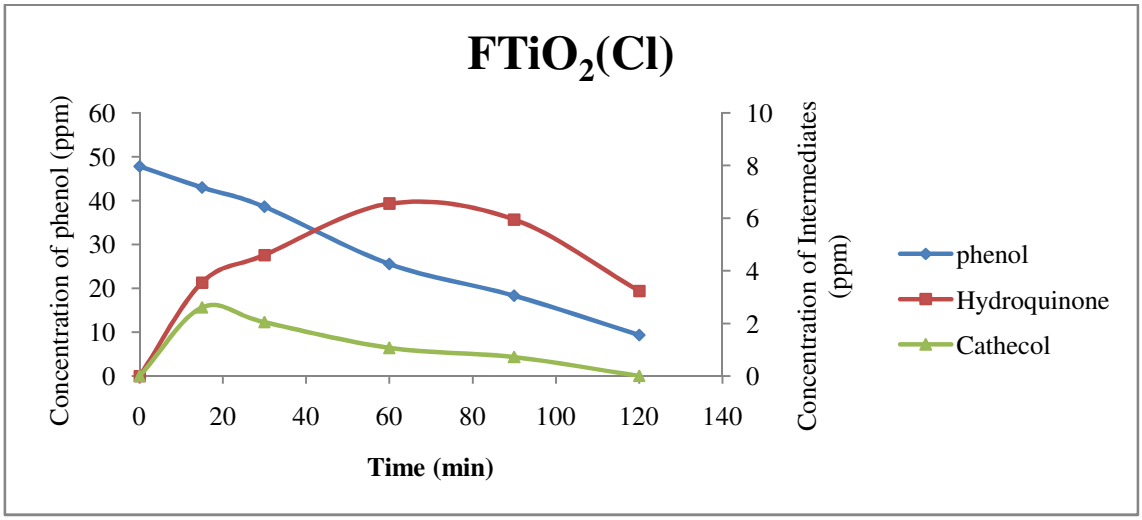

Figure IV.19- concentration profile for phenol degradation and its degradation intermediates, catechol and hydroquinone with $FTiO_2$(Cl)

We can see that catechol and hydroquinone don't appear when using the $FZrO_2$and FWO_3,syn as well as in the non fluorinated ones.

But even though in the previous study they don't appear for the synthesized ZnO, in this study it appeared for the corresponding fluorinated one with observation of a continuation in the formation of the intermediates.

By analyzing the evolution of phenol degradation intermediates for the fluorinated commercial ZnO, it is observed that as the phenol degrades so quick, catechol and hydroquinone don't appear. However, this intermediates appeared in the non-fluorinated commercial ZnO, and the degradation of phenol was not so fast as using FZnO,com.

By analyzing the evolution of phenol degradation intermediates for the fluorinated TiO_2(Cl), it is observed that as the phenol degrades, catechol and hydroquinone appear up to a maximum value from which they degrade completely, exactly as in the case of TiO_2(Cl). However, the maximum intermediates concentrations are not the same for that two catalysts. We can see that the maximum formation of hydroquinone for both

TiO_2(Cl) and $FTiO_2$(Cl) is reached at 60 min of phenol degradation. The valor are 5ppm for TiO_2(Cl) and 7ppm for $FTiO_2$(Cl).

4- Conclusion:

The sought objective in any photocatalytic degradation reaction is the total mineralization of the organic substance. It may happen that the intermediate products formed are more toxic than the initial pollutant. To ensure this, a follow-up of the evolution of oxygen consumption or a control of the rate of CO_2 formation (TOC) during the reaction was necessary to confirm complete degradation. During our study, we followed the variation of the concentration of phenol and its degradation intermediates when using different catalysts and their corresponding fluorinated ones, and we have identified the intermediate products of the reaction by high performance liquid chromatography (HPLC).

We concluded that TiO_2(Cl), commercial ZnO catalysts degrade faster phenol than the others. The $FTiO_2$(Cl) and FZnO,com degrade it better that the non-fluorinated ones.

However, taking into account the low chemical stability of ZnO for pH values below 5 and above 8 [10,11], TiO_2 will be used for the next studies along this research.

References:

[1] AKYOL, A., YATMAZ, H. C., et BAYRAMOGLU, M. Photocatalytic decolorization of Remazol Red RR in aqueous ZnO suspensions. Applied Catalysis B: Environmental, 2004, vol. 54, no 1, p. 19-24.

[2] AMANO, Fumiaki, ISHINAGA, Eri, et YAMAKATA, Akira. Effect of particle size on the photocatalytic activity of WO3 particles for water oxidation. The Journal of Physical Chemistry C, 2013, vol. 117, no 44, p. 22584-22590.

[3] ZHANG, Zhibo, WANG, Chen-Chi, ZAKARIA, Rama, et al. Role of particle size in nanocrystalline TiO2-based photocatalysts. The Journal of Physical Chemistry B, 1998, vol. 102, no 52, p. 10871-10878.

[4] THIELE, Ernest W. Relation between catalytic activity and size of particle. Industrial & Engineering Chemistry, 1939, vol. 31, no 7, p. 916-920.

[5] ANJU, S. G., YESODHARAN, Suguna, et YESODHARAN, E. P. Zinc oxide mediated sonophotocatalytic degradation of phenol in water. Chemical Engineering Journal, 2012, vol. 189, p. 84-93.

[6] C. H. Chiou, C. Y. Wu, & R. S. Juang. Influence of operating parameters on photocatalytic degradation of phenol in UV/TiO2 process. Chemical Engineering Journal, 139.2 (2008): 322-329.

[7] OSKOEI, V., DEHGHANI, M. H., NAZMARA, S., et al. Removal of humic acid from aqueous solution using UV/ZnO nano-photocatalysis and adsorption. Journal of Molecular Liquids, 2016, vol. 213, p. 374-380.

[8] ZHANG, Liwu, CHENG, Hanyun, ZONG, Ruilong, et al. Photocorrosion suppression of ZnO nanoparticles via hybridization with graphite-like carbon and enhanced photocatalytic activity. The Journal of Physical Chemistry C, 2009, vol. 113, no 6, p. 2368-2374.

[9] HUANG, Xianhuai, LEAL, Marlen, et LI, Qilin. Degradation of natural organic matter by TiO2 photocatalytic oxidation and its effect on fouling of low-pressure membranes. Water research, 2008, vol. 42, no 4-5, p. 1142-1150.

[10] ZHOU, Jun, XU, N. Sheng, et WANG, Zhong L. Dissolving behavior and stability of ZnO wires in biofluids: a study on biodegradability and biocompatibility of ZnO nanostructures. Advanced Materials, 2006, vol. 18, no 18, p. 2432-2435.

[11] UMAR, Ahmad, RAHMAN, Mohammed Muzibur, KIM, Sang Hoon, et al. Zinc oxide nanonail based chemical sensor for hydrazine detection. Chemical Communications, 2008, no 2, p. 166-168.

CHAPTER V

EFECT OF TI-F SURFACE INTERACTION ON THE PHOTOCATALYTIC DEGRADATION OF PHENOL, ANILINE AND FORMIC ACID

Efect of Ti-F surface interaction on the photocatalytic degradation of phenol, aniline and formic acid

1- Introduction :

The capacity of TiO_2 to degrade organic compounds has been demonstrated in several studies. However, the efficiency of this semiconductor needs to be improved for it to be an effective tool for pollutant removal. Various processes have been developed with the aim of enhancing and optimizing its photocatalytic properties. Fluoride has been used as precursor to synthesize new catalysts in which the exposure of certain crystalline faces is increased [1-5]. Research has also been conducted on surface modification of TiO_2 with fluorine (F-TiO_2). Fluorine has a higher electronegativity than oxygen and a specific affinity for adsorption onto TiO_2 acting as a Lewis base. The presence of fluoride anions has shown positive effects in aqueous phase increasing the degradation rate of phenol [6], benzoic acid [7], cyanuric acid (Triazine-2,4,6-Triol) [8], benzene, 4-chlorophenol [9], as well as several dyes [10, 11].

Different studies have shown that TiO_2 fluorination does not change the band gap of this semiconductor as the p orbitals of the fluorine have a lower energy than those of the oxygen atoms [12-14]. It has also been shown that the strong electron acceptor capacity of the Ti-F groups present on the surface hinders recombination of photo-generated electrons and holes, thereby enhancing photocatalytic efficiency [12-15]. It has been reported that the increased degradation rate is due to the increase in the concentration of OH· radicals in solution as the fluorides displace the OH^- groups from the surface [6]. In this respect, the following mechanisms have been proposed [6]:

$$\equiv \mathbf{Ti-OH} + \mathbf{e^-_{(CB)}} + \mathbf{h^+_{(VB)}} \rightarrow \equiv \mathbf{Ti--^{\bullet}OH} \qquad \textbf{(V.1)}$$

$$\equiv \mathbf{Ti-OH_2} + \mathbf{h^+_{(VB)}} \rightarrow \equiv \mathbf{Ti--^{\bullet}OH} + \mathbf{H^+_{ads}} \qquad \textbf{(V.2)}$$

$$\equiv Ti - O - Ti \equiv + h^{+}_{(VB)} + H_2O_{ads} \rightarrow \equiv Ti - O^{\bullet} - -H - O - Ti \equiv + H^{+}_{ads} \quad (V.3)$$

$$\equiv Ti - OH + F^{-}_{ads} + H^{+}_{ads} \rightarrow \equiv Ti - F + H_2O \quad (V.4)$$

$$\equiv Ti - F + h^{+}_{(VB)} + H_2O_{ads} \rightarrow \equiv Ti - F + {}^{\bullet}OH_{free} + H^{+}_{ads} \quad (V.5)$$

However, the physical chemistry of this process as well as many other aspects of the effect of fluorine on the TiO_2 surface have not been fully clarified [15].

It has been reported that the doping of anatase TiO_2 with elements like F with extra electrons gives rise to *n*-type materials with significantly different properties to those of the original catalyst [16]. The extra electrons provided by the F^- ions are stabilized on the titanium ions of the crystal lattice giving rise to Ti^{3+} ions homogenously spread over the crystal lattice. Titanium dioxide is a reducible oxide whose composition depends, among other factors, on oxygen pressure in the atmosphere. The extra electron provided by the fluorine will be found in the Ti 3*d* orbitals a few tenths of an electron-volt below the lower end of the conduction band [17]. TiO_2 doping with fluorine gives rise to two types of fluoride species. The first of these arises when the F^- ion replaces the O^{2-} ions of the crystal lattice resulting in Ti-F-Ti bonds. This leads to the formation of Ti^{3+} species in the bulk, giving rise to localized Ti^{3+} states just below the conduction band. This type of doping inhibits oxygen adsorption and consequently the formation of superoxide radicals, suggesting that the sites with defects are localized in the bulk and not on the surface. The second species consists of F^- ions on the surface of the solid which replace surface hydroxyl groups giving rise to Ti-F terminal groups without generating reduced sites [17]. The Ti^{3+} sites that are generated may be systems entirely localized in sections of the catalyst or systems in which there is a total delocalization of electron density in all the ions of the metal, with the energy levels of these states just below the conduction band [16]. Studies undertaken to date suggest that the second of these possibilities

appears to be the most probable [18]. Displacement of the negative charge, which takes place at the edges of the energy levels, favors the charge transference rate and lowers the recombination rate. The accumulation of electrons trapped in the conduction band in a photo-stationary state results in the surface charge of the TiO_2 suspended particles changing to negative [19]. Most of the electrons would be localized on Ti(III)-OH surface sites.

It has been reported in other studies that an increase in the degradation rate takes place when the anatase phase is doped with fluorine, but that this rate decreases when the rutile phase of the TiO_2 is doped [20]. It was also shown in the same study that the increase in the degradation rate does not always require pre-adsorption of the fluoride ions. A Helmholtz double layer was proposed by the authors of the study in which the fluoride ions would be situated on the internal and external planes of this double layer, facilitating desorption of the surface bonded OH· radicals to the solution upon irradiation of the TiO_2. The most active radical fluorides are those found in the outer Helmholtz layer, and are the most efficient at provoking desorption of the surface bonded OH· radicals. The inner layer fluoride ions, namely those adsorbed onto the surface or bonded to Ti^{4+} sites, have a lower capacity to form a bond with the surface bonded OH· via hydrogen-fluorine bridges. The key to this proposal lies in the argument that desorption to the solution of the surface bonded hydroxyl radicals on the irradiated TiO_2 is thermodynamically possible through an H-F bond formation [20].

It should also be noted that a positive effect has not been observed in all studies involving TiO_2 doping with fluorine. For example, a slowing down of the degradation rate of dichloroacetate [21] and of the degradation rate in gas phase of some compounds [22] has been observed. As previously stated, the fluoride ion has a specific affinity for adsorption on TiO_2 acting as a Lewis base and so would decrease and modify the density of surface states and, in this way, slow

down certain degradation processes [15]. It should also be noted that although the formation of $OH\cdot$ radicals is higher in F-TiO_2, the oxidation processes in which there is hole transfer are inhibited [21].

In order to acquire a more in-depth knowledge and understanding of the behavior of these fluorinated materials, a study is undertaken in the present thesis of the degradation of phenol, formic acid and aniline with two TiO_2 catalysts with different anatase and rutile phase proportions. For this purpose, the P25 catalyst with 80% anatase and 20% rutile phase and the Sigma Aldrich (SA) catalyst with purely anatase phase were selected. Both materials have approximately the same surface area (about 50 $m^2 \cdot g^{-1}$). These two catalysts were fluorinated using high concentrations of NaF at pH 6.5 and selecting the filtration method to obtain the corresponding F-P25 and F-SA catalysts.

Various organic compounds have been described in the bibliography to assess the photocatalytic activity of materials with different physical-chemical properties. These include coumarin, terephthalic acid, phenol, aniline and/or formic acid, depending principally, among other aspects, on determining what type of radical intervenes or whether adsorption is a determinant factor in the process [23, 24]. Considering the working pH values, the degradation mechanisms and the results described in the bibliography, formic acid, aniline and phenol were selected in the present work as test molecules to characterize the catalysts.

2. Experimental :

2.1 Used photocatalysts :

Two commercial TiO_2 photocatalysts were used: Evonik Aeroxide P25 (P25) and anatase Sigma Aldrich (SA). We used also the corresponding fluorinated ones (synthesized as mentioned in chapter 3 paragraph 1.3.3).

2.2 Characterization of materials :

The surface concentration of fluorine on the catalysts was semi-quantitatively determined by EDAX analysis. Analyses of the crystalline structure were performed by X-ray diffraction. Anatase-rutile fractions were calculated taking into account the relative diffraction peak intensities of crystalline planes (101) and (111) of anatase and rutile, respectively. BET surface area measurements and diffuse reflectance UV-Vis spectra (DRS-UV-Vis) were carried out and band gap values were calculated by the Kubelka-Munk function, according to the Tandon-Gupta method. Field emission scanning electron microscopy (FESEM) images were obtained using a Hitachi S-4800 microscope.

The Brönsted and Lewis acid sites determination was done through interaction of ammonia with the surface of the catalysts. This interaction was followed by Fourier transform infrared spectroscopy (FTIR).

2.3 Photocatalytic experiments :

The degradation tests were performed as described in chapter 3. The solution was left for 15 minutes in the darkness to reach the adsorption-desorption quasi-equilibrium.

All the studies were performed with a 0.51 mM concentration of phenol, aniline or formic acid. The studies with formic acid were performed at pH 3, those with phenol at pH 5 and those with aniline at pH 7, with the aim of ensuring that the molecule under study had the appropriate electrical charge to facilitate its approximation to the photocatalyst surface. A constant pH was maintained throughout the test.

2.4 Analytical determinations :

Concentrations of phenol, aniline and formic acid at different reaction times were measured using the first HPLC equipment mentioned in chapter 3 for phenol and

aniline, but using the second HPLC equipment for formic acid.

The concentrations of phenol and muconic acid in the studies performed with mixtures of these compounds were made using an EC 250/4 Nucleodur 100-5 C18ec column (250 mm x 4 mm ID, 5 µm particles). The mobile phase used was acetonitrile/water/H_3PO_4 15/85/0.1. Detector wavelength in these studies was 264nm. The total organic carbon (TOC) analyses were carried out.

3. Results and discussion :

3.1 BET area, EDAX, SEM, XRD and DRS-UV-Vis analyses :

Table V.1 shows the most important results of the BET, EDAX, DRX and DRS-UV-Vis analyses. P25 and Sigma-Aldrich (SA) catalysts have respective surface areas of 50.9 and 47.3 $m^2 \cdot g^{-1}$. The fluorinated catalysts, F-P25 and F-SA, have similar surface areas (51.3 and 45.4 $m^2 \cdot g^{-1}$ respectively). The anatase/rutile phase ratios of the P25 and F-P25 are 82.3/17.7 and 85.5/14.5 respectively, while the SA and F-SA catalysts only have anatase phase. The mean particle size was also determined; it was noted that they were very similar in the P25 and F-P25, but that there was a difference in size of approximately 7 nm between the anatase particles of the SA and F-SA. The differences observed are attributable to the filtration process of the catalyst in the synthesis of the fluorinated materials. The band gap values obtained from the UV-Vis analyses are all very similar, with no significant changes observed when fluorinating the catalysts. Thus, as seen in other studies, surface fluorination of the catalysts does not modify the optical properties of these materials [25, 26]. The images obtained from the SEM analyses of the F-P25, F-SA and SA catalysts show a similar distribution of aggregates (Fig.V.1). However, SEM analyses of the P25 show a different distribution of aggregates, which can also be attributed to the filtration process.

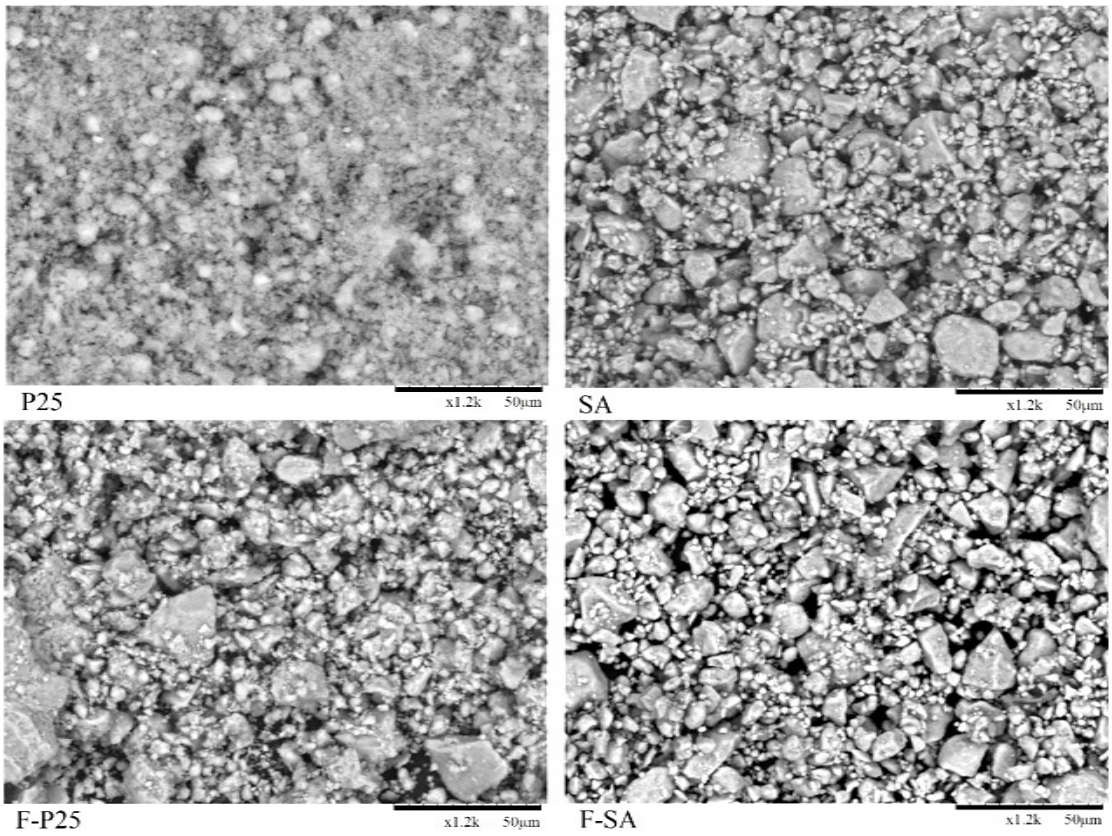

Figure V.1 : Imagen SEM of the fluorinated and non-fluorinated P25 and SA catalysts.

Table V.1 also shows the Ti/F and F/Na ratios obtained from the EDAX analyses. The analyses also showed the presence of sodium on the surface of the fluorinated materials, though its concentration is significantly lower than the molar concentration of fluorine. This shows that the fluorine is mostly interacting with the catalyst surface and is not as NaF, though the presence of this salt on the surface cannot discarded. Note that the Ti/F proportions in both fluorinated catalysts are similar.

	Surface area ($m^2 \cdot g^{-1}$)	Anatase/rutile phase ratios	Cristallite size (nm)		Band gap (eV)	Molar ratio	
			Anatase	Rutile		Ti/F	F/Na
P25	50.9	82.3/17.7	20.56	33.01	3.16	---	---
F-P25	51.3	85.5/14.5	19.84	34.70	3.0	20.97	2.47
SA	47.3	100/0	13.93	--	3.16	---	---
F-SA	45.4	100/0	20.57	--	3.18	19.43	2.12

Table V.1 : Surface area, anatase/rutile phase ratios, crystallite size, band gap and Ti/F and F/Na molar ratios

3.2 Characterization of the adsorbed water, hydroxyl groups and surface charge :

Figure V.2 shows the spectra of the fluorinated and non-fluorinated P25 and SA catalysts. Note in particular the position of the baseline in each of these catalysts, the band attributed to isolated hydroxyl groups (3698 cm^{-1}) and the bands attributed to adsorbed water (3600-3000 cm^{-1} and 1640 cm^{-1}).

An important feature to note in the spectra of Figure V.2 is the position of the baseline. As a result of the presence of surface or shallow electron traps, electrons are fed to the conduction band via thermal processes such as those generated by the infrared radiation used to obtain the spectra. The electrons promoted to the conduction band have a similar behavior to that described for delocalized electrons confined to a three-dimensional box with infinite walls; the high density of generated states gives rise to the continuous presence of excited electrons leading to a baseline increase of the infrared spectrum [16].

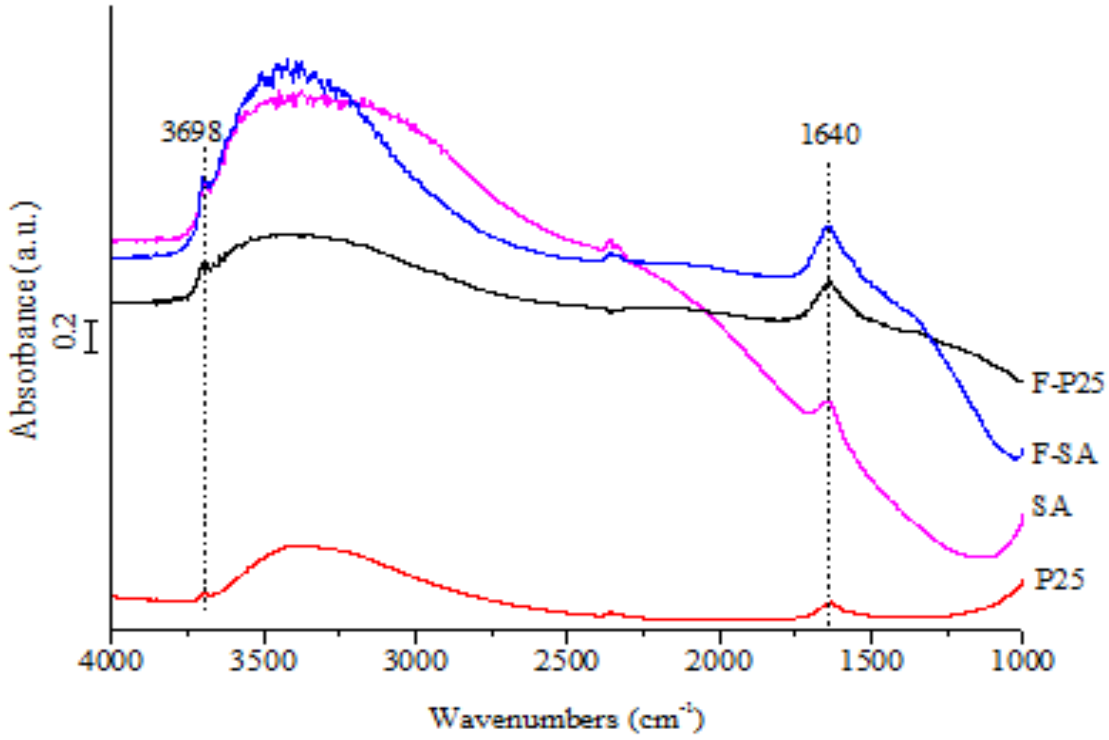

Figure V.2 : FTIR spectra of the fluorinated and non-fluorinated P25 and SA catalysts.

The baseline position of the SA catalyst, the one with only anatase phase, is higher than that of the P25. On modification of P25 with fluorine, a baseline increase takes place which takes it to the same level as that observed in the SA catalyst. When TiO_2 is modified with fluorine, at least a fraction of the excess electrons introduced by the fluorine are localized by lattice Ti^{4+} cations. The presence of reduced Ti^{3+} centers in the as-prepared, fully oxidized solid indicates that the F-TiO_2 system can be described in terms of an n-type semiconductor provoking the baseline increase observed in the F-P25 catalysts [17]. Modification of the baseline also takes place with the F-SA catalyst in the region between 2500-1000 cm^{-1} as a consequence of the presence of fluoride.

The fluorination process has been described through reaction (V.6) [4].

$$\equiv \mathbf{Ti-OH} + \mathbf{F^-} \rightarrow \equiv \mathbf{Ti-F} + \mathbf{OH^-} \quad (pK = 6.2) \qquad \textbf{(V.6)}$$

Bearing in mind the pK of reaction (V.6), the highest percentage of fluorination is produced around pH 3 [27,28]. However, in the present work, impregnation with NaF was performed at pH 6.5, and so in the spectra of the fluorinated catalysts (Fig. V.2) bands of isolated hydroxyl groups (3698 cm^{-1}) are still observed and in an even relatively higher proportion than with the P25 and SA catalysts.

3.3 Determination of Lewis and Brönsted acid sites :

Ammonia can interact with Brönsted and Lewis acidic surface sites forming ammonium ions and acid-base adducts, respectively. The presence of these species can be perfectly identified via FTIR. The interaction of NH_3 with the Lewis acid sites gives rise to bands centered around 1200 cm^{-1}, the higher the wavenumber the greater the strength of the Lewis sites. The non-adsorbed NH_4^+ gives rise to a band centered around 1445 cm^{-1}, and the shift of this band to higher wavenumbers would indicate the presence of adsorbed ammonium.

The spectra obtained from the interaction of ammonia with the catalysts are shown in Figure V.3. A broad band centered around 1200 cm^{-1} can be observed in the initial spectrum of the P25 attributed to $\delta_S NH_3$ ammonia adsorbed on Lewis sites. The asymmetry and width of the band suggest that it may be composed of Lewis acid sites of different types. A broad band can also be observed at 1445 cm^{-1} which is attributed to the $\delta_{as} NH_4^+$ vibration. The width of this band may be due to its being formed of free ammonium produced by the abstraction of a proton from the P25 surface present in a Brönsted acid site and adsorbed ammonia [29, 30]. A further band can be observed at 1315 cm^{-1} and a shoulder at 1558 cm^{-1} which cannot be attributed to ammonia adsorbed on either Lewis or Brönsted acid sites. It has been suggested in some studies that these bands most likely represent various deformation vibrations of NH_x species, which are formed on the surface in relatively small amounts as a result of NH_3 adsorption [31].

In the spectrum obtained of the interaction of NH_3 with the SA catalyst, the band attributed to the $\delta_{as}NH_4^+$ vibration is found at the same wavenumber, 1445 cm^{-1}, as in the P25 studies. However, the band attributed to the Lewis acid sites is found at 1216 cm^{-1} and the band corresponding to compounds generated by the decomposition of the ammonia has low intensity.

In the spectrum of NH_3 interaction with the F-P25 and F-SA catalysts (Fig.V.2), the absence of the band attributed to NH_3 adsorbed on Lewis acid sites should be noted. However, in these catalysts the band attributed to δ_{as} NH_4^+ (1445 cm^{-1}) was observed and a band at 1340 cm^{-1}.

The initial spectrum observed with F-TiO_2 can be explained as the interaction of NH_3 with surface fluorine through the following reaction [32, 33].

$$\equiv \mathbf{Ti} - \mathbf{F} + \mathbf{NH_3} \rightarrow \mathbf{HF} + \equiv \mathbf{TiNH_2} \qquad \textbf{(V.7)}$$

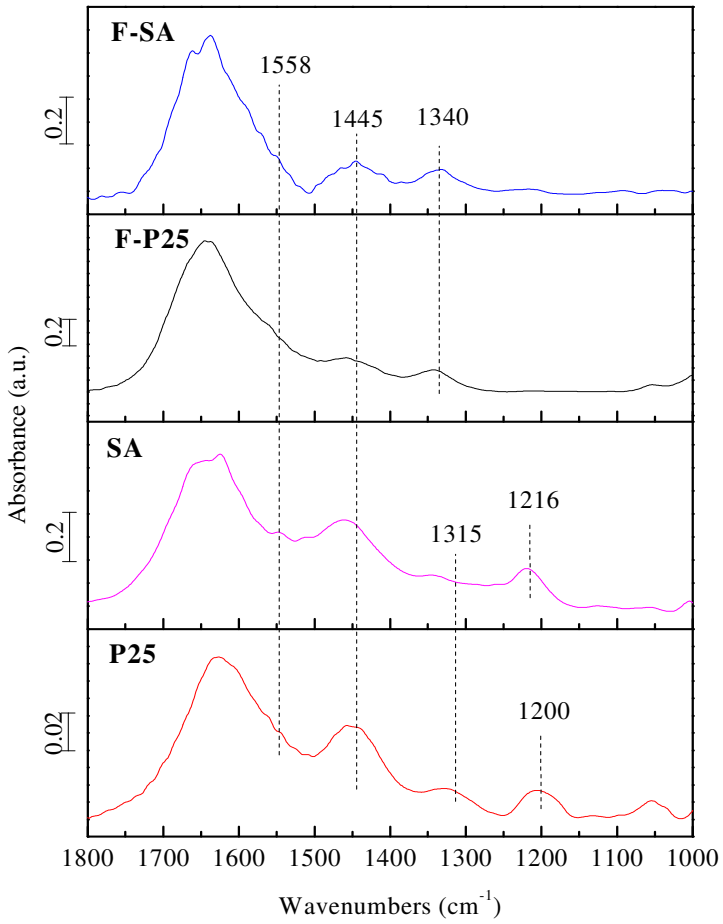

Figure V.3 : FTIR spectra of the interaction of the NH_3 with the catalysts.

The non-detection of the band attributed to Lewis acid sites at around 1200 cm^{-1} in the fluorinated catalysts would suggest that in these materials the surface Ti atoms are fluorinated or strongly bonded to hydroxyl groups.

3.4 Photocatalytic degradation studies :

As indicated in the experimental section in chapter 3, the formic acid, aniline and phenol degradation studies were all performed at the same concentration (0.51mM). The pH of the solution in the different studies was 7, 5 and 3 for the aniline, phenol and formic acid, respectively.

Figures V.4, V.5 and V.6 show the degradation results of formic acid, aniline and phenol, respectively. With all the substrates studied, the F-P25 catalyst showed

the greatest photocatalytic efficiency in degradation. The F-SA and P25 had similar degradation curves for all the molecules, while the SA has the worst photocatalytic activity.

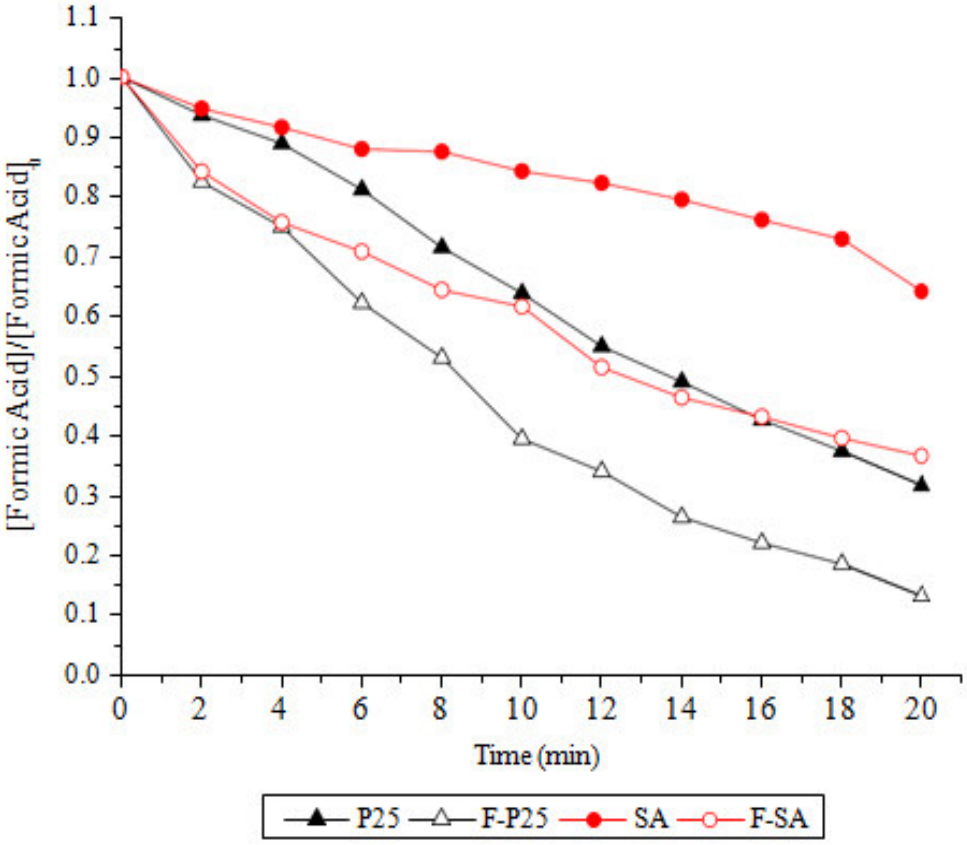

Figure V.4 : Evolution of the concentration of formic acid during photocatalytic oxidation, pH=3.

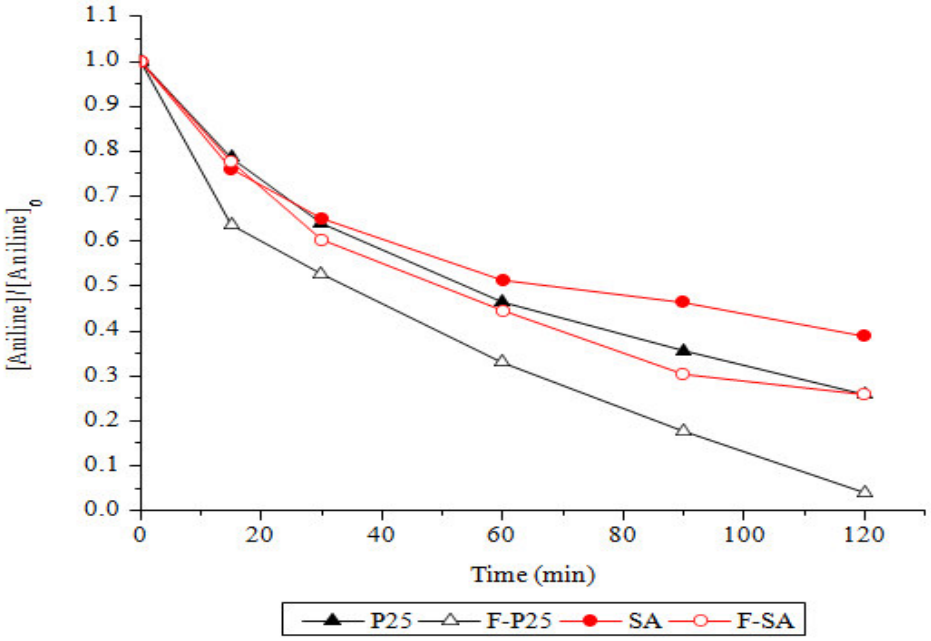

Figure V.5 : Evolution of the concentration of aniline during photocatalytic oxidation, pH=7.

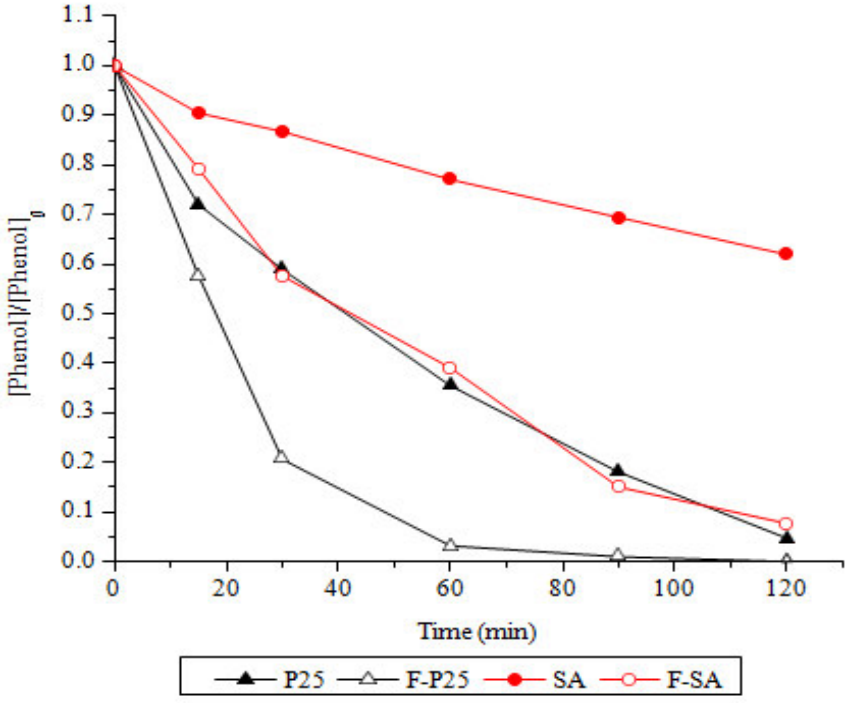

Figure V.6 : Evolution of the concentration of phenol during photocatalytic oxidation, pH=5.

Figure V.7 shows the degradation constants for each catalyst and each substrate obtained from the results shown in Figures V.4- V.6. As can be observed, the rate constants display the following sequence with all the substrates:

F-P25 > F-SA ≈ P25 > SA

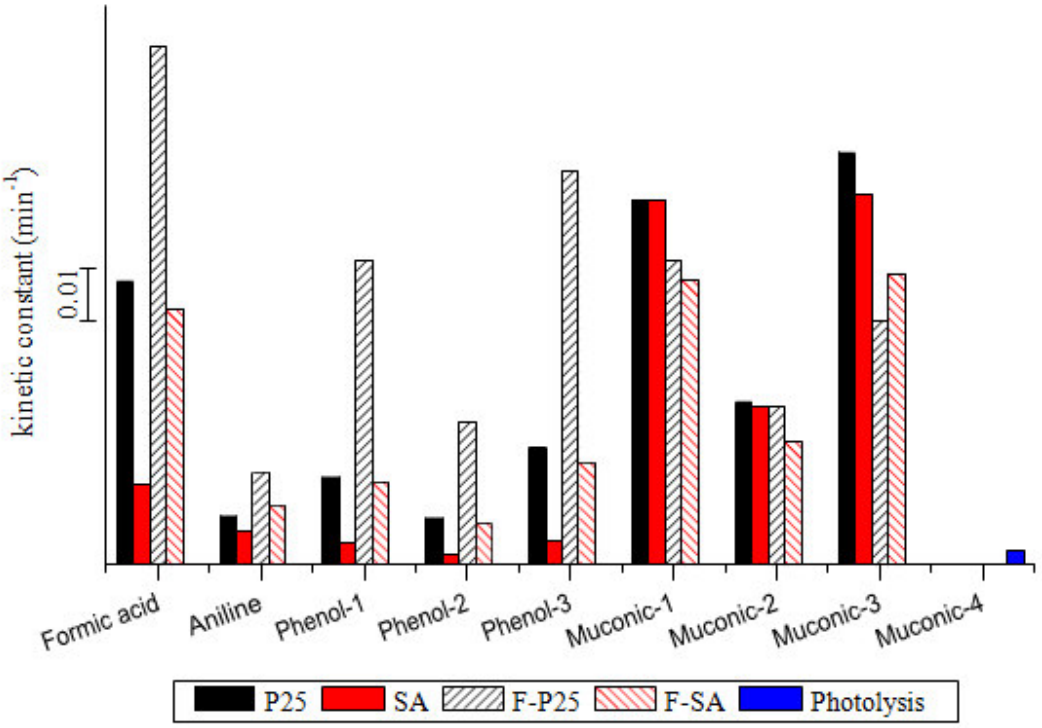

Figure V.7 : Apparent first order kinetic constants for formic acid, aniline, phenol and muconic acid photocatalytic oxidation in presence of the different catalysts.

Phenol-1 :k_{phenol} in study with phenol 0.51 mM; Phenol-2: k_{phenol} in study with mixtures phenol:muconic acid (0.51 mM: 0.51 mM); Phenol-3: k_{phenol} in study with mixtures phenol:muconic acid (0.25 mM : 0.25 mM).

Muconic-1: $k_{muconicacid}$ in study with muconic acid 0.51 mM; Muconic-2 $k_{muconicacid}$ in study with mixtures phenol:muconic acid (0.51 mM: 0.51 mM); Muconic-3: $k_{muconicacid}$ in study with mixturesphenol:muconic acid (0.25 mM : 0.25 mM); Muconic-4: $k_{muconicacid}$ in muconic acidphotolysis.

With all catalysts, the highest rate constant is found for formic acid degradation, followed by phenol and the slowest for aniline. The rate constant with P25 in the formic acid degradation is 3.25 times greater than that of phenol, in the SA it is 2.15 times greater and in the fluorinated catalysts it is 1.5 times greater. Again with the P25, the degradation rate constant of phenol is, in turn, 1.8 times greater than that of aniline, whereas with the SA catalyst the rates are similar and in the fluorinated catalysts it is 3.7 times higher in the F-P25 and 2.5 times higher in the F-SA. The degradation sequence appears to be related to the oxidation state of the carbon in the compound. Thus, the more oxidized the substrate under study the faster the degradation.

To compare the efficiency of the fluorinated catalysts, the ratio between the rate constants of F-P25/P25 and of F-SA/SA with the different substrates was calculated (Fig.V.8). The ratios obtained for phenol and aniline are practically the same for both catalysts. That is, for the phenol and aniline the same increase in the rate constant takes place when the catalysts are fluorinated. The highest increase in the rate constant is with the phenol. With the fluorinated P25 catalyst, the same increase in the rate constant is seen in aniline and formic acid degradation. However, with the SA catalyst a higher increase is observed in the degradation rate constant of formic acid than of aniline.

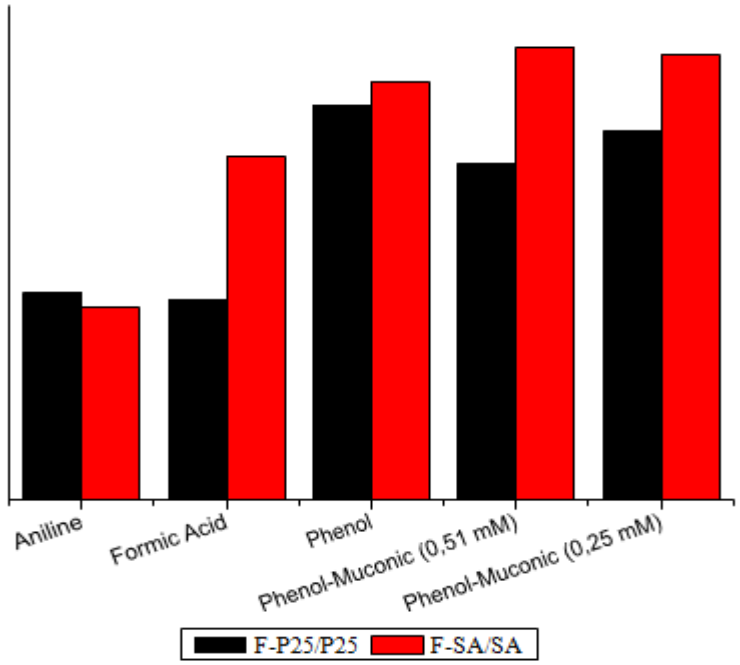

Figure V.8 : Ratio between apparent first order kinetic constants obtained for the fluorinated/bare catalysts (F-P25/P25 and F-SA/SA).

With a view to a greater in-depth study, tests were carried out with phenol in the presence of muconic acid with each at the same concentration of 0.51 mM (Fig.V.9 A), and at half that concentration (0.25 mM) (Fig.V.9 B). These studies were performed to see whether the presence of a phenol degradation intermediate (muconic acid) at high concentrations would vary the parameters determined in the previous studies. The rate constants obtained in these studies were compared with those of phenol alone, aniline and formic acid (Fig. V.7). Also shown in Figure V.7 are the degradation rate constants of the muconic acid alone (0.51 mM) and the phenol-muconic acid mixtures. The $k_{phenol-2}$ in the studies performed with phenol-muconic acid mixtures (0.5mM-0.5mM) decrease by almost half with all the catalysts compared to the $k_{phenol-1}$ (studies with 0.51mM phenol alone) (Fig.V.7). In contrast, the $k_{phenol-3}$ values obtained in the studies performed with 0.25 mM-0.25 mM phenol-muconic acid mixtures are similar to the $k_{phenol-1}$ values. The same fact was observed in the degradation rate constants of the

muconic acid (Fig.V.7). Given that phenol is barely adsorbed onto the catalyst [34], this could be indicating a competition for the generated radicals. It was also observed in these tests that the phenol degradation rate constant follows the same sequence as in the previous studies. That is, the highest rate constant is obtained with the F-P25, followed by the F-SA which has a similar rate constant to the P25, and finally the SA. The correlation between the F- P25/P25 and F-SA/SA phenol degradation rate constants was also calculated (Fig.V.8), with very similar degradation rate constant increases being obtained after fluorination as in the previous studies. On the other hand, no increase was observed in the muconic acid degradation rate constant with the fluorinated catalysts. In fact, there even appears a slight decrease in the value when the catalysts are fluorinated.

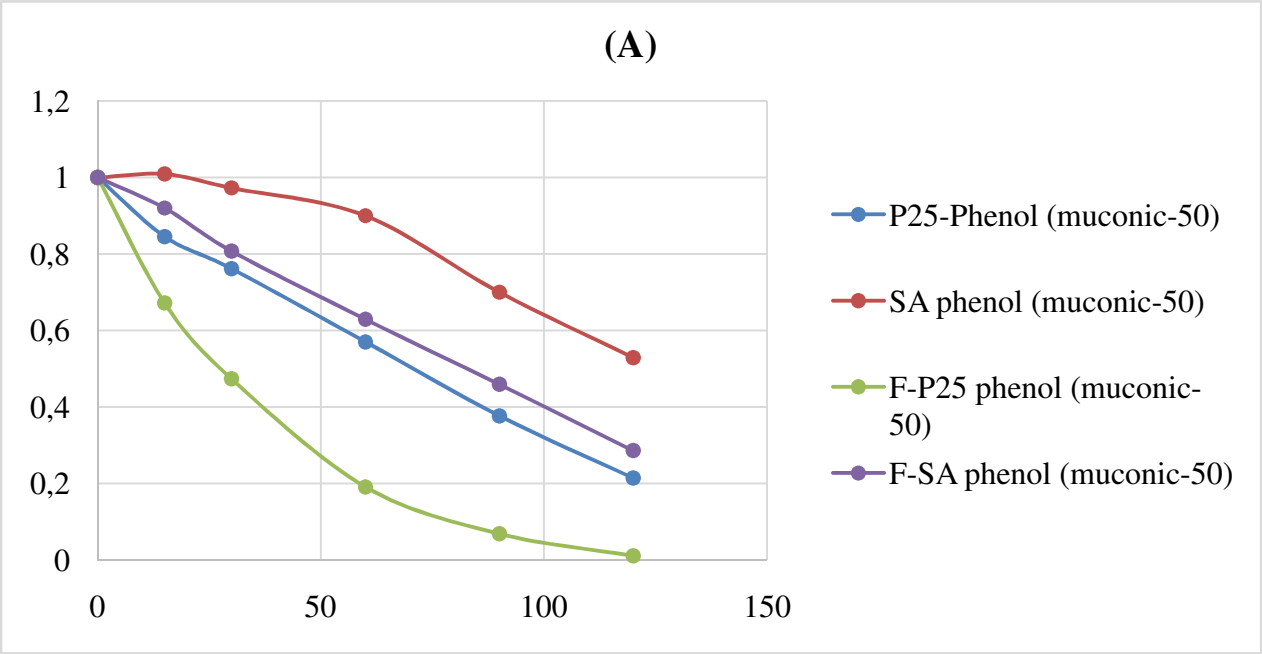

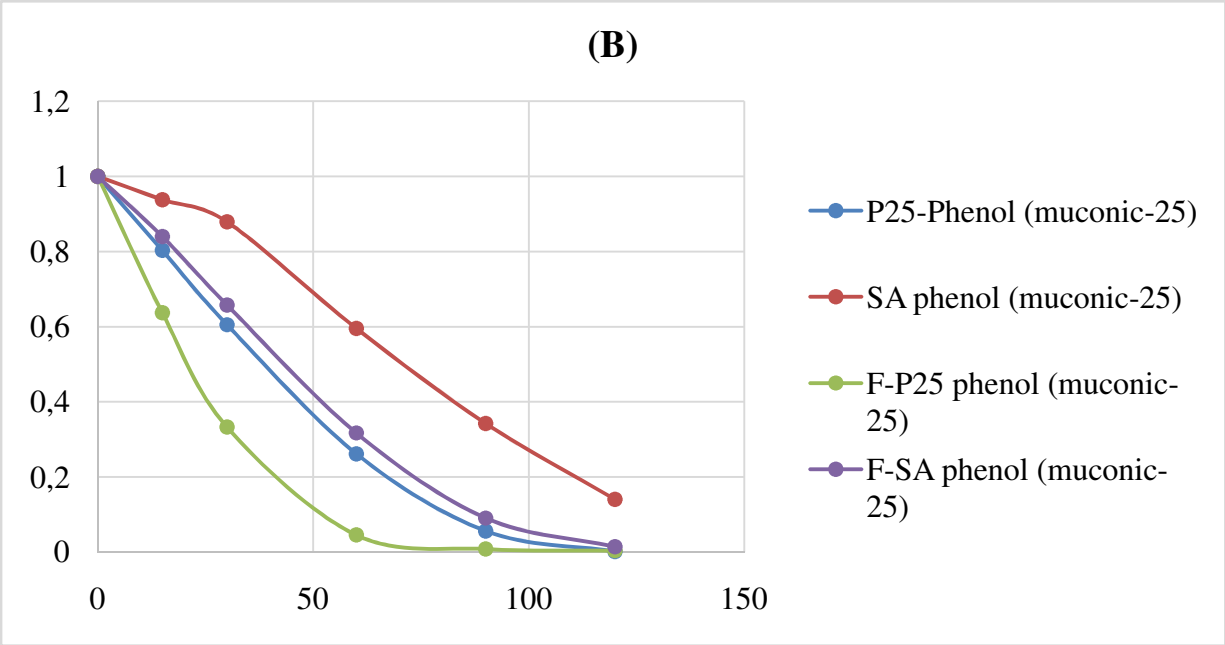

Figure V.9 : Evolution of the concentration of phenol during photocatalytic oxidation of mixtures phenol:muconic acid (pH=5), 0.51 mM:0.51 mM (A) and 0.25 mM:0.25 mM (B).

A control was also performed of the main intermediates of phenol degradation (hydroquinone, catechol and resorcinol). Figures V.10 and V.11 show the concentrations and evolution of these intermediates. In the studies with phenol alone, the concentrations of intermediates follow the sequence [resorcinol] ≥ [hydroquinone] > [catechol] with all the catalysts. With the F-P25, the concentrations of these intermediates decrease very rapidly. In the studies performed in the presence of muconic acid (0.51 mM), the concentrations of resorcinol are significantly smaller and the concentration of intermediates has the following sequence [hydroquinone] > [catechol] >[resorcinol].

A control was also performed of TOC. In order to evaluate the concentration of degradation intermediates other than dihydroxylated phenolic compounds, the concentrations of organic matter corresponding to phenol, hydroquinone, catechol, resorcinol and muconic acid determined in previous analyses (Fig.V.12) were subtracted from the experimentally determined TOC. As can be seen, in all

the studies the F-P25, which presents the highest k_{phenol}, has less capacity to mineralize the intermediates generated from the degradation of the dihydroxylated compounds.

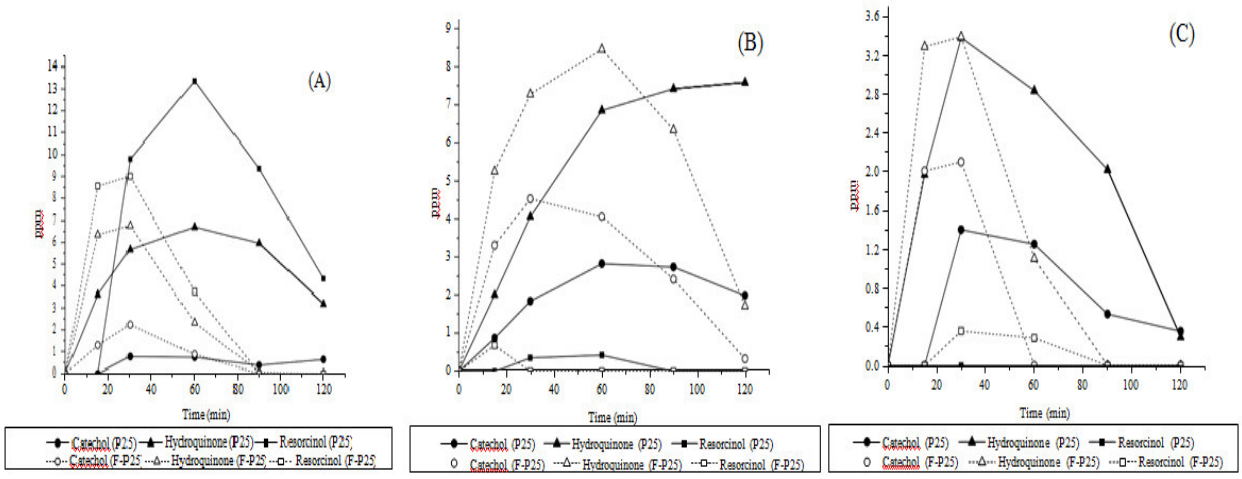

Figure V.10 : Evolution of intermediates catechol, hydroquinone and resorcinol during phenol degradation (A), mixtures phenol: muconic acid 0.51mM:0.51 mM (B) and mixtures phenol: muconic acid 0.25 mM:0.25 mM (C) with P25 and F-P25.

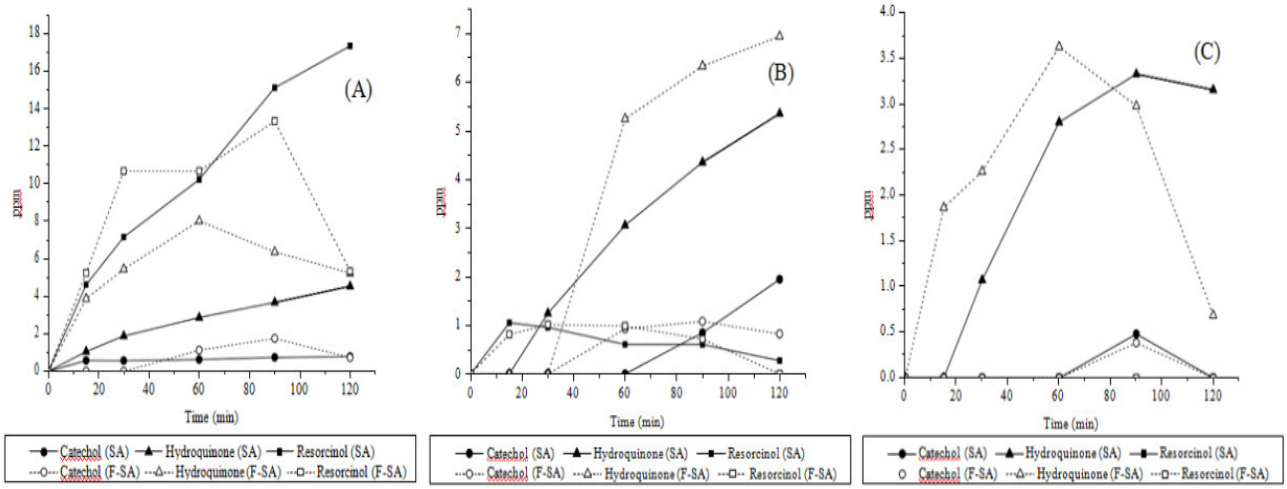

Figure V.11 : Evolution of intermediates catechol, hydroquinone and resorcinol during phenol degradation (A), mixtures phenol: muconic acid 0.51mM:0.51 mM (B) and mixtures phenol: muconic acid 0.25 mM:0.25 mM)(C) with SA and F-SA.

3.5 Discussion of the results :

The photocatalytic processes can be summarized in the following reactions [34]:

$$TiO_2 + h\nu \rightarrow h^+ + e^- \quad \textbf{(V.8)}$$

$$h^+ + \text{organic}_{(ads/inter)} \rightarrow \text{oxidized product} \quad \textbf{(V.9)}$$

$$\equiv Ti - OH_2 + h^+ \rightarrow Ti - (\ ^{\bullet}OH_{surf}) + H^+ \quad \textbf{(V.10)}$$

$$^{\bullet}OH_{surf} + \text{organic}_{(ads/inter)} \rightarrow \text{oxidized product} \quad \textbf{(V.11)}$$

$$O_{2(ads)} + e^- \rightarrow O^{2-} \quad \textbf{(V.12)}$$

$$O^{\bullet -}{}_2 + H^+ \rightarrow HO^{\bullet}; \qquad 2\,HO^{\bullet}{}_2 \rightarrow H_2O_2 \quad \textbf{(V.13)}$$

$$H_2O_{2(aqu)} + e^- \rightarrow {}^{\bullet}OH_{(free)} + OH^- \quad \textbf{(V.14)}$$

$$^{\bullet}OH_{(free)} + \text{organic}_{(aqu)} \rightarrow \text{oxidized product} \quad \textbf{(V.15)}$$

$$H_2O_2 + \text{organic}_{(aqu)} \rightarrow \text{oxidized product} \quad \textbf{(V.16)}$$

The oxidative species h^+ and $OH^{\bullet}_{surf}$ would give rise to oxidation processes on the catalyst surface or at the surface-solution (inter) interface, while the oxidative species $OH^{\bullet}_{(free)}$ and H_2O_2 would give rise to oxidation processes in the solution. Different studies [16-19] have shown that, with the introduction of fluorine atoms on the TiO_2 surface and their interaction with the Ti surface atoms, states are generated with high negative charge density. This has been observed in the FTIR studies of the F- P25 and F-SA catalysts described in this thesis. The presence of surface states of high negative charge density means that during illumination the photogenerated holes are trapped at the surface and the electrons forced to make their way to more internal Ti atoms in the crystalline structure [35]. Thus, the holes can react with the surface oxygen atoms and/or the adsorbed water favoring reactions (V.9)-(V.11) or generating new $OH^{\bullet}_{free}$ radicals via

reaction (V.17) [15].

$$h^+ + \equiv Ti - F + \ H_2O \ \rightarrow \equiv Ti - F + \ {}^{\bullet}OH_{(free)} + \ H^+ \qquad \textbf{(V.17)}$$

Depending on the reaction conditions, the reagents used and the reaction mechanism, the formation and/or participation of these radicals can be favored. [36-38].

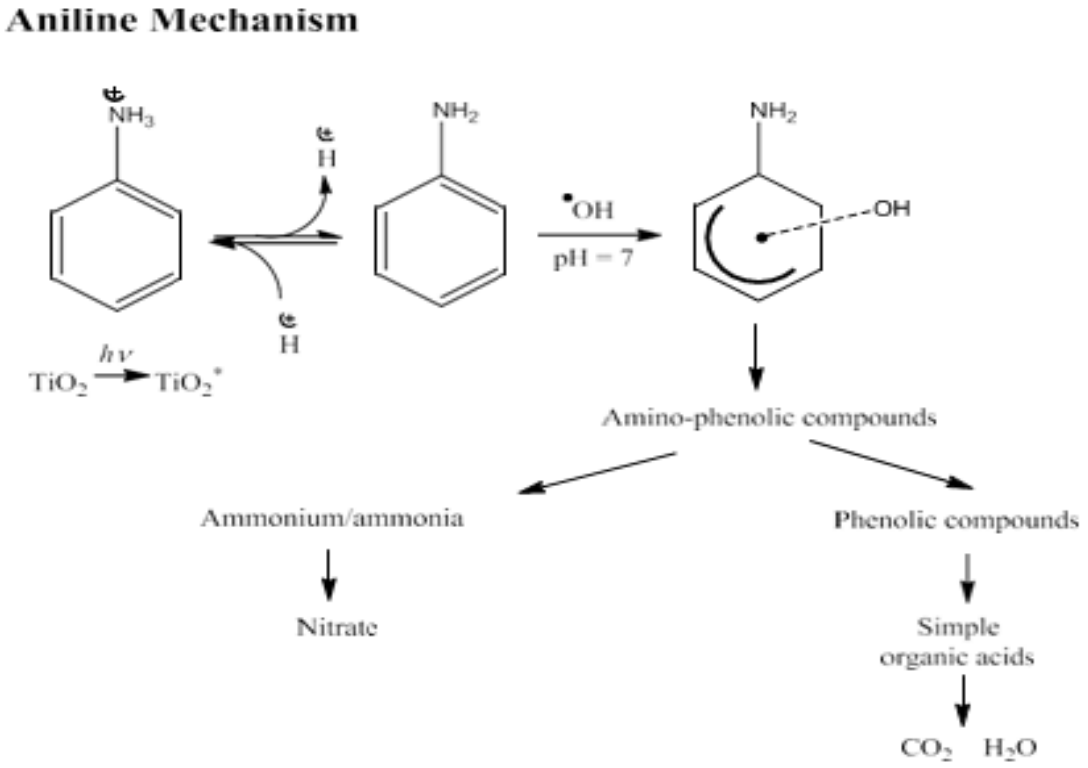

Diagram V.1: Degradation mechanisms of aniline

Degradation of formic acid can take place via reaction of the adsorbed (ads) formic acid or of the formic acid present at the solution/surface interface of the catalysts (inter) with the surface hydroxyl radicals ($OH^{\bullet}_{surf}$) or holes (reactions (V.18) and (V.19), respectively) or via the reaction of the formic acid in solution with free hydroxyl radicals ($OH^{\bullet}_{free}$) (reaction (V.20)).

Formic acid mechanism :

$$HCOO^-_{(ads)/inter} + {}^{\bullet}OH_{surf} \rightarrow H_2O + CO^{\bullet -}{}_2 \quad \textbf{(V.18)}$$

$$HCOO^-_{(ads)/inter} + h^+ \rightarrow CO^{\bullet -}{}_2 + H^+ \quad \textbf{(V.19)}$$

$$HCOO^-_{(aqu)} + {}^{\bullet}OH_{free} \rightarrow H_2O + CO^{\bullet -}{}_2 \quad \textbf{(V.20)}$$

In the formic acid degradation studies described in previous sections, it was observed that the rate constant was 3.5 times higher in the P25 than in the SA. The P25 is characterized as having anatase and rutile phases. It has been reported that the faces of the anatase phase have different potential energy [39]. The electrons and holes generated migrate to different faces depending on their potential energy allowing, in this way, their separation. In fact, it has also been reported that there are preferential faces of the anatase phase for photooxidation processes and preferential faces for photoreduction [38]. However, in catalysts like the P25 in which anatase and rutile phases coexist, it has been reported that, due to the low diffusivity of electrons in the rutile phase (89 times lower than in anatase), a greater separation is favored of the e^-/h^+ pair so a transfer of the holes is produced from the anatase to the rutile phase [39]. This would favor reactions (V.9)–(V.16) in the P25 with respect to the SA. In the fluorinated catalysts, an increase was observed in the rate constant of 1.8 times in the F- P25 with respect to the P25 and of 3.13 times in the F-SA with respect to the SA. As previously indicated, when fluorinating the catalysts reactions (V.9), (V.11) and/or (V.17) can be favored.

The degradation mechanisms of aniline and phenol, at the working pH values, are described in diagrams 1 and 2.

In the phenol degradation mechanism, depending on the intermediate generated, it can be determined which reaction is favored between (V.9), (V.11) and (V.15) or (V.17). It has thus been reported that resorcinol is generated from the reaction

of phenol directly with the holes (reaction (V.9)), hydroquinone from its reaction with the $OH\cdot_{surf}$ (reaction (V.11)) and catechol from its reaction with the $OH\cdot_{free}$ (reaction (V.15) or (V.17)) [34]. In other studiesperformed with fluorinated catalysts on phenol degradation, in addition to an increase in the phenol degradation rate constant (in the fluorinated catalysts), a significant increase was also observed in catechol concentrations with respect to hydroquinone concentrations [6, 20, 41, 42]. This has been attributed to reaction (V.17) being favored in these catalysts. However, in the different phenol degradation studies in the present work (with and without muconic acid) performed with the F-P25 and F-SA catalysts, although there was an increase between 3.6 and 4 times in the phenol degradation rate constant, in no test was observed a higher concentration of catechol than of hydroquinone. This would suggest that reaction (V.17) is not taking place in the studies performed with phenol with the F-P25 and F-SA catalysts. In these catalysts, the reactions which appear to be taking place are (V.9) and (V.11), with reaction (V.15) taking place to a lesser degree. That is, in these catalysts it seems that what is influential are the electrostatic effects that decrease the reaction rate of the e^-/h^+ pair and which in this way promote reaction with the $OH\cdot_{surf}$ (reaction (V.11)) or with the holes (reaction (V.9)). In fact, in the characterization studies the presence was observed of isolated hydroxyl groups in an even higher proportion than in the P25 and SA, as well as Brönsted acid sites.

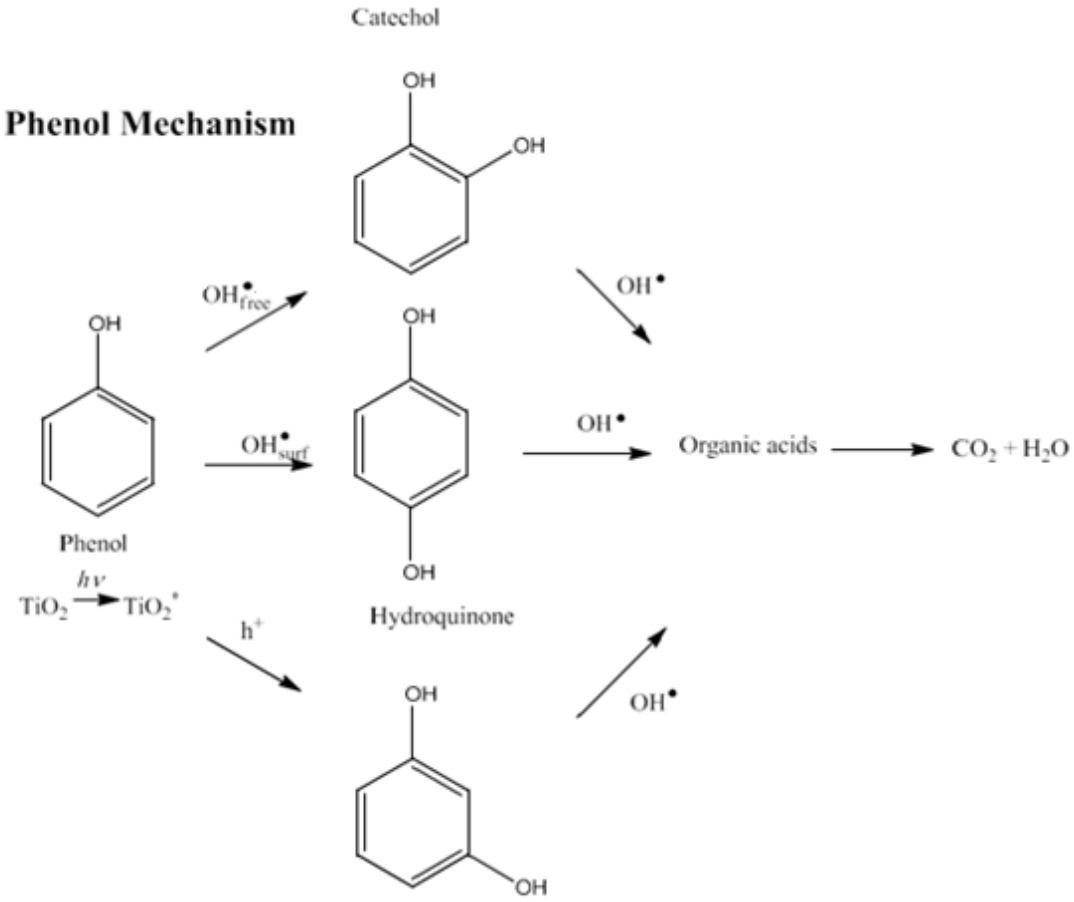

Diagram V.2: Degradation mechanisms of phenol

In the phenol degradation studies in the presence of 0.5 mM muconic acid concentrations, it was observed that the phenol degradation rate constant was reduced practically by half in all the catalysts compared to the studies without this acid. Also reduced by half was the $k_{muconic}$ compared to that of the studies without the presence of phenol. It was observed in the analysis of the intermediates that in the studies with muconic acid the concentrations of resorcinol was drastically reduced. This would suggest that reaction (V.9) of phenol with the holes would be inhibited in the presence of muconic acid. Muconic acid can be degraded by direct reaction of carboxylic acids with the holes (Kolbe reaction) or by means of the attack of OH· radicals on olefinic groups.

The fact that the concentration of resorcinol decreases in these conditions and not that of hydroquinone or catechol would suggest that, in the presence of muconic acid, phenol does not have access to the holes but does have access to the $OH\cdot_{surf}$, in this way partially inhibiting muconic acid degradation. For this reason, the rate constants of both are reduced by half. Meanwhile, the $k_{muconic}$ with the fluorinated catalysts is in all cases lower than that of the P25 and SA. This may be due to electrostatic repulsions which partially inhibit access to the surface of the fluorinated catalysts in the ionized form of this acid and to a significant number of Ti surface atoms being bonded to the fluorine (Table V.1). The muconic acid at the study pH=5 is principally in ionized form. However, the phenol and aniline are, at the study pH, in a suitable molecular form to be at the surface/solution interface.

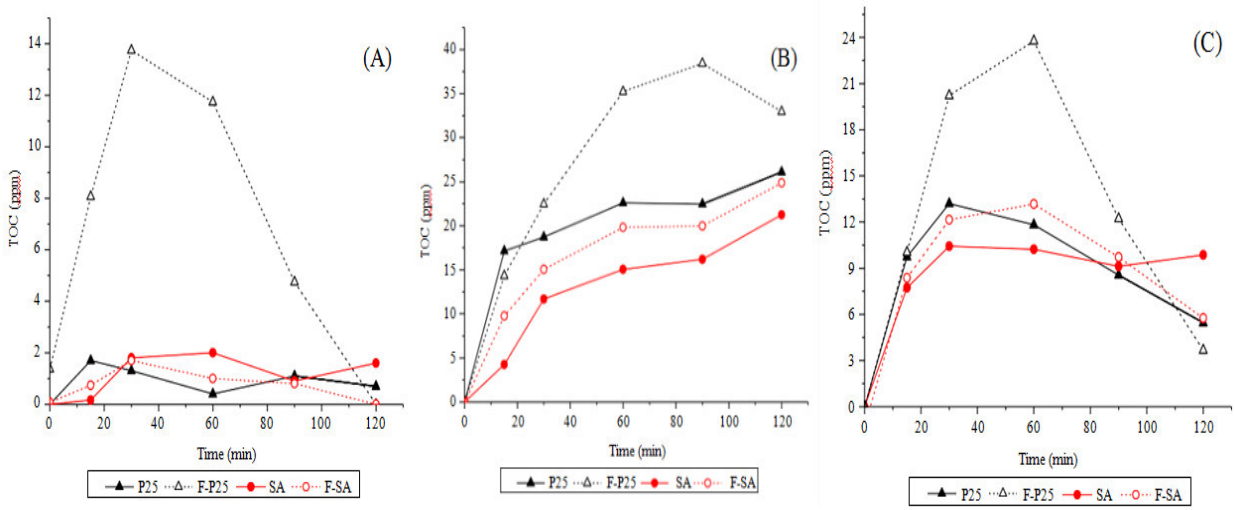

Figure V.12 : TOC evolution no corresponding to phenol, hydroquinone, catechol, resorcinol or muconic acid during phenol degradation (A), mixtures phenol: muconic acid 0.51mM:0.51 mM (B) and mixtures phenol:muconic acid 0.25 mM:0.25 mM (C).

As previously mentioned, in the three studies performed with phenol and in the study performed with aniline, approximately the same increase was observed in

the k_{phenol} of the F-P25 and F-SA with respect to the P25 and SA, respectively (Fig.V.8). That is, although the P25 has a higher k_{phenol} than the SA, when fluorinating both catalysts there takes place practically the same increase in the rate constant. This would suggest that in the fluorination process performed in this study the photoactive sites are being promoted in the same proportion.

The differences in the fluorination process carried out in this work compared to those carried out in other studies are that a much higher NaF concentration was used in this study and a specific type of aggregate was selected via filtration. Under these conditions, it has been reported in the bibliography that the process that takes place is [28]:

$$\equiv \mathbf{Ti} - \mathbf{OH}^{NaF} \equiv \mathbf{Ti} - \mathbf{F}^{NaF} \equiv \mathbf{Ti} - \mathbf{F} - \mathbf{F}^{-} \qquad \textbf{(V.21)}$$

Therefore, in the F-P25 and F-SA the typical Ti-F centers that give rise to reaction (V.17) do not appear, but the electrostatic effect is produced which favors e^-/h^+ pair separation. This would also explain the fact that the F-SA has similar rate constants to the P25 with all the substrates studied. This may indicate that the electrostatic effect of the fluoride ion on the anatase phase of the F-SA provokes a similar decrease in the recombination rate of the e^-/h^+ pair to that provoked by the rutile phase in the P25.

4. Conclusions:

The synthesis method for the fluorinated materials used in this study (F-P25 and F-SA) generated new catalysts with different properties to those described in other works. The characterization studies performed with the F-P25 and F-SA catalysts reveal a practically identical surface area and band gap. Small differences are observed in mean particle size between the SA and F-SA and in the anatase/rutile proportions between the P25 and F-P25 which are attributable to the catalyst filtration process. There was also detected in the F-P25 and F-SA the presence of isolated hydroxyl groups in a higher relative proportion (in

relation to the non-fluorinated catalysts), the absence of Lewis acid sites where the NH_3 could be adsorbed and the presence of Brönsted acid sites. It was also determined that interaction of Ti with fluorine atoms generates surface electron traps which cause a baseline increase in the FTIR spectra.

In the studies performed with formic acid, aniline, phenol and phenol-muconic acid mixtures, the k_{formic}, $k_{aniline}$, and k_{phenol} of the fluorinated catalysts are higher than those of the P25 and SA. With molecules whose adsorption on the catalyst surface is limited, as is the case of phenol and aniline, and whose degradation can take place at the surface/solution interface, the F-P25 and F-SA catalysts generate similar increases in the k_{phenol} with respect to the P25 and SA, respectively. The intermediates identified in phenol degradation suggest that in the fluorinated catalysts the formation of $OH\bullet_{free}$ is not favored. The results obtained indicate that the F-P25 and F-SA promote at the same intensity the sites responsible for the formation of $OH\bullet_{surf}$ and surface h^+.

In this way, it was determined that the fluoride adsorbed on the surface of the F-P25 and F-SA catalysts generates electrostatic fields which favor the reactions of $OH\bullet_{surf}$ and $h^+$with adsorbed molecules or at the surface/solution interface.

These new catalysts could be promising for processes in gas phase in which the intervention of $OH\bullet_{surf}$ and h^+ radicals is a determining factor.

References:

[1] J. Low, B. Cheng, J. Yu, Surface modification and enhanced photocatalytic CO2 reduction performance of TiO2: a review, Appl. Surf. Sci. 392 (2017)658–686.

[2] E. M. Samsudin, S. B. Abd Hamid, Effect of band gap engineering in anionic-doped TiO_2photocatalyst, Appl. Surf. Sci. 391 (2017)326–336.

[3] E. M. Samsudin, S. B. Abd Hamid, J. Ching Juan, W. J. Basirun, G. Centib, Synergetic effects in novel hydrogenated F-doped TiO_2photocatalysts, Appl. Surf. Sci. 370 (2016)380–393.

[4] E. M. Samsudina, S. B. AbdHamida, J. Ching Juana, W. J. Basiruna, A. E. Kandjanib, S. K. Bhargavaba, Effective role of trifluoroacetic acid (TFA) to enhancethephotocatalytic activity of F-doped TiO_2 prepared by modified sol–gelmethod, Appl. Surf. Sci. 365 (2016)57–68.

[5] A.A. Sadovnikov , A.E. Baranchikov , Y.V. Zubavichus , O.S. Ivanova , V.Y. Murzin, V.V. Kozik , V.K. Ivanov , Photocatalytically active fluorinated nano-titania synthesized by microwave-assisted hydrothermal treatment, J. Photochem. Photobiol. A: Chem. 303–304 (2015)36–43.

[6] C. Minero, G. Mariella, V. Maurino, E. Pelizzetti, Photocatalytic transformation of organic compounds in the presence of inorganic anions. 1. Hydroxyl-mediated and direct electron-transfer reactions of phenol on a titanium dioxide−fluoride system, Langmuir 16 (2000) 2632-2641.

[7] D. Vione, C. Minero, V. Maurino, M.E. Carlotti, T. Picatonottoa, E. Pelizzetti, Degradation of phenol and benzoic acid in the presence of a TiO2-based heterogeneous photocatalyst, Appl. Catal. B: Environ 58 (2005)79-88.

[8] Y-C Oh, W.S. Jenks, Photocatalytic degradation of a cyanuric acid, a recalcitrant species, J. Photochem. Photobiol. A 162 (2004)323-328.

[9] **S.** Kim, H. Park, W. Choi, Effects of TiO_2 Surface fluorination on photocatalytic reactions and photoelectrochemical behaviors, J. Phys. Chem. B 108 (2004)6402-6411.

[10] KONSTANTAKOU, Maria, STERGIOPOULOS, Thomas, LIKODIMOS, Vlassis, et al. Influence of fluorine plasma treatment of TiO2 films on the behavior of dye solar cells employing the Co (II)/(III) redox couple. The Journal of Physical Chemistry C, 2014, vol. 118, no 30, p. 16760-16775.

[11] K. Lv, Y. Xu, Effects of polyoxometalate and fluoride on adsorption and photocatalytic degradation of organic dye X3B on TiO_2: the difference in the production of reactive species, J. Phys. Chem. B 110 (2006)6204-6212.

[12] J. H. Pan, Z. Cai, Y. Yu, X.S. Zhao, Controllable synthesis of mesoporous F–TiO_2 spheres for effective photocatalysis, J. Mater. Chem. 21 (2011)11430-11438.

[13] J. Yu, Q. Xiang, J. Ran, S. Mann, One-step hydrothermal fabrication and photocatalytic activity of surface-fluorinated TiO_2 hollow microspheres and tabularanatase single micro-crystals with high-energy facets, CrystEngComm. 12 (2010) 872- 879.

[14] J. Yu, W. Wang, B. Cheng, B-L- Su, Enhancement of photocatalytic activity of mesporous TiO_2 powders by hydrothermal surface fluorination treatment, J. Phys. Chem. C 113 (2009) 6743-6750.

[15] X. F. Cheng, W. H. Leng, D. P. Liu, Y. M. Xu, J. Q. Zhang, C. N. Cao, Electrochemical preparation and characterization of surface-fluorinatedTiO_2 nanoporous film and its enhanced photoelectrochemical and photocatalytic properties, J. Phys. Chem. C 112 (2008) 8725–8734.

[16] J. Biedrzycki, S. Livraghi, E. Giamello, S. Agnoli, G. Granozzi, Fluorine- and niobium-doped TiO_2: chemical and spectroscopic properties of polycrystalline n-type- doped anatase, J. Phys. Chem. C 118 (2014)8462–8473.

[17] A. M. Czoska, S. Livraghi, M. Chiesa, E. Giamello, S. Agnoli, G. Granozzi, E.Finazzi, C. Di Valentin, G. Pacchioni, The nature of defects in fluorine-doped TiO_2, J. Phys. Chem. C 112 (2008)8951–8956.

[18] C. Di Valentin, G. Pacchioni, A. Selloni, Reduced and n-type doped TiO_2: Nature of Ti^{3+} Species, J. Phys. Chem. C 113 (2009)20543–20552.

[19] W. W. Dunn, Y. Aikawa, A. J. Bard, Characterization of particulate titanium dioxide photocatalysts by photoelectrophoretic and electrochemical measurements, J. Am. Chem. Soc. 103 (1981)3456-3459.

[20] Y. Xu, K. Lv, Z. Xiong, W. Leng, W. Du, D. Liu, X. Xue, Rate enhancement and rate inhibition of phenol degradation over irradiated anatase and rutile TiO2 on the addition of NaF: new insight into the mechanism, J. Phys. Chem. C 111 (2007) 19024- 19032.

[21] PARK, Hyunwoong et CHOI, Wonyong. Effects of TiO2 surface fluorination on photocatalytic reactions and photoelectrochemical behaviors. The Journal of Physical Chemistry B, 2004, vol. 108, no 13, p. 4086-4093.

[22] M. Lewandowski, D. F. Ollis, Halide acid pretreatments of photocatalysts for oxidation of aromatic air contaminants: rate enhancement, rate inhibition, and a thermodynamic rationale, J. Catal. 217 (2003)38-46.

[23] Q. Xiang, J. Yu, P. K. Wong, Quantitative characterization of hydroxyl radicals produced by various Photocatalysts, J. Colloid Interface Sci. 357 (2011)163–167.

[24] K. Ishibashi, A. Fujishima, T. Watanabe, K. Hashimoto, Detection of active oxidative species in TiO_2photocatalysis using the fluorescence technique, Electrochem.Commun. 2 (2000)207-210.

[25] J. Tang, H. Quan, J. Ye, Photocatalytic Properties and Photoinduced Hydrophilicity of Surface-Fluorinated TiO2, Chem. Mater. 19 (2007)116-122.

[26] LI, Di, HANEDA, Hajime, HISHITA, Shunichi, et al. Fluorine-doped TiO2 powders prepared by spray pyrolysis and their improved photocatalytic activity for decomposition of gas-phase acetaldehyde. Journal of Fluorine Chemistry, 2005, vol. 126, no 1, p. 69-77.

[27] M. Shariq Vohra, S. Kim, W. Choi, Effects of surface fluorination of TiO_2 on the photocatalytic degradation of tetramethylammonium, J. Photochem. Photobiol. A: Chem. 160 (2003)55–60.

[28] S. Liu, J. Yu, B. Cheng, M. Jaroniec, Fluorinated semiconductor photocatalysts: Tunable synthesis and unique properties, Adv. Colloid Interface Sci. 173 (2012)35–53.

[29] B. Bahrami, V. G. Komvokis, U. G. Singh, M. S. Ziebarth, O. S. Alexeev, M. D.Amiridis, In situ FTIR characterization of NH_3 adsorption and reaction with O_2 and CO on Pd-based FCC emission control additives, Appl. Catal. A: General 391(2011)11–21.

[30] A.C. Sola, D. Garzón Sousa, J. Araña, O. González Díaz, J.M. Doña Rodríguez, P. Ramírez de la Piscina, N. Homs, Differences in the vapour phase photocatalytic degradation of ammonia and ethanol in the presence of water as a function of TiO_2 characteristics and the presence of O_2, Catal. Today 266(2016)53-61.

[31] K. Hadjiivanov, H. Kno. Zinger**,** Species formed after NO adsorption and NO**+** O_2 co-adsorption on TiO2 : an FTIR spectroscopic study, Phys. Chem. Chem. Phys. 2 (2000)2803-2806.

[32] P. Pagsberg, B. Sztube, E. Ratajczak, A. Sillesen, Spectrokinetic studies of the gas phase reactions NH_2 + NOx initiated by pulse radiolysis. Acta Chem. Scand. 45 (1991) 329-334.

[33] X. Zhang, Q. S. Li, Direct dynamics study on the reaction of N2H4 with F atom: a hydrogen abstraction reaction? J. Phys. Chem. A, 110 (2006) 11636-11644]

[34] K. Lv, X. Guo, X. Wu, Q. Li, W. Ho, M. Li, H. Ye, D. Du, Photocatalytic selective oxidation of phenol to producedihydroxy benzenes in a TiO2/UV system: Hydroxyl radical versus hole, Appl. Catal. B 199 (2016)405-411.

[35] H. Sheng, Q. Li, W. Ma, H. Ji, C. Chen, J. Zhao, Photocatalytic degradation of organic pollutants on surface anionized TiO2: Common effect of

anions for high hole- availability by water, Appl. Catal. B: Environ. 138– 139 (2013)212–218.

[36] J. Araña, E. Pulido Melián , V.M. Rodríguez López, A. Peña Alonso, J.M. Doña Rodríguez , O. González Díaz , J. Pérez Peña, Photocatalytic degradation of phenol and phenolic compounds Part I. Adsorption and FTIR study, J. Hazard. Mater. 146 (2007) 520–528.

[37] M. Canle L. , J.A. Santaballa, E. Vulliet, On the mechanism of TiO_2-photocatalyzed degradation of aniline derivatives, J. Photochem. Photobiol. A 175 (2005)192–200.

[38] M. F. J. Dijkstra, H. J. Panneman, J. G. M. Winkelman, J. J. Kelly, A. A. C. M. Beenackers. Modeling the photocatalytic degradation of formic acid in a reactor with immobilized catalyst, Chem. Eng. Sci. 57 (2002) 4895 –4907.

[39] X. Ma, Y. Dai, M. Guo, B. Huang, Relative photooxidation and photoreduction activities of the {100},{101}, and {001} surfaces of anatase TiO_2, Langmuir 29 (2013) 13647−13654.

[40] B. Sun, Alexandre V. Vorontsov, P. G. Smirniotis, Role of platinum deposited on TiO_2 in phenol photocatalytic oxidation, Langmuir 19 (2003) 3151–315.

[41] N. Watanabe, S. Horikoshi, H. Hidaka, N. Serpone, On the recalcitrant nature of the triazinic ring species, cyanuric acid, to degradation in Fenton solutions and in UV- illuminated TiO_2 (naked) and fluorinated TiO_2 aqueous dispersions, J. Photochem.Photobiol. A: Chem. 174 (2005)229–238.

[42] C. Minero, G. Mariella, V. Maurino, D. Vione, and E. Pelizzetti, Photocatalytic Transformation of Organic Compounds in the Presence of Inorganic Ions. 2. Competitive Reactions of Phenol and Alcohols on a Titanium Dioxide-Fluoride System, Langmuir 2000, 16,8964-8972.

CHAPTER VI

GAS PHASE STUDIES

Part 1 : TiO_2 and F-TiO_2 photocatalytic deactivation in gas phase (ethanol)

TiO_2 and F-TiO_2 photocatalytic application in gas phase (ethanol)

1. Introduction

Different strategies have been used to enhance the activity of these materials by impeding their deactivation and reducing the e^-/h^+ recombination reactions. One of these strategies is the surface modification of TiO_2 with fluorine (F- TiO_2). Fluorine has a higher electronegativity than oxygen and has a specific affinity for adsorption onto TiO_2 acting as a Lewis base. The presence of fluoride anions has shown positive effects in aqueous phase increasing the degradation rate of different compounds [1–3]. It has been shown that the strong electron acceptor capacity of the Ti-F groups present on the surface hinders recombination of photo-generated electrons and holes, thereby enhancing photocatalytic efficiency [4,5]. However, many aspects of the effect of fluorine on the TiO_2 surface have not been fully clarified specially in photocatalytic processes in gas phase.

The aim of chapter is to study TiO_2 deactivation processes during the degradation of ethanol in gas phase, using catalysts composed only by anatase phase and anatase/rutile phase mixtures. A study is also undertaken of the effect of fluorination of these materials on deactivation. These studies were carried out with mixtures of air, ethanol and water. The water vapor can compete with the adsorption centers, but can also favor the diffusion processes of molecules and radicals during the photocatalytic process. It has also been reported that water may participate in stabilization of the adsorbed molecules or of the photogenerated holes [6,7]. The adsorption process was performed continuously in view to increase the signal of minority species which may be generated during the adsorption process.

2. Experimental

2.1. Characterization of materials

The surface concentration of fluorine on the catalysts was semi-quantitatively determined by EDAX analysis.Analyses of the crystalline structure were performed by X-ray diffraction. Anatase-rutile fractions were calculated taking into account the relative diffraction peak intensities of crystalline planes (101) and (111) of anatase and rutile, respectively. Field emission scanning electron microscopy (FESEM) images, BET surface area measurements and diffuse reflectance UV–Vis spectra (DRS-UV–Vis) were carried out. Band gap values were calculated from diffuse reflectance spectra by using the Kubelka-Munk function, according to the Tandon-Gupta method [8].

2.2. Photocatalytic experiments

The photocatalytic experiments were performed with four commercial catalysts (P25, SA, P90 and PC100) and the two fluorinated catalysts (F-P25 and F-SA). The interaction and photocatalytic degradation of ethanol were followed by Fourier Transform Infrared Spectroscopy (FTIR). 10 mg of catalyst were used in each experiment.A UV lamp was used as source in the degradation studies.

Once the substrate was adsorbed and the initial spectrum was taken, the irradiation was initiated and the FTIR analysis was periodically performed in order to study the evolution of species during the degradation process.

Catalysts were subjected to an air flow of 50 $mL \cdot min^{-1}$ in which the concentrations of ethanol and water were, respectively, 8.5 and 32.9 $mmol \cdot min^{-1}$ for 60 min and then placed in the cell for analysis. The system is summarized in figure VI.1.

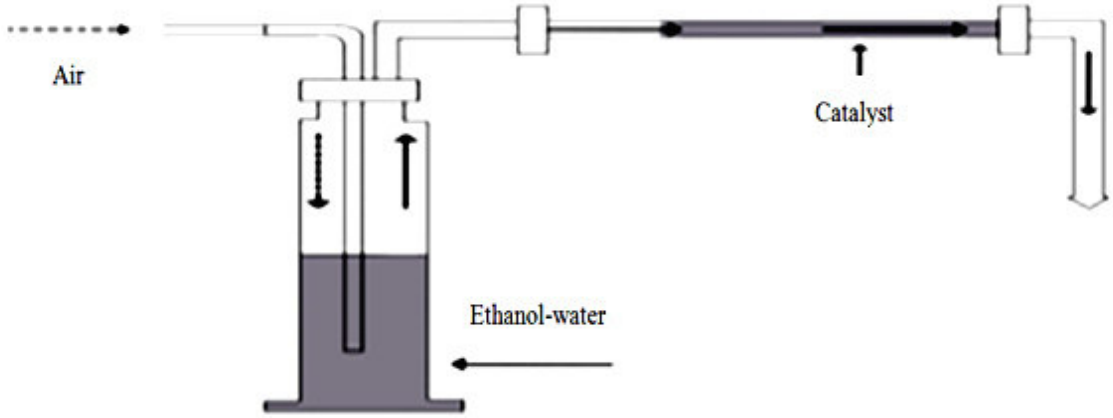

Figure VI.1: System used to study adsorption of ethanol onto catalysts.

Blank experiments of photolytic evolution of ethanol were carried out in the absence of catalyst and under the same experimental conditions; reactants remained unaltered throughout the assay.

3. Results and discussion

3.1. DRS BET area, EDAX, SEM, XRD and UV–Vis DRS analyses

	Surface area ($m^2 \cdot g^{-1}$)	Anatase/rutile phase ratios	Band gap (eV)	Molar ratio	
				Ti/F	F/Na
P25	50.9	82.3 / 17.7	3.16	-	-
F-P25	52.9	82.4 / 17.6	3.00	20.32	2.50
SA	47.3	100 / 0	3.16	-	-
F-SA	46.1	100 / 0	3.18	18.46	2.09
P90	95.2	89.4 / 10.6	3.25	-	-
PC100	94.7	100 / 0	3.14	-	-

Table VI.1 - Characteristics results of the studied catalysts

Table VI.1 shows the most important results of the BET, EDAX, DRX and UV–Vis DRS analyses. The P90 and PC100 catalysts have the largest surface area (95.2 and 94.7$m^2 \cdot g^{-1}$, respectively), while the P25, SA, F-P25 and F-SA catalysts have similar surface areas (of around 50 $m^2 \cdot g^{-1}$). The P25, F-P25 and P90 have anatase and rutile in

their structure, while the SA, F-SA and PC100 catalysts are only composed of anatase phase (figure VI.2 shows the X-ray diffraction pattern of the P25, F-P25, SA and F-SA).

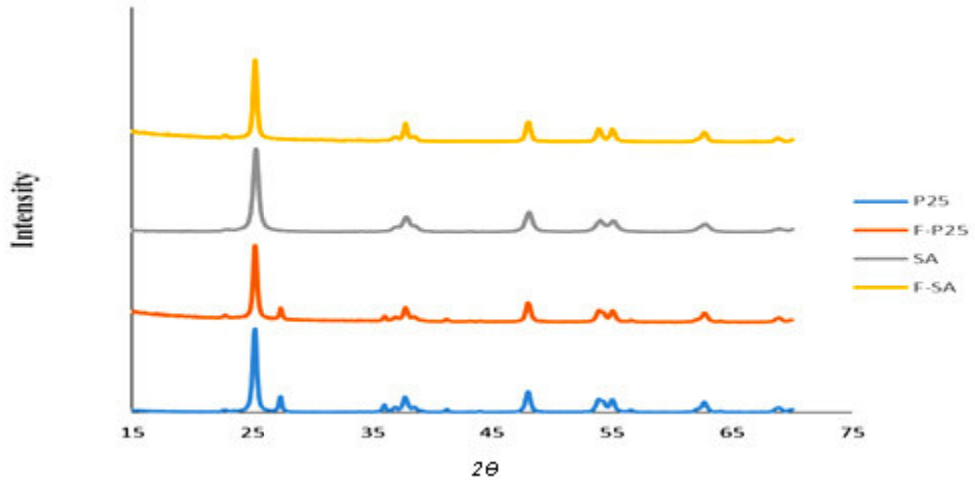

Figure VI.2: XRD of fluorinated and non-fluorinated catalysts

The band gap values obtained from the UV–Vis analyses are all very similar, with no significant changes observed when fluorinating the catalysts (figure VI.3 displays the UV–Vis DRS spectra of the P25, F-P25, SA and F-SA).

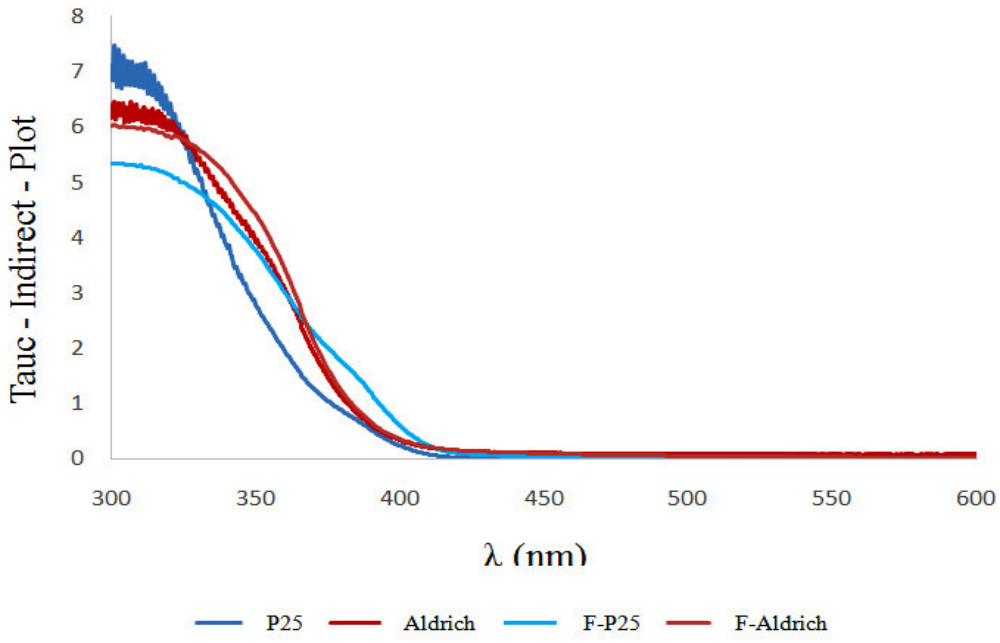

Figure VI.3: UV-Vis spectra of fluorinated and non-fluorinated catalysts

Thus, as shown in other studies, surface fluorination of the catalysts does not modify the optical properties of these materials [9,10]. The images obtained from the SEM analyses of F-P25, F-SA and SA showed a similar distribution of aggregates. However, SEM analyses of P25 showed different distribution (Figure VI.4).

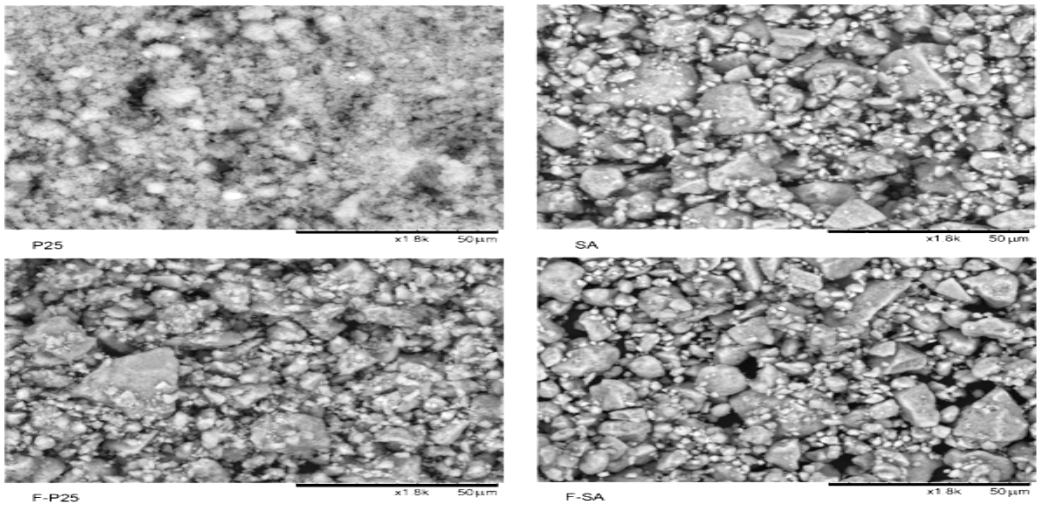

Figure VI.4: SEMof fluorinated and non-fluorinated catalysts

Table VI.1 also shows the Ti/F and F/Na ratios obtained from the EDAX analysis. The surface composition studies also showed the presence of sodium on the surface of these materials, though its concentration is significantly lower than the molar concentration of fluorine. This shows that the fluorine is mostly interacting with the catalyst surface and is not as NaF, though the presence of this salt on the surface cannot be avoided.

3.2. Characterization of the adsorbed water, hydroxyl groups and surface charge

Figure VI.5 shows the FTIR spectra of the fluorinated and non-fluorinated P25, SA, P90 and PC100 catalysts. Note in particular the band attributed to isolated hydroxyl groups (3698 cm^{-1}), the bands attributed to adsorbed water (3600–3000 cm^{-1} and 1640 cm^{-1}), and finally the position of the baseline of each of the catalysts.

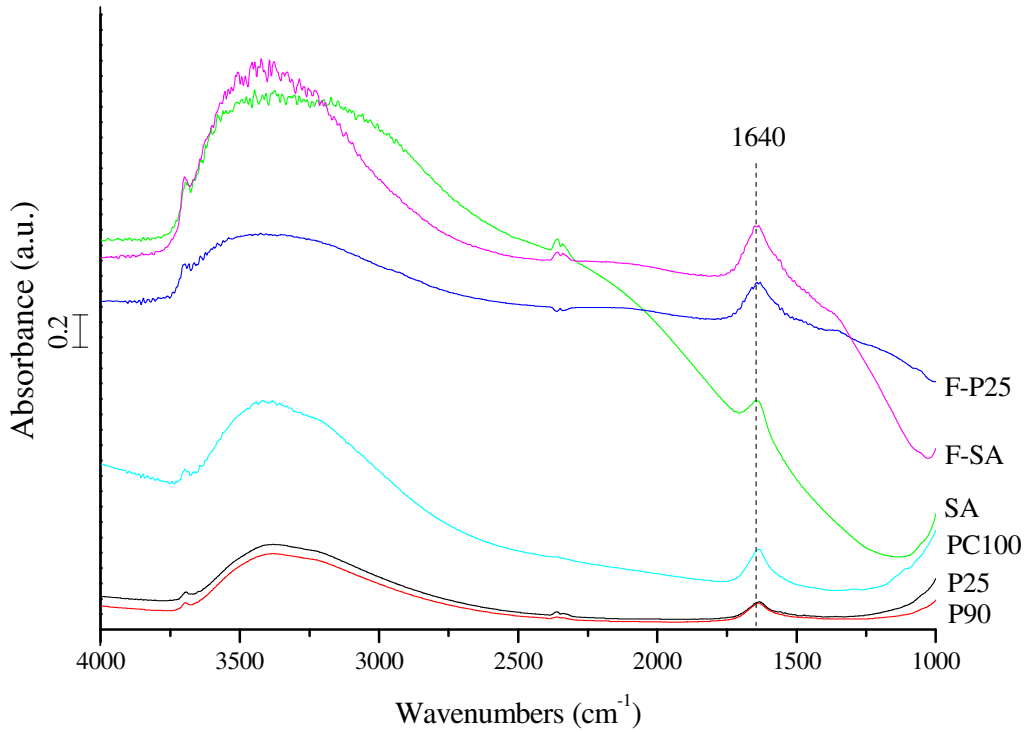

Figure VI.5: FTIR spectra of the fluorinated and non-fluorinated catalysts

The band observed in all catalysts at 1640 cm^{-1} is assigned to the water bending mode (υ_2), while the broad band between 3650 and 3000 cm^{-1} is attributed to antisymmetric (υ_3) and symmetric (υ_1) stretching vibration modes of the water [11,12].

An important aspect to note in the spectra of figure VI.5 is the position of the baseline. As a result of the presence of surface or shallow electron traps, electrons are fed to the conduction band via thermal processes such as those generated by the infrared radiation used to obtain the spectra. The electrons promoted to the conduction band have a similar behavior to that described for delocalized electrons confined to a three-dimension box with infinite walls; the high density of generated states gives rise to the continuous presence of excited electrons leading to a baseline increase of the infrared spectrum [13]. The baseline position of the SA and PC100 catalysts, the ones with only anatase phase, is higher than that of the P25 and P90. On modification of P25 with fluorine, a baseline increase takes place which takes it to the same level as that observed in the SA catalyst. When TiO_2 is modified with fluorine, at least a fraction of the excess electrons introduced by the fluorine are localized by lattice Ti^{4+}

cations. The presence of reduced Ti^{3+} centers in the as-prepared, fully oxidized solid indicates that the F-TiO_2 system can be described in terms of an n-type semiconductor provoking the baseline increase observed in the F-P25 catalysts [14]. This could be related with the change in the aggregate distribution observed in SEM analyses.

3.3. Ethanol photocatalytic degradation studies

Once ethanol was adsorbed onto the surface, the catalysts were illuminated for 90 min and the different species formed were studied by FTIR. Figure VI.6 shows the evolution of the adsorbed species in the region between 4000 and 1000 cm^{-1} for the P25 and F-P25 catalysts.

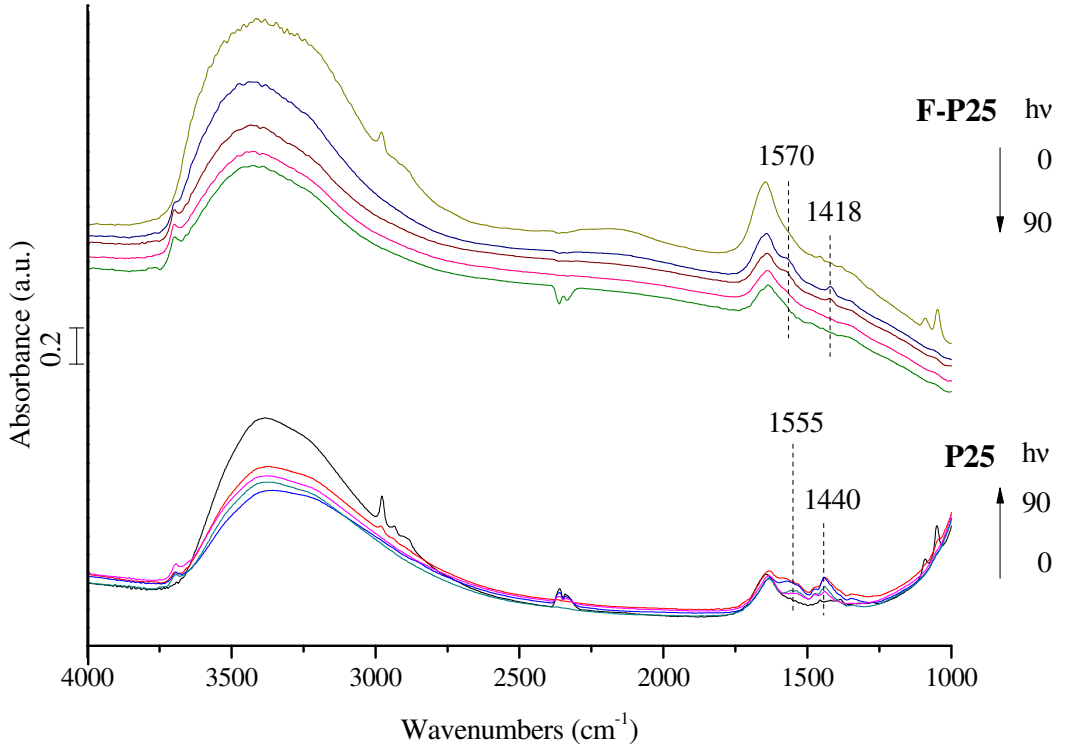

Figure VI.6: Evolution of the spectra of P25 and F-P25 after ethanol adsorption and after different periods of time under illumination

Similar spectra were obtained with the other catalysts (SA, P90 and PC100). The main difference observed with the different catalysts was the nature of the acetates formed after the first few minutes of irradiation corresponding to the bands observed between 1580–1540 cm^{-1} and 1450–1430 cm^{-1} and attributed to $\upsilon(COO)_{as}$ and $\upsilon(COO)_{s}$. FigureVI.7 compares the spectra of the acetates obtained for the different catalysts

after 20 min of illumination. Note that the asymmetric vibration of the acetates identified in both catalysts is found at approximately the same wavenumber. However, the symmetric vibration is found at 1440 cm^{-1} in the P25 and P90, and at 1418 cm^{-1} in the SA and PC100. The differences observed may be due to the presence of rutile phase in the first two catalysts. Indeed, similar changes were observed in studies carried out using acetic acid with TiO_2 with different phases [15].

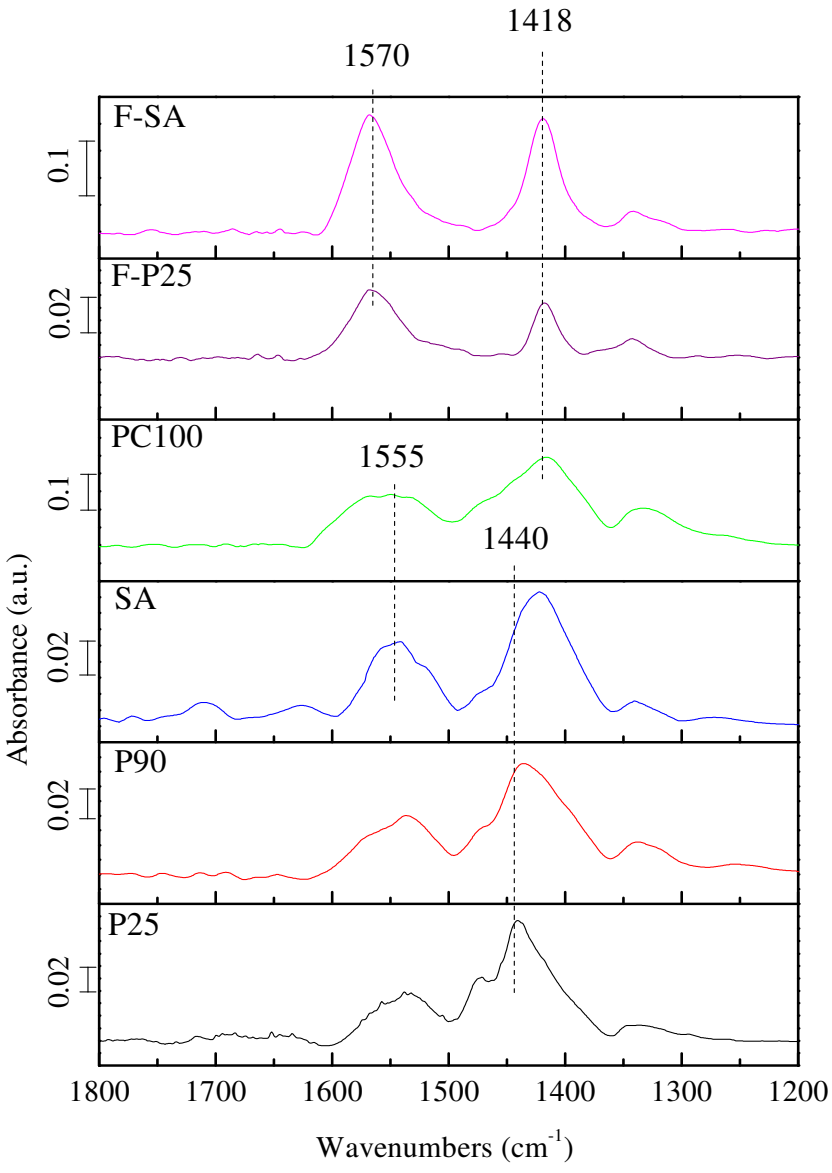

Figure VI.7: Comparison of the acetates spectra during ethanol degradation on the different catalysts after 20 min of illumination.

It can therefore be argued that the shift observed in the symmetric vibration in the P25 and P90 catalysts is due to the presence of rutile phase. Bands were also observed in

the SA catalyst around 1715 and 1270 cm^{-1} which can be attributed to acetaldehyde or acetic acid [16].

The photocatalytic degradation of ethanol has been described through the following reaction stages [17,18]:

$$CH_3CH_2OH \rightarrow CH_3CHO \rightarrow CH_3COOH \quad \textbf{(VI.1)}$$

$$CH_3COOH \rightarrow HCHO \rightarrow HCOOH \rightarrow CO_2 \quad \textbf{(VI.2)}$$

During the photocatalytic studies undertaken in the present work, it was possible to clearly follow the evolution of the ethanol and acetates adsorbed on the surface and the process that was observed can be summarized in Reactions (VI.1) and (VI.2). The other intermediates which are generated must be degraded very quickly and for this reason they were not observed. Therefore, in order to make a proper analysis of the species generated in this study and their evolution during illumination, acetate (1440 or 1418cm^{-1}) and ethanol (1050 cm^{-1}) tracings were performed. Figure VI.8 A–C show the evolution of the bands attributed to the symmetric vibration (υ(COO)s) of the acetates and the symmetric vibration (υ(CO)) of the ethanol. A progressive increase of the intensity of the band attributed to the υ(COO)s can be observed in the P90 and P25 catalysts during the first 15–20 min (Reaction (VI.1)), followed by a progressive decrease (Reaction (VI.2)). The beginning of the decrease of the intensity of this band coincides with the disappearance of the ethanol band at 1050 cm^{-1} (υ(CO)). Thus, it would appear that Reaction (VI.2) does not start until the whole Reaction (VI.1) has concluded.

A progressive increase of the intensity of the band attributed to the υ(COO)s can also be observed in the PC100 and SA catalysts during the first few minutes. However, after this initial period the intensity of the band does not change for the next 20 min, and subsequently it slowly decreases.

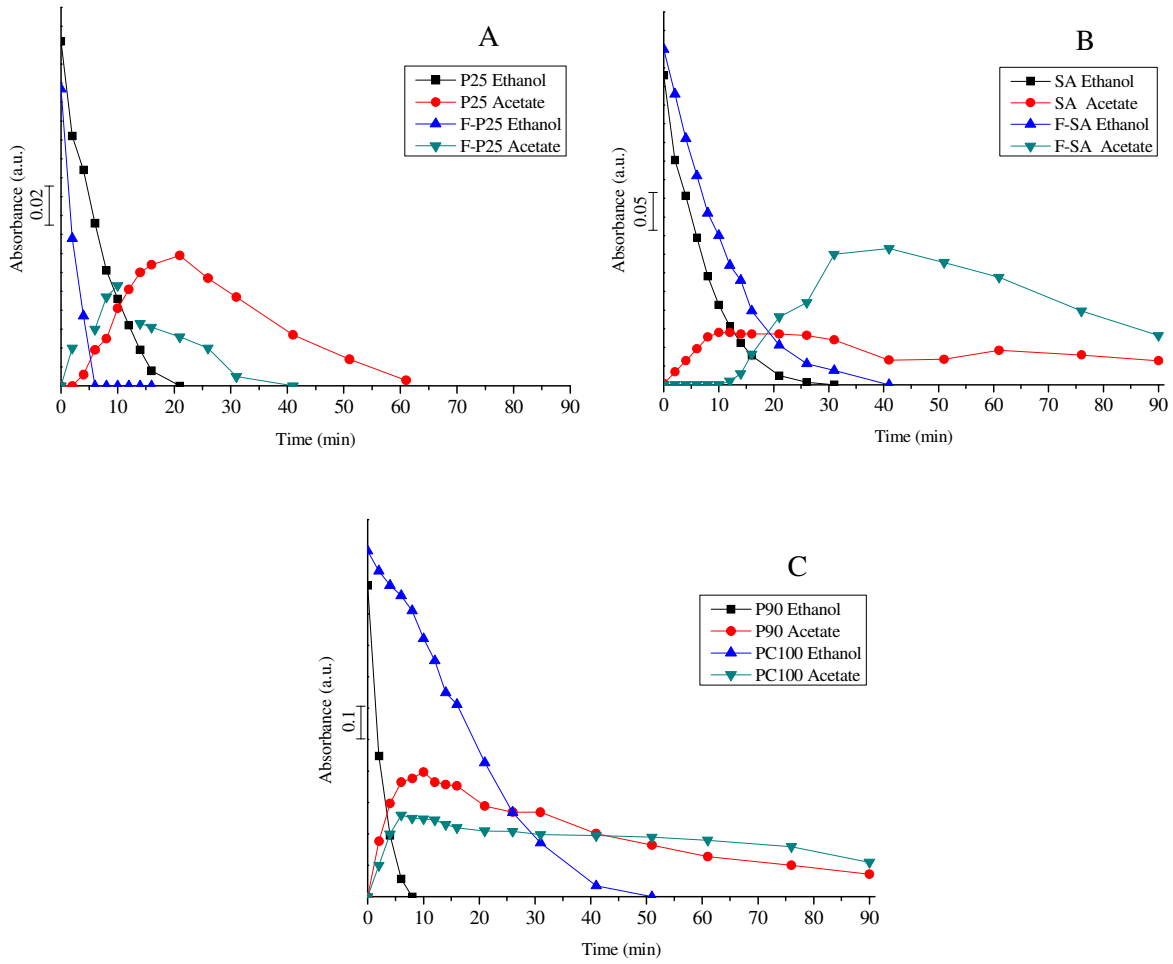

Figure VI.8: Evolution over the time of the different IR bands during UV radiation of (A) P25 and F-P25, (B) SA and F-SA and (C) P90 and PC100

3.4. Deactivation studies

In order to elucidate the deactivation processes of these catalysts, a new study was undertaken in which, after the first 20 min of illumination (that is when the ethanol signal at 1050 cm^{-1} was no longer observed), the catalyst was once again impregnated with ethanol for 1h. It was then again illuminated under the same conditions as previously. This process was repeated a total of 7 times (cycles).

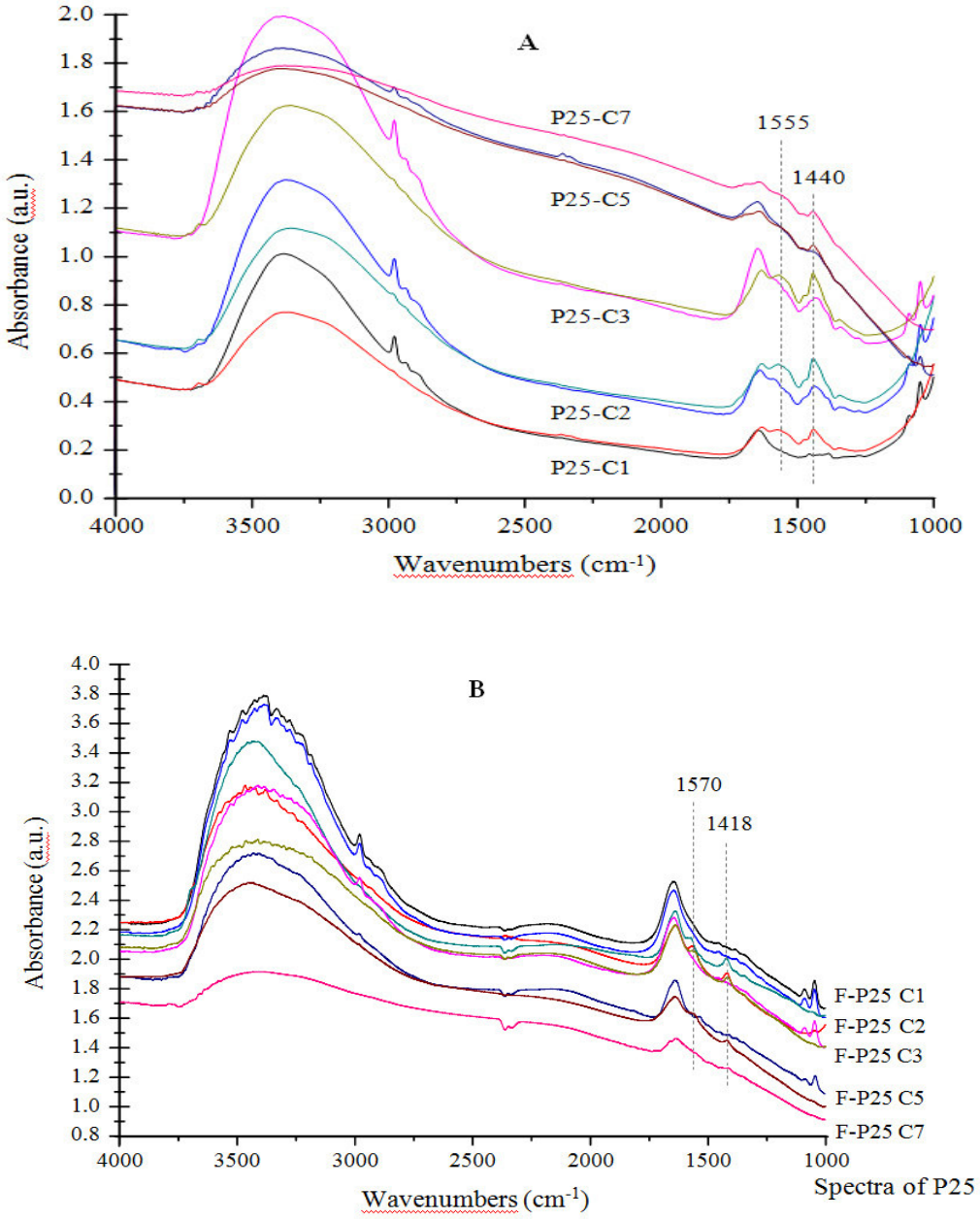

Figure VI.9: Spectra of P25 (A) and F-P25 (B) at 0 and 20 min of illumination in cycles (C) 1, 2, 3, 5 and 7 during the deactivation studies

Figure VI.9A shows the initial spectra of each of these cycles 1, 2, 3, 5 and 7 for P25, and the spectra obtained after 20 min of illumination (the spectra obtained in these tests for P90 were practically identical and are thus not shown). In the studies with SA and PC100, no increase was observed in the formation of acetates after the first cycle. However, adsorbed ethanol was observed after the first cycle. It has been reported that ethanol can be adsorbed onto organic compounds present on the surface[19].

FigureVI.10 shows the increase in the intensity of the band attributed to υ(COO)s for each catalyst after each cycle.

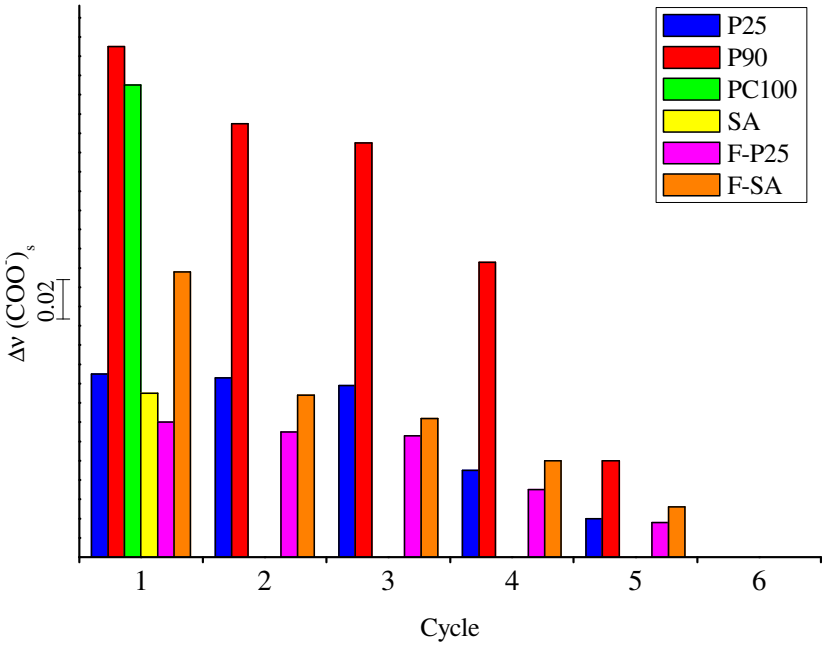

Figure VI.10: Increase of the band associated with the vibration υ(COO)s of acetates produced after each cycle during the deactivation studies.

This increase progressively diminishes as the number of cycles increases, indicating deactivation processes. After first cycles, in the P25 (Figure VI.9A) and P90 catalysts, the band attributed to the υ(COO)s of acetates possibly adsorbed on the rutile surface decreases significantly in intensity and only the band present at 1418 cm^{-1} is observed, attributed to the υ(COO)s of acetates adsorbed on the anatase surface (Figure VI.9A). This would suggest that the acetates present on the rutile surface are very weakly adsorbed (probably hydrated as reported in other studies [15]). The decrease in the intensity of all the bands after the third cycle should also be noted (Figure VI.10). It is also observed that the baseline of the initial spectrum of each cycle increases its position with respect to the previous cycle (Figure VI.9A). As previously indicated, the increase in the baseline of the spectrum is attributed to an accumulation of surface electrons close to the conduction band. The progressive injection of electrons through the adsorption of the acetate on the anatase phase may be responsible for modification of the position of baseline and the deactivation observed in the P25 and P90 catalysts.

In the SA and PC100, deactivation takes place faster as in these catalysts surface electrons are present from the initial instants (Figure VI.5).

3.5. Studies with fluorinated catalysts

Given that with commercial catalysts deactivation processes were observed as a consequence of the increase in the negative charge on the catalysts, similar studies were carried out with the fluorinated catalysts F-P25 and F-SA. Firstly, a degradation test was performed for 90 min, as with the previous catalysts. Figure VI.6 shows a comparison of the spectra obtained with the F-P25 and the P25. Note that, unlike the P25, there takes place with the F-P25 a progressive decrease in the baseline position with illumination time. This can be more clearly observed in the studies with the F-SA (Figure VI.11).

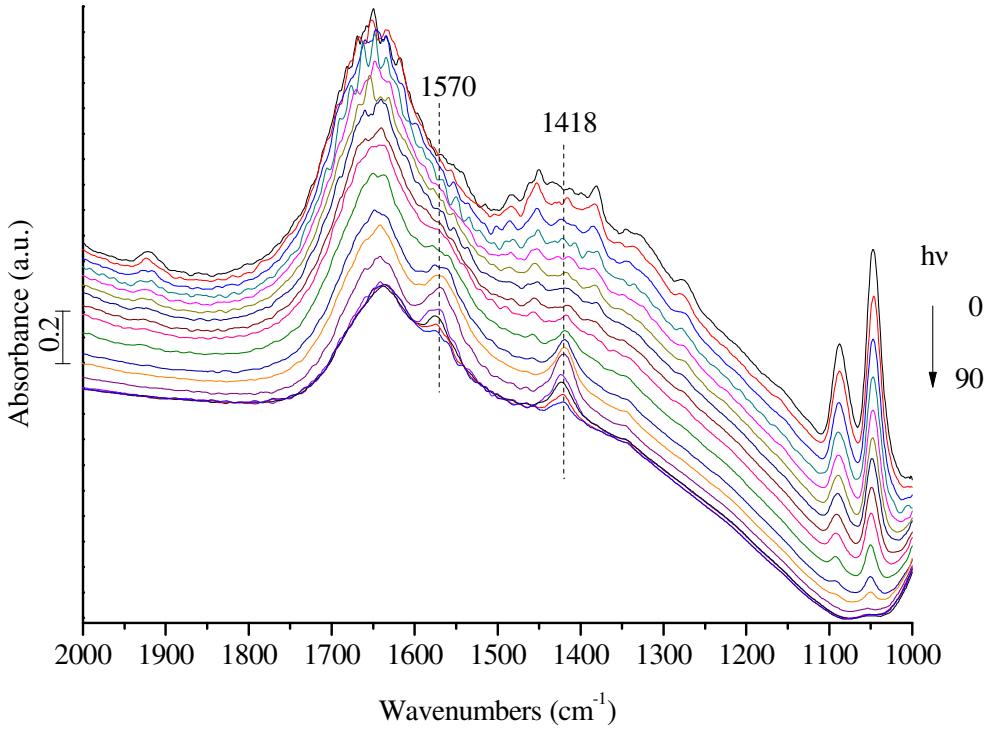

Figure VI.11: Evolution of the spectra of F-SA after ethanol adsorption and after different periods of time under illumination.

It should also be noted that the wavenumber and the shape of the bands attributed to the υ(COO)as and υ(COO)s are different to those observed in the studies of the non-

fluorinated catalysts (Figure VI.7). With the fluorinated catalysts (F-P25 and F-SA), these bands are narrower, the symmetric and asymmetric vibrations have the same intensity and are found at 1570 and 1418 cm^{-1}, respectively. The shape of these bands and the wavenumber are similar to those of sodium acetate [20]. The EDAX analyses revealed the presence of sodium on the surface of these catalysts after fluorination, suggesting that formation of these acetates is feasible

As a consequence of the high density of states with high negative surface charge of semiconductors with adsorbed F^- ions, during illumination the photogenerated holes would be trapped on the surface and the electrons forced to move to more interior Ti atoms of the crystalline structure [21]. The holes can then react with the oxygen atoms and/or surface water giving rise to radicals or with the electrons trapped on the surface, as can be deduced from Figures VI.6 and VI.11.This would explain the decrease in the baseline position during illumination of the fluorinated catalysts. Ethanol degradation with the fluorinated catalysts is slightly faster than with the P25 and SA (Figure VI.8A and B) due to the above described effect.

The same deactivation studies were also performed as with the other catalysts. FigureVI.9B shows a comparison of baseline evolution of the F-P25 after different cycles (cycle 1, 2, 3, 5 and 7) with that obtained for P25. At the start of each new cycle no acetates are observed, as these must have been dissolved and carried away during the ethanol impregnation. The baseline of the spectra decreases progressively after each cycle. When both catalysts are deactivated (F-P25 and P25), the spectra are practically identical and the baseline of the spectrum is found in similar position. Exactly the same behavior was observed with the F-SA.

On the other hand, deactivation with the P25 and P90 catalysts is produced by adsorption of the acetates on the anatase phase. It has been reported that diffusivity of electrons in rutile phase is 89 times lower than in anatase, and that therefore a transfer of holes can take place from the anatase to rutile phase [22]. When the density of electrons in the anatase phase increases this transfer would be more impeded. In the cycles performed with the P25 and P90, it was observed that after hydrated acetates are formed on the rutile surface they could be transferred and adsorbed on the anatase

phase and a baseline increase results as a consequence of the transfer of electrons. The increase of acetates on the anatase phase must be increasing the charge density in this phase and decreasing hole transfer.

As was seen in Figure VI.9B, the final spectrum after deactivation of the fluorinated catalysts (as a consequence of the loss of electrons trapped on the surface) and the final spectrum of the P25 catalyst (after the progressive adsorption of acetates, FigureVI.9A) are very similar in terms of the intensity of the hydration bands and baseline position. That is, it appears that a similar deactivated state is reached in which, as a consequence of electron transfer, the two processes which accelerated the reaction are deactivated. The fact that the final spectrum is the same may indicate that only the electron transfer processes described here are intervening in the deactivation process.

4. Conclusions

In the P25 and P90 catalysts, it was observed that acetates resulting from ethanol degradation are found hydrated on the surface of the rutile phase. It was found that if these acetates are not degraded, they could migrate and are adsorbed on the anatase surface, provoking a transfer of electrons to surface layers which progressively deactivate the catalyst.

In the catalysts with purely anatase phase (SA and PC100), deactivation is immediate if the acetates are not removed before again adsorbing ethanol. Surface-trapped electrons were identified in these catalysts, probably generated in their synthesis process, which may accelerate catalyst deactivation.

The characterization studies performed with the F-P25 and F-SA catalysts showed that in the fluorination process carried out in this study there is no significant modification to either surface area size, optical properties or crystalline phase distribution. However, the fluorination process does modify the concentration of surface electron traps, aggregates distribution and the interaction of acetates with the catalyst surface. In these semiconductors, a decrease in the concentration of electrons in the surface traps was observed during irradiation which was attributed to its reaction with the

holes. The progressive decrease in the concentration of electrons in the traps may be the reason for the deactivation of these materials during ethanol degradation due, in part, to the diminishing effect of the electrostatic field.

It was therefore observed that the charge transfers processes, by different routes, in the P25, SA, F-P25 and F-SA catalysts ultimately give rise to a similar deactivated state.

Part 2 : FTIR STUDY OF NH_3 PHOTOCATALYTIC DEGRADATION IN GAS PHASE WITH TiO_2 AND F-TiO_2

FTIR study of NH_3photocatalytic degradation in gas phase with $TiO_2$and F-TiO_2

1. Introduction

Fluorine has a higher electronegativity than oxygen and has a specific affinity for adsorption onto TiO_2 acting as a Lewis base. Different studies have shown that TiO_2 doping with fluorine does not change the band gap of this semiconductor as the *p* orbitals of the fluorine have a lower energy than those of the oxygen atoms [23-25]. However, it has been shown that the strong electron acceptor capacity of the Ti-F groups present on the surface hinders recombination of photo-generated electrons and holes, thereby enhancing photocatalytic efficiency [23-26]. It has been reported that the increased degradation rate is due to the increase in the concentration of OH• radicals in solution as the fluorides displace the -OH groups from the surface [1]. In this respect, the following mechanisms have been proposed:

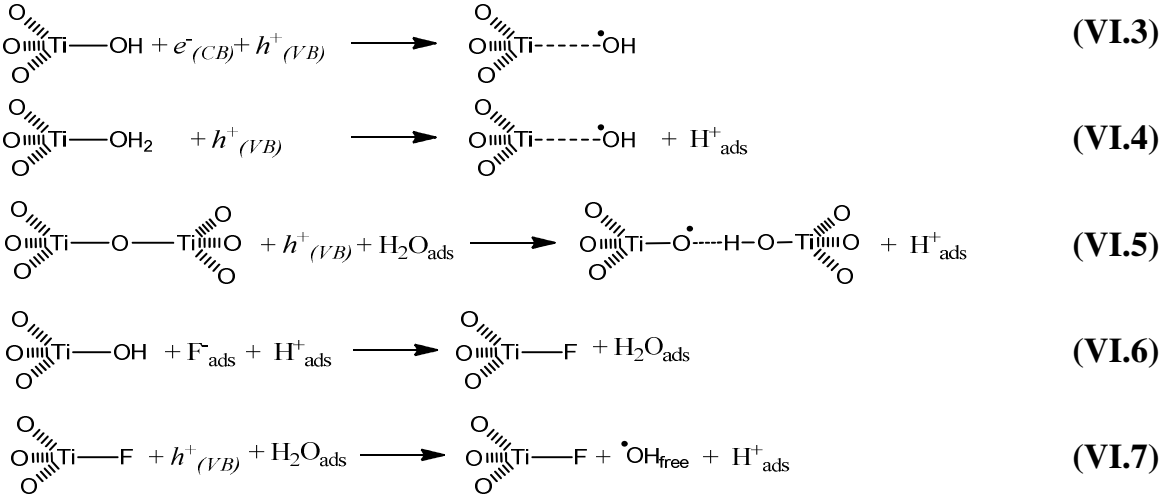

However, the physical chemistry of this process as well as many other aspects of the effect of fluorine on the TiO_2 surface have not been fully clarified [26].

It has been reported that the doping of anatase TiO_2 with elements like F with extra electrons gives rise to *n*-type materials with significantly different properties to those of the original catalyst [27]. The extra electrons provided by the F^- ions are stabilised on the titanium ions of the crystal lattice giving rise to Ti^{3+} ions homogenously scattered over the crystal lattice. Titanium dioxide is a reducible oxide whose

composition depends, among other factors, on oxygen pressure in the atmosphere. The extra electron provided by the fluorine will be found in the Ti 3*d* orbitals a few tenths of an electron-volt below the lower end of the conduction band [28]. TiO_2doping with fluorine gives rise to two types of fluoride species. The first of these arises when the F^- ion replaces the O^{2-} ions of the crystal lattice resulting in Ti-F-Ti bonds. This leads to the formation of Ti^{3+} species in the bulk, giving rise to localized Ti^{3+} states just below the conduction band. This type of doping inhibits oxygen adsorption and consequently the formation of superoxide radicals, suggesting that the sites with defects are localized in the bulk and not on the surface. The second species consists of F^- ions on the surface of the solid which replace surface hydroxyl groups giving rise to Ti-F terminal groups without generating reduced sites [28]. The Ti^{3+} sites that are generated may be systems entirely localized in sections of the catalyst or systems in which there is a total delocalization of electron density in all the ions of the metal, with the energy levels of these states just below the conduction band [27]. Studies undertaken to date suggest that the second of these possibilities appears to be the most probable [29]. Displacement of the negative charge, which takes place at the edges of the energy levels favors the charge transference rate and lowers the recombination rate. The accumulation of electrons trapped in the conduction band in a photo-stationary state results in the surface charge of the TiO_2 suspended particles changing to negative [30]. Most of the electrons would be localized on Ti(III)-OH surface sites.

It has been reported in other studies that when doping TiO_2 with fluorine, this increase in the degradation rate was observed but it was decreased with rutile phase [31]. It has also been shown that the increase in the degradation rate does not always require pre-adsorption of the fluoride ions. A Helmholtz double layer has thus been proposed in which the fluoride ions would be situated on the internal and external planes of this double layer, facilitating desorption of the surface bonded OH• radicals to the solution upon irradiation of the TiO_2. The most active radical fluorides are those found in the outer Helmholtz layer, and are the most efficient at provoking desorption of the surface bonded OH• radicals. The inner layer fluoride ions, namely those adsorbed onto the surface or bonded to Ti^{4+} sites, have a lower capacity to form a bond with the

surface bonded OH• via hydrogen-fluorine bridges. The key to this proposal lies in the argument that desorption to the solution of the surface bonded hydroxyl radicals on the irradiated TiO_2 is thermodynamically possible through an H-F bond [31].

It should also be noted that a positive effect has not been observed in all studies involving TiO_2 doping with fluorine. For example, a slowing down of the degradation rate of dichloroacetate [32] and of the degradation rate in gas phase of some compounds [33] has been observed. As previously stated, the fluoride ion has a specific affinity for adsorption on TiO_2 acting as a Lewis base, and so would decrease and modify the density of surface states and, in this way, slow down certain degradation processes [26]. It should also be noted that although the formation of OH• radicals is higher in F-TiO_2, the oxidation processes in which there is hole transfer are inhibited [32].

As previously stated, most studies with F-TiO_2 catalysts have been performed in aqueous phase and very few in gas phase. In the few studies performed in gas phase, the effect of the fluoride is not very clear [33]. The present study analyses the effect of modifying with fluorine the surface of P25 catalysts on the degradation of ammonia in gas phase. The formation and diffusion of OH• radicals is more evident in aqueous phase, but the effect of the fluorine may be different in gas phase. In addition, the effect of the negative surface charge generated by the adsorption of fluorine onto the catalyst surface may have different repercussions for studies in gas phase than those observed in aqueous phase.

Most studies undertaken with ammonia to characterize different materials have been performed under conditions very different to those that would correspond to their possible application. For example, the catalysts are subjected to drying processes at high temperatures and the tests are performed with low and controlled pressures of ammonia. The studies described here were performed passing a flow of saturated moist air through an aqueous solution of ammonia, simulating more realistic conditions. This was done to generate products through interaction of the NH_3 (extracted with the air flow) with the catalyst surface and determine the behaviour of the catalysts under study in these conditions. The water vapour can compete with the

adsorption centres, but can also favour the diffusion processes of molecules and radicals during the photocatalytic process. It has also been reported that water may participate in stabilisation of the adsorbed molecules or of the generated holes [34-36]. The adsorption process was performed continuously with a view to augmenting the signal of minority species which may be generated during the adsorption process.

2. Experimental

2.1. Used catalysts

Four commercial TiO_2photocatalysts were used: P25, Aldrich (SA), P90 and PC100. And the fluorinated ones of the corresponding commercial TiO_2catalysts.

2.2. Photocatalytic experiments

The photocatalytic interaction and degradation of ammonia were followed by FTIR. Around 10 mg of catalyst were used in each experiment. An UV lamp was used in the degradation studies. Once the substrate was adsorbed and the initial spectrum was taken, the irradiation was initiated and the FTIR analysis was periodically performed to study the evolution of species during the degradation process.

Catalysts were treated with gas generated by bubbling air through an NH_3/aqueous solution at room temperature with flow rate of $6.24 \cdot 10^{-4}$ mol·min^{-1} [37] for 60 min. Then the catalyst was placed in the cell for analysis. The used system is described in the chapter 3.

Blank experiments of photocatalytic degradation of ammonia were carried out in the absence of catalyst and under the same experimental conditions; reactants remained unaltered throughout the assay.

The spectra shown in all figures were taken at 0, 3, 5, 10, 15, 20 25, 30, 40, 50, 60, 75 and 90 min. The spectra obtained in each reaction assay are shown in these figures.

3. Results and discussion

3.1. Macroscopic characteristics

Evonik-P25 (P25) and Sigma Aldrich (SA) catalysts have an equal surface area of more or less 50 $m^2 \cdot g^{-1}$,and the Evonik-P90 (P90) and Millenium-PC100 (PC100) a surface area of more or less 95 $m^2 \cdot g^{-1}$. The anatase/rutile phase ratios of the P25 and P90 catalysts are 82.3/17.7 and 89.4/10.6, respectively, while the SA and PC100 catalysts only have anatase phase.

The following table shows the anatase/rutile ratios, particle size and superficial area of these studied commercial catalysts.

Catalyst	Anatase/Rutile %	Superficial area ($m^2 \cdot g^{-1}$)	Diameter (nm)	
			Anatase	Rutile
P25	82.3/17.7	50.9	26	49
P90	89.4/10.6	95.2	13	19
PC100	100/0	94.7	15	-
Aldrich	100/0	47.3	21	-

Table VI.2 - Physical characteristics of the studied catalysts

The P25/Aldrich and PC100/P90 pairs, have similar particle sizes for the anatase phase, having values of 21-26 nm and 13-15 nm respectively. Concerning the superficial areas, it can be clearly seen that the PC100 and P90 have the largest superficial area.

Different studies have shown a strong relation between particle size and photoactivity. In fact, it has been indicated that the size of the particles can influence on the absorption efficiency, the diffusion of light and the dynamics of the charge carriers. The optimum size of the particles is therefore the result of an effective competition in light absorption, diffusion efficiency, dynamic of charge carriers and superficial area [38-40].

Table VI.3 shows the Ti/F and F/Na ratios obtained from the EDAX analysis. It should firstly be noted that the fluorinated catalysts with larger surface area (F-P90 and F-PC100) have a significantly higher relative concentration of fluorine, which would appear to be related to the anatase particle size. The surface analysis studies also showed the presence of sodium on the surface of these materials, though its concentration is significantly lower than the molar concentration of fluorine. This shows that the fluorine is mostly interacting with the catalyst surface as F^- but not as NaF, though the presence of this salt on the surface cannot be discarded.

	Ti/F	**F/Na**
F-P25	20.32	2.50
F-SA	18.46	2.09
F-P90	42.48	1.46
F-PC100	30.30	7.92

Table VI.3 –Ti/F and F/Na molar ratios from the EDAX surface analysis.

3.2. Characterisation of the adsorbed water, hydroxyl groups and surface charge

Figure VI.12 shows the spectra of the fluorinated and non-fluorinated P25, SA, P90 and PC100 catalysts. Note in particular the band attributed to isolated hydroxyl groups (3698 cm^{-1}), the bands attributed to adsorbed water (3600-3000 cm^{-1} and 1640 cm^{-1}) and finally the position of the baseline in each of the catalysts. The presence of isolated hydroxyl groups reveals the existence of defects or oxygen vacancies on the surface of these catalysts [41, 42].

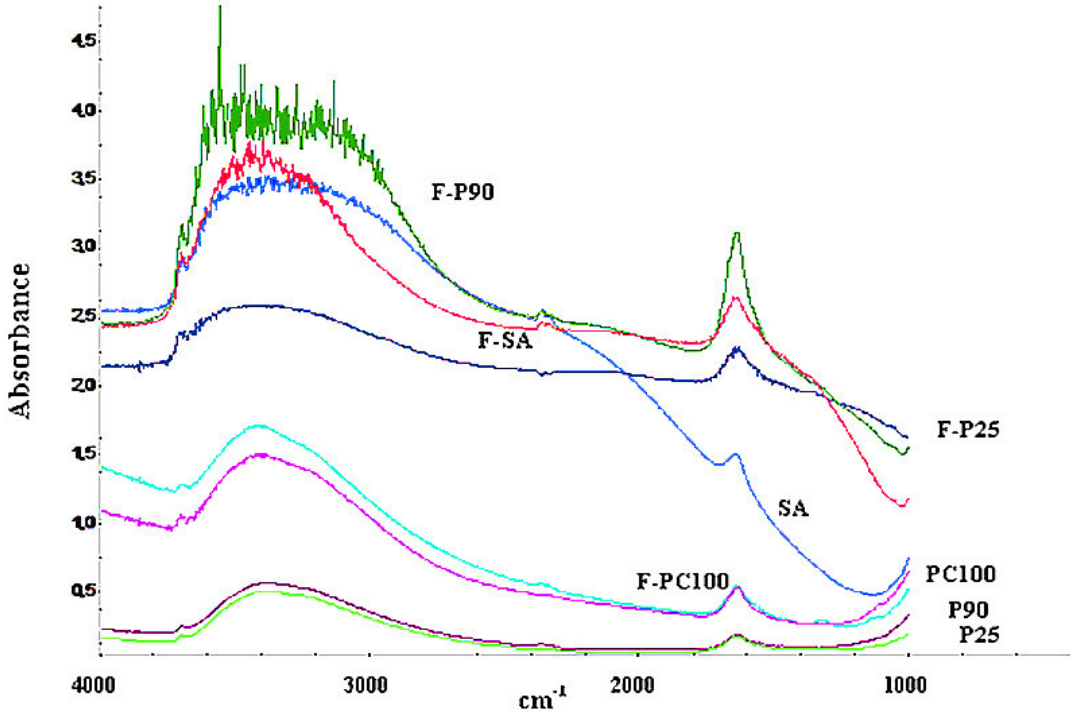

Figure VI.12: FTIR spectra of the fluorinated and non-fluorinated P25, SA, P90 and PC100 catalysts.

The band observed in all catalysts at 1640 cm^{-1} is assigned to the water bending mode (ν_2), while the broad band between 3650 and 3000 cm^{-1} is attributed to antisymmetric (ν_3) and symmetric (ν_1) stretchingvibration modes of the water [43, 44]. As can be seen, the P25, P90, PC100, F-P25 and F-PC100 spectra differ from those of the other catalysts. In these catalysts, the bands attributed to ν_3 and ν_1 vibrations appear very close to each other, and the relative intensity of these with respect to ν_2 is much higher. This may be related to various water layers interacting via hydrogen bridges [44]. With the remaining catalysts (SA, F-SA and F-P90), the band between 3650 and 3000 cm^{-1} can be attributed to isolated water molecules directly interacting via hydrogen bridges with the catalyst surface. The intensity of this interaction force has been designated strong for the bands at 3230 and 3070 cm^{-1} and weak for the corresponding bands between 3600 and 3415 cm^{-1} [43, 45].

With the P25, P90, PC100 and F-PC100 catalysts, the relative intensity of the isolated OH groups with respect to the water bands is much lower than that observed with the

other catalysts. The presence of a greater number of surface defects may also have an influence on the different interaction of the water.

As stated above, another important aspect to note in the spectra of Figure VI.12 is the position of the baseline. As a result of the presence of surface or shallow electron traps (Ti^{3+} type surface defects),electrons are fed to the conduction band via thermal processes such as those generated by the infrared radiation used to obtain these spectra. The electrons promoted to the conduction band have a similar behavior to that described for delocalized electrons confined to a three-dimension box with infinite walls; the high density of generated states gives rise to the continuous presence of excited electrons leading to a baseline increase of the infrared spectrum [46]. The baseline position of the SA and PC100 catalysts, the ones with only anatase phase, is much higher than that of the P25 and P90, in particular the P25. On modification of these catalysts with fluorine a baseline increase takes place which takes it to the same level as that observed in the SA catalyst. When modifying the SA and PC100 catalysts with fluorine there is only a very slight modification of the baseline position. As mentioned in the introduction, when TiO_2 is modified with fluorine, at least a fraction of the excess electrons introduced by the fluorine are localized by lattice Ti^{4+} cations. The presence of reduced Ti^{3+}centers in the as prepared fully oxidized solid indicates that the F-TiO_2 system can be described in terms of an *n*-type semiconductor provoking the baseline increase observed in the F-P25 and F-P90 catalysts [47]. Before its modification with fluorine, the SA had a high baseline position but, unlike the F-SA catalyst, the slope of the baseline falls rapidly as the wavenumber decreases. This may be related to the change in the O/Ti ratio observed in the initial analysis of this catalyst. The fact that no baseline increase is observed in the SA and PC100 catalysts when fluorinated may be due to their already having surface electron traps before adding the fluorine.

It should also be noted that those catalysts with a higher baseline position and therefore a higher number of surface-trapped electrons also have a higher relative intensity of the band attributed to isolated hydroxyl groups with respect to the water

band. That is, it seems that the negative charge generated by the surface-trapped electrons may be influencing water adsorption.

3.3. Interaction and photocatalytic degradation of ammonia

Ammonia can interact with Brönsted and Lewis acidic surface sites forming ammonium ions and acid-base adducts, respectively. The presence of these species can be perfectly identified via FTIR. It has been reported that bands corresponding to the asymmetric and symmetric vibrations of the ammonia adsorbed on the Lewis acid centers can be observed between 1660-1620 and 1250-1000 cm^{-1}, respectively [48,49]. The higher the wavenumber the greater the strength of the Lewis sites. The non-adsorbed NH_4^+ gives rise to a band centred around 1445 cm^{-1}, and the shift of this band to higher wavenumbers would indicate the presence of adsorbed ammonium. Bands corresponding to the ammonia adsorbed on the Brönsted acid centers between 1660-1620 and 1500-1400 cm^{-1} [48]. It has also been reported in various studies that interaction of $NH_3$with the surface of a metal oxide can result in its direct oxidation depending on the surface characteristics of the material under study, even at room temperature. A summary of the first stages which may take place in ammonia oxidation when interacting with the surface of a metal oxide is shown in diagram 1 [50].

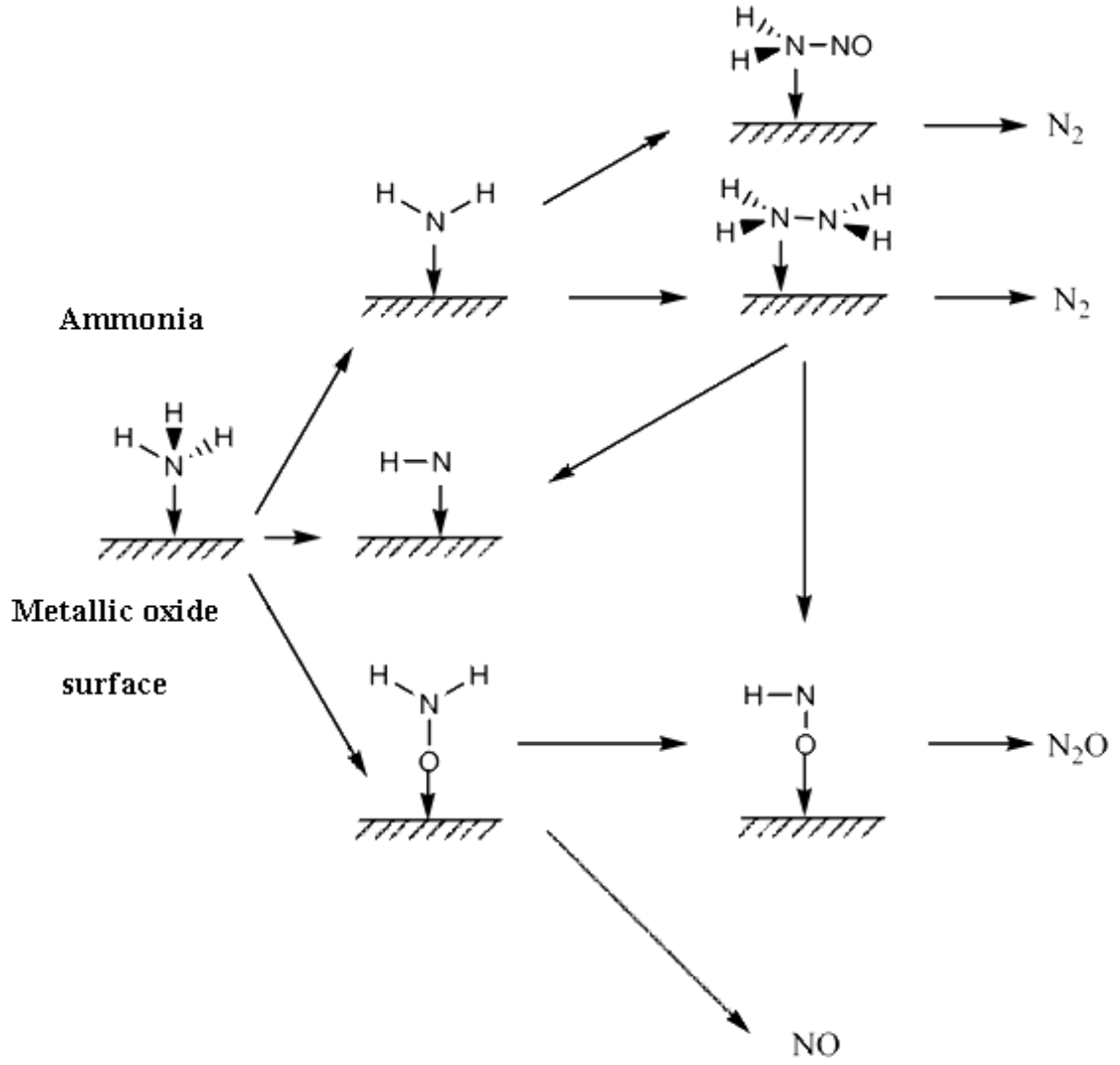

Diagram VI-1: Ammonia oxidation

Different initial oxidation processes of ammonia upon interaction with the surface have been reported [51-53]:

$$\mathbf{NH_3 + M^{n+} \rightarrow NH_2^{\bullet} + M^{(n-1)+} + H^+} \qquad \textbf{(VI.8)}$$

$$\mathbf{NH_3 + O_{lattice} \rightarrow NH_2^{\bullet} + OH^{\bullet}} \qquad \textbf{(VI.9)}$$

The NH_2 radical that is formed reacts rapidly, forming different species depending on the reaction conditions and the nature of the surface. So, among other compounds, hydrazine (N_2H_4), hydroxylamine (NH_2OH), nitric oxide (NO) or NH_2-NO can be formed. Under the ammonia adsorption conditions of the present studies, namely in a

continuous flow of saturated moist air, some of the reactions shown in diagram 1 may take place, to a greater or lesser extent, at room temperature.

3.3.1. Studies with P25

The spectra obtained from the interaction of ammonia with the P25 catalyst under illumination are shown in Figure VI.13. A broad band centered around 1200 cm^{-1} can be observed in the initial spectrum of the P25 attributed to $\delta_s NH_3$ ammonia adsorbed on Lewis sites. The asymmetry and width of the band indicate that it may be composed by the presence of Lewis acid sites of other types of compounds. A broad band can also be observed at 1449 cm^{-1} which is attributed to the $\delta_{as} NH_4^+$ vibration. The width of this band may be due to its being formed of free ammonium produced by the abstraction of a proton from the P25 surface present in a Brönsted acid site and adsorbed ammonium [54]. A further band can be observed at 1315 cm^{-1} and a shoulder at 1550 cm^{-1} which cannot be attributed to ammonia adsorbed on either Lewis or Brönsted acid sites. It has been suggested in some studies that these bands most likely represent various deformation vibrations of NH_x species, which are formed on the surface in relatively small amounts as a result of NH_3 decomposition [55].

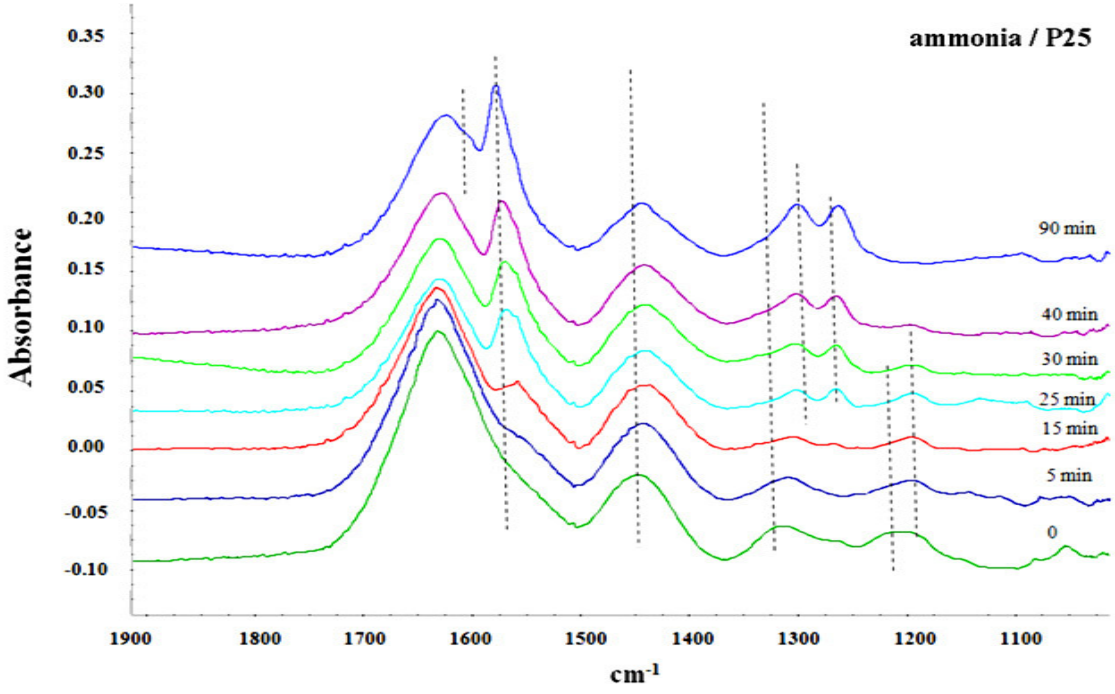

Figure VI.13: FTIR spectra of ammonia interaction with the P25 catalyst and its evolution under illumination.

A progressive decrease in intensity of the band centered at 1315 cm^{-1} and one of the components of the broad band centered at 1200 cm^{-1} was observed during the first 8 minutes of illumination of the P25 catalyst, as well as the progressive definition of a band at 1558 cm^{-1}. After this period of time, the progressive decrease of the band centered at 1195 cm^{-1} was observed and the formation of new bands at 1305, 1265 and 1580 cm^{-1} and a shoulder at 1607 cm^{-1}. These latter bands can be perfectly attributed to monodentate, bidentate or bridge nitrates [56], while the band observed at 1558 cm^{-1} could be attributed to NO^- [57]. The band attributed to the $\delta_{as}NH_4^+$ vibration decreases slightly in intensity leaving at the end of the process a more defined band at 1445 cm^{-1} which is attributed to non-adsorbed free ammonium. The process observed with the P25 catalyst is well described by the mechanism described in other studies on ammonium oxidation [58]. The oxygen reacts with the photogenerated electrons (reaction VI.10). The adsorbed ammonia then oxides directly by reaction with the holes (reaction VI.11) giving rise to $O_2^{\bullet-}$ radicals, which give rise to NO^- which is oxidized by O_2 to NO_2^- or NO_3^-.

$$\mathbf{O_{2,ads} + e_{tr}^- \rightarrow O_{2,ads}^{\bullet-}} \quad \textbf{(VI.10)}$$

$$\mathbf{NH_{3,ads} + h_{tr}^+ \rightarrow NH_{2,ads}^{\bullet} + H_{ads}^+} \quad \textbf{(VI.11)}$$

$$\mathbf{NH_{2,ads}^{\bullet} + O_{2,ads}^{\bullet-} \rightarrow NO_{ads}^- + H_2O_{ads}} \quad \textbf{(VI.12)}$$

$$\mathbf{2\,NO_{ads}^- + O_{2,ads} \rightarrow 2NO_{2,ads}^-} \quad \textbf{(VI.13)}$$

$$\mathbf{NO_{ads}^- + O_{2,ads} \rightarrow NO_{3,ads}^-} \quad \textbf{(VI.14)}$$

3.3.2. Studies with SA

The spectra obtained from the interaction of ammonia with the SA catalyst under illumination are shown in Figure VI.14. In the spectrum obtained of the interaction of NH_3 with the SA catalyst, the band attributed to the $\delta_{as}NH_4^+$ vibration is found at the same wavenumber, 1446 cm^{-1}, as in the P25 studies. However, the band attributed to the Lewis acid sites is found at 1216 cm^{-1} and the band corresponding to compounds generated by the decomposition of the ammonia is found at 1326 cm^{-1}. Hardly any

change can be observed in the spectra during the first 8 minutes of illumination. However, beyond this illumination time a progressive decrease is observed of the bands at 1326 and 1216 cm^{-1}, as well as the formation of solvated nitrates though bands are also observed [59] at lower intensity, attributed to adsorbed nitrates (bands at 1578 and 1265 cm^{-1}).

In other words, the main difference observed between this catalyst (SA) and the P25 is the formation of solvated nitrates as well as adsorbed nitrates as reaction products. The described surface analysis studies showed for this catalyst a high negative surface charge which may be playing a role in the formation of solvated nitrates.

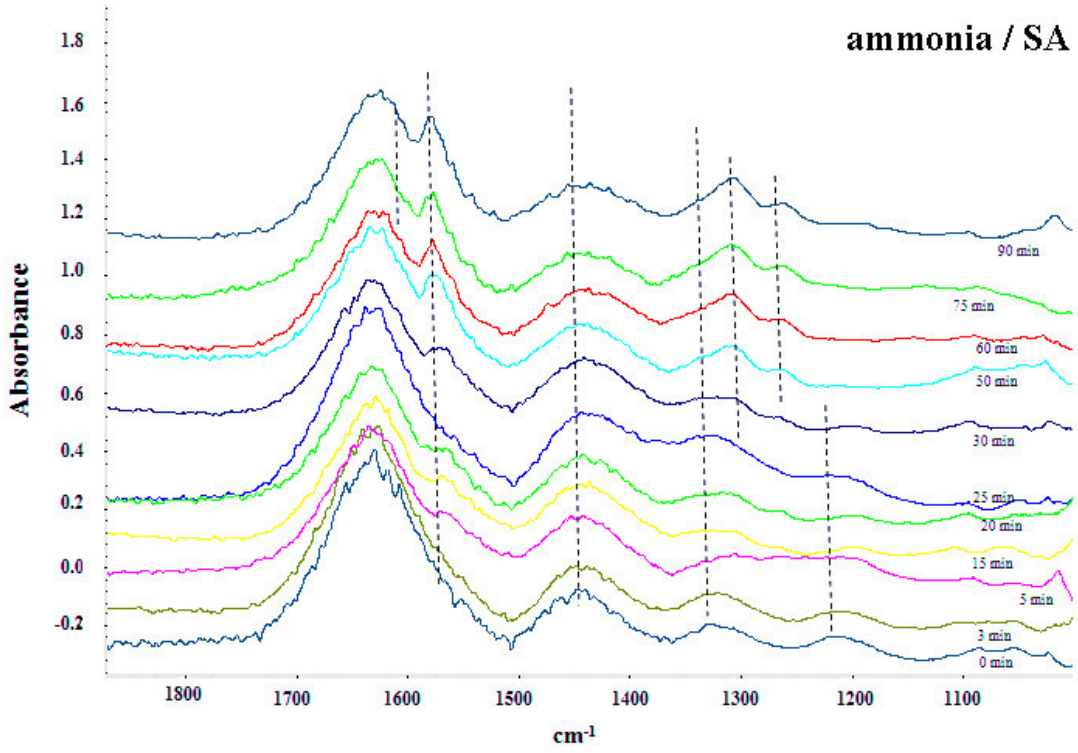

Figure VI.14: FTIR spectra of the ammonia interaction with the SA catalyst and its evolution under illumination.

3.3.3. Studies with P90

The initial spectrum obtained of the interaction of NH_3 with the P90 catalyst (FigureVI.15) is practically the same as that obtained with the P25 though there is a smaller contribution of Lewis acid sites of lower acidity (band around 1195 cm^{-1}). As

with the P25, the definition of a shoulder about 1553 cm^{-1} and 1300 cm^{-1} as well as the progressive decrease of the band at 1215 cm^{-1} and 1320 cm^{-1} is observed during the first ten minutes of illumination.

After the first 20 minutes of illumination the bands of adsorbed nitrates can be clearly seen (bands at 1572, 1318 and 1264 cm^{-1}), and with the same proportions as seen with the P25 catalyst. It should be noted that, unlike the P25, an important decrease of the band attributed to ammonia adsorbed on the Brönsted acid sites at 1446 cm^{-1} is observed during illumination of this catalyst.

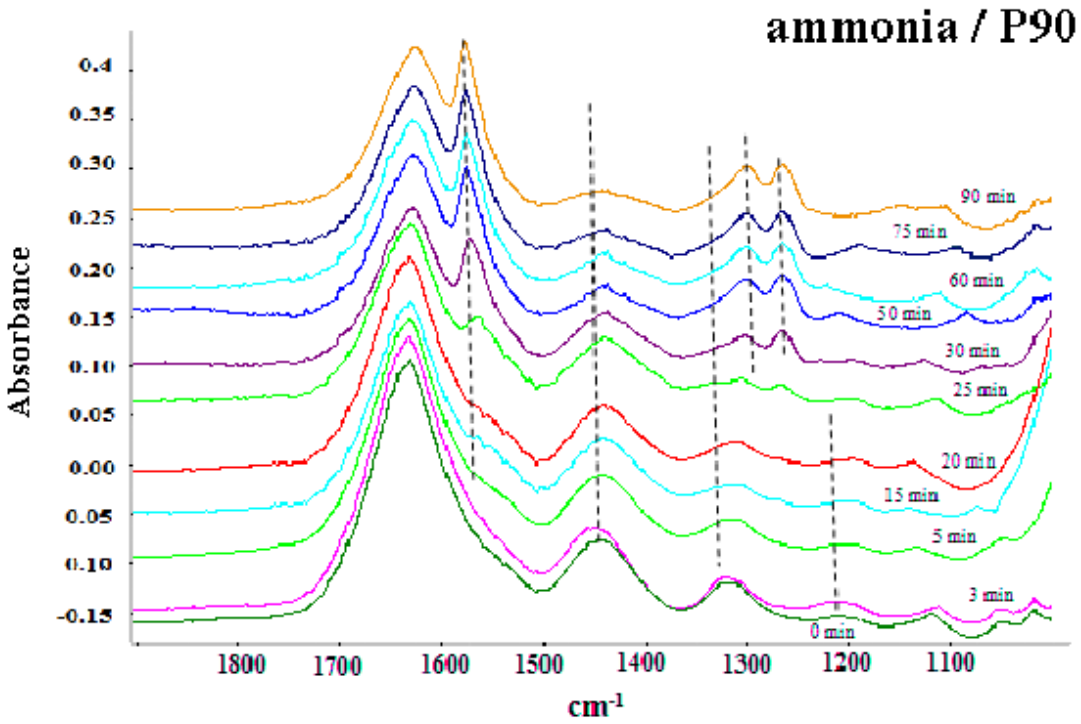

Figure VI.15: FTIR spectra of ammonia interaction with the P90 catalyst and its evolution under illumination.

3.3.4. Studies with PC100

The first thing to note in the spectrum obtained of the interaction of NH_3 with the PC100 catalyst (Figure VI.16) is the significantly lower intensity of the band attributed to Lewis acid sites compared to that of Brönsted acid sites, and the significant intensity of the band attributed to compounds generated by the decomposition and subsequent oxidation of the adsorbed NH_3 as a result of its interaction compared to that observed

with the other catalysts. This suggests that with this catalyst the Lewis acid sites are mostly very strong and are found close to also strong Brönsted acid sites. This may be related to the smaller particle size of the PC100 catalyst which favors the proximity of sites when there is only anatase phase, as this was not observed with the P90 catalyst.

When this catalyst is illuminated it is observed a clearer definition of the bands attributed to high ν_3 vibrations at 1605 and 1582 cm^{-1} which are related with the bands attributed to low ν_3 vibrations at 1299 and 1266 cm^{-1} of adsorbed nitrates. During the illumination it was observed that the band attributed to the $\delta_{as}NH_4^+$ at 1446 cm^{-1} decreases in intensity and shifts to lower wavenumbers (1435 cm^{-1}). A pronounced shoulder is also observed in the band at 1299 cm^{-1} which may be due to the presence of solvated nitrate, as also observed with the SA catalyst.

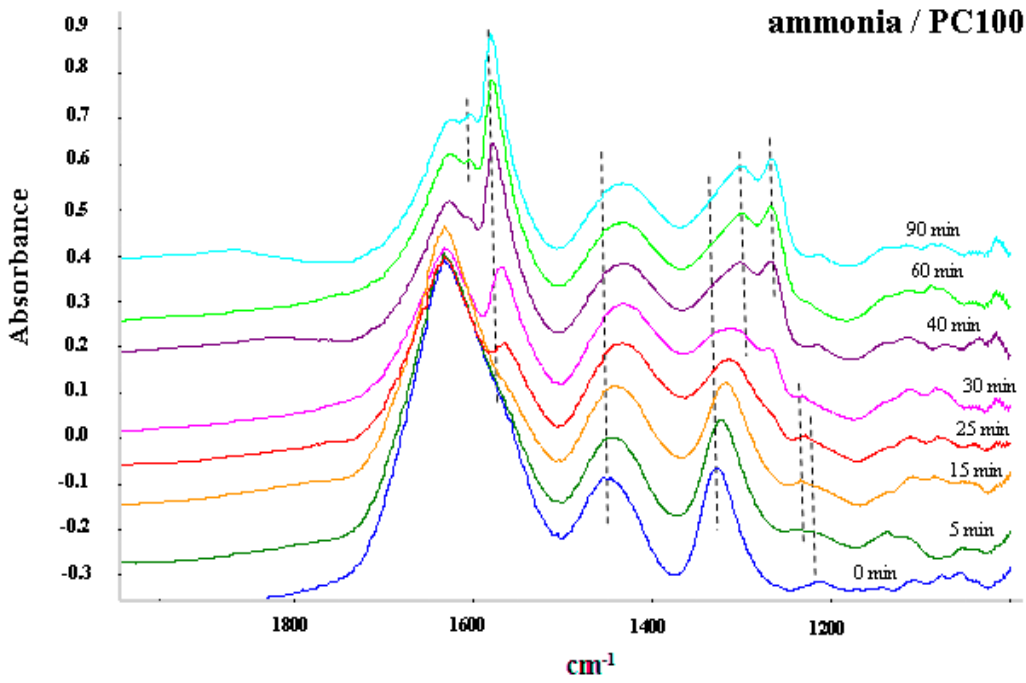

Figure VI.16: FTIR spectra of the interaction of ammonia with PC100 and its evolution under illumination.

3.3.5 Studies with F-P25

In the initial spectrum of NH_3 interaction with the F-P25 catalyst (Figure VI.17 A), should be noted the absence of the band attributed to NH_3 adsorbed on Lewis acid sites. The band attributed to $\delta_{as}NH_4^+$ is displaced to higher wavenumbers at 1459 cm^{-1},

indicating that it is adsorbed, and the band corresponding to DOAA is also shifted to higher wavenumbers (1340 cm^{-1}). During the first 12 minutes of illumination, the progressive decrease is observed of the band attributed to the $\delta_{as}NH_4^+$ (1459 cm^{-1}), the band corresponding to DOAA is barely modified and the formation of a new band can be seen at 2169 cm^{-1} which is attributed to N_2O (Figure VI.17 B) [60]. After the first 12 minutes of reaction, a progressive decrease can be seen of the band attributed to DOAA and the formation of two new bands at 1408 and 1358 cm^{-1} which are attributed to H_2O-HNO_3 adducts [61]. These latter compounds stop being produced after 30 minutes and beyond this reaction time there was no variation in the spectrum.

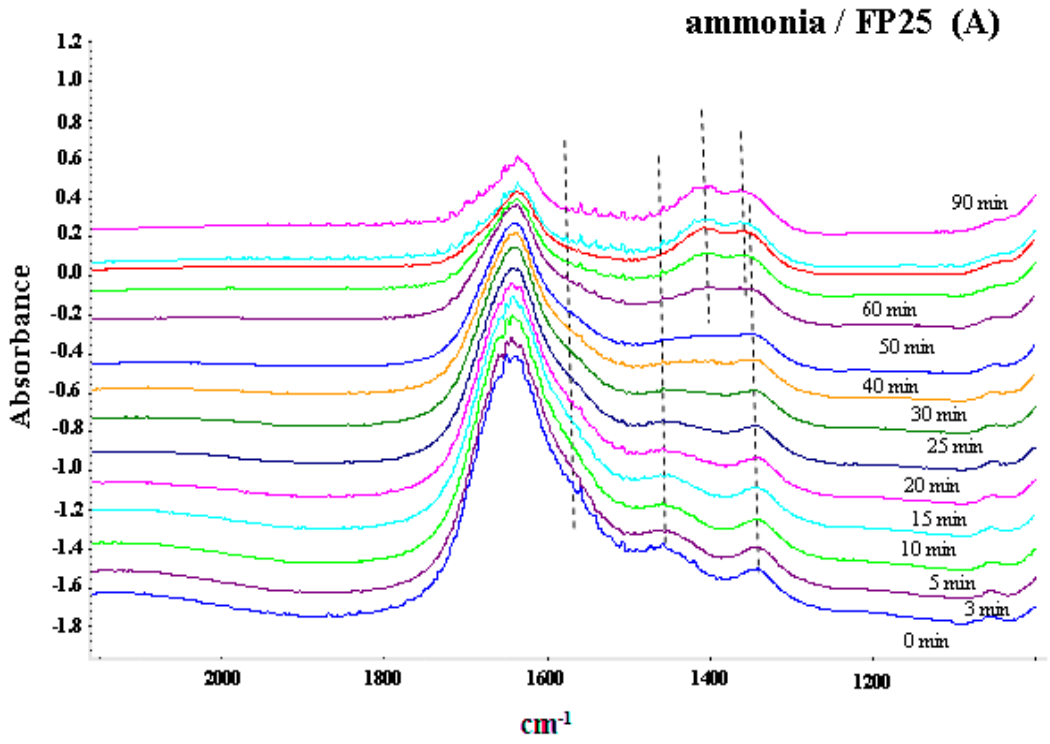

Figure VI.17.A: FTIR spectra of the interaction of ammonia with F-P25 and its evolution under illumination.

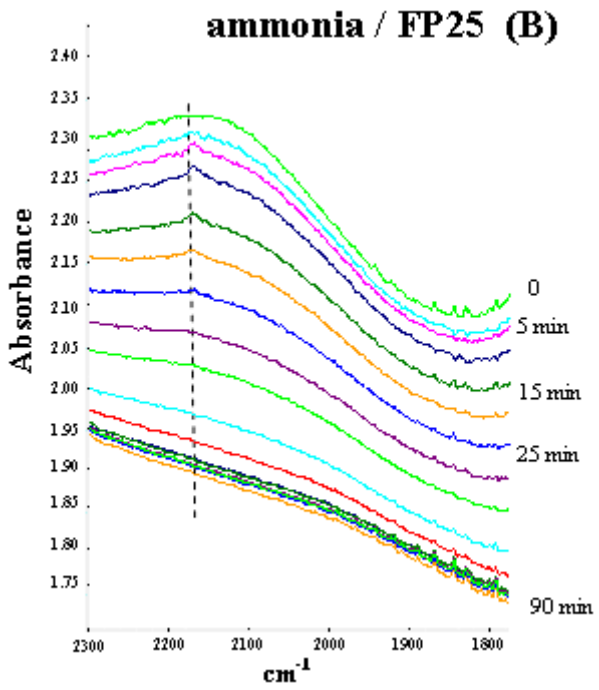

Figure VI.17.B: FTIR spectra of the interaction of ammonia with F-P25 and its evolution under illumination in the region between 2300 and 1800 cm^{-1}.

The formation of N_2O can take place through the following reactions [60]:

$$O_{2,ads} \rightarrow 2O_{ads} \quad \text{(VI.15)}$$

$$NH_{3,ads} + O_{ads} \rightarrow NH_{ads} + H_2O_{ads} \quad \text{(VI.16)}$$

$$NH_{ads} + O_{ads} \rightarrow HNO_{ads} \quad \text{(VI.17)}$$

$$NH_{ads} + HNO_{ads} \rightarrow N_{2,ads} + H_2O_{ads} \quad \text{(VI.18)}$$

$$HNO_{ads} + HNO_{ads} \rightarrow N_2O_{ads} + H_2O_{ads} \quad \text{(VI.19)}$$

$$NH_{ads} + O_{2,ads} \rightarrow NO_{ads} + OH_{ads}^{\bullet} \quad \text{(VI.20)}$$

$$NH_{2,ads} + NO_{ads} \rightarrow N_{2,ads} + H_2O_{ads} \quad \text{(VI.21)}$$

$$NH_{ads} + NO_{ads} \rightarrow N_2O + H_{ads}^{\bullet} \quad \text{(VI.22)}$$

$$H_{ads}^{\bullet} + OH_{ads}^{\bullet} \rightarrow H_2O_{ads} \quad \text{(VI.23)}$$

The formation of H_2O-HNO_3 was observed from the reaction of NO_2 with the catalyst surface [62].

3.3.6. Studies with F-SA

The photocatalytic degradation of NH_3 observed with the F-SA catalyst is very similar to that of the P25: no bands of ammonia adsorbed on Lewis acid sites are observed, a decrease of the band centered at 1459 cm^{-1} takes place in the first few minutes, and H_2O-HNO_3 is generated.

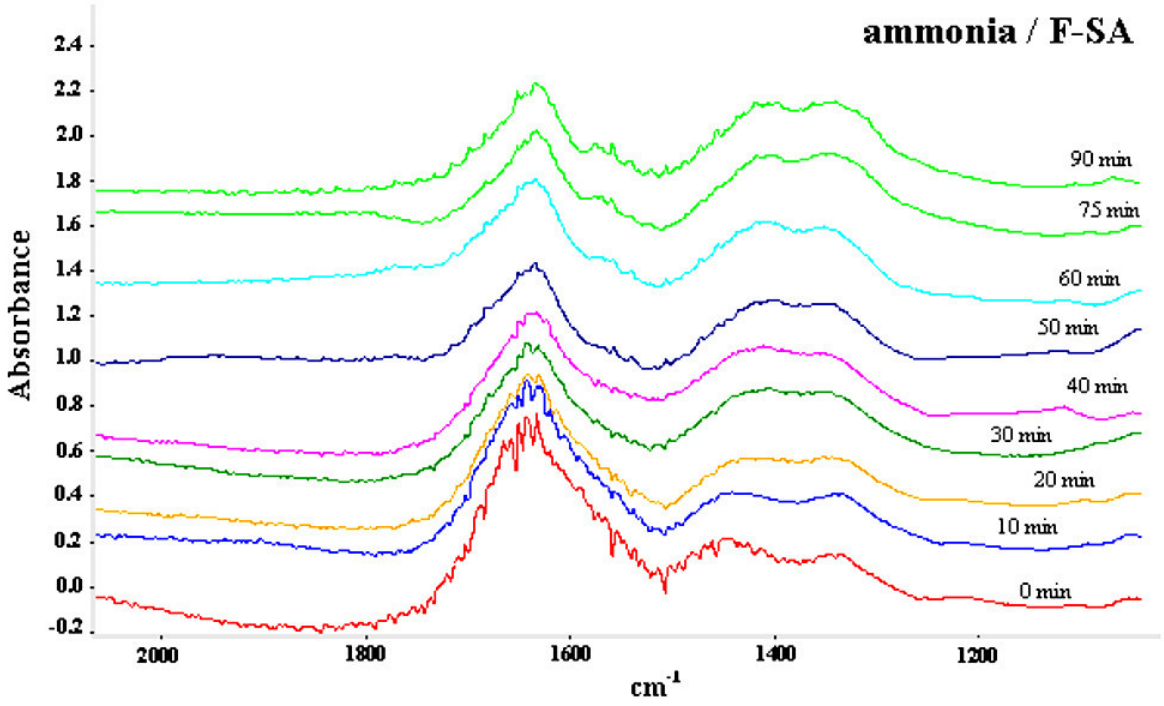

Figure VI.18:FTIR spectra of the interaction of ammonia with F-SA and its evolution under illumination.

3.3.7. Studies with F-P90

Interaction of NH_3 with the F-P90 catalyst does give rise to bands attributed to Lewis acid sites. However, as with the F-P25 and the F-SA, the band attributed to DOAA is shifted to 1335 cm^{-1}. Under illumination, the behaviour of the F-P90 catalyst is the same as that observed with the F-P25: during the first few minutes there is a

progressive decrease of the band at 1459 cm^{-1}, the formation of N_2O is observed (band at 1269 cm^{-1}) and after the first 6 minutes of illumination the bands attributed to H_2O-HNO_3 begin to form. However, with this catalyst formation of the bands attributed to H_2O-HNO_3 continues up to 90 minutes and is also observed the formation of adsorbed nitrates (band at 1580 cm^{-1}).

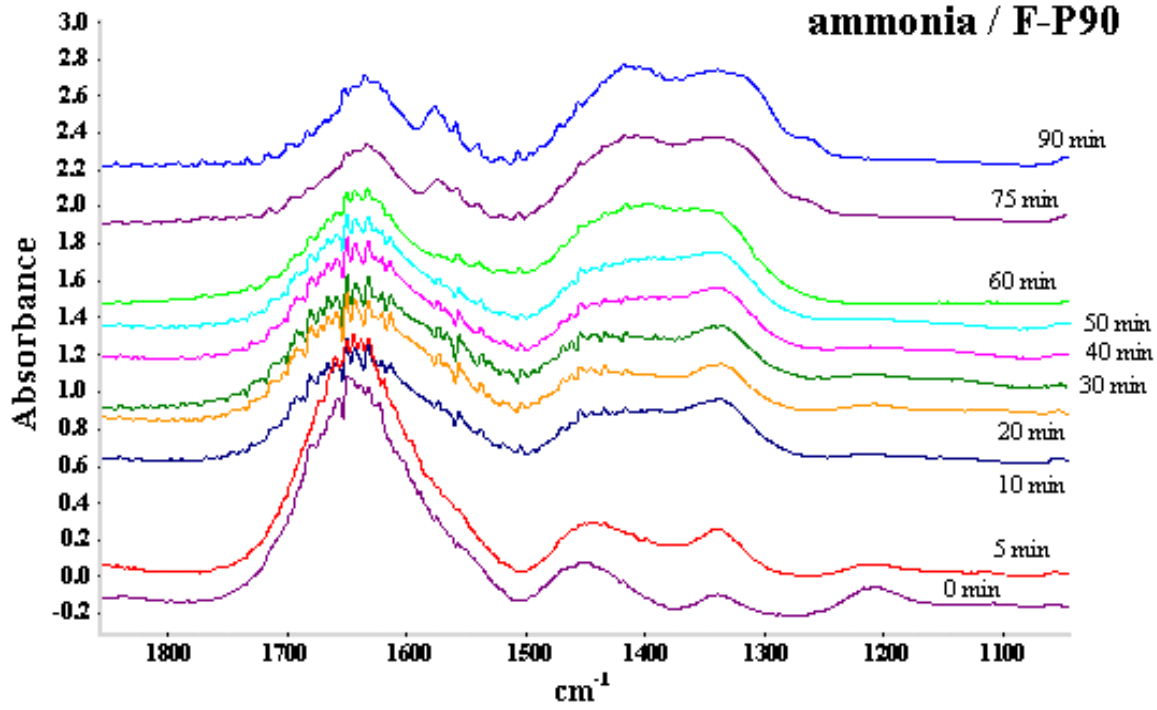

Figure VI.19.A: FTIR spectra of the interaction of ammonia with F-P90 and its evolution under illumination.

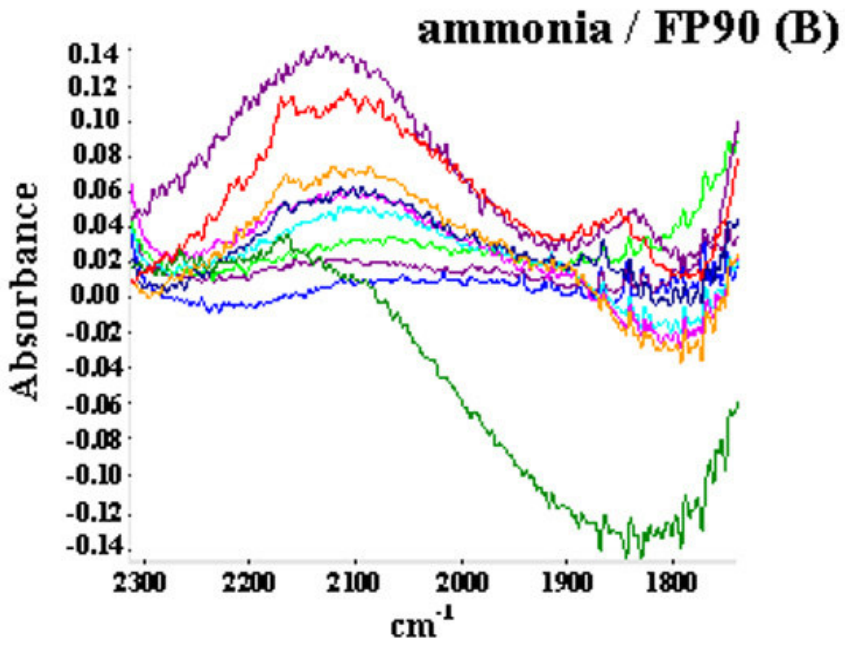

Figure VI.19.B: FTIR spectra of the interaction of ammonia with F-P90 and its evolution under illumination in the region between 2300 and 1800 cm^{-1}

3.3.8. Studies with theF-PC100 catalyst

As with the P90 catalyst, it is observed the formation of adsorbed nitrates with the F-PC100 (Figure VI.20) during illumination. Also observed, though not so clearly, are HNO_3-H_2O and N_2O adducts.

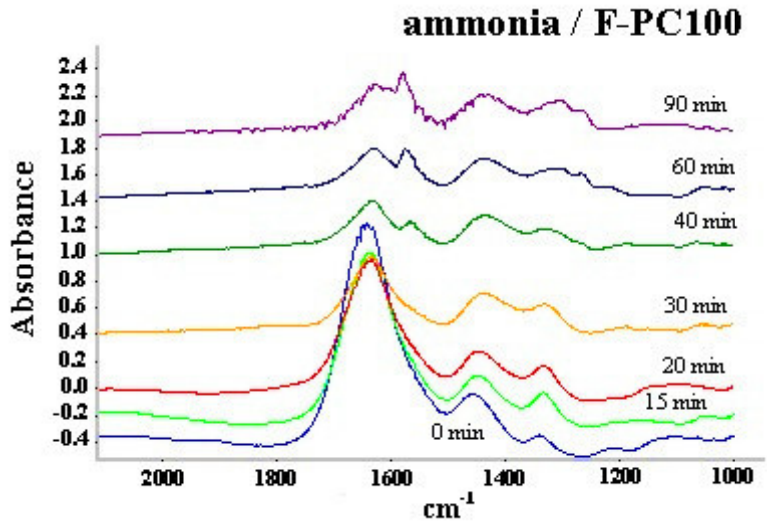

Figure VI.20: FTIR spectra of the interaction of ammonia with F-PC100 and its evolution under illumination.

4. Discussion of results

The results obtained show that the interaction of ammonia on the TiO_2 can give rise to NH_4^+ adsorbed on Brönsted acid sites or free NH_4^+, NH_3 adsorbed on Lewis acid sites and to the decomposition of the ammonia as a consequence of its interaction, probably due to the proximity of sites of relatively high strength. The free NH_4^+ was not photocatalytically oxidised, but the NH_4^+ adsorbed on the Brönsted acid sites was. Photocatalytic oxidation was also observed for the rest of species.

When modifying the catalysts with fluorine it was observed that, in general, an increase of the negative surface charge takes place which may be related to the formation of Ti^{3+} electron traps as reported in other studies [63]. The surface analysis studies showed that the catalysts of greater surface area and so smaller particle size (F-PC100 and F-P90) have a higher concentration of adsorbed fluoride. It was also determined in the NH_3 interaction studies that Lewis acid sites are not present in the F-P25 and SA catalysts. Fluorination as performed in this study comprised a mixture of NaF/water in which the F- ions present react with surface Lewis sites. All the P25 Lewis sites seem to be neutralised with the fluoride and for this reason no NH_3 adsorbed on Lewis acid sites were observed. In contrast, the Brönsted/Lewis ratio of the P90 and PC100 catalysts was only slightly modified by fluorination. In the FTIR characterisation studies of the initial spectra of the catalysts, it was determined that for the PC100 catalyst there was an only slight change of the baseline when modified with fluorine, whereas a significant change was observed with the P90. This may be due to the fact that P90 has rutile particles of larger size than those of anatase. That is, if adsorbability of fluorine is lower on smaller size particles and the anatase particles are smaller than the rutile, this would explain why an increase of the baseline was observed in the P90 but not in the P100 and why the same photocatalytic performance and NH_3 interaction were not observed with the F-P25 and F-SA catalysts as with the F-P90 and F-PC100.

In the P25 studies under illumination (Figure VI.13), it can be seen that the progressive decrease of the bands attributed to NH_3 adsorbed on Lewis acid sites is correlated to the formation of adsorbed nitrates. However, with the F-P25 and F-SA catalysts, there

is progressive formation of N_2O during the first few minutes from adsorbed NH_4^+ and of H_2O-HNO_3 adducts from the DOAA. That is, the mechanism described in reactions VI.10 - VI.14 takes place at Lewis acid sites with the non-fluorinated catalysts, whereas the mechanism by which NH_3 adsorbed on Brönsted acid sites is oxidised to H_2O-HNO_3 adducts takes place with the fluorinated catalysts.

Various studies have shown that surface oxygen bridges intervene in the reaction with the holes [64]:

$$\mathbf{h_{tr}^+ + O_{br,s}^{2-} \rightarrow O_{br,s}^{\bullet -}} \qquad \textbf{(VI.24)}$$

The $O_s^{\bullet -}$ anion radicals could react with surface bonded NH_4^+ species via the reaction:

$$\mathbf{NH_{4,ads}^+ + O_{br,s}^{\bullet -} \rightarrow HN_{ads}^{\bullet -} + H_2O_{ads} + H_{ads}^+} \qquad \textbf{(VI.25)}$$

The reaction of $HN^{\bullet -}$ radicals with oxygen would give rise to $NO^\bullet$ and the reaction of this radical with oxygen produces NO_2:

$$\mathbf{HN_{ads}^{\bullet -} + O_{2,ads} \rightarrow NO_{ads}^\bullet + OH_{ads}^-} \qquad \textbf{(VI.26)}$$

$$\mathbf{NO_{ads}^\bullet + \frac{1}{2}O_{2,ads} \rightarrow NO_{2,ads}^\bullet} \qquad \textbf{(VI.27)}$$

With the F-P25 and F-SA catalysts, after elimination of adsorbed NH_4^+ was also observed the elimination of NH_x species generated from the interaction of NH_3 with the catalyst surface and its decomposition. At the same time as the bands of NH_x species decrease takes place the formation of H_2O-HNO_3 adducts. As previously mentioned, these were observed after interaction of NO_2 with the catalyst surface, which suggests that the NH_x species must be evolving into NO and NO_2. In view of the fact that NH_x species were also observed in the non-fluorinated catalysts but not H_2O-HNO_3 adducts, it seems clear that adsorbed fluoride could be intervening in the process via the following reactions:

$$\mathbf{NH_{x,ads}^- + h_{tr}^+ \rightarrow NH_{x,ads}^\bullet} \qquad \textbf{(VI.28)}$$

$$\mathbf{F_{ads}^- + h_{tr}^+ \rightarrow F_{ads}^\bullet} \qquad \textbf{(VI.29)}$$

$$\mathbf{NH_{x,ads}}^{-} + \left(\frac{\mathbf{2+x}}{\mathbf{2}}\right)\mathbf{O_{2,ads}}^{\bullet-} \rightarrow \mathbf{NO_{ads}}^{-} + \frac{\mathbf{x}}{\mathbf{2}}\mathbf{H_2O_{ads}} \quad \textbf{(VI.30)}$$

$$\mathbf{NO_{ads}}^{-} + \mathbf{F_{ads}}^{\bullet} \rightarrow \mathbf{NO_{ads}} + \mathbf{F_{ads}}^{-} \quad \textbf{(VI.31)}$$

In the non-fluorinated catalysts, NO^- would react with O_2 via reactions VI.13 and VI.14, forming adsorbed nitrates. However, no adsorbed nitrates were observed with the catalysts in which fluoride surface concentrations were high and there was a clear resulting increase of the baseline, with this being attributed to reactions VI.29 - VI.31.

As previously stated, the F-TiO_2 catalysts can be considered *n*-type semiconductors [65]. These catalysts act as trap sites of photogenerated electrons, and these sites are much stronger than Ti(III)-OH sites due to the strong electronegativity of fluoride [30, 66]. The high surface charge of the fluorinated catalysts due to the injection of electrons into the $TiO_2$from the fluorine and the high capacity of the F-Ti(III) sites to retain photogenerated electrons would inhibit the VI.10 reaction. Reaction with photogenerated holes of surface oxygen bridges close to Ti(III) atoms weakens the bond between titanium atoms and crystal lattice oxygen [67]. This would favour the reaction VI.15.

NH_3 is adsorbed only on Brönsted acid sites with the F-P25 and F-SA. The Brönsted acid sites are localised at surface oxygen bridge sites. All of this would favour the reactions VI.15 - VI.23 for the F-P25 and F-SA catalysts.

The formation of N_2O observed with the F-P25 and F-SA catalysts (reaction VI.22) is further evidence of the NH_3 degradation mechanism described for them. N_2O is only observed during the first few minutes of illumination probably due to this time being when a higher concentration of $NH^{\bullet}$ and NO radicals are generated and so the probability of interaction with them is higher. At a later time during the illumination, NO reacts with oxygen giving rise to NO_2. In parallel studies that were performed, it was observed that NO_2 dimerizes to N_2O_4 which disproportionates reacting with adsorbed water to give rise to H_2O-HNO_3adducts. The type of adduct H_2O-HNO_3 formed depends on the amount of water available [59].

The SA was the only non-fluorinated catalyst in which the formation of this adduct was observed, though in the form of low water content and low relative concentrations of adsorbed nitrates. The SA catalyst also has an important negative surface charge, which could be favouring the mechanism as also described for the fluorinated catalysts.

5. Conclusions

- It was determined in the study presented in this part of work that:
- Modifying TiO_2 with fluorine results in an increase of negative surface charge which is attributed to the formation of surface Ti^{3+} electron trap sites.
- The increase in negative surface charge was preferentially observed in those catalysts of smaller surface area (P25 and SA) or, in other words, of larger-sized particles with anatase phase.
- The photocatalytic oxidation of $NH_3$when using the non-fluorinated catalysts takes place via the mechanism shown in reactions VI.10-VI.14 *g*iving rise to adsorbed nitrates as final products.
- The fluoride interacts with Lewis acid sites in the catalysts of larger particle size, inhibiting the interaction of $NH_3$with these sites. The photocatalytic oxidation of NH_3 adsorbed on Brönsted acid sites with these catalysts takes place via reactions which generate H_2O-HNO_3adducts and not adsorbed nitrates.

  The adsorbed fluorides appear to intervene directly in the degradation mechanism throughthe formation of $F^{\bullet}$ radicals which neutralize NO^-ions responsible for the formation of adsorbed nitrates. Oxidation of ammonia adsorbed on Brönstedacid sites via oxygen bridges also appears to be favored by the presence of fluorides on the surface.

References:

[1] MINERO, C., MARIELLA, G., MAURINO, V., et al. Photocatalytic transformation of organic compounds in the presence of inorganic anions. 1. Hydroxyl-mediated and direct electron-transfer reactions of phenol on a titanium dioxide− fluoride system. Langmuir, 2000, vol. 16, no 6, p. 2632-2641.

[2] KIM, Soonhyun, PARK, Hyunwoong, et CHOI, Wonyong. Comparative study of homogeneous and heterogeneous photocatalytic redox reactions: PW12O403-vs TiO2. The Journal of Physical Chemistry B, 2004, vol. 108, no 20, p. 6402-6411.

[3] MURCIA, J. J., HIDALGO, M. C., NAVÍO, J. A., et al. Study of the phenol photocatalytic degradation over TiO2 modified by sulfation, fluorination, and platinum nanoparticles photodeposition. Applied Catalysis B: Environmental, 2015, vol. 179, p. 305-312.

[4] KONSTANTAKOU, Maria, STERGIOPOULOS, Thomas, LIKODIMOS, Vlassis, et al. Influence of fluorine plasma treatment of TiO2 films on the behavior of dye solar cells employing the Co (II)/(III) redox couple. The Journal of Physical Chemistry C, 2014, vol. 118, no 30, p. 16760-16775.

[5] YU, Jiaguo, XIANG, Quanjun, RAN, Jingrun, et al. One-step hydrothermal fabrication and photocatalytic activity of surface-fluorinated TiO 2 hollow microspheres and tabular anatase single micro-crystals with high-energy facets. CrystEngComm, 2010, vol. 12, no 3, p. 872-879.

[6] PANARELLI, Enzo Gabriele, LIVRAGHI, Stefano, MAURELLI, Sara, et al. Role of surface water molecules in stabilizing trapped hole centres in titanium dioxide (anatase) as monitored by electron paramagnetic resonance. Journal of Photochemistry and Photobiology A: Chemistry, 2016, vol. 322, p. 27-34.

[7] MILLER, Kristi L., FALCONER, John L., et MEDLIN, J. Will. Effect of water on the adsorbed structure of formic acid on TiO2 anatase (1 0 1). Journal of catalysis, 2011, vol. 278, no 2, p. 321-328.

[8] TANDON, S. P. et GUPTA, J. P. Measurement of forbidden energy gap of semiconductors by diffuse reflectance technique. physica status solidi (b), 1970, vol. 38, no 1, p. 363-367.

[9] TANG, Junwang, QUAN, Hengdao, et YE, Jinhua. Photocatalytic properties and photoinduced hydrophilicity of surface-fluorinated TiO2. Chemistry of materials, 2007, vol. 19, no 1, p. 116-122.

[10] LI, Di, HANEDA, Hajime, HISHITA, Shunichi, et al. Fluorine-doped TiO2 powders prepared by spray pyrolysis and their improved photocatalytic activity for decomposition of gas-phase acetaldehyde. Journal of Fluorine Chemistry, 2005, vol. 126, no 1, p. 69-77.

[11] TONG, Hai-Jie, YU, Jun-Ying, ZHANG, Yun-Hong, et al. Observation of conformational changes in 1-propanol– water complexes by FTIR spectroscopy. The Journal of Physical Chemistry A, 2010, vol. 114, no 25, p. 6795-6802.

[12] AL-ABADLEH, Hind A. et GRASSIAN, V. H. FT-IR study of water adsorption on aluminum oxide surfaces. Langmuir, 2003, vol. 19, no 2, p. 341-347.

[13] THOMPSON, Tracy L. et YATES, John T. Surface science studies of the photoactivation of TiO2 new photochemical processes. Chemical Reviews, 2006, vol. 106, no 10, p. 4428-4453.

[14] BIEDRZYCKI, Jakub, LIVRAGHI, Stefano, GIAMELLO, Elio, et al. Fluorine- and niobium-doped TiO2: Chemical and spectroscopic properties of polycrystalline n-type-doped anatase. The Journal of Physical Chemistry C, 2014, vol. 118, no 16, p. 8462-8473.

[15] MATTSSON, Andreas et OSTERLUND, L. Adsorption and photoinduced decomposition of acetone and acetic acid on anatase, brookite, and rutile TiO2 nanoparticles. The Journal of Physical Chemistry C, 2010, vol. 114, no 33, p. 14121-14132.

[16] SOLA, A. C., SOUSA, D. Garzón, ARAÑA, J., et al. Differences in the vapour phase photocatalytic degradation of ammonia and ethanol in the presence of water as a function of TiO2 characteristics and the presence of O2. Catalysis Today, 2016, vol. 266, p. 53-61.

[17] VORONTSOV, Alexandre V. et DUBOVITSKAYA, Vera P. Selectivity of photocatalytic oxidation of gaseous ethanol over pure and modified TiO2. Journal of Catalysis, 2004, vol. 221, no 1, p. 102-109.

[18] PILKENTON, Sarah, HWANG, Son-Jong, et RAFTERY, Daniel. Ethanol photocatalysis on TiO2-coated optical microfiber, supported monolayer, and powdered catalysts: An in situ NMR study. The Journal of Physical Chemistry B, 1999, vol. 103, no 50, p. 11152-11160.

[19] PIERA, Eva, AYLLÓN, José A., DOMÉNECH, Xavier, et al. TiO2 deactivation during gas-phase photocatalytic oxidation of ethanol. Catalysis Today, 2002, vol. 76, no 2-4, p. 259-270.

[20] SASAKI, Jennifer, ASCHMANN, Sara M., KWOK, Eric SC, et al. Products of the gas-phase OH and NO3 radical-initiated reactions of naphthalene. Environmental Science & Technology, 1997, vol. 31, no 11, p. 3173-3179.

[21] SHENG, Hua, LI, Qin, MA, Wanhong, et al. Photocatalytic degradation of organic pollutants on surface anionized TiO2: Common effect of anions for high hole-availability by water. Applied Catalysis B: Environmental, 2013, vol. 138, p. 212-218.

[22] SUN, Bo, VORONTSOV, Alexandre V., et SMIRNIOTIS, Panagiotis G. Role of platinum deposited on TiO2 in phenol photocatalytic oxidation. Langmuir, 2003, vol. 19, no 8, p. 3151-3156.

[23] PAN, Jia Hong, CAI, Zhongyu, YU, Yong, et al. Controllable synthesis of mesoporous F–TiO 2 spheres for effective photocatalysis. Journal of Materials Chemistry, 2011, vol. 21, no 30, p. 11430-11438.

[24] YU, Jiaguo, XIANG, Quanjun, RAN, Jingrun, et al. One-step hydrothermal fabrication and photocatalytic activity of surface-fluorinated TiO 2 hollow microspheres and tabular anatase single micro-crystals with high-energy facets. CrystEngComm, 2010, vol. 12, no 3, p. 872-879.

[25] YU, Jiaguo, WANG, Wenguang, CHENG, Bei, et al. Enhancement of photocatalytic activity of mesporous TiO2 powders by hydrothermal surface fluorination treatment. The Journal of Physical Chemistry C, 2009, vol. 113, no 16, p. 6743-6750.

[26] CHENG, X. F., LENG, W. H., LIU, D. P., et al. Electrochemical preparation and characterization of surface-fluorinated TiO2 nanoporous film and its enhanced

photoelectrochemical and photocatalytic properties. The Journal of Physical Chemistry C, 2008, vol. 112, no 23, p. 8725-8734.

[27] BIEDRZYCKI, Jakub, LIVRAGHI, Stefano, GIAMELLO, Elio, et al. Fluorine- and niobium-doped TiO2: Chemical and spectroscopic properties of polycrystalline n-type-doped anatase. The Journal of Physical Chemistry C, 2014, vol. 118, no 16, p. 8462-8473.

[28] CZOSKA, A. M., LIVRAGHI, S., CHIESA, M., et al. The nature of defects in fluorine-doped TiO2. The Journal of Physical Chemistry C, 2008, vol. 112, no 24, p. 8951-8956.

[29] DI VALENTIN, Cristiana, PACCHIONI, Gianfranco, et SELLONI, Annabella. Reduced and n-type doped TiO2: nature of Ti3+ species. The Journal of Physical Chemistry C, 2009, vol. 113, no 48, p. 20543-20552.

[30] DUNN, Wendell W., AIKAWA, Yosihiro, et BARD, Allen J. Characterization of particulate titanium dioxide photocatalysts by photoelectrophoretic and electrochemical measurements. Journal of the American Chemical Society, 1981, vol. 103, no 12, p. 3456-3459.

[31] XU, Yiming, LV, Kangle, XIONG, Zhigang, et al. Rate enhancement and rate inhibition of phenol degradation over irradiated anatase and rutile TiO2 on the addition of NaF: new insight into the mechanism. The Journal of Physical Chemistry C, 2007, vol. 111, no 51, p. 19024-19032.

[32] PARK, Hyunwoong et CHOI, Wonyong. Effects of TiO2 surface fluorination on photocatalytic reactions and photoelectrochemical behaviors. The Journal of Physical Chemistry B, 2004, vol. 108, no 13, p. 4086-4093.

[33] LEWANDOWSKI, M. et OLLIS, D. F. Halide acid pretreatments of photocatalysts for oxidation of aromatic air contaminants: rate enhancement, rate inhibition, and a thermodynamic rationale. Journal of Catalysis, 2003, vol. 217, no 1, p. 38-46.

[34] PANARELLI, Enzo Gabriele, LIVRAGHI, Stefano, MAURELLI, Sara, et al. Role of surface water molecules in stabilizing trapped hole centres in titanium dioxide (anatase) as monitored by electron paramagnetic resonance. Journal of Photochemistry and Photobiology A: Chemistry, 2016, vol. 322, p. 27-34.

[35] MILLER, Kristi L., FALCONER, John L., et MEDLIN, J. Will. Effect of water on the adsorbed structure of formic acid on TiO2 anatase (1 0 1). Journal of catalysis, 2011, vol. 278, no 2, p. 321-328.

[36] MAIRA, A. J., YEUNG, King Lun, SORIA, J., et al. Gas-phase photo-oxidation of toluene using nanometer-size TiO2 catalysts. Applied Catalysis B: Environmental, 2001, vol. 29, no 4, p. 327-336.

[37] PATOCZKA, Jerzy et WILSON, David J. Kinetics of the desorption of ammonia from water by diffused aeration. Separation Science and Technology, 1984, vol. 19, no 1, p. 77-93.

[38] LINSEBIGLER, Amy L., LU, Guangquan, et YATES JR, John T. Photocatalysis on TiO2 surfaces: principles, mechanisms, and selected results. Chemical reviews, 1995, vol. 95, no 3, p. 735-758.

[39] JUNG, Kyeong Youl, PARK, Seung Bin, et IHM, Son-Ki. Linear relationship between the crystallite size and the photoactivity of non-porous titania ranging from nanometer to micrometer size. Applied Catalysis A: General, 2002, vol. 224, no 1-2, p. 229-237.

[40] BAKARDJIEVA, Snejana, SUBRT, Jan, PULISOVA, Petra, et al. Photoactivity of Anatase–Rutile TiO 2 Nanocrystalline Mixtures Obtained by Heat Treatment of Titanium Peroxide Gel. MRS Online Proceedings Library Archive, 2011, vol. 1352.

[41] SZCZEPANKIEWICZ, Steven H., COLUSSI, A. J., et HOFFMANN, Michael R. Infrared spectra of photoinduced species on hydroxylated titania surfaces. The Journal of Physical Chemistry B, 2000, vol. 104, no 42, p. 9842-9850.

[42] PAZÉ, C., BORDIGA, S., LAMBERTI, C., et al. Acidic Properties of H− β Zeolite As Probed by Bases with Proton Affinity in the 118− 204 kcal mol-1 Range: A FTIR Investigation. The Journal of Physical Chemistry B, 1997, vol. 101, no 24, p. 4740-4751.

[43] TONG, Hai-Jie, YU, Jun-Ying, ZHANG, Yun-Hong, et al. Observation of conformational changes in 1-propanol− water complexes by FTIR spectroscopy. The Journal of Physical Chemistry A, 2010, vol. 114, no 25, p. 6795-6802.

[44] Hind A , AL-ABADLEH. and GRASSIAN, V. H. FT-IR study of water adsorption on aluminum oxide surfaces. Langmuir, 2003, vol. 19, no 2, p. 341-347.

[45] SCATENA, L. F., BROWN, M. G., et RICHMOND, G. L. Water at hydrophobic surfaces: weak hydrogen bonding and strong orientation effects. Science, 2001, vol. 292, no 5518, p. 908-912.

[46] THOMPSON, Tracy L. et YATES, John T. Surface science studies of the photoactivation of TiO2 new photochemical processes. Chemical Reviews, 2006, vol. 106, no 10, p. 4428-4453.

[47] BIEDRZYCKI, Jakub, LIVRAGHI, Stefano, GIAMELLO, Elio, et al. Fluorine- and niobium-doped TiO2: Chemical and spectroscopic properties of polycrystalline n-type-doped anatase. The Journal of Physical Chemistry C, 2014, vol. 118, no 16, p. 8462-8473.

[48] SKARLIS, Stavros A., BERTHOUT, David, NICOLLE, André, et al. IR spectroscopy analysis and kinetic modeling study for NH3 adsorption and desorption on H-and Fe-BEA catalysts. The Journal of Physical Chemistry C, 2013, vol. 117, no 14, p. 7154-7169.

[49] H. A. Al-Abadleh, V. H. Grassian, FT-IR Study of Water Adsorption on Aluminum Oxide Surfaces, Langmuir, 19 (2003),pp. 341-347.

[50] QI, Gongshin et YANG, Ralph T. Characterization and FTIR Studies of MnO x– CeO2 Catalyst for Low-Temperature Selective Catalytic Reduction of NO with NH3. The Journal of Physical Chemistry B, 2004, vol. 108, no 40, p. 15738-15747.

[51] QI, Gongshin et YANG, Ralph T. Characterization and FTIR Studies of MnO x– CeO2 Catalyst for Low-Temperature Selective Catalytic Reduction of NO with NH3. The Journal of Physical Chemistry B, 2004, vol. 108, no 40, p. 15738-15747.

[52] CURTIN, T., O'REGAN, F., DECONINCK, C., et al. The catalytic oxidation of ammonia: influence of water and sulfur on selectivity to nitrogen over promoted copper oxide/alumina catalysts. Catalysis today, 2000, vol. 55, no 1-2, p. 189-195.

[53] AMORES, JosèManuel Gallardo, ESCRIBANO, Vicente Sanchez, RAMIS, Gianguido, et al. An FT-IR study of ammonia adsorption and oxidation over anatase-

supported metal oxides. Applied Catalysis B: Environmental, 1997, vol. 13, no 1, p. 45-58.

[54] BAHRAMI, Behnam, KOMVOKIS, Vasileios G., SINGH, Udayshankar G., et al. In situ FTIR characterization of NH3 adsorption and reaction with O2 and CO on Pd-based FCC emission control additives. Applied Catalysis A: General, 2011, vol. 391, no 1-2, p. 11-21.

[55] BAHRAMI, Behnam, KOMVOKIS, Vasileios G., ZIEBARTH, Michael S., et al. NH3 decomposition and oxidation over noble metal-based FCC CO combustion promoters. Applied Catalysis B: Environmental, 2013, vol. 130, p. 25-35.

[56] ISHII, Hisao, SUGIYAMA, Kiyoshi, ITO, Eisuke, et al. Energy level alignment and interfacial electronic structures at organic/metal and organic/organic interfaces. Advanced materials, 1999, vol. 11, no 8, p. 605-625.

[57] DAVYDOV, Anatoli. The nature of oxide surface centers. John Wiley & Sons, Ltd, 2003.

[58] XU, Yiming, LV, Kangle, XIONG, Zhigang, et al. Rate enhancement and rate inhibition of phenol degradation over irradiated anatase and rutile TiO2 on the addition of NaF: new insight into the mechanism. The Journal of Physical Chemistry C, 2007, vol. 111, no 51, p. 19024-19032.

[59] OSSEO-ASARE, K. Aggregation, reversed micelles, and microemulsions in liquid-liquid extraction: the tri-n-butyl phosphatediluent-water-electrolyte system. Advances in colloid and interface science, 1991, vol. 37, no 1-2, p. 123-173.

[60] ZHANG, Li et HE, Hong. Mechanism of selective catalytic oxidation of ammonia to nitrogen over Ag/Al2O3. Journal of Catalysis, 2009, vol. 268, no 1, p. 18-25.

[61] LAANE, Jaan (ed.). Frontiers of molecular spectroscopy. Elsevier, 2011.

[62] GOODMAN, A. L., UNDERWOOD, G. M., et GRASSIAN, V. H. Heterogeneous reaction of NO2: Characterization of gas-phase and adsorbed products from the reaction, 2NO2 (g)+ H2O (a)→ HONO (g)+ HNO3 (a) on hydrated silica particles. The Journal of Physical Chemistry A, 1999, vol. 103, no 36, p. 7217-7223.

[63] RUZICKA, Jan-Yves, BAKAR, Faridah Abu, THOMSEN, Lars, et al. XPS and NEXAFS study of fluorine modified TiO 2 nano-ovoids reveals dependence of Ti 3+ surface population on the modifying agent. RSC Advances, 2014, vol. 4, no 40, p. 20649-20658.

[64] CUNNINGHAM, J., GOOLD, E. L., HODNETT, B. K., et al. Photoassisted gas-solid reactions, photocatalytic processes and endergonic photoconversions over pure and surface-doped metal oxides. In : Studies in Surface Science and Catalysis. Elsevier, 1984. p. 283-290.

[65] BIEDRZYCKI, Jakub, LIVRAGHI, Stefano, GIAMELLO, Elio, et al. Fluorine- and niobium-doped TiO2: Chemical and spectroscopic properties of polycrystalline n-type-doped anatase. The Journal of Physical Chemistry C, 2014, vol. 118, no 16, p. 8462-8473.

[66] HE, Zhiqiao, WEN, Lina, WANG, Da, et al. Photocatalytic reduction of CO2 in aqueous solution on surface-fluorinated anatase TiO2 nanosheets with exposed {001} facets. Energy & Fuels, 2014, vol. 28, no 6, p. 3982-3993.

[67] CARP, Oana, HUISMAN, Carolien L., et RELLER, Armin. Photoinduced reactivity of titanium dioxide. Progress in solid state chemistry, 2004, vol. 32, no 1-2, p. 33-177.

CHAPTER VII

FINAL CONCLUSIONS

CONCLUSIONES FINALES

La primera parte del trabajo que utiliza diferentes catalizadores sintetizados y comerciales, concluimos que:

- Los catalizadores de TiO_2(Cl) y ZnO comerciales degradan el fenol más rápido que los otros catalizadores probados.
- TiO_2(Cl) actúa tan bien como P25, por lo que planeamos continuar nuestros estudios postdoctorales sobre este catalizador.

El estudio en fase líquida utilizando diferentes tipos de fotocatalizadores muestra que:

- Entre los materiales estudiados, el TiO_2 tanto comercial como sintetizado, es el material que muestra la mejor combinación de estabilidad y reactividad para aplicaciones fotocatalíticas.
- La fluoración de los catalizadores aumenta la reactividad para la degradación de fenol, utilizado como modelo de contaminante.
- La actividad de los fotocatalizadores dopados con flúor disminuye significativamente cuando son reutilizados.
- Mientras que la fluoración del catalizador P25 ralentiza la degradación del ácido fórmico y la anilina, se observa el efecto opuesto para los catalizadores Aldrich.

Sobre los estudios de fotodegradación con etanol, concluimos que:

- Las tasas de degradación con catalizadores dopados son más altas que con catalizadores no dopados.
- La producción de acetato cuando se usan catalizadores dopados es menor que cuando se usan catalizadores sin modificar.

- Los catalizadores fluorados se desactivan gradualmente durante los sucesivos usos, lo que se atribuye a un empobrecimiento en F superficial.

A partir de los estudios de fotodegradación con amoníaco, dedujimos:

- La oxidación fotocatalítica del amoníaco utilizando fotocatalizadoresno dopados produce nitratos adsorbidos.
- La oxidación fotocatalítica del amoníaco utilizando fotocatalizadores fluorados produce aductos superficiales HNO_3-H_2O.

CONCLUSIONS FINALES

La première partie du travail qui utilise différents catalyseurs synthétisés et commerciaux, nous concluons que:

- Les catalyseurs TiO_2(Cl) et ZnO commercial dégradent le phénol plus rapidement que les autres catalyseurs testés.
- TiO_2(Cl) agit aussi bien que P25, donc nous prévoyons de poursuivre nos études postdoctorale sur ce catalyseur.

L'étude en phase liquide utilisant différents types de photocatalyseurs montre que:

- Parmi les matériaux étudiés, le TiO_2 commercial et synthétisé est le matériau qui présente la meilleure combinaison de stabilité et de réactivité pour les applications photocatalytiques.
- La fluoration des catalyseurs augmente la réactivité pour la dégradation du phénol, utilisé comme polluant modèle.
- L'activité des photocatalyseurs dopés au fluor diminue de manière significative lorsqu'ils sont réutilisés.
- Tandis que la fluoration du catalyseur P25 ralentit la dégradation de l'acide formique et de l'aniline, l'effet inverse est observé pour le catalyseur Aldrich.

Concernant les études de photodégradation avec l'éthanol, on conclut que:

- Les taux de dégradation avec les catalyseurs dopés sont plus élevés qu'avec les catalyseurs non dopés.
- La production d'acétate lors de l'utilisation des catalyseurs dopés est plus faible que lors de l'utilisation des catalyseurs non modifiés.

- Les catalyseurs fluorés sont progressivement désactivés lors d'utilisations successives, ce qui est attribué à un appauvrissement superficiel en F.

A partir des études de photodégradation avec l'ammoniac, nous avons déduit:

- L'oxydation photocatalytique de l'ammoniac en utilisant des photocatalyseurs non dopés, produit des nitrates adsorbés.
- L'oxydation photocatalytique de l'ammoniac en utilisant des photocatalyseurs fluorés, produit des adducts de surface HNO_3-H_2O.

FINAL CONCLUSIONS

The first part of work using different synthesized and commercial catalysts, we conclude that:

- TiO_2(Cl) and commercial ZnO catalysts degrade phenol faster than the other proven catalysts.
- TiO_2(Cl) act as well as P25, so we plan to continue our postdoctoral studies on this catalyst.

The study in liquid phase using different types of commercial TiO_2 shows that:

- Among studied materials, both commercial and synthesized TiO_2 are the materials that show the best combination of stability and reactivity for photocatalytic applications.
- Fluorination of the catalysts increases thereactivity for the degradation of phenol, used as pollutant model.
- The activity of the photocatalysts doped with fluorine significantly when they are reused.
- While fluorination of P25 catalyst slows down the degradation of formic acid and aniline, the opposite effect is observed for the Aldrich catalysts.

Concerning the photodegradation studies with ethanol, we conclude that:

- Degradation rates with the doped catalysts are higher than with undopped ones.
- Acetates production when using doped catalysts is lower than when using bare catalysts.
- Fluorinated catalysts are gradually deactivated during subsequent uses, which is attributed to surface F impoverishment.

From the photodegradation studies with ammonia, we deduced:

- Photocatalytic oxidation of ammonia using undopedphotocatalysts results in adsorbed nitrates.
- Photocatalytic oxidation of ammonia using fluorinated photocatalysts produces HNO_3-H_2O surface adducts.

Chemical Physics Letters 684 (2017) 164–170

Contents lists available at ScienceDirect

Chemical Physics Letters

journal homepage: www.elsevier.com/locate/cplett

Research paper

TiO_2 and F-TiO_2 photocatalytic deactivation in gas phase

W. El-Alami [a,b,c], D. Garzón Sousa [b,c], J.M. Díaz González [b,c], C. Fernández Rodríguez [b,c], O. González Díaz [b,c], J.M. Doña Rodríguez [b,c], M. El Azzouzi [a], J. Araña [b,c,*]

[a] Faculty des Sciences, University Mohammed V, Agdal, BP 1014-Avenue Ibn Batoutta, Rabat, Morocco
[b] CIDIA-FEAM Universidad de Las Palmas de Gran Canaria, Edificio del Parque Científico Tecnológico de la ULPGC, Campus de Tafira, 35017 Las Palmas de Gran Canaria, Spain[1]
[c] Instituto de Estudios Ambientales y Recursos Naturales (i-UNAT), ULPGC, Spain

ARTICLE INFO

Article history:
Received 27 April 2017
In final form 27 June 2017
Available online 28 June 2017

Keywords:
TiO_2
Photocatalysis
Ethanol
Acetates
FTIR

ABSTRACT

TiO_2 deactivation processes during gas-phase degradation of ethanol were studied. To force the deactivation processes, various cycles were performed, avoiding the degradation of acetates. It was observed that acetates adsorbed on the anatase phase of catalysts provoke the transference of electrons to surface traps which modify the electron states of the semiconductor.

The same deactivation studies were also performed with fluorinated TiO_2. It was noted that the electrons present in the surface traps, as a consequence of the Ti-F interaction, react with the holes during irradiation and provoke a change in the electron states of the semiconductor.

© 2017 Elsevier B.V. All rights reserved.

1. Introduction

TiO_2 has been studied and used preferentially in aqueous phase where the processes of deactivation are less frequent as the water can facilitate removal of intermediates from the surface [1]. By contrast, in gas phase, the adsorption of reagents and/or reaction intermediates can more easily produce poisoning of the semiconductor surface. This has been seen in studies with both inorganic [2,3] and organic [4] compounds. In many studies, there have been difficulties to identify the substrate which resulted in surface inactivation and/or of the nature of the active centres. Deactivation of the TiO_2 materials has also been attributed to the water or to the extraction of oxygen from the crystalline lattice for its participation in the stages of generation of radicals [5,6].

Different strategies have been used to enhance the activity of these materials by impeding their deactivation and reducing the e^-/h^+ recombination reactions. One of these strategies is surface modification of TiO_2 with fluorine (F-TiO_2). Fluorine has a higher electronegativity than oxygen and has a specific affinity for adsorption onto TiO_2 acting as a Lewis base. The presence of fluoride anions has shown positive effects in aqueous phase increasing the degradation rate of different compounds [7–9]. It has been shown that the strong electron acceptor capacity of the Ti-F groups present on the surface hinders recombination of photo-generated electrons and holes, thereby enhancing photocatalytic efficiency [10,11]. However, many aspects of the effect of fluorine on the TiO_2 surface have not been fully clarified specially in photocatalytic processes in gas phase.

The aim of the present work is to study TiO_2 deactivation processes during the degradation of ethanol in gas phase, using catalysts composed only by anatase phase and anatase/rutile phase mixtures. A study is also undertaken of the effect of fluorination of these materials on deactivation. These studies were carried out with mixtures of air, ethanol and water. The water vapour can compete with the adsorption centres, but can also favour the diffusion processes of molecules and radicals during the photocatalytic process. It has also been reported that water may participate in stabilisation of the adsorbed molecules or of the photogenerated holes [12,13]. The adsorption process was performed continuously in view to increase the signal of minority species which may be generated during the adsorption process.

2. Experimental

2.1. Synthesis of fluorinated catalysts

Two commercial TiO_2 photocatalysts were used: Evonik Aeroxide P25 (P25) and anatase Sigma Aldrich (SA). For synthesis of the

* Corresponding author at: CIDIA-FEAM Universidad de Las Palmas de Gran Canaria, Edificio del Parque Científico Tecnológico de la ULPGC, Campus de Tafira, 35017 Las Palmas de Gran Canaria, Spain.
E-mail address: farana@dqui.ulpgc.es (J. Araña).
[1] Unidad Asociada al CSIC a través del Instituto de Ciencias de Materiales de Sevilla, ICMS.

http://dx.doi.org/10.1016/j.cplett.2017.06.056
0009-2614/© 2017 Elsevier B.V. All rights reserved.

fluorinated catalysts, 10 g of the corresponding commercial TiO_2 catalyst were placed into 250 mL of a 2 M NaF solution at pH 3 in order to favour fluorine adsorption. This solution was stirred continuously for 30 min and then filtered. The catalyst obtained after filtration was washed with 1 L of water and the non-desorption of fluoride and sodium was observed. The catalyst was subsequently dried at 100 °C for 12 h.

2.2. Characterisation of materials

The surface concentration of fluorine on the catalysts was semi-quantitatively determined by EDAX analysis (Quantax 70, Bruker). Three image amplifications were carried out for this analysis (300, 3000 and 30000) with 5 sampling points in each increase and an exposure time of 300 s.

Analyses of the crystalline structure were performed by X-ray diffraction (XRD Bruker D8 Advance) with a source of Cu $K\alpha_1$ radiation (λ = 0.15406 nm) at 1.6 kW (40 kV, 40 mA). Anatase-rutile fractions were calculated taking into account the relative diffraction peak intensities of crystalline planes (101) and (111) of anatase and rutile, respectively. BET surface area measurements were carried out by N_2 adsorption at 77 K using a Micromeritics 2010 instrument. Diffuse reflectance UV–Vis spectra (DRS-UV–Vis) were recorded on a Varian Cary 5 spectrometer equipped with an integrating sphere using PTFE (poly-tetrafluoroethylene) as reference to study the optoelectronic properties of the samples. Diffuse reflectance spectra were recorded and band gap values were calculated by the Kubelka-Munk function, according to the Tandon-Gupta method [14]. Field emission scanning electron microscopy (FESEM) images were obtained using a Hitachi S-4800 microscope.

2.3. Photocatalytic experiments

The photocatalytic experiments were performed with four commercial catalysts (P25, SA, P90 and PC100) and the two fluorinated catalysts (F-P25 and F-SA). The interaction and photocatalytic degradation of ethanol were followed by Fourier Transform Infrared Spectroscopy (FTIR) with a Thermo-Scientific-Nicolet iS10 spectrophotometer and a custom-made cell equipped with CaF_2 windows performing 32 scans with a spectral resolution of 4 cm^{-1}. 10 mg of catalyst were used in each experiment.

A 60 W Philips Solarium HB175 lamp equipped with four 15 W Philips CLEO fluorescent tubes with emission between 300 and 400 nm (λ_{max} = 365 nm, irradiance: 9 mW cm^{-2}) was used as UV source in the degradation studies. Once the substrate was adsorbed and the initial spectrum was taken, the irradiation was initiated and the FTIR analysis was periodically performed in order to study the evolution of species during the degradation process.

Catalysts were subjected to an air flow of 50 mL·min^{-1} in which the concentrations of ethanol and water were, respectively, 8.5 and 32.9 mmol·min^{-1} for 60 min and then placed in the cell for analysis. The system has been described in a previous work [15] and is summarised in Fig. 1S of the supplementary materials.

Blank experiments of photolytic evolution of ethanol were carried out in the absence of catalyst and under the same experimental conditions; reactants remained unaltered throughout the assay.

3. Results and discussion

3.1. BET area, EDAX, SEM, XRD and UV–vis DRS analyses

Table 1 shows the most important results of the BET, EDAX, DRX and UV–Vis DRS analyses. The P90 and PC100 catalysts have the

Table 1
Surface area, anatase/rutile phase ratios, band gap and Ti/F and F/Na molar ratios.

	Surface area (m^2 g^{-1})	Anatase/rutile phase ratios	Band gap (eV)	Molar ratio	
				Ti/F	F/Na
P25	50.9	82.3/17.7	3.16	–	–
F-P25	52.9	82.4/17.6	3.0	20.32	2.50
SA	47.3	100/0	3.16	–	–
F-SA	46.1	100/0	3.18	18.46	2.09
P90	95.2	89.4/10.6	3.25	–	–
PC100	94.7	100/0	3.14	–	–

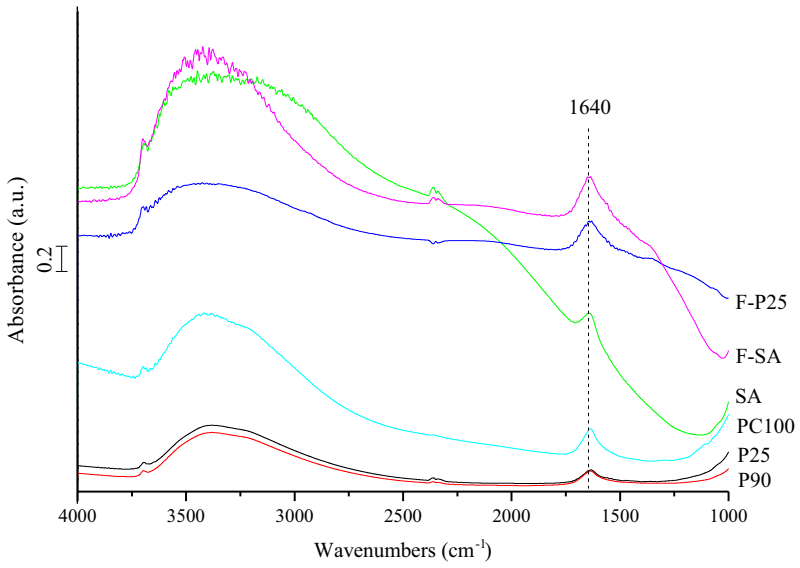

Fig. 1. FTIR spectra of the fluorinated and non-fluorinated P25, SA, P90 and PC100 catalysts.

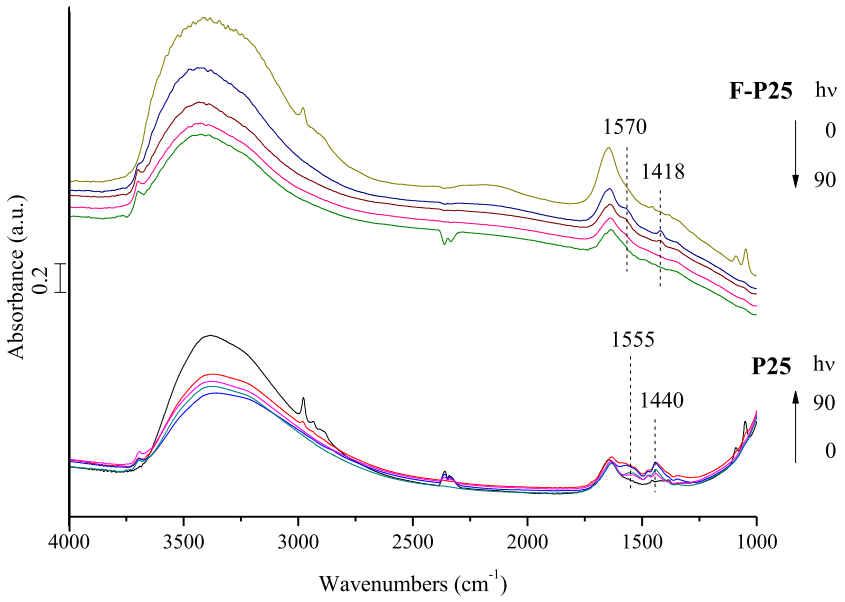

Fig. 2. Evolution of the spectra of P25 and F-P25 after ethanol adsorption and after different periods of time under illumination.

largest surface area (95.2 and 94.7 $m^2\,g^{-1}$, respectively), while the P25, SA, F-P25 and F-SA catalysts have similar surface area sizes (of around 50 $m^2 \cdot g^{-1}$). The P25, F-P25 and P90 have anatase and rutile in their structure, while the SA, F-SA and PC100 catalysts are only composed of anatase phase (Fig. 2S of supplementary materials shows the X-ray diffraction pattern of the P25, F-P25, SA and F-SA). The band gap values obtained from the UV–Vis analyses are all very similar, with no significant changes observed when fluorinating the catalysts (Fig. 3S of supplementary materials displays the UV–vis DRS spectra of the P25, F-P25, SA and F-SA). Thus, as shown in other studies, surface fluorination of the catalysts does not modify the optical properties of these materials [16,17]. The images obtained from the SEM analyses of F-P25, F-SA and SA showed a similar distribution of aggregates. However SEM analyses of P25 showed different distribution (Fig. 4S of supplementary materials).

Table 1 also shows the Ti/F and F/Na ratios obtained from the EDAX analysis. The surface composition studies also showed the presence of sodium on the surface of these materials, though its concentration is significantly lower than the molar concentration of fluorine. This shows that the fluorine is mostly interacting with the catalyst surface and is not as NaF, though the presence of this salt on the surface cannot be discarded.

3.2. Characterisation of the adsorbed water, hydroxyl groups and surface charge

Fig. 1 shows the spectra of the fluorinated and non-fluorinated P25, SA, P90 and PC100 catalysts. Note in particular the band attributed to isolated hydroxyl groups (3698 cm^{-1}), the bands attributed to adsorbed water (3600–3000 cm^{-1} and 1640 cm^{-1}), and finally the position of the baseline of each of the catalysts.

The band observed in all catalysts at 1640 cm^{-1} is assigned to the water bending mode (ν_2), while the broad band between 3650 and 3000 cm^{-1} is attributed to antisymmetric (ν_3) and symmetric (ν_1) stretching vibration modes of the water [18,19].

An important aspect to note in the spectra of Fig. 1 is the position of the baseline. As a result of the presence of surface or shallow electron traps, electrons are fed to the conduction band via thermal processes such as those generated by the infrared radiation used to obtain the spectra. The electrons promoted to the conduction band have a similar behaviour to that described for delocalised electrons confined to a three-dimension box with infinite walls; the high density of generated states gives rise to the continuous presence of excited electrons leading to a baseline

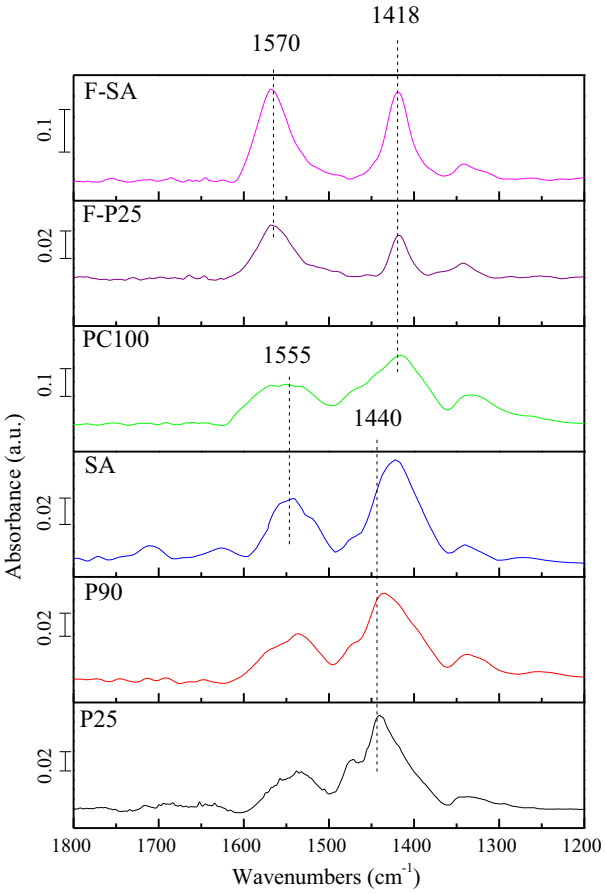

Fig. 3. Comparison of the acetates spectra during ethanol degradation on the different catalysts after 20 min of illumination.

increase of the infrared spectrum [20]. The baseline position of the SA and PC100 catalysts, the ones with only anatase phase, is higher than that of the P25 and P90. On modification of P25 with fluorine, a baseline increase takes place which takes it to the same level as that observed in the SA catalyst. When TiO_2 is modified with fluorine, at least a fraction of the excess electrons introduced by the fluorine are localised by lattice Ti^{4+} cations. The presence of reduced Ti^{3+} centres in the as-prepared, fully oxidized solid indicates that the F-TiO_2 system can be described in terms of an *n*-type semiconductor provoking the baseline increase observed in the F-P25 catalysts [21]. This could be related with the change in the aggregate distribution observed in SEM analyses.

3.3. Ethanol photocatalytic degradation studies

Once ethanol was adsorbed onto the surface, the catalysts were illuminated for 90 min and the different species formed were studied by FTIR. Fig. 2 shows the evolution of the adsorbed species in the region between 4000 and 1000 cm^{-1} with the P25 catalyst. Similar spectra were obtained with the other catalysts (SA, P90 and PC100). The main difference observed with the different catalysts was the nature of the acetates formed after the first few minutes of irradiation corresponding to the bands observed between 1580–1540 cm^{-1} and 1450–1430 cm^{-1} and attributed to $\nu\,(COO)_{as}$ and $\nu\,(COO)_s$. Fig. 3 compares the spectra of the acetates obtained for the different catalysts after 20 min of illumination. Note that the asymmetric vibration of the acetates identified in both catalysts is found at approximately the same wavenumber. However, the symmetric vibration is found at 1440 cm^{-1} in the P25 and P90, and at 1418 cm^{-1} in the SA and PC100. The differences observed may be due to the presence of rutile phase in the first two catalysts. Indeed, similar changes were observed in studies carried out with acetic acid with TiO_2 with different phases [22]. It can therefore be argued that the shift observed in the symmetric vibration in the P25 and P90 catalysts is due to the presence of rutile phase. Bands were also observed in the SA catalyst around 1715 and 1270 cm^{-1} which can be attributed to acetaldehyde or acetic acid [23].

The photocatalytic degradation of ethanol has been described through the following reaction stages [24,25]:

$$CH_3CH_2OH \rightarrow CH_3CHO \rightarrow CH_3COOH \quad (1)$$

$$CH_3COOH \rightarrow HCHO \rightarrow HCOOH \rightarrow CO_2 \quad (2)$$

During the photocatalytic studies undertaken in the present work, it was possible to clearly follow the evolution of the ethanol and acetates adsorbed on the surface and the process that was observed can be summarised in Reactions (1) and (2). The other intermediates which are generated must be degraded very quickly and for this reason they were not observed. Therefore, in order to make a proper analysis of the species generated in this study and their evolution during illumination, acetate (1440 or 1418 cm^{-1}) and ethanol (1050 cm^{-1}) tracings were performed. Fig. 4A–C show the evolution of the bands attributed to the symmetric vibration ($\nu\,(COO)_s$) of the acetates and the symmetric vibration ($\nu\,(CO)$) of the ethanol. A progressive increase of the intensity of the band attributed to the $\nu\,(COO)_s$ can be observed in the P90 and P25 catalysts during the first 15–20 min (Reaction (1)), followed by a progressive decrease (Reaction (2)). The beginning of the decrease of the intensity of this band coincides with the disappearance of the ethanol band at 1050 cm^{-1} ($\nu\,(CO)$). Thus, it would appear that Reaction (2) does not commence until all Reaction (1) has concluded. A progressive increase of the intensity of the band attributed to the ν

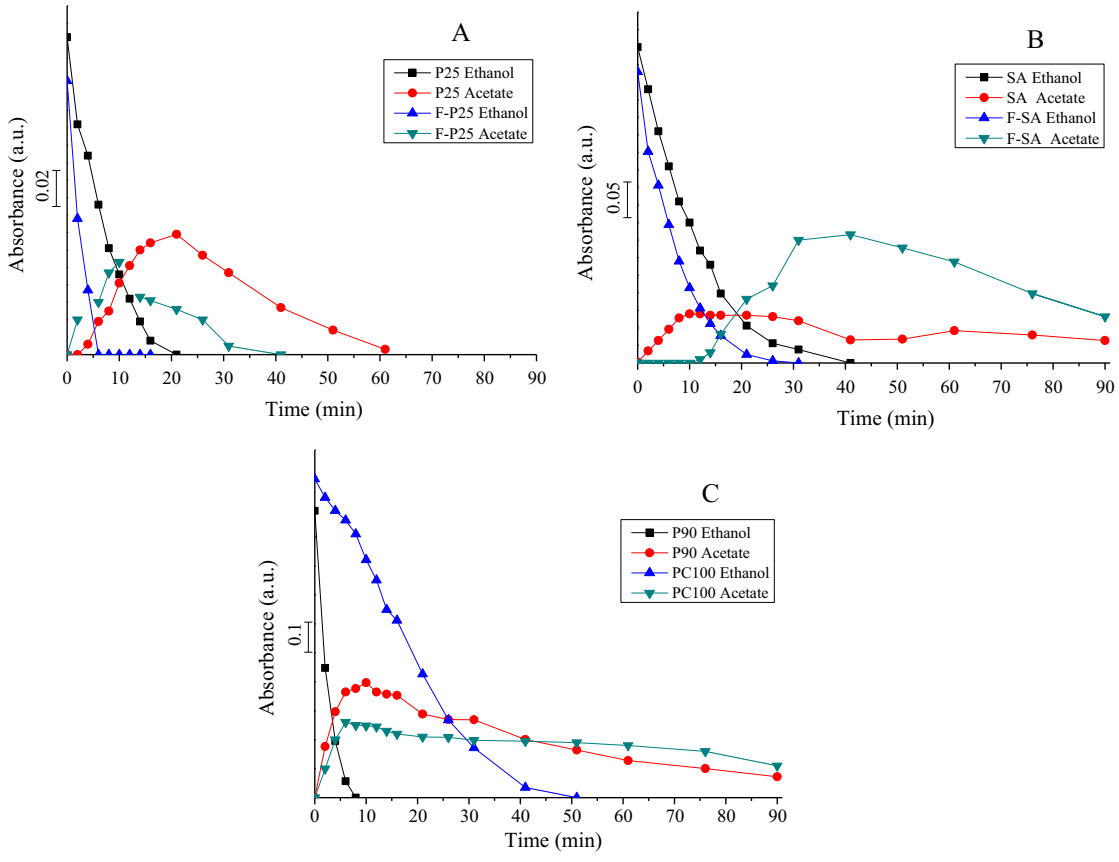

Fig. 4. Evolution over the time of the different IR bands during UV radiation of (A) P25 and F-P25, (B) SA and F-SA and (C) P90 and PC100.

$(COO)_s$ can also be observed in the PC100 and SA catalysts during the first few minutes. However, after this initial period the intensity of the band does not change for the next 20 min, and subsequently it slowly decreases.

3.4. Deactivation studies

In order to elucidate the deactivation processes of these catalysts, a new study was undertaken in which, after the first 20 min of illumination (that is when the ethanol signal at 1050 cm^{-1} was no longer observed), the catalyst was once again impregnated with ethanol for 1 h. It was then again illuminated under the same conditions as previously. This process was repeated a total of 7 times (cycles). Fig. 5A shows the initial spectra of each of these cycles 1, 2, 3, 5 and 7 with the P25, and the spectra obtained after 20 min of illumination (the spectra obtained in these tests with the P90 were practically identical and are thus not shown). In the studies with the SA and PC100, no increase was observed in the formation of acetates after the first cycle. However, adsorbed ethanol was observed after the first cycle. It has been reported that ethanol can be adsorbed onto organic compounds present on the surface [26]. Fig. 6 shows the increase in the intensity of the band attributed to $\nu\,(COO)_s$ for each catalyst after each cycle. This increase progressively diminishes as the number of cycles increases, indicating deactivation processes. After first cycles, in the P25 (Fig. 5A) and P90 catalysts, the band attributed to the $\nu\,(COO)_s$ of acetates possibly adsorbed on the rutile surface decreases significantly in intensity and only the band present at 1418 cm^{-1} is observed, attributed to the $\nu\,(COO)_s$ of acetates adsorbed on the anatase surface (Fig. 5A). This would suggest that the acetates present on the rutile surface are very weakly adsorbed (probably hydrated as reported in other studies [22]). The decrease in the intensity of all the bands after the third cycle should also be noted (Fig. 6). It is also observed that the baseline of the initial spectrum of each cycle increases its position with respect to the previous cycle (Fig. 5A). As previously indicated, the increase in the baseline of the spectrum is attributed to an accumulation of surface electrons close to the conduction band. The progressive transmission of electrons through the adsorption of the acetate on the anatase phase may be responsible for modification of the position of baseline and the deactivation observed in the P25 and P90 catalysts. In the SA and PC100, deactivation takes place faster as in these catalysts surface electrons are from the initial instants (Fig. 1).

3.5. Studies with fluorinated catalysts

Given that with commercial catalysts deactivation processes were observed as a consequence of the increase in the negative

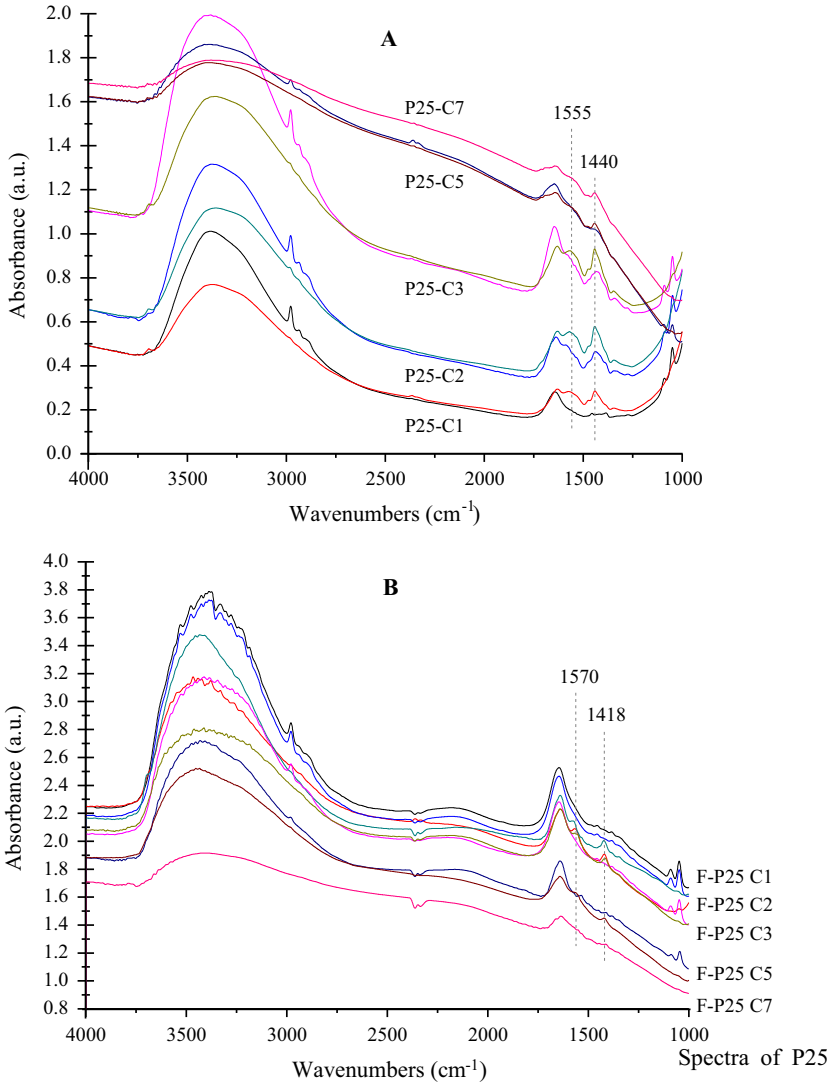

Fig. 5. Spectra of P25 (A) and F-P25 (B) at 0 and 20 min of illumination in cycles (C) 1, 2, 3, 5 and 7 during the deactivation studies.

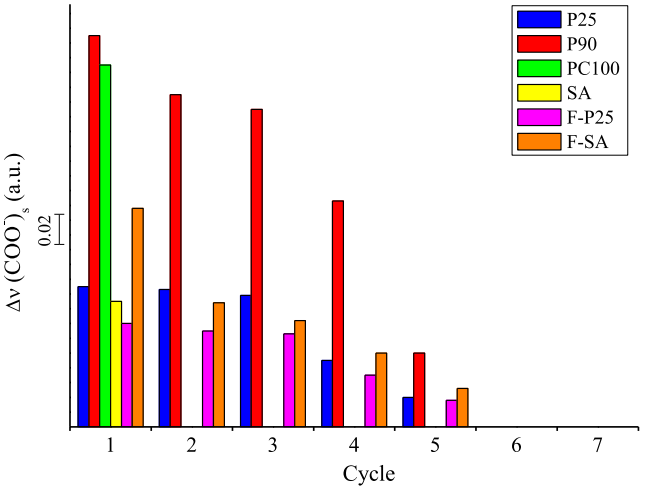

Fig. 6. Increase of the band associated with the vibration ν $(COO)_s$ of acetates produced after each cycle during the deactivation studies.

charge on the catalysts, similar studies were carried out with the fluorinated catalysts F-P25 and F-SA. Firstly, a degradation test was performed for 90 min, as with the previous catalysts. Fig. 2 shows a comparison of the spectra obtained with the F-P25 and the P25. Note that, unlike the P25, there takes place with the F-P25 a progressive decrease in the baseline position with illumination time. This can be more clearly observed in the studies with the F-SA (Fig. 7). It should also be noted that the wavenumber and the shape of the bands attributed to the ν $(COO)_{as}$ and ν $(COO)_s$ are different to those observed in the studies of the non-fluorinated catalysts (Fig. 3). With the fluorinated catalysts (F-P25 and F-SA), these bands are narrower, the symmetric and asymmetric vibrations have the same intensity and are found at 1570 and 1418 cm^{-1}, respectively. The shape of these bands and the wavenumber are similar to those of sodium acetate [27]. The EDAX analyses revealed the presence of sodium on the surface of these catalysts after fluorination, suggesting that formation of these acetates is feasible.

As a consequence of the high density of states with high negative surface charge of semiconductors with adsorbed F^- ions, during illumination the photogenerated holes would be trapped on the surface and the electrons forced to move to more interior Ti atoms of the crystalline structure [28]. The holes can then react with the oxygen atoms and/or the water giving rise to radicals or with the electrons trapped on the surface, as can be deduced from Figs. 2 and 7. This would explain the decrease in the baseline position during illumination of the fluorinated catalysts. Ethanol degradation with the fluorinated catalysts is slightly faster than with the P25 and SA (Fig. 4A and B) due to the above described effect.

The same deactivation studies were also performed as with the other catalysts. Fig. 5 B shows a comparison of baseline evolution of the F-P25 after different cycles (cycle 1, 2, 3, 5 and 7) with that obtained for P25. At the start of each new cycle no acetates are observed, as these must have been dissolved and carried away during the ethanol impregnation. The baseline of the spectra decreases progressively after each cycle. When both catalysts are deactivated (F-P25 and P25), the spectra are practically identical and the baseline of the spectrum is found in similar position. Exactly the same behaviour was observed with the F-SA.

On the other hand, deactivation with the P25 and P90 catalysts is produced by adsorption of the acetates on the anatase phase. It has been reported that diffusivity of electrons in rutile phase is 89 times lower than in anatase, and that therefore a transfer of holes can take place from the anatase to rutile phase [29]. When the density of electrons in the anatase phase increases this transfer would be more impeded. In the cycles performed with the P25 and P90, it was observed that after hydrated acetates are formed on the rutile surface they could be transferred and adsorbed on the anatase phase and a baseline increase results as a consequence of the transfer of electrons. The increase of acetates on the anatase phase must be increasing the charge density in this phase and decreasing hole transfer.

As was seen in Fig. 5B, the final spectrum after deactivation of the fluorinated catalysts (as a consequence of the loss of electrons trapped on the surface) and the final spectrum of the P25 catalyst (after the progressive adsorption of acetates, Fig. 5A) are very similar in terms of the intensity of the hydration bands and baseline position. That is, it appears that a similar deactivated state is

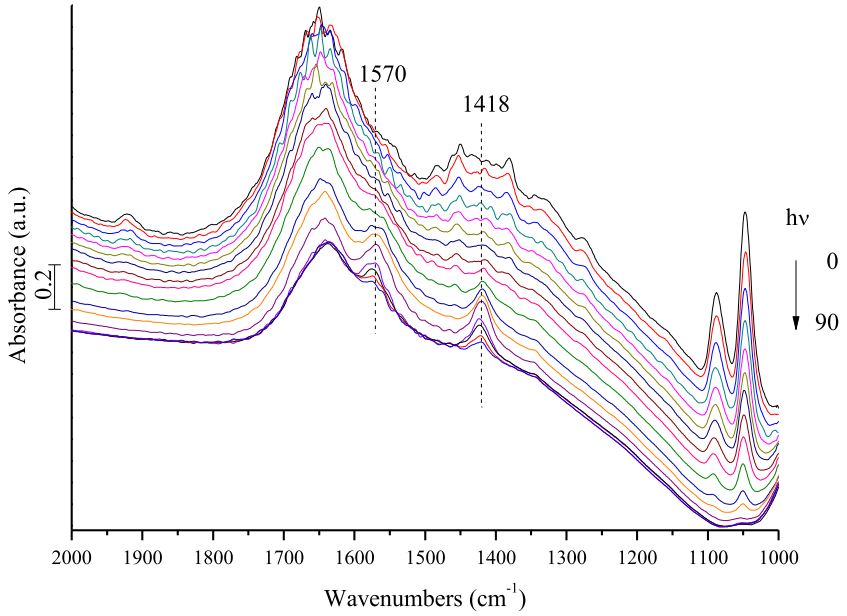

Fig. 7. Evolution of the spectra of F-SA after ethanol adsorption and after different periods of time under illumination.

reached in which, as a consequence of electron transfer, the two processes which accelerated the reaction are deactivated. The fact that the final spectrum is the same may indicate that only the electron transfer processes described here are intervening in the deactivation process.

4. Conclusions

In the P25 and P90 catalysts, it was observed that acetates resulting from ethanol degradation are found hydrated on the surface of the rutile phase. It was found that if these acetates are not degraded, they could migrate and are adsorbed on the anatase surface, provoking a transfer of electrons to surface layers which progressively deactivate the catalyst.

In the catalysts with purely anatase phase (SA and PC100), deactivation is immediate if the acetates are not removed before again adsorbing ethanol. Surface-trapped electrons were identified in these catalysts, probably generated in their synthesis process, which may accelerate catalyst deactivation.

The characterisation studies performed with the F-P25 and F-SA catalysts showed that in the fluorination process carried out in this study there is no significant modification to either surface area size, optical properties or crystalline phase distribution. However, the fluorination process does modify the concentration of surface electron traps, aggregates distribution and the interaction of acetates with the catalyst surface. In these semiconductors, a decrease in the concentration of electrons in the surface traps was observed during irradiation which was attributed to its reaction with the holes. The progressive decrease in the concentration of electrons in the traps may be the reason for the deactivation of these materials during ethanol degradation due, in part, to the diminishing effect of the electrostatic field.

It was therefore observed that the charge transfer processes, by different routes, in the P25, SA, F-P25 and F-SA catalysts ultimately give rise to a similar deactivated state.

Acknowledgements

We are grateful for the financial support of the Spanish Ministry of Economy and Competitiveness through the projects CTQ2015-64664-C2-1-P and the Spanish Ministry of Science and Innovation for the UNLP10-3E-726 infrastructure, co-financed with ERDF funds. D. Garzón Sousa would like to thank the University of Las Palmas de Gran Canaria for its funding through its PhD Grant Program and Wiâm El-Alami would like to thank the Erasmus Program for its funding through a mobility grant.

Appendix A. Supplementary material

Supplementary data associated with this article can be found, in the online version, at http://dx.doi.org/10.1016/j.cplett.2017.06.056.

References

[1] N. González-García, J.A. Ayllón, X. Doménech, J. Peral, Appl. Catal. B: Environ. 52 (2004) 69–77.
[2] A. Alonso-Telleza, R. Massona, D. Robertb, N. Kellera, V. Kellera, J. Photochem. Photobiol. A 250 (2012) 58–65.
[3] A. Folli, S.B. Campbell, J.A. Anderson, D.E. Macphee, J. Photochem. Photobiol. A 220 (2011) 85–934.
[4] Y. Ono, T. Rachi, M. Yokouchi, Y. Kamimoto, A. Nakajima, K. Okada, Mater. Res. Bull. 48 (2013) 2272–2278.
[5] D.S. Muggli, J.L. Falconer, J. Catal. 191 (2000) 318–325.
[6] H. Wang, C. You, Chem. Eng. J. 292 (2016) 199–206.
[7] C. Minero, G. Mariella, V. Maurino, E. Pelizzetti, J. Langmuir 16 (2000) 2632–2641.
[8] S. Kim, H. Park, W. Choi, J. Phys. Chem. B 108 (2004) 6402–6411.
[9] J.J. Murcia, M.C. Hidalgo, J.A. Navío, J. Araña, J.M. Doña-Rodríguez, Appl. Catal. B: Environ. 179 (2015) 305–312.
[10] M. Konstantakou, T. Stergiopoulos, V. Likodimos, G.C. Vougioukalakis, L. Sygellou, A.G. Kontos, A. Tserepi, P. Falaras, J. Phys. Chem. C 118 (30) (2014) 16760–16775.
[11] J. Yu, Q. Xiang, J. Ran, S. Mann, Cryst. Eng. Commun. 12 (2010) 872–879.
[12] E.G. Panarelli, S. Livraghi, S. Maurelli, V. Polliotto, M. Chiesa, E. Giamello, J. Photochem. Photobiol. A 322–323 (2016) 27–34.
[13] K.L. Miller, J.L. Falconer, J.W. Medlin, J. Catal. 278 (2011) 321–328.
[14] S.P. Tandon, J.P. Gupta, Phys. Status Solid. (b) 38 (1) (1970) 363–367.
[15] J. Araña, J.M. Doña-Rodríguez, O. González-Díaz, E. Tello Rendón, J.A. Herrera Melián, G. Colón, J.A. Navío, J. Pérez Peña J. Mol. Catal. A: Chem. 215 (2004) 153–160.
[16] J. Tang, H. Quan, J. Ye, Chem. Mater. 19 (2007) 116–122.
[17] Di Lia, Hajime Hanedaa, Shunichi Hishitaa, Naoki Ohashia, Nitin K. Labhsetwar, J. Fluorine Chem. 126 (2005) 69–77.
[18] H.-J. Tong, J.-Y. Yu, Y.-H. Zhang, J.P. Reid, J. Phys. Chem. A 114 (2010) 6795–6802.
[19] H.A. Al-Abadleh, V.H. Grassian, Langmuir 19 (2003) 341–347.
[20] T.L. Thompson, J.T. Yates, Jr., Chem. Rev. 106 (2006) 4428–4453.
[21] J. Biedrzycki, S. Livraghi, E. Giamello, S. Agnoli, G. Granozzi, J. Phys. Chem. C 118 (2014) 8462–8473.
[22] A. Mattsson, L. Österlund, J. Phys. Chem. C 114 (2010) 14121–14132.
[23] A.C. Sola, D. Garzón Sousa, J. Araña, O. González Díaz, J.M. Doña Rodríguez, P. Ramírez de la Piscina, N. Homs, Catal. Today 266 (2016) 53–61.
[24] Alexandre V. Vorontsov, Vera P. Dubovitskaya, J. Catal. 221 (2004) 102–109.
[25] Sarah Pilkenton, Son-Jong Hwang, Daniel Raftery, J. Phys. Chem. B 103 (1999) 11152–11160.
[26] E. Piera, J.A. Ayllón, X. Doménech, J. Peral, Catal. Today 76 (2002) 259–270.
[27] The Aldrich Library of FT-IR Spectra, 2nd ed., 3-volume set Milwaukee, WI, 1997.
[28] Hu.a. Sheng, Qin Li, Wanhong Ma, Hongwei Ji, Chuncheng Chen, Jincai Zhao, Appl. Catal. B: Environ. 138–139 (2013) 212–218.
[29] B. Sun, A.V. Vorontsov, P.G. Smirniotis, Role of platinum deposited on TiO_2 in phenol photocatalytic oxidation, Langmuir 19 (2003), 3151–315.

Journal of Photochemistry and Photobiology A: Chemistry 348 (2017) 139–149

Contents lists available at ScienceDirect

Journal of Photochemistry and Photobiology A: Chemistry

journal homepage: www.elsevier.com/locate/jphotochem

Invited paper

Efect of Ti—F surface interaction on the photocatalytic degradation of phenol, aniline and formic acid

W. El-Alami[a,b,c], D. Garzón Sousa[b,c,*], C. Fernández Rodríguez[b,c], O. González Díaz[b,c], J.M. Doña Rodríguez[b,c], M. El Azzouzi[a], J. Araña[b,c,*]

[a] Faculté des Sciences, Université Mohammed V, Agdal, BP 1014 Avenue Ibn Batoutta, Rabat, Morocco
[b] CIDIA-FEAM Universidad de La Palmas de Gran Canaria, Edificio del Parque Científico Tecnológico de la ULPGC, Campus de Tafira, 35017 La Palmas de Gran Canaria, (Unidad Asociada al CSIC a través del Instituto de Ciencias de Materiales de Sevilla, ICMS), Spain
[c] Instituto de Estudios Ambientales y Recursos Naturales (i-UNAT)-ULPGC, Spain

ARTICLE INFO

Article history:
Received 27 April 2017
Received in revised form 27 July 2017
Accepted 7 August 2017
Available online 22 August 2017

Keywords:
F-TiO_2
FTIR
Phenol
Aniline
Formic acid

ABSTRACT

A study is undertaken of the effect of fluorinating two TiO_2 catalysts, both with the same surface area but one composed only of pure anatase phase (SA) and the other of mixed anatase and rutile phases (P25), on the degradation of phenol, formic acid and aniline. The catalysts were characterised by FTIR, BET, EDAXs, SEM, XRD and DRS-UV–vis studies. The method used for synthesis of the F-P25 and F-SA resulted in fluorinated catalysts with properties different to those of other fluorinated catalysts reported in the bibliography. The results obtained show that, unlike other studies in which the formation of free hydroxyl radicals ($^{\bullet}OH_{free}$) was enhanced with the fluorinated catalysts, in the F-P25 and F-SA catalysts it was the formation of surface hydroxyl radicals ($^{\bullet}OH_{surf}$) which was significantly enhanced. In this way, the F-P25 and F-SA catalysts gave rise to higher degradation rate constants of phenol (k_{phenol}), aniline ($k_{aniline}$) and formic acid (k_{formic}) than the P25 and SA catalysts.

© 2017 Elsevier B.V. All rights reserved.

1. Introduction

The capacity of TiO_2 to degrade organic compounds has been demonstrated in numerous studies. However, the efficiency of this semiconductor needs to be improved for it to be an effective tool for pollutant removal. Various processes have been developed with the aim of enhancing and optimizing its photocatalytic properties. Fluoride has been used as precursor to synthesise new catalysts in which the exposure of certain crystalline faces is increased [1–5]. Research has also been conducted on surface modification of TiO_2 with fluorine (F-TiO_2). Fluorine has a higher electronegativity than oxygen and a specific affinity for adsorption onto TiO_2 acting as a Lewis base. The presence of fluoride anions has shown positive effects in aqueous phase increasing the degradation rate of phenol [6], benzoic acid [7], cyanuric acid (Triazine-*2*, *4*, *6*-Triol) [8], benzene, *4*-chlorophenol [9], as well as several dyes [10,11].

Different studies have shown that TiO_2 fluorination does not change the band gap of this semiconductor as the *p* orbitals of the fluorine have a lower energy than those of the oxygen atoms [12–14]. It has also been shown that the strong electron acceptor capacity of the Ti—F groups present on the surface hinders recombination of photo-generated electrons and holes, thereby enhancing photocatalytic efficiency [12–15]. It has been reported that the increased degradation rate is due to the increase in the concentration of $^{\bullet}OH$ radicals in solution as the fluorides displace the ^{-}OH groups from the surface [6]. In this respect, the following mechanisms have been proposed [6]:

$$\equiv Ti - OH + e^{-}_{(CB)} + h^{+}_{(VB)} \rightarrow \equiv Ti - -^{\circ}OH \quad \text{(I)}$$

$$\equiv Ti - OH_2 + h^{+}_{(VB)} \rightarrow \equiv Ti - -^{\circ}OH + H^{+}_{ads} \quad \text{(II)}$$

$$\equiv Ti - O - Ti \equiv + h^{+}_{(VB)} + H_2O_{ads} \rightarrow \equiv Ti - O^{\circ} - -H - O - Ti \equiv + H^{+}_{ads} \quad \text{(III)}$$

* Corresponding authors at: CIDIA-FEAM Universidad de La Palmas de Gran Canaria, Edificio del Parque Científico Tecnológico de la ULPGC, Campus de Tafira, 35017 La Palmas de Gran Canaria, (Unidad Asociada al CSIC a través del Instituto de Ciencias de Materiales de Sevilla, ICMS), Spain.
E-mail addresses: d.garzon.sousa@gmail.com (D. G. Sousa), javier.arana@ulpgc.es (J. Araña).

http://dx.doi.org/10.1016/j.jphotochem.2017.08.010
1010-6030/© 2017 Elsevier B.V. All rights reserved.

$$\equiv Ti - OH + F^-_{ads} + H^+_{ads} \rightarrow \equiv Ti - F + H_2O \quad \text{(IV)}$$

$$\equiv Ti - F + h^+_{(VB)} + H_2O_{ads} \rightarrow \equiv Ti - F + {}^{\circ}OH_{free} + H^+_{ads} \quad \text{(V)}$$

However, the physical chemistry of this process as well as many other aspects of the effect of fluorine on the TiO_2 surface have not been fully clarified [15].

It has been reported that the doping of anatase TiO_2 with elements like F with extra electrons gives rise to *n*-type materials with significantly different properties to those of the original catalyst [16]. The extra electrons provided by the F^- ions are stabilised on the titanium ions of the crystal lattice giving rise to Ti^{3+} ions homogenously spread over the crystal lattice. Titanium dioxide is a reducible oxide whose composition depends, among other factors, on oxygen pressure in the atmosphere. The extra electron provided by the fluorine will be found in the Ti 3*d* orbitals a few tenths of an electron-volt below the lower end of the conduction band [17]. TiO_2 doping with fluorine gives rise to two types of fluoride species. The first of these arises when the F^- ion replaces the O^{2-} ions of the crystal lattice resulting in Ti—F—Ti bonds. This leads to the formation of Ti^{3+} species in the bulk, giving rise to localised Ti^{3+} states just below the conduction band. This type of doping inhibits oxygen adsorption and consequently the formation of superoxide radicals, suggesting that the sites with defects are localised in the bulk and not on the surface. The second species consists of F^- ions on the surface of the solid which replace surface hydroxyl groups giving rise to Ti—F terminal groups without generating reduced sites [17]. The Ti^{3+} sites that are generated may be systems entirely localised in sections of the catalyst or systems in which there is a total delocalisation of electron density in all the ions of the metal, with the energy levels of these states just below the conduction band [16]. Studies undertaken to date suggest that the second of these possibilities appears to be the most probable [18]. Displacement of the negative charge, which takes place at the edges of the energy levels, favours the charge transference rate and lowers the recombination rate. The accumulation of electrons trapped in the conduction band in a photo-stationary state results in the surface charge of the TiO_2 suspended particles changing to negative [19]. Most of the electrons would be localised on Ti(III)-OH surface sites.

It has been reported in other studies that an increase in the degradation rate takes place when the anatase phase is doped with fluorine, but that this rate decreases when the rutile phase of the TiO_2 is doped [20]. It was also shown in the same study that the increase in the degradation rate does not always require pre-adsorption of the fluoride ions. A Helmholtz double layer was proposed by the authors of the study in which the fluoride ions would be situated on the internal and external planes of this double layer, facilitating desorption of the surface bonded $^{\bullet}OH$ radicals to the solution upon irradiation of the TiO_2. The most active radical fluorides are those found in the outer Helmholtz layer, and are the most efficient at provoking desorption of the surface bonded $^{\bullet}OH$ radicals. The inner layer fluoride ions, namely those adsorbed onto the surface or bonded to Ti^{4+} sites, have a lower capacity to form a bond with the surface bonded $^{\bullet}OH$ via hydrogen-fluorine bridges. The key to this proposal lies in the argument that desorption to the solution of the surface bonded hydroxyl radicals on the irradiated TiO_2 is thermodynamically possible through an H—F bond [20].

It should also be noted that a positive effect has not been observed in all studies involving TiO_2 doping with fluorine. For example, a slowing down of the degradation rate of dichloroacetate [21] and of the degradation rate in gas phase of some compounds [22] has been observed. As previously stated, the fluoride ion has a specific affinity for adsorption on TiO_2 acting as a Lewis base, and so would decrease and modify the density of surface states and, in this way, slow down certain degradation processes [15]. It should also be noted that although the formation of $^{\bullet}OH$ radicals is higher in F-TiO_2, the oxidation processes in which there is hole transfer are inhibited [21].

In order to acquire a more in-depth knowledge and understanding of the behaviour of these fluorinated materials, a study is undertaken in the present work of the degradation of phenol, formic acid and aniline with two TiO_2 catalysts with different anatase and rutile phase proportions. For this purpose, the P25 catalyst with 80% anatase and 20% rutile phase and the Sigma Aldrich (SA) catalyst with purely anatase phase were selected. Both materials have approximately the same surface area (about 50 $m^2\,g^{-1}$). These two catalysts were fluorinated using high concentrations of NaF at pH 6.5 and selecting the filtration method to obtain the corresponding F-P25 and F-SA catalysts.

Various organic compounds have been described in the bibliography to assess the photocatalytic activity of materials with different physical-chemical properties. These include coumarin, terephthalic acid, phenol, aniline and/or formic acid, depending principally, among other aspects, on determining what type of radical intervenes or whether adsorption is a determinant factor in the process [23,24]. Considering the working pH values, the degradation mechanisms and the results described in the bibliography, formic acid, aniline and phenol were selected in the present work as test molecules to characterise the catalysts.

2. Experimental

2.1. Synthesis of fluorinated catalysts

Two commercial TiO_2 photocatalysts were used: Evonik Aeroxide P25 (P25) and anatase Sigma Aldrich (SA). For the synthesis of the fluorinated catalysts, 10 g of the corresponding commercial TiO_2 catalyst were placed into 250 mL of a 2 M NaF solution (pH 6.5). This solution was stirred continuously for 30 min and then filtered. The catalyst obtained after filtration was washed with 1 L of water and the non-desorption of fluoride and sodium was observed. The catalyst was subsequently dried at 100 °C for 12 h. It should be noted that different filters were tested with different pore diameters and that important photocatalytic performances were only obtained with the Whatman TM 1005-125 (grade 5, diameter: 12.5 cm, pore size: 2.5 μm).

2.2. Characterisation of materials

The surface concentration of fluorine on the catalysts was semi-quantitatively determined by EDAX analysis (Quantax 70, Bruker). Three image amplifications were carried out for this analysis (300, 3000 and 30,000) with 5 sampling points in each increase and an exposure time of 300 s.

Analyses of the crystalline structure were performed by X-ray diffraction (XRD Bruker D8 Advance) with a source of Cu $K\alpha_1$ radiation (λ = 0.15406 nm) at 1.6 kW (40 kV, 40 mA). Anatase-rutile fractions were calculated taking into account the relative diffraction peak intensities of crystalline planes (101) and (111) of anatase and rutile, respectively. BET surface area measurements were carried out by N_2 adsorption at 77 K using a Micromeritics 2010 instrument. Diffuse reflectance UV–vis spectra (DRS-UV–vis) were recorded on a Varian Cary 5 spectrometer equipped with an integrating sphere using PTFE (poly-tetra-fluoroethylene) as reference to study the optoelectronic properties of the samples. Diffuse reflectance spectra were recorded and band gap values

were calculated by the Kubelka-Munk function, according to the Tandon-Gupta method. Field emission scanning electron microscopy (FESEM) images were obtained using a Hitachi S-4800 microscope.

The Brönsted and Lewis acid sites determination was done through interaction of ammonia with the surface of the catalysts. This interaction was followed by Fourier transform infrared spectroscopy (FTIR) with a Thermo-Scientific-Nicolet iS10 spectrophotometer and a custom-made cell equipped with CaF_2 windows performing 32 scans with a spectral resolution of 4 cm^{-1}. 10 mg of catalyst were used in each experiment. Catalysts were treated with a stream of saturated moist air with an NH_3 molar flow rate of $6.24 \cdot 10^{-4}$ mol min^{-1} for 60 min and then placed in the cell for analysis. The system has been described in a previous work [25].

2.3. Photocatalytic experiments

The degradation tests were performed in 250 mL Pyrex glass batch reactors, filled with 200 mL of the pollutant aqueous solution and 1 g/L of P25, SA, F-P25 or F-SA. A constant stirring was maintained at 750 rpm. A 60W Philips Solarium HB175 equipped with four 15W Philips CLEO fluorescent tubes with emission spectrum from 300 to 400 nm (maximum around 365 nm) and with an average irradiation power of about 9 mW was used as UV source in the photocatalytic studies. The pH was adjusted with diluted H_2SO_4 or NaOH. Before irradiation was turned on, the solution was left for 15 min in the darkness to reach the adsorption-desorption quasi-equilibrium. Adsorption was lower than 5% after this period with all catalysts.

All the studies were performed with a 0.51 mM concentration of phenol, aniline or formic acid. The studies with formic acid were performed at pH 3, those with phenol at pH 5 and those with aniline at pH 7, with the aim of ensuring that the molecule under study had the appropriate electrical charge to facilitate its approximation to the photocatalyst surface. A constant pH was maintained throughout the test.

2.3.1. Analytical determinations

Concentrations of phenol, aniline and formic acid at different reaction times were HPLC-measured using a Supelco Discovery C18 (25 cm × 4.6 mm ID, 5 μm particles) for phenol and aniline and a Supelcogel C-610H (30 cm × 7.8 mm ID) for formic acid. The mobile phase used were acetonitrile-water-acetic acid (30:69:5:0.5% vol) for phenol, acetonitrile- acetate buffer 0.01 M (30:70) for aniline and phosphoric acid-water (0.1:99.9) for formic acid. Detector wavelength was 270 nm for phenol and 230 nm for aniline and formic acid. Quantification was performed by least-squares fit.

The concentrations of phenol and muconic acid in the studies performed with mixtures of these compounds were made using an EC 250/4 Nucleodur 100-5 C18ec column (250 mm × 4 mm ID, 5 μm particles). The mobile phase used was acetonitrile/water/H_3PO_4 15/85/0.1. Detector wavelength in these studies was 264 nm. Quantification was also performed by least-squares fit.

The total organic carbon (TOC) analyses were determined using an analyser (TOC-VCSN, Shimadzu).

3. Results and discussion

3.1. BET area, EDAX, SEM, XRD and DRS-UV–vis analyses

Table 1 shows the most important results of the BET, EDAX, DRX and DRS-UV–vis analyses. P25 and SA catalysts have respective surface areas of 50.9 and 47.3 $m^2 g^{-1}$. The fluorinated catalysts, F-P25 and F-SA, have similar surface areas (51.3 and 45.4 m^2/g respectively). The anatase/rutile phase ratios of the P25 and F-P25 are 82.3/17.7 and 85.5/14.5 respectively, while the SA and F-SA catalysts only have anatase phase. The mean particle size was also determined; it was noted that they were very similar in the P25 and F-P25, but that there was a difference in size of approximately 7 nm between the anatase particles of the SA and F-SA. The differences observed are attributable to the filtration process of the catalyst in the synthesis of the fluorinated materials. The band gap values obtained from the UV–vis analyses are all very similar, with no significant changes observed when fluorinating the catalysts. Thus, as seen in other studies, surface fluorination of the catalysts does not modify the optical properties of these materials [26,27]. The images obtained from the SEM analyses of the F-P25, F-SA and SA catalysts show a similar distribution of aggregates (Fig. 1). However SEM analyses of the P25 show a different distribution of aggregates, which can also be attributed to the filtration process.

Table 1 also shows the Ti/F and F/Na ratios obtained from the EDAX analyses. The analyses also showed the presence of sodium on the surface of the fluorinated materials, though its concentration is significantly lower than the molar concentration of fluorine. This shows that the fluorine is mostly interacting with the catalyst surface and is not as NaF, though the presence of this salt on the surface cannot de discarded. Note that the Ti/F proportions in both fluorinated catalysts are similar.

3.2. Characterisation of the adsorbed water, hydroxyl groups and surface charge

Fig. 2 shows the spectra of the fluorinated and non-fluorinated P25 and SA catalysts. Note in particular the position of the baseline in each of these catalysts, the band attributed to isolated hydroxyl groups (3698 cm^{-1}) and the bands attributed to adsorbed water (3600–3000 cm^{-1} and 1640 cm^{-1}).

An important feature to note in the spectra of Fig. 2 is the position of the baseline. As a result of the presence of surface or shallow electron traps, electrons are fed to the conduction band via thermal processes such as those generated by the infrared radiation used to obtain the spectra. The electrons promoted to the conduction band have a similar behaviour to that described for delocalised electrons confined to a three-dimensional box with infinite walls; the high density of generated states gives rise to the continuous presence of excited electrons leading to a baseline increase of the infrared spectrum [16]. The baseline position of the

Table 1
Surface area, anatase/rutile phase ratios, crystallite size, band gap and Ti/F and F/Na molar ratios.

	Surface area ($m^2 g^{-1}$)	Anatase/rutile phase ratios	Cristallite size (nm)		Band gap (eV)	Molar ratio	
			Anatase	Rutile		Ti/F	F/Na
P25	50.9	82.3/17.7	20.56	33.01	3.16	–	–
F-P25	51.3	85.5/14.5	19.84	34.70	3.0	20.97	2.47
SA	47.3	100/0	13.93	–	3.16	–	–
F-SA	45.4	100/0	20.57	–	3.18	19.43	2.12

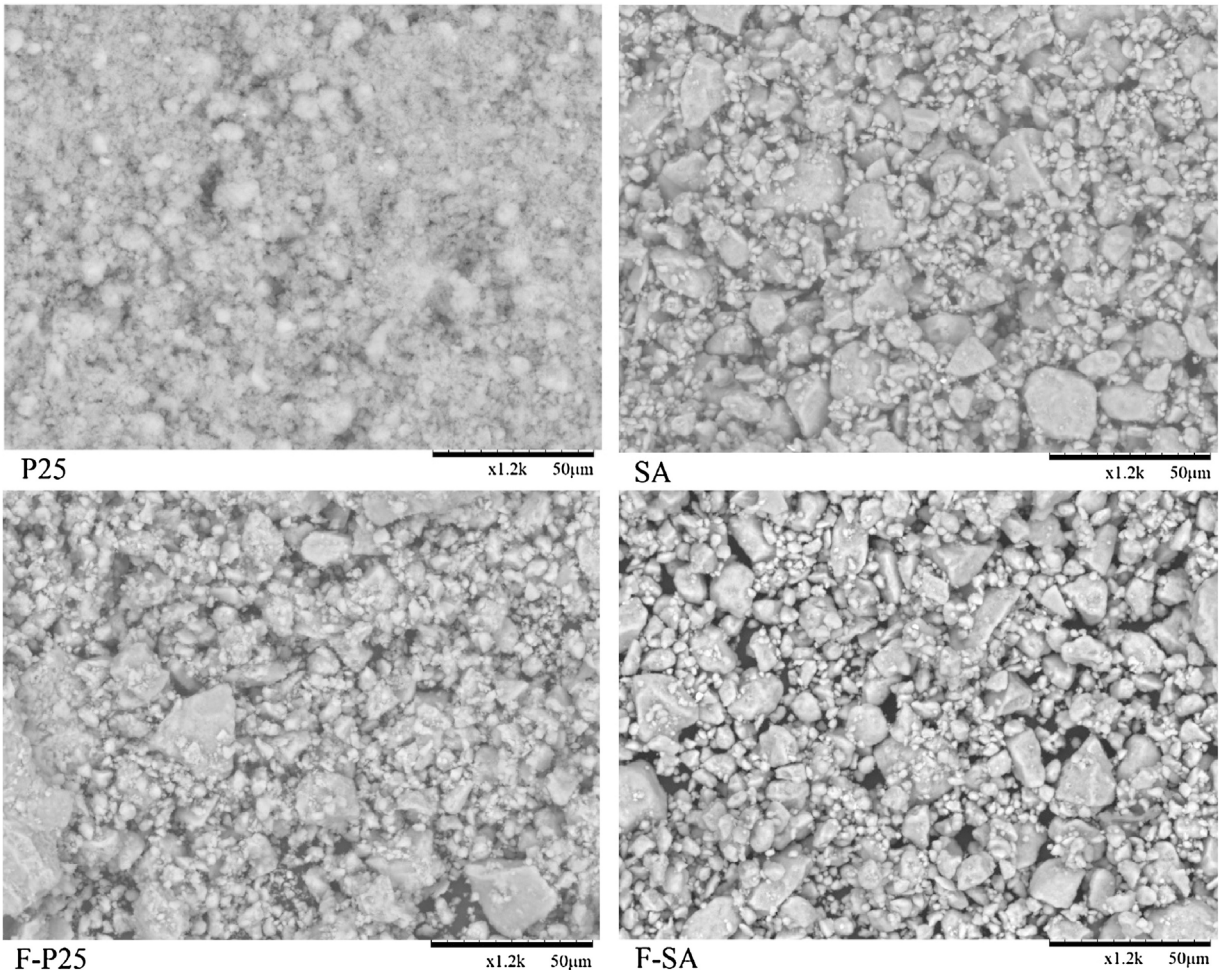

Fig. 1. Imagen SEM of the fluorinated and non-fluorinated P25 and SA catalysts.

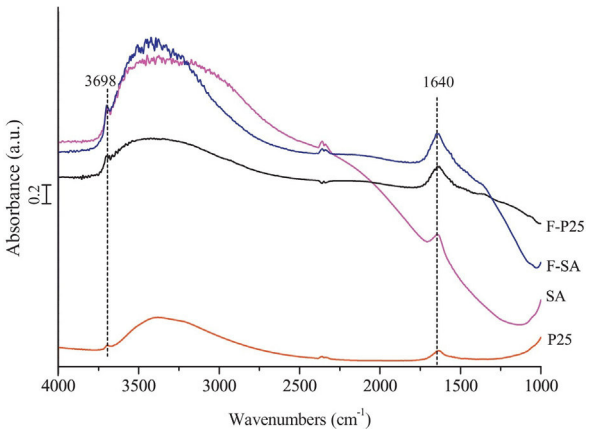

Fig. 2. FTIR spectra of the fluorinated and non-fluorinated P25 and SA catalysts.

SA catalyst, the one with only anatase phase, is higher than that of the P25. On modification of P25 with fluorine, a baseline increase takes place which takes it to the same level as that observed in the SA catalyst. When TiO_2 is modified with fluorine, at least a fraction of the excess electrons introduced by the fluorine are localised by lattice Ti^{4+} cations. The presence of reduced Ti^{3+} centres in the as-prepared, fully oxidised solid indicates that the F-TiO_2 system can be described in terms of an *n*-type semiconductor provoking the baseline increase observed in the F-P25 catalysts [17]. Modification of the baseline also takes place with the F-SA catalyst in the region between 2500 and 1000 cm^{-1} as a consequence of the presence of fluoride.

The fluorination process has been described through Reaction (1) [4].

$$\equiv Ti - OH + F^- \rightarrow \equiv Ti - F + OH^- (pK = 6.2) \quad (1)$$

Bearing in mind the pK of Reaction (1), the highest percentage of fluorination is produced around pH 3 [28,29]. However, in the present work, impregnation with NaF was performed at pH 6.5, and so in the spectra of the fluorinated catalysts (Fig. 2) bands of isolated hydroxyl groups (3698 cm^{-1}) are still observed and in an even relatively higher proportion than with the P25 and SA catalysts.

3.3. Determination of Lewis and Brönsted acid sites

Ammonia can interact with Brönsted and Lewis acidic surface sites forming ammonium ions and acid-base adducts, respectively. The presence of these species can be perfectly identified via FTIR. The interaction of NH_3 with the Lewis acid sites gives rise to bands centred around 1200 cm^{-1}; the higher the wavenumber the greater the strength of the Lewis sites. The non-adsorbed NH_4^+ gives rise to a band centred around 1445 cm^{-1}, and the shift of this band to higher wavenumbers would indicate the presence of adsorbed ammonium.

The spectra obtained from the interaction of ammonia with the catalysts are shown in Fig. 3. A broad band centred around 1200 cm^{-1} can be observed in the initial spectrum of the P25 attributed to $\delta_s NH_3$ ammonia adsorbed on Lewis sites. The asymmetry and width of the band suggest that it may be composed of Lewis acid sites of different types. A broad band can also be observed at 1445 cm^{-1} which is attributed to the $\delta_{as}NH_4^+$ vibration. The width of this band may be due to its being formed of free ammonium produced by the abstraction of a proton from the P25 surface present in a Brönsted acid site and adsorbed ammonia [30,31]. A further band can be observed at 1315 cm^{-1} and a shoulder at 1558 cm^{-1} which cannot be attributed to ammonia adsorbed on either Lewis or Brönsted acid sites. It has been suggested in some studies that these bands most likely represent various deformation vibrations of NH_x species, which are formed on the surface in relatively small amounts as a result of NH_3 adsorption [32].

In the spectrum obtained of the interaction of NH_3 with the SA catalyst, the band attributed to the $\delta_{as}NH_4^+$ vibration is found at the same wavenumber, 1445 cm^{-1}, as in the P25 studies. However, the band attributed to the Lewis acid sites is found at 1216 cm^{-1} and the band corresponding to compounds generated by the decomposition of the ammonia has low intensity.

In the spectrum of NH_3 interaction with the F-P25 and F-SA catalysts (Fig. 2), the absence of the band attributed to NH_3 adsorbed on Lewis acid sites should be noted. However, in these catalysts the band attributed to $\delta_{as}NH_4^+$ (1445 cm^{-1}) was observed and a band at 1340 cm^{-1}.

The initial spectrum observed with F-TiO_2 can be explained as the interaction of NH_3 with surface fluorine through the following reaction [33,34].

$$\equiv Ti{-}F + NH_3 \rightarrow HF + \equiv TiNH_2$$

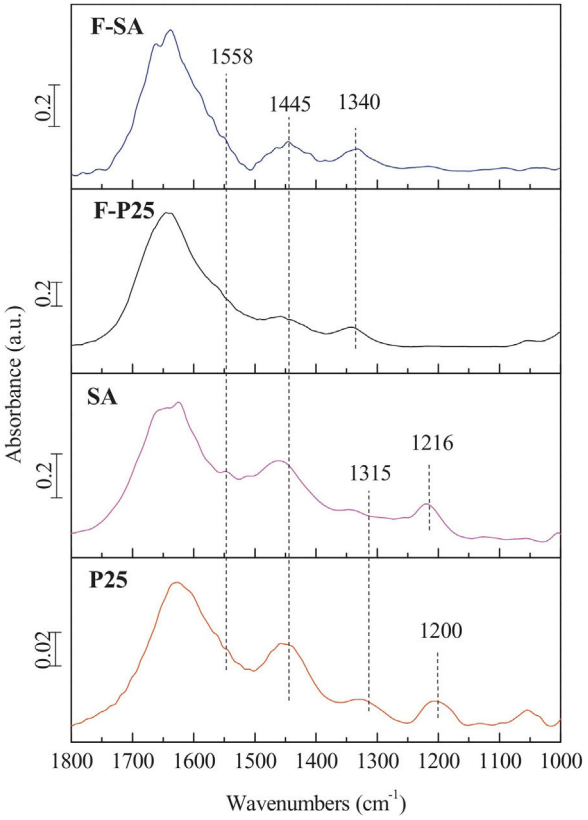

Fig. 3. FTIR spectra of the interaction of the NH_3 with the catalysts.

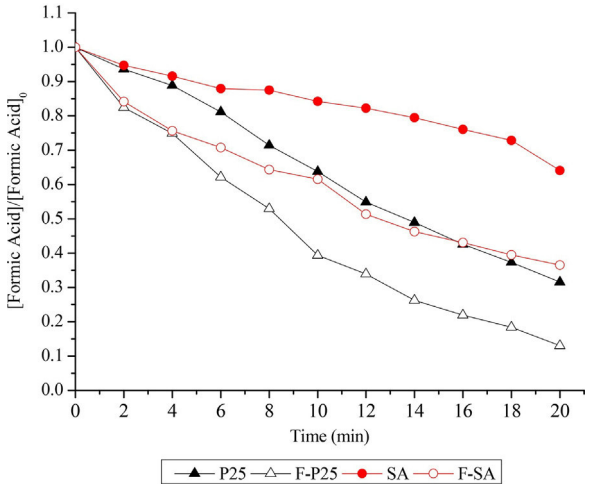

Fig. 4. Evolution of the concentration of formic acid during photocatalytic oxidation.

The non-detection of the band attributed to Lewis acid sites at around 1200 cm^{-1} in the fluorinated catalysts would suggest that in these materials the surface Ti atoms are fluorinated or strongly bonded to hydroxyl groups.

3.4. Photocatalytic degradation studies

As indicated in the experimental section, the formic acid, aniline and phenol degradation studies were all performed at the same concentration (0.51 mM). The pH of the solution in the different studies was 7, 5 and 3 for the aniline, phenol and formic acid, respectively.

Figs. 4–6 show the degradation results of formic acid, aniline and phenol, respectively. With all the substrates studied, the F-P25 catalyst showed the greatest photocatalytic efficiency in degradation. The F-SA and P25 had similar degradation curves for all the molecules, while the SA has the worst photocatalytic activity.

Fig. 7 shows the degradation constants for each catalyst and each substrate obtained from the results shown in Figs. 4–6. As can be observed, the rate constants display the following sequence with all the substrates:

F-P25 > F-SA ≈ P25 > SA

With all catalysts, the highest rate constant is found with formic acid degradation, followed by phenol and with the slowest for

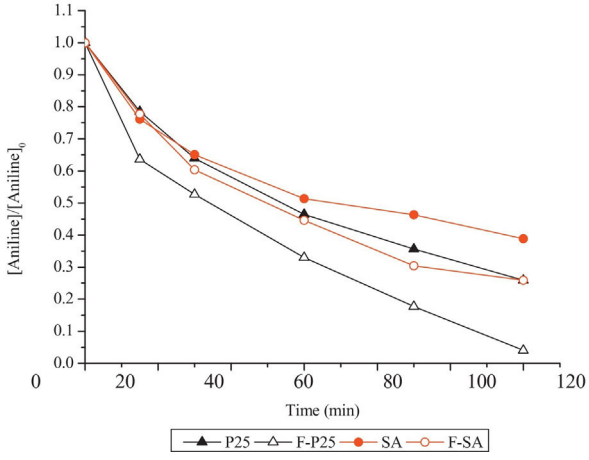

Fig. 5. Evolution of the concentration of aniline during photocatalytic oxidation.

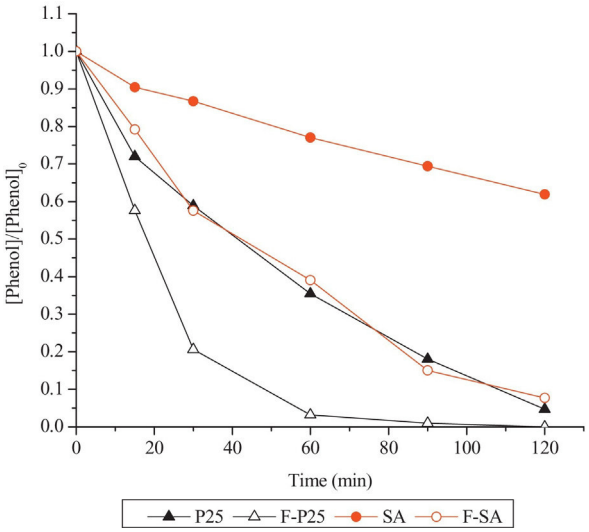

Fig. 6. Evolution of the concentration of phenol during photocatalytic oxidation.

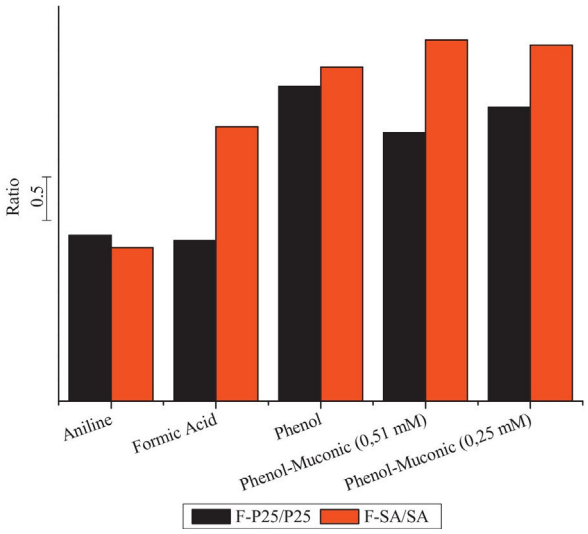

Fig. 8. Ratio between apparent first order kinetic constants obtained for the fluorinated/bare catalysts (F-P25/P25 and F-SA/SA).

aniline. The rate constant with P25 in the formic acid degradation is 3.25 times greater than that of phenol, in the SA it is 2.15 times greater and in the fluorinated catalysts it is 1.5 times greater. Again with the P25, the degradation rate constant of phenol is, in turn, 1.8 times greater than that of aniline, whereas with the SA catalyst the rates are similar and in the fluorinated catalysts it is 3.7 times higher in the F-P25 and 2.5 times higher in the F-SA. The degradation sequence appears to be related to the oxidation state of the carbon in the compound. Thus, the more oxidised the substrate under study the faster the degradation.

To compare the efficiency of the fluorinated catalysts, the ratio between the rate constants of F-P25/P25 and of F-SA/SA with the different substrates was calculated (Fig. 8). The ratios obtained for phenol and aniline are practically the same for both catalysts. That is, for the phenol and aniline the same increase in the rate constant takes place when the catalysts are fluorinated. The highest increase in the rate constant is with the phenol. With the fluorinated P25 catalyst, the same increase in the rate constant is seen in aniline and formic acid degradation. However, with the SA catalyst a higher increase is observed in the degradation rate constant of formic acid than of aniline.

With a view to a greater in-depth study, tests were carried out with phenol in the presence of muconic acid with each at the same concentration of 0.51 mM (Fig. 9A), and at half that concentration (0.25 mM) (Fig. 9B). These studies were performed to see whether the presence of a phenol degradation intermediate (muconic acid) at high concentrations would vary the parameters determined in the previous studies. The rate constants obtained in these studies were compared with those of phenol alone, aniline and formic acid

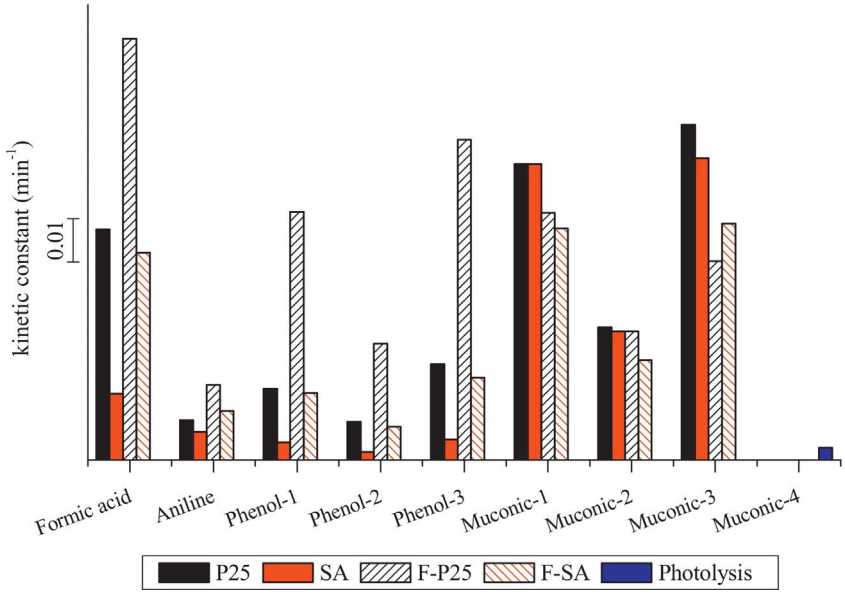

Fig. 7. Apparent first order kinetic constants for formic acid, aniline, phenol and muconic acid photocatalytic oxidation in presence of the different catalysts.
Phenol-1: k_{phenol} in study with phenol 0.51 mM; Phenol-2: k_{phenol} in study with mixtures phenol:muconic acid (0.51 mM: 0.51 mM); Phenol-3: k_{phenol} in study with mixtures phenol:muconic acid (0.25 mM: 0.25 mM).
Muconic-1: $k_{muconicacid}$ in study with muconic acid 0.51 mM; Muconic–2 $k_{muconicacid}$ in study with mixtures phenol:muconic acid (0.51 mM: 0.51 mM); Muconic-3: $k_{muconicacid}$ in study with mixtures phenol:muconic acid (0.25 mM: 0.25 mM); Muconic-4: $k_{muconicacid}$ in muconic acid photolysis.

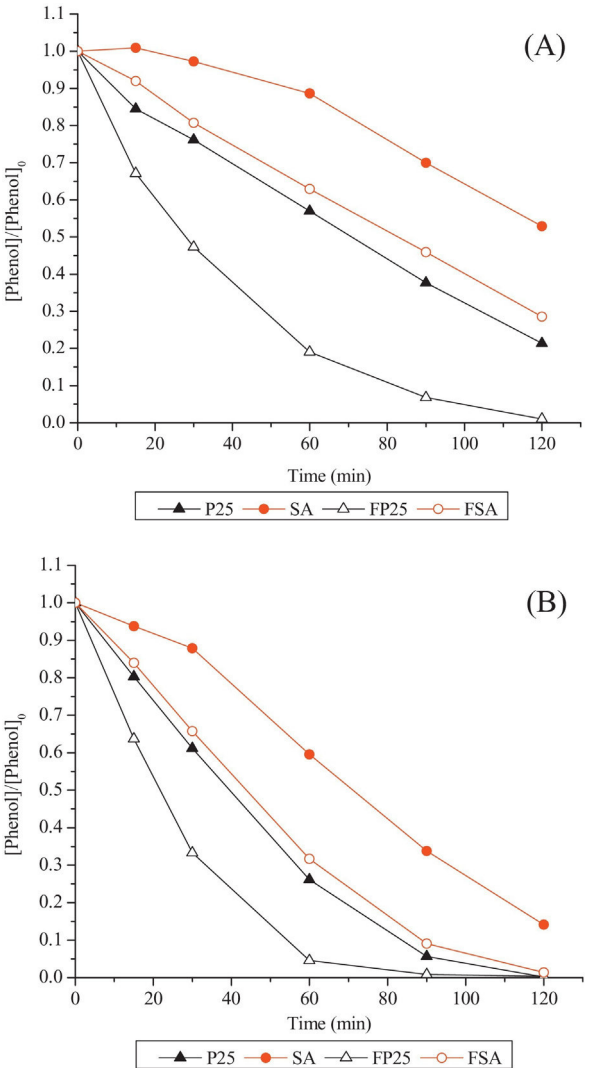

Fig. 9. Evolution of the concentration of phenol during photocatalytic oxidation of mixtures phenol:muconic acid 0.51 mM:0.51 mM (A) and 0.25 mM:0.25 mM (B).

(Fig. 7). Also shown in Fig. 7 are the degradation rate constants of the muconic acid alone (0.51 mM) and the phenol-muconic acid mixtures. The $k_{phenol\text{-}2}$ in the studies performed with phenol-muconic acid mixtures (0.5 mM–0.5 mM) decrease by almost half with all the catalysts compared to the $k_{phenol\text{-}1}$ (studies with 0.51 mM phenol alone) (Fig. 7). In contrast, the $k_{phenol\text{-}3}$ values obtained in the studies performed with 0.25 mM–0.25 mM phenol-muconic acid mixtures are similar to the $k_{phenol\text{-}1}$ values. The same thing was observed in the degradation rate constants of the muconic acid (Fig. 7). Given that phenol is barely adsorbed onto the catalyst [35], this could be indicating competition for the generated radicals. It was also observed in these tests that the phenol degradation rate constant follows the same sequence as in the previous studies. That is, the highest rate constant is obtained with the F-P25, followed by the F-SA which has a similar rate constant to the P25, and finally the SA. The correlation between the F-P25/P25 and F-SA/SA phenol degradation rate constants was also calculated (Fig. 8), with very similar degradation rate constant increases being obtained after fluorination as in the previous studies. On the other hand, no increase was observed in the muconic acid degradation rate constant with the fluorinated catalysts. In fact, there even appears a slight decrease in the value when the catalysts are fluorinated.

A control was also performed of the main intermediates of phenol degradation (hydroquinone, catechol and resorcinol). Figs. 10 and 11 show the concentrations and evolution of these intermediates. In the studies with phenol alone, the concentrations of intermediates follow the sequence [resorcinol] ≥ [hydroquinone] > [catechol] with the all catalysts. With the F-P25, the concentrations of these intermediates decrease very rapidly. In the studies performed in the presence of muconic acid (0.51 mM), the concentrations of resorcinol are significantly smaller and the concentration of intermediates has the following sequence [hydroquinone] > [catechol] > [resorcinol].

A control was also performed of TOC. In order to evaluate the concentration of degradation intermediates other than dihydroxylated phenolic compounds, the concentrations of organic matter corresponding to phenol, hydroquinone, catechol, resorcinol and muconic acid determined in previous analyses (Fig. 12) were subtracted from the experimentally determined TOC. As can be seen, in all the studies the F-P25, which presents the highest k_{phenol}, has less capacity to mineralise the intermediates generated from the degradation of the dihydroxylated compounds.

3.5. Discussion of the results

The photocatalytic processes can be summarized in the following reactions [35]:

$$TiO_2 + h\nu \rightarrow h^+ + e^- \quad (2)$$

$$h^+ + organic_{(ads/inter)} \rightarrow oxidized\ product \quad (3)$$

$$\equiv Ti{-}OH_2 + h^+ \rightarrow Ti - (^{\bullet}OH_{surf}) + H^+ \quad (4)$$

$$^{\circ}OH_{surf} + organic_{(ads/inter)} \rightarrow oxidized\ product \quad (5)$$

$$O_{2(ads)} + e^- \rightarrow O_2^{\circ -} \quad (6)$$

$$O_2^{\circ -} + H^+ \rightarrow HO_2^{\circ};\ 2HO_2^{\circ} \rightarrow H_2O_2 \quad (7)$$

$$H_2O_{2(aqu)} + e^- \rightarrow {}^{\circ}OH_{(free)} + OH^- \quad (8)$$

$$^{\circ}OH_{(free)} + organic_{(aqu)} \rightarrow oxidized\ product \quad (9)$$

$$H_2O_2 + organic_{(aqu)} \rightarrow oxidized\ product \quad (10)$$

The oxidative species h^+ and $^{\bullet}OH_{surf}$ would give rise to oxidation processes on the catalyst surface or at the surface-solution (inter) interface, while the oxidative species $^{\bullet}OH_{(free)}$ and H_2O_2 would give rise to oxidation processes in the solution.

Different studies [16–19] have shown that, with the introduction of fluorine atoms on the TiO_2 surface and their interaction with the Ti surface atoms, states are generated with high negative charge density. This has been observed in the FTIR studies of the F-P25 and F-SA catalysts described in this paper. The presence of the surface states of high negative charge density means that during illumination the photogenerated holes are trapped on the surface and the electrons forced to make their way to more internal Ti atoms in the crystalline structure [36]. Thus, the holes can react

with the surface oxygen atoms and/or the adsorbed water favouring Reactions (3)–(5) or generating new $^{\bullet}OH_{free}$ radicals via Reaction (11) [15].

$$h^{+} + \equiv Ti - F + H_2O \rightarrow \equiv Ti - F + {}^{\circ}OH_{(free)} + H^{+} \quad (11)$$

Depending on the reaction conditions, the reagents used and the reaction mechanism, the formation and/or intervention of these radicals can be favoured. The mechanisms described for the degradation of formic acid, aniline and phenol are outlined in Diagrams 1–3 [37–39].

Aniline Mechanism

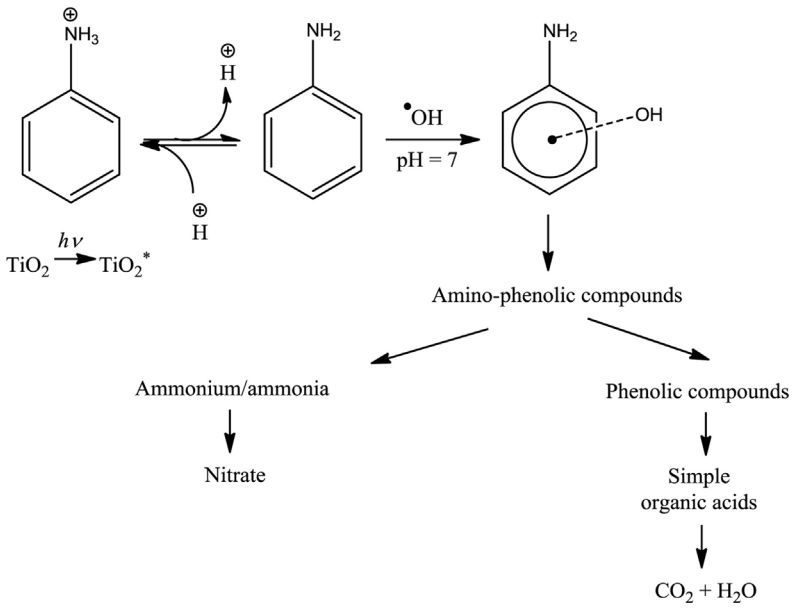

Degradation of formic acid can take place via reaction of the adsorbed (ads) formic acid or of the formic acid present at the solution/surface interface of the catalysts (inter) with the surface hydroxyl radicals ($^{\bullet}OH_{surf}$) or holes (Reactions (12) and (13), respectively) or via the reaction of the formic acid in solution with free hydroxyl radicals ($^{\bullet}OH_{free}$) (Reaction (14)).

Formic mechanism

$$HCOO^{-}_{(ads)/inter} + {}^{\circ}OH_{surf} \rightarrow CO_2^{\circ -} + H_2O \quad (12)$$

$$HCOO^{-}_{(ads)/inter} + h^{+} \rightarrow CO_2^{\circ -} + H^{+} \quad (13)$$

$$HCOO^{-}_{(aqu)} + {}^{\circ}OH_{free} \rightarrow CO_2^{\circ -} + H_2O \quad (14)$$

In the formic acid degradation studies described in previous sections, it was observed that the rate constant was 3.5 times higher in the P25 than in the SA. The P25 is characterised as having anatase and rutile phases. It has been reported that the faces of the anatase phase have different conduction potential energy [40]. The electrons and holes generated migrate to different faces depending on their potential energy allowing, in this way, their separation. In fact, it has also been reported that there are preferential faces of the anatase phase for photooxidation processes and preferential faces for photoreduction [40]. However, in catalysts like the P25 in which anatase and rutile phases coexist, it has been reported that, due to the low diffusivity of electrons in the rutile phase (89 times lower than in anatase), a greater separation is favoured of the e^{-}/h^{+} pair as a transfer of the holes is produced from the anatase to the rutile phase [41]. This would favour Reactions (3)–(10) in the P25 with respect to the SA. In the fluorinated catalysts, an increase was observed in the rate constant of 1.8 times in the F-P25 with respect to the P25 and of 3.13 times in the F-SA with respect to the SA. As previously indicated, when fluorinating the catalysts Reactions (3), (5) and/or (11) can be favoured.

The degradation mechanisms of aniline and phenol, at the working pH values, are described in Diagrams 2 and 3.

In the phenol degradation mechanism, depending on the intermediate generated, it can be determined which reaction is favoured between (3), (5) and (9) or (11). It has thus been reported that resorcinol is generated from the reaction of phenol directly with the holes (Reaction (3)), hydroquinone from its reaction with the $^{\bullet}OH_{surf}$ (Reaction (5)) and catechol from its reaction with the $^{\bullet}OH_{free}$ (Reaction (9) or (11)) [35]. In other studies performed with fluorinated catalysts on phenol degradation, in addition to an increase in the phenol degradation rate constant (in the fluorinated catalysts), a significant increase was also observed in catechol concentrations with respect to hydroquinone concentrations [6,20,42,43]. This has been attributed to Reaction (11) being favoured in these catalysts. However, in the different phenol degradation studies in the present work (with and without muconic acid) performed with the F-P25 and F-SA catalysts, although there was an increase of between 3.6 and 4 times in the phenol degradation rate constant, in no test was there observed a higher concentration of catechol than of hydroquinone. This would suggest that Reaction (11) is not taking place in the studies performed with phenol with the F-P25 and F-SA catalysts. In these catalysts, the reactions which appear to be taking place are (3) and (5), with Reaction (9) taking place to a lesser degree. That is, in these catalysts it seems that what is influential are the electrostatic effects that decrease the reaction rate of the e-/h+ pair and which in this way promote reaction with the $^{\bullet}OH_{surf}$ (Reaction (5)) or with the holes (Reaction (3)). In fact, in the characterisation studies the presence was observed of isolated hydroxyl groups in an even higher proportion than in the P25 and SA, as well as Brönsted acid sites.

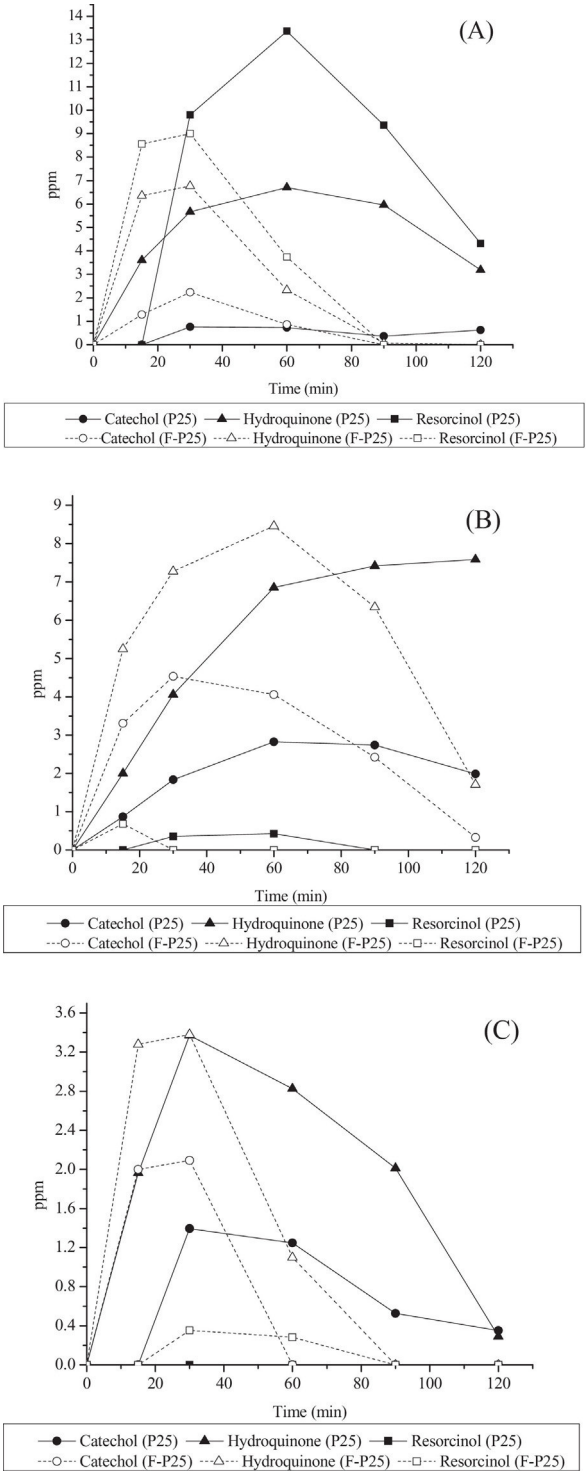

Fig. 10. Evolution of intermediates catechol, hydroquinone and resorcinol during phenol degradation (A), mixtures phenol: muconic acid 0.51 mM:0.51 mM (B) and mixtures phenol: muconic acid 0.25 mM:0.25 mM (C) with P25 and F-P25.

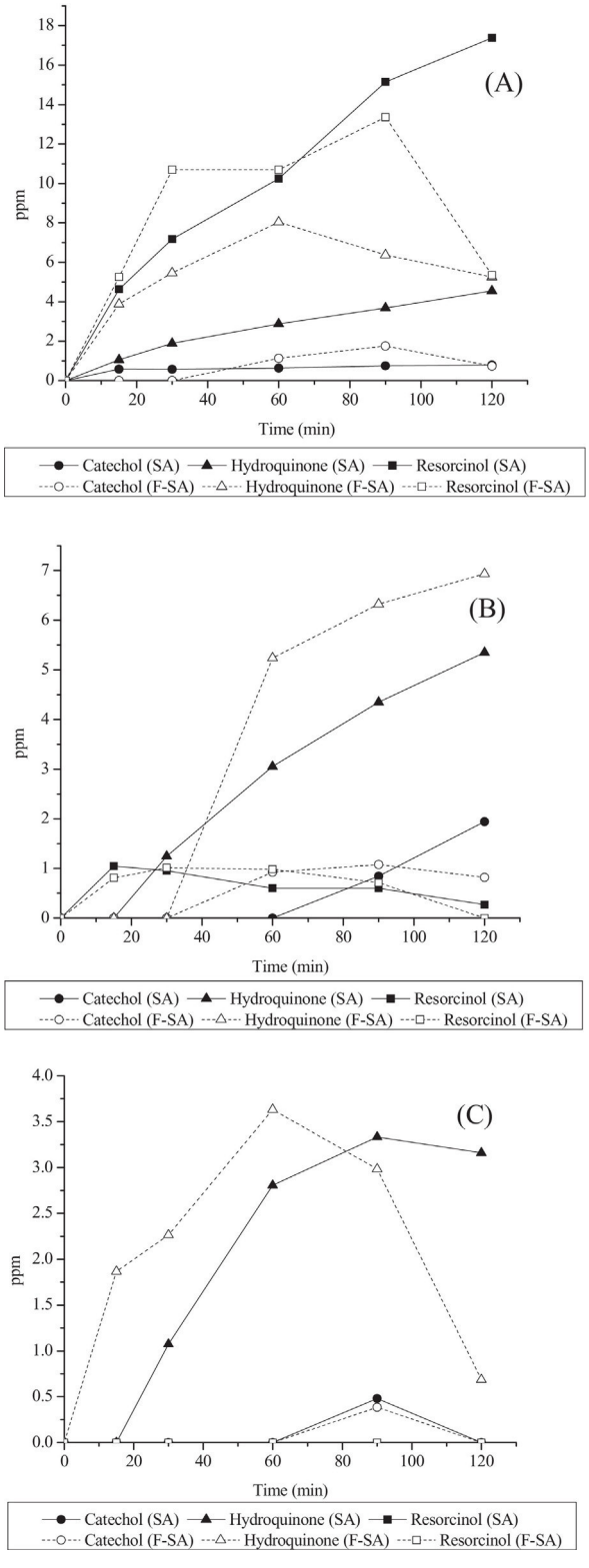

Fig. 11. Evolution of intermediates catechol, hydroquinone and resorcinol during phenol degradation (A), mixtures phenol: muconic acid 0.51 mM:0.51 mM (B) and mixtures phenol: muconic acid 0.25 mM:0.25 mM (C) with SA and F-SA.

In the phenol degradation studies in the presence of 0.5 mM muconic acid concentrations, it was observed that the phenol degradation rate constant was reduced practically by half in all the catalysts compared to the studies without this acid. Also reduced by half was the $k_{muconic}$ compared to that of the studies without the presence of phenol. It was observed in the analysis of the intermediates that in the studies with muconic acid the concentrations of resorcinol were drastically reduced. This would suggest that Reaction (3) of phenol with the holes would be inhibited in the presence of muconic acid. Muconic acid can be degraded by direct reaction of carboxylic acids with the holes (Kolbe reaction) or by means of the attack of $^{\bullet}OH$ radicals on olefinic groups. The fact that the concentration of resorcinol decreases in these conditions and

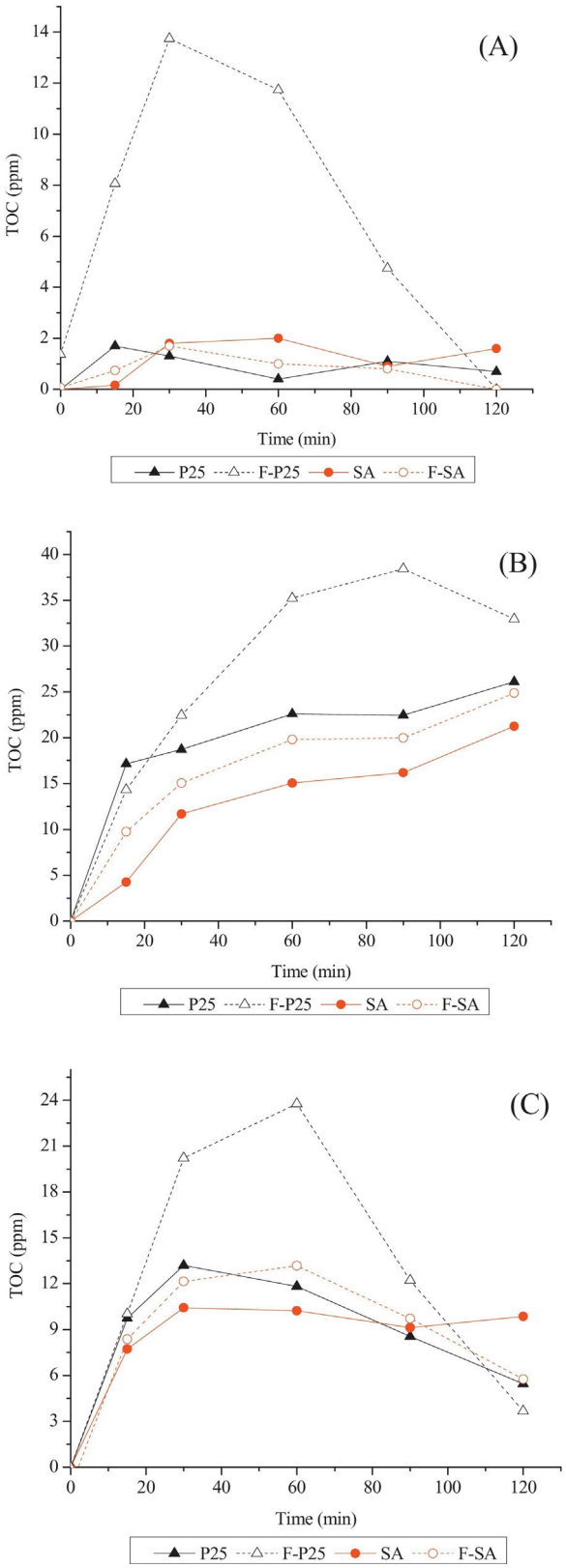

Fig. 12. TOC evolution no corresponding to phenol, hydroquinone, catechol, resorcinol or muconic acid during phenol degradation (A), mixtures phenol: muconic acid 0.51 mM:0.51 mM (B) and mixtures phenol:muconic acid 0.25 mM:0.25 mM (C).

not that of hydroquinone or catechol would suggest that, in the presence of muconic acid, phenol does not have access to the holes but does have access to the $^{\bullet}OH_{surf}$, in this way partially inhibiting muconic acid degradation. For this reason, the rate constants of both are reduced by half. Meanwhile, the $k_{muconic}$ with the fluorinated catalysts is in all cases lower than that of the P25 and SA. This may be due to electrostatic repulsions which partially inhibit access to the surface of the fluorinated catalysts in the ionized form of this acid and to a significant number of Ti surface atoms being bonded to the fluorine (Table 1). The muconic acid at the study pH is principally in ionized form. However, the phenol and aniline are, at the study pH, in a suitable molecular form to be at the surface/solution interface.

As previously mentioned, in the three studies performed with phenol and in the study performed with aniline, approximately the same increase was observed in the k_{phenol} of the F-P25 and F-SA with respect to the P25 and SA, respectively (Fig. 8). That is, although the P25 has a higher k_{phenol} than the SA, when fluorinating both catalysts there takes place practically the same increase in the rate constant. This would suggest that in the fluorination process performed in this study the photoactive sites are being promoted in the same proportion.

The differences in the fluorination process carried out in this work compared to those carried out in other studies are that a much higher NaF concentration was used in this study and a specific type of aggregate was selected via filtration. Under these conditions, it has been reported in the bibliography that the process that takes place is [29]:

$$\equiv Ti - OH^{NaF} \equiv Ti - F^{NaF} \equiv Ti - F - F^{-}$$

Therefore, in the F-P25 and F-SA the typical Ti—F centres that give rise to Reaction (11) do not appear, but the electrostatic effect is produced which favours e-/h+ pair separation. This would also explain the fact that the F-SA has similar rate constants to the P25 with all the substrates studied. This may indicate that the electrostatic effect of the fluoride ion on the anatase phase of the F-SA provokes a similar decrease in the recombination rate of the e^{-}/h^{+} pair to that provoked by the rutile phase in the P25.

4. Conclusions

The synthesis method for the fluorinated materials used in this study (F-P25 and F-SA) generated new catalysts with different properties to those described in other works. The characterisation studies performed with the F-P25 and F-SA catalysts reveal a practically identical surface area and band gap. Small differences are observed in mean particle size between the SA and F-SA and in the anatase/rutile proportions between the P25 and F-P25 which are attributable to the catalyst filtration process. The presence was also seen in the F-P25 and F-SA of isolated hydroxyl groups in a higher relative proportion (in relation to the non-fluorinated catalysts), the absence of Lewis acid sites where the NH_3 is adsorbed and the presence of Brönsted acid sites. It was also determined that interaction of Ti with fluorine atoms generates surface electron traps which cause a baseline increase in the FTIR spectra.

In the studies performed with formic acid, aniline, phenol and phenol-muconic acid mixtures, the k_{formic}, $k_{aniline}$, and k_{phenol} of the fluorinated catalysts are higher than those of the P25 and SA. With molecules whose adsorption on the catalyst surface is limited, as is the case of phenol and aniline, and whose degradation can take place at the surface/solution interface, the F-P25 and F-SA catalysts generate similar increases in the k_{phenol} with respect to the P25 and SA, respectively. The intermediates identified in phenol degradation suggest that in the fluorinated catalysts the formation of $^{\bullet}OH_{free}$ is not favoured. The results obtained indicate that the F-P25

and F-SA promote at the same intensity the sites responsible for the formation of $^{\bullet}OH_{surf}$ and surface h^{+}.

In this way, it was determined that the fluoride adsorbed on the surface of the F-P25 and F-SA catalysts generates electrostatic fields which favour the reactions of $^{\bullet}OH_{surf}$ and h^{+} with adsorbed molecules or at the surface/solution interface.

These new catalysts could be promising for processes in gas phase in which the intervention of $^{\bullet}OH_{surf}$ and h^{+} radicals is a determining factor.

Acknowledgements

We are grateful for the financial support of the Spanish Ministry of Economy and Competitiveness through the projects CTQ2015-64664-C2-1-P and the Spanish Ministry of Science and Innovation for the UNLP10-3E-726 infrastructure, co-financed with ERDF funds. D. Garzón Sousa would like to thank the University of La Palmas de Gran Canaria for its funding through its PhD Grant Program and Wiâm El-Alami would also like to thank the UNetBA Erasmus Program for its funding through a mobility grant.

References

[1] J. Low, B. Cheng, J. Yu, Surface modification and enhanced photocatalytic CO_2 reduction performance of TiO_2: a review, Appl. Surf. Sci. 392 (2017) 658–686.
[2] E.M. Samsudin, S.B. Abd Hamid, Effect of band gap engineering in anionic-doped TiO_2 photocatalyst, Appl. Surf. Sci. 391 (2017) 326–336.
[3] E.M. Samsudin, S.B. Abd Hamid, J. Ching Juan, W.J. Basirun, G. Centib, Synergetic effects in novel hydrogenated F-doped TiO_2 photocatalysts, Appl. Surf. Sci. 370 (2016) 380–393.
[4] E.M. Samsudina, S.B. Abd Hamida, J. Ching Juana, W.J. Basiruna, A.E. Kandjanib, S.K. Bhargavaba, Effective role of trifluoroacetic acid (TFA) to enhance thephotocatalytic activity of F-doped TiO_2 prepared by modified sol–gelmethod, Appl. Surf. Sci. 365 (2016) 57–68.
[5] A.A. Sadovnikov, A.E. Baranchikov, Y.V. Zubavichus, O.S. Ivanova, V.Y. Murzin, V.V. Kozik, V.K. Ivanov, Photocatalytically active fluorinated nano-titania synthesized by microwave-assisted hydrothermal treatment, J. Photochem. Photobiol. A: Chem. 303–304 (2015) 36–43.
[6] C. Minero, G. Mariella, V. Maurino, E. Pelizzetti, Photocatalytic transformation of organic compounds in the presence of inorganic anions. 1. Hydroxyl-mediated and direct electron-transfer reactions of phenol on a titanium dioxide-fluoride system, Langmuir 16 (2000) 2632–2641.
[7] D. Vione, C. Minero, V. Maurino, M.E. Carlotti, T. Picatonottoa, E. Pelizzetti, Degradation of phenol and benzoic acid in the presence of a TiO_2-based heterogeneous photocatalyst, Appl. Catal. B: Environ. 58 (2005) 79–88.
[8] Y.-C. Oh, W.S. Jenks, Photocatalytic degradation of a cyanuric acid, a recalcitrant species, J. Photochem. Photobiol. A 162 (2004) 323–328.
[9] S. Kim, H. Park, W. Choi, Effects of TiO_2 Surface fluorination on photocatalytic reactions and photoelectrochemical behaviors, J. Phys. Chem. B 108 (2004) 6402–6411.
[10] M. Konstantakou, T. Stergiopoulos, V. Likodimos, G.C. Vougioukalakis, L. Sygellou, A.G. Kontos, A. Tserepi, P. Falaras, I. nfluence of fluorine plasma treatment of TiO_2 Films on the behavior of dye solar cells employing the Co(II)/(III) redox couple, J. Phys. Chem. C 118 (2014) 16760–16775.
[11] K. Lv, Y. Xu, Effects of polyoxometalate and fluoride on adsorption and photocatalytic degradation of organic dye X3B on TiO_2: the difference in the production of reactive species, J. Phys. Chem. B 110 (2006) 6204–6212.
[12] J.H. Pan, Z. Cai, Y. Yu, X.S. Zhao, Controllable synthesis of mesoporous F–TiO_2 spheres for effective photocatalysis, J. Mater. Chem. 21 (2011) 11430–11438.
[13] J. Yu, Q. Xiang, J. Ran, S. Mann, One-step hydrothermal fabrication and photocatalytic activity of surface-fluorinated TiO_2 hollow microspheres and tabular anatase single micro-crystals with high-energy facets, CrystEngComm 12 (2010) 872–879.
[14] J. Yu, W. Wang, B. Cheng, B.-L.- Su, Enhancement of photocatalytic activity of mesporous TiO_2 powders by hydrothermal surface fluorination treatment, J. Phys. Chem. C 113 (2009) 6743–6750.
[15] X.F. Cheng, W.H. Leng, D.P. Liu, Y.M. Xu, J.Q. Zhang, C.N. Cao, Electrochemical preparation and characterization of surface-fluorinated TiO_2 nanoporous film and its enhanced photoelectrochemical and photocatalytic properties, J. Phys. Chem. C 112 (2008) 8725–8734.
[16] J. Biedrzycki, S. Livraghi, E. Giamello, S. Agnoli, G. Granozzi, Fluorine- and niobium-doped TiO_2: chemical and spectroscopic properties of polycrystalline n-type-doped anatase, J. Phys. Chem. C 118 (2014) 8462–8473.
[17] A.M. Czoska, S. Livraghi, M. Chiesa, E. Giamello, S. Agnoli, G. Granozzi, E. Finazzi, C. Di Valentin, G. Pacchioni, The nature of defects in fluorine-doped TiO_2, J. Phys. Chem. C 112 (2008) 8951–8956.
[18] C. Di Valentin, G. Pacchioni, A. Selloni, Reduced and *n*-type doped TiO_2: nature of Ti^{3+} species, J. Phys. Chem. C 113 (2009) 20543–20552.
[19] W.W. Dunn, Y. Aikawa, A.J. Bard, Characterization of particulate titanium dioxide photocatalysts by photoelectrophoretic and electrochemical measurements, J. Am. Chem. Soc. 103 (1981) 3456–3459.
[20] Y. Xu, K. Lv, Z. Xiong, W. Leng, W. Du, D. Liu, X. Xue, Rate enhancement and rate inhibition of phenol degradation over irradiated anatase and rutile TiO_2 on the addition of NaF: new insight into the mechanism, J. Phys. Chem. C 111 (2007) 19024–19032.
[21] H. Park, W. Choi, Effects of TiO_2 surface fluorination on photocatalytic reactions, J. Phys. Chem. B 108 (2004) 4086–4093.
[22] M. Lewandowski, D.F. Ollis, Halide acid pretreatments of photocatalysts for oxidation of aromatic air contaminants: rate enhancement, rate inhibition, and a thermodynamic rationale, J. Catal. 217 (2003) 38–46.
[23] Q. Xiang, J. Yu, P.K. Wong, Quantitative characterization of hydroxyl radicals produced by various Photocatalysts, J. Colloid Interface Sci. 357 (2011) 163–167.
[24] K. Ishibashi, A. Fujishima, T. Watanabe, K. Hashimoto, Detection of active oxidative species in TiO_2 photocatalysis using the fluorescence technique, Electrochem. Commun. 2 (2000) 207–210.
[25] J. Araña, A. Peña Alonso, J.M. Doña Rodríguez, J.A. Herrera Melián, O. González Díaz, J. Pérez Peña, Comparative study of MTBE photocatalytic degradation with TiO_2 and Cu-TiO_2, Appl. Catal. B: Environ. 78 (2008) 355–363.
[26] J. Tang, H. Quan, J. Ye, Photocatalytic properties and photoinduced hydrophilicity of surface-fluorinated TiO_2, Chem. Mater. 19 (2007) 116–122.
[27] D. Li, H. Haneda, S. Hishita, N. Ohashi, N.K. Labhsetwar, Fluorine-doped TiO_2 powders prepared by spray pyrolysis and their improved photocatalytic activity for decomposition of gas-phase acetaldehyde, J. Fluor. Chem. 126 (2005) 69–77.
[28] M. Shariq Vohra, S. Kim, W. Choi, Effects of surface fluorination of TiO_2 on the photocatalytic degradation of tetramethylammonium, J. Photochem. Photobiol. A: Chem. 160 (2003) 55–60.
[29] S. Liu, J. Yu, B. Cheng, M. Jaroniec, Fluorinated semiconductor photocatalysts: tunable synthesis and unique properties, Adv. Colloid Interface Sci. 173 (2012) 35–53.
[30] B. Bahrami, V.G. Komvokis, U.G. Singh, M.S. Ziebarth, O.S. Alexeev, M.D. Amiridis, In situ FTIR characterization of NH_3 adsorption and reaction with O_2 and CO on Pd-based FCC emission control additives, Appl. Catal. A: Gen. 391 (2011) 11–21.
[31] A.C. Sola, D. Garzón Sousa, J. Araña, O. González Díaz, J.M. Doña Rodríguez, P. Ramírez de la Piscina, N. Homs, Differences in the vapour phase photocatalytic degradation of ammonia and ethanol in the presence of water as a function of TiO_2 characteristics and the presence of O_2, Catal. Today 266 (2016) 53–61.
[32] K. Hadjiivanov, H. Knözinger, Species formed after NO adsorption and NO+ O_2 co-adsorption on TiO_2: an FTIR spectroscopic study, Phys. Chem. Chem. Phys. 2 (2000) 2803–2806.
[33] P. Pagsberg, B. Sztube, E. Ratajczak, A. Sillesen, Spectrokinetic studies of the gas phase reactions NH_2 + NO_x initiated by pulse radiolysis, Acta Chem. Scand. 45 (1991) 329–334.
[34] X. Zhang, Q.S. Li, Direct dynamics study on the reaction of N_2H_4 with F atom: a hydrogen abstraction reaction? J. Phys. Chem. A 110 (2006) 11636–11644.
[35] K. Lv, X. Guo, X. Wu, Q. Li, W. Ho, M. Li, H. Ye, D. Du, Photocatalytic selective oxidation of phenol to producedihydroxy benzenes in a TiO_2/UV system: hydroxyl radical versus hole, Appl. Catal. B 199 (2016) 405–411.
[36] H. Sheng, Q. Li, W. Ma, H. Ji, C. Chen, J. Zhao, Photocatalytic degradation of organic pollutants on surface anionized TiO2: common effect of anions for high hole-availability by water, Appl. Catal. B: Environ. 138–139 (2013) 212–218.
[37] J. Araña, E. Pulido Melián, V.M. Rodríguez López, A. Peña Alonso, J.M. Doña Rodríguez, O. González Díaz, J. Pérez Peña, Photocatalytic degradation of phenol and phenolic compounds Part I. Adsorption and FTIR study, J. Hazard. Mater. 146 (2007) 520–528.
[38] M. Canle L, J.A. Santaballa, E. Vulliet, On the mechanism of TiO_2-photocatalyzed degradation of aniline derivatives, J. Photochem. Photobiol. A 175 (2005) 192–200.
[39] M.F.J. Dijkstra, H.J. Panneman, J.G.M. Winkelman, J.J. Kelly, A.A.C.M. Beenackers, Modeling the photocatalytic degradation of formic acid in a reactor with immobilized catalyst, Chem. Eng. Sci. 57 (2002) 4895–4907.
[40] X. Ma, Y. Dai, M. Guo, B. Huang, Relative photooxidation and photoreduction activities of the {100},{101}, and {001} surfaces of anatase TiO_2, Langmuir 29 (2013) 13647–13654.
[41] B. Sun, Alexandre V. Vorontsov, P.G. Smirniotis, Role of platinum deposited on TiO_2 in phenol photocatalytic oxidation, Langmuir 19 (2003) 3151–3315.
[42] N. Watanabe, S. Horikoshi, H. Hidaka, N. Serpone, On the recalcitrant nature of the triazinic ring species cyanuric acid, to degradation in Fenton solutions and in UV-illuminated TiO_2 (naked) and fluorinated TiO_2 aqueous dispersions, J. Photochem. Photobiol. A: Chem. 174 (2005) 229–238.
[43] C. Minero, G. Mariella, V. Maurino, D. Vione, E. Pelizzetti, Photocatalytic transformation of organic compounds in the presence of inorganic ions 2. Competitive reactions of phenol and alcohols on a titanium dioxide-fluoride system, Langmuir 16 (2000) 8964–8972.